Contents

General Information

The EMN Cancun Meeting 2015 will take place at The Westin Resort & Spa, Cancun, Mexico. The conference will be held from June 8 to June 11, 2015.

Workshops on selected focus topics will include invited and contributed oral presentations from Monday to Wednesday, and the poster session will be presented on the afternoon of Tuesday (June 9).

Registration Desk Hours

The EMN Cancun Meeting 2015 registration desk, located in The Westin Resort & Spa, will be open during the following hours:

Sunday, June 7th…….....14:00pm - 18:00pm
Monday, June 8th…….7:00am - 18:00pm
Tuesday, June 9th…….7:00am - 18:00pm
Wednesday, June 10th……..7:00am - 18:00pm

Publication Information

Authors of accepted presentations are encouraged but not required to submit their full manuscripts for publication reviewing as journal articles or book chapters. The following are possible publishing titles:

- Nanoscale Research Letters (Springer)
- NRL Advances (Springer)
  Open access publishing is not without costs. For EMN submissions, Springer will provide a 50% discount for each article accepted for publication. Fee will to be paid by the author if the article is accepted for publication.
- Frontiers of Materials Science (Springer)
- Journal of Semiconductors (IOP)
- Lecture Notes in Nanoscale Science and Technology (Springer)
- Springer Series in Materials Science (Springer)

International Advisory Committee

Oliver AMBACHER, Fraunhofer IAF, Freiburg, Germany
Wanda ANDREONI, Ecole Polytechnique Federale de Lausanne, Switzerland
Sergei BARANOVSKI, Philipps University Marburg, Germany
Kunji CHEN, Nanjing University, China
Hideo HOSONO, Tokyo Institute of Technology, Japan
Jasper KNOESTER, University of Groningen, The Netherlands
Sandor KUGLER, Budapest University of Technology & Economics, Hungary
Yurii E. LOZOVIK, Institute for Spectroscopy, Russia
Rodrigo MARTINS, UNINOVA, Portugal
John ROBERTSON, University of Cambridge, UK
John F. **WAGER**, Oregon State University, USA
Hongqi XU, Peking University, China

International Program Committee

Elena V. BASIUK, Universidad Nacional Autonoma de Mexico, Mexico
Holger EISELE, Technical University Berlin, Germany
Elvira FORTUNATO, Universidade Nova de Lisboa, Portugal
Bernard GIL, University of Montpellier, France
Sven HOFLING, University of St Andrews, UK
Berend T. JONKER, Naval Research Laboratory, USA
Young Hee LEE, Sungkyunkwan University, Korea
Andy SACHRAJDA, National Research Council of Canada, Canada
Luis VINA, Autonomous University of Madrid, Spain
Su-Huai WEI, National Renewable Energy Laboratory, USA
Dieter WEISS, University of Regensburg, Germany

International Organizing Committee

Vladimir A. BASIUK, Universidad Nacional Autónoma de México, México
Ray MURRAY, Imperial College London, UK
Enrique Calleja PARDO, Polytechnical University of Madrid, Spain
Peyman SERVATI, University of British Columbia, Canada
Zhiming WANG, University of Electronic Science and Technology of China, China

Program at-a-glance

Monday Morning, June 8	
Keynote	08:00-08:25AM Room A
Materials I	08:25-10:05AM Room A
Photonics and Optoelectronics I	10:20-12:25PM Room A
Monday Afternoon, June 8	
Welcome and Introduction	13:30-13:35PM Room B
Laser I	13:30-15:10PM Room C
Amorphous and Nano-crystalline I	13:30-15:10PM Room D
Excitons in organic systems	13:35-15:35PM Room B
Process and Device I	15:10-15:35PM Room C
General I	15:10-15:35PM Room D
Biological and biocompatible systems	15:55-17:15PM Room B
Process and Device I	15:55-17:35PM Room C

General I	15:55-17:00PM Room D

Tuesday Morning, June 9

Singlet fission	08:45-10:05AM Room B
Process and Device II	08:25-10:05AM Room C
Materials II	08:00-10:05AM Room D
Charge transfer and transport	10:20-11:40AM Room B
Photonics and Optoelectronics II	10:20-12:25PM Room C
Physics I	10:20-11:50AM Room D

Tuesday Afternoon, June 9

Exciton dynamics and transport I	13:50-15:10PM Room B
III-Nitrides for Energy Conversion and Solid State Lighting	13:30-14:45PM Room C
Photonics and Optoelectronics III	14:45-15:10PM Room C
Laser II	13:30-15:10PM Room D
Poster Session	**15:10-15:55PM**

Exciton dynamics and transport I	15:55-16:35PM Room B
Photonics and Optoelectronics III	15:55-16:20PM Room C
Amorphous and Nano-crystalline II	16:20-17:10PM Room C
Nanomedicine I	16:00-17:40PM Room D
Exciton dynamics and transport II	16:35-17:55PM Room B

Wednesday Morning, June 10

Process and Device III	08:10-10:05AM Room B
Materials III	08:00-10:05AM Room C
General III	08:20-09:50AM Room D
Physics II	09:50-10:05AM Room D
Photonics and Optoelectronics IV	10:20-11:50AM Room B
Materials IV	10:20-11:50PM Room C
Physics II	10:20-12:00PM Room D

Wednesday Afternoon, June 10

Laser III	14:00-15:40PM Room B
Nanomedicine II	14:00-15:15PM Room C
General II	15:15-16:50PM Room C
Nanomedicine III	14:00-15:40PM Room D
Nanomedicine IV	15:55-17:40PM Room D
Photonics and Optoelectronics V	15:55-17:50PM Room B

Monday Jun. 8 Room A		
7:00-8:00AM	Breakfast	
Session: Keynote Speakers Chair: Anna Kozlowska		
8:00-8:25AM	A01: High-performance, low-cost, single-crystal-like device layers and controlled self-assembly of nanostructures within device layers for wide-ranging energy and electronic applications	**Amit Goyal** University at Buffalo USA Page1
Session: Materials I Chair: Amit Goyal		
8:25-8:50AM	A02: Graphene layer as surface transparent electrode, advantages and drawbacks	**Anna Kozlowska** Institute of Electronic Materials Technology Poland Page 1
8:50-9:15AM	A03: Microelectrochemical capillary experiments in energy material research	**Ulrike Langklotz** Fraunhofer-Institut für Keramische Technologien und Systeme Germany Page 2
9:15-9:40AM	A04: Multi-Dye-Stacked Light-Harvesting Antennas Grown by Liquid-Phase Molecular Layer Deposition for Sensitization of ZnO	**Tetsuzo Yoshimura** Tokyo University of Technology Japan Page 3
9:40-10:05AM	A05: Surface characterization and optical properties of phosphor materials	**Hendrik Swart** University of Free State South Africa Page 4
10:05-10:20AM	Session Break	
Session: Photonics and Optoelectronics I Chair: Amit Goyal		
10:20-10:45AM	A06: Excited state dynamics in nanomaterials for solar energy applications	**Oleg Prezhdo** University of Southern California USA Page 5
10:45-11:10AM	A07: Multiphoton microscopy for investigation of optical nonlinearities in layered materials	**Lasse Karvonen** Aalto University Finland Page 6
11:10-11:35AM	A08: Phase camera for observing nanoscale aberrations of an optical cavity	**Kazuhiro Agatsuma** National Institute for Subatomic Physics The Netherlands Page 8

11:35-12:00PM	A09: Enhanced nonlinear optical response in plasmonic nanomaterials	**Tiziana Cesca** University of Padova Italy Page 8
12:00-12:25PM	A10: Property-controlled III-N quantum dots for quantum photonics	**Hui Deng** University of Michigan USA Page 10
12:30-13:30PM	Lunch Break	
Monday Jun. 8 Room B		
13:30-13:35PM	**Welcome and Introduction Chair: Jasper Knoester**	
Session: Excitons in organic systems Chair: Jenny Clark		
13:35-14:15PM	B01: Short-Range and Long-Range Excitonic Coupling in Molecular Aggregates: Introducing a New Design Paradigm for Organic Materials	**Frank Spano** Temple University, USA Page 10
14:15 -14:55PM	B02: Soft Supra-Molecular Nanotubes for Robust Light Harvesting?	**Dorthe Eisele** CUNY, USA Page 11
14:55-15:35PM	B03: Benchmarking calculations of excitonic couplings between chlorophylls	**Ivan Kassal** The University of Queensland Australia Page 12
15:35-15:55PM	Session Break	
Session: Biological and biocompatible systems Chair: David Vanden Bout		
15:55-16:35PM	B04: Elucidation of the Mechanisms of Photoprotection in Single LHCII Complexes	**Gabriela Schlau Cohen** MIT, USA Page 12
16:35-17:15PM	B05: Conformational Memory of Single Photosynthetic Pigment-Protein Complexes A Precursor of Non-Photochemical Quenching?	**Juergen Koehler** University Of Bayreuth Germany Page 13
18:00PM	Dinner Social	

Monday Jun. 8 Room C		
Session: Laser I Chair: Nadjib Semmar		
13:30-13:55PM	C01: Coherent control of a molecular ionization process by using Fourier-synthesized laser fields	**Hideki Ohmura** National Institute of Advanced Industrial Science and Technology Japan Page 14
13:55 -14:20PM	C02: Material gain in dilute nitrides materials using 8-band and 10-band models	**Marta Gladysiewicz-Kudrawiec** Wroclaw University of Technology Poland Page 15
14:20 -14:45PM	C03: Multiple optical injection in semiconductor laser	**Najm M. Al-Hosiny** Aljouf University Saudi Arabia Page 15
14:45 -15:10PM	C04: Organic thin-film solid-state lasers: towards applications	**Sebastien Chenais** PARIS 13 University and CNRS France Page 16
Session: Process and Device I Chair: Hideki Ohmura		
15:10-15:35PM	C05: Real-Time Laser Based Diagnostics for Complex Thin Films Thermo-physical and Thermo-electrical Properties Characterization	**Nadjib Semmar** University of Orleans/CNRS France Page 17
15:35-15:55PM	Session Break	
15:55-16:20PM	C06: Principle of innovative laser-dicing of silicon wafer -Stealth Dicing	**Etsuji Ohmura** Osaka University Japan Page 18
16:20-16:45PM	C07: Gate-bias dependent carrier distribution visualization in SiC power-MOSFET using super-higher-order SNDM	**Yasuo Cho** Tohoku University Japan Page 19
16:45-17:10PM	C08: Charge modulation spectroscopy and electric field induced optical second harmonic generation measurement for analysing organic device	**Eunju Lim** Dankook University Korea Page 20
17:10-17:35PM	C09: Towards the fabrication of 3D-LiNbO3 nanostructures	**Gwenn Ulliac** Institute of FEMTO-ST France Page 21
18:00PM	Dinner Social	

Monday Jun. 8 Room D		
Session: Amorphous and Nano-crystalline I Chair: Vitezslav Benda		
13:30-13:55PM	D01: TiO2-based nanostructures for photocatalytic applications synthesized by vapor-phase pulsed laser ablation	**Takehito Yoshida** National Institute of technology Japan Page 22
13:55 -14:20PM	D02: Nanoparticles and Nanostructures Produced by Ultra-short Laser Ablation in Liquid	**Roberto Teghil** Universita della Basilicata Italy Page 24
14:20 -14:45PM	D03: Deposition and Characterization of Silicon/Nitrogen-Doped Diamond-Like Carbon Films	**Hideki Nakazawa** Hirosaki University Japan Page 25
14:45 -15:10PM	D04: Avalanche amorphous Selenium (a-Se) for optical and x-ray imaging	**Alla Reznik** Lakehead University Canada Page 26
Session: General I Chair: Takehito Yoshida		
15:10-15:35PM	D05: Photovoltaic cells and modules towards terrawatt era	**Vitezslav Benda** Czech Technical University in Prague Czech Republic Page 27
15:35-15:55PM	Session Break	
15:55-16:20PM	D06: Quantitative Analysis of Coal Using Laser Induced Breakdown Spectroscopy	**Zhe Wang** Tsinghua University China Page 28
16:20-16:35PM	D07: Catalyst-free growth of ZnO nanowires on sapphire substrates by various steps of laser processing	**Tetsuya Shimogaki** Kyushu University Japan Page 28
16:35-17:00PM	D08: Integrated Circuits for Analog Optical Applications	**Vincent Urick** Naval Research Lab USA Page 29
18:00PM	Dinner Social	

Tuesday Jun. 9 Room B		
7:00-8:00AM	Breakfast	
Session: Singlet fission Chair: Libai Huang		
8:45-9:25AM	B06: Singlet Fission in Polyene-type Materials	**Jenny Clark** University of Sheffield, UK UK Page 30
9:25-10:05AM	B07: Uncovering Structure-Function Relationships for Singlet Exciton Fission	**Sean Roberts** University of Texas at Austin, USA Page 31
10:05-10:20AM	Session Break	
Session: Charge transfer and transport Chair: Frank Spano		
10:20-11:00AM	B08: Extended Charge Carrier Lifetimes in Hierarchical Donor-Acceptor Supramolecular Polymer Films	**Amy Scott** University of Miami USA Page 33
11:00-11:40AM	B09: Signatures of charge transfer in the fifth-order nonlinear response	**Arend Dijkstra** Max-Planck Institute for Structure and Dynamics of Matter Germany Page 33
12:30-13:30PM	Lunch Break	
Session: Exciton dynamics and transport I Chair: Gabriela Schlau-Cohen		
13:50-14:30PM	B10: Energy Transport in Nanotubular Supramolecular Cyanine Aggregate Systems	**David Vanden Bout** University of Texas at Austin, USA Page 34
14:30 -15:10PM	B11: Direct imaging of long-range exciton transport in porphyrin aggregates by ultrafast microscopy	**Libai Huang** Purdue University, USA Page 35
15:10-15:55PM	Poster Session	
15:55-16:35PM	B12: Exciton dynamics in tubular porphyrin aggregates	**Anna Stradomska** University of Glasgow, Scotland Scotland Page 35
Session: Exciton dynamics and transport II Chair: Dorthe Eisele		
16:35-17:15PM	B13: Coherent Transport in Light-harvesting and Nano-scale Systems	**Jianshu Cao** MIT, USA Page 36

17:15-17:55PM	B14: Modeling Excitation Energy Transport in Supramolecular Systems	**Jasper Knoester** University of Groningen The Netherlands Page 37
18:00PM	Dinner Social	

Tuesday Jun. 9 Room C		
7:00-8:00AM	Breakfast	
Session: Process and Device II Chair: Volker J. Sorger		
8:25-8:50AM	C10: Physics of Metal/Ge Interfaces; Fermi-level Unpinning and Interface Disorders	**Takashi Nakayama** Chiba University Japan Page 37
8:50-9:15AM	C11: Synthesis and Characterization of Cd-free Buffer layers to be used in thin films solar Cells	**William Vallejo** Atlantic University Colombia Page 38
9:15-9:40AM	C12: Growth and doping control of diamond semiconductor for junction device applications	**Hiromitsu Kato** Energy Technology Research Institute, AIST Japan Page 39
9:40-10:05AM	C13: Interferometric imaging for the detection of nanoparticles and for airborne instrumentation	**Sawitree Saengkaew** University of Rouen France Page 40
10:05-10:20AM	Session Break	
Session: Photonics and Optoelectronics II Chair: William Vallejo		
10:20 -10:45AM	C14: 2-D Materials for strong light-matter-interaction and photo conversion devices	**Volker J. Sorger** The George Washington University USA Page 41
10:45-11:10AM	C15: Sensitive Terahertz-wave detection and imaging by nonlinear frequency up-conversion	**Hiroaki Minamide** RIKEN Japan Page 43
11:10-11:35AM	C16: New developments in guided-mode resonance nanophotonics	**Robert Magnusson** University of Texas at Arlington USA Page 44

11:35-12:00PM	C17: An Optimized Spectral Response the HBT InP/InGaAs as an Optoelectronic Mixer mm-wave Radio over Fiber	**Sevia M. Idrus** Universiti Teknologi Malaysia Malaysia Page 45
12:00-12:25PM	C18: Cu_2O-based solar cells using oxide semiconductors	**Toshihiro Miyata** Kanazawa Institute of Technology Japan Page 46
12:30-13:30PM	Lunch Break	
Session: III-Nitrides for Energy Conversion and Solid State Lighting Chair: Graham Turnbull		
13:30-13:55PM	C19: Recent progress in fabrication process for highly efficient GaN LEDs	**Joon Seop Kwak** Sunchon National University South Korea Page 46
13:55 -14:20PM	C20: Is electron accumulation in InN intrinsic or may it be a material for photovoltaic applications?	**Holger Eisele** Technical University of Berlin, Germany Germany Page 47
14:20 -14:45PM	C21: Surface modification of III-Nitride epilayers by Chemical Mechanical Planarization (CMP)	**Dibakar Das** University of Hyderabad India Page 48
Session: Photonics and Optoelectronics III Chair: Joon Seop Kwak		
14:45 -15:10PM	C22: Organic semiconductor light sources for visible light communications	**Graham Turnbull** University of St Andrews USA Page 48
15:10-15:55PM	Poster Session	
15:55-16:20PM	C23: Optical cavity spectroscopy for environment, military and medicine applications	**Jacek Wojtas** Military University of Technology Poland Page 50
Session: Amorphous and Nano-crystalline II Chair: Jacek Wojtas		
16:20-16:45PM	C24: Enhancing the luminescent properties of Si nanoparticles by applying the additional continuous laser during ablation in liquid	**Dusan Popovic** University of Belgrade Serbia Page 51
16:45-17:10PM	C25: Newly Developed Soft Magnetic NANOMET® Powder Cores with High Magnetic Flux Density	**Yan Zhang** Tohoku University Japan Page 52
18:00PM	Dinner Social	

Tuesday Jun. 9 Room D		
7:00-8:00AM	Breakfast	
Session: Materials II Chair: Masaaki Tanaka		
8:00-8:25AM	D09: Graphene and graphene based nanostructures as molecular transporters	**Ewa Mijowska** West Pomeranian University of Technology Poland Page 52
8:25-8:50AM	D10: Plasmonic nanostructure instability by surface diffusion	**James Chon** Swinburne University of Technology Australia Page 53
8:50-9:15AM	D11: Effects of kosmotrope and chaotrope interactions at the micelle surfaces on the formation of lyotropic biaxial nematic phases: Intrinsically Biaxial Micelle Model	**Erol Akpinar** Abant Izzet Baysal University Turkey Page 54
9:15-9:40AM	D12: Studying the effect of zeolite inclusion in aluminum alloy on measurement of its hardness using electron density measurement	**Osama Khalil** MTI University Egypt Page 55
9:40-10:05AM	D13: Ferromagnetic semiconductors and heterostructures for semiconductor spintronics: New n-type electron-induced ferromagnetic semiconductor and its quantum wells	**Masaaki Tanaka** University of Tokyo Japan Page 55
10:05-10:20AM	Session Break	
Session: Physics I Chair: Ewa Mijowska		
10:20 -10:45AM	D14: Switchable photo-induced current of strongly correlated ferroelectric thin films	**Norifumi Fujimura** Osaka Prefecture University Japan Page 56
10:45-11:10AM	D15: Dynamic Modeling and Control of Membrane Filtration Process	**Norhaliza Abdul Wahab** Universiti Teknologi Malaysia Malaysia Page 57
11:10-11:35AM	D16: Quantum spin dynamics and spin-orbit coupling at terahertz frequencies in strained germanium quantum wells	**Michele Failla** University of Warwick UK Page 58
11:35-11:50AM	D17: First-principle Vs Experimental design of Diluted Magnetic Semiconductor	**Omar Mounkachi** Moroccan Foundation for Advanced Science, Innovation and Reseach Morocco Page 60

12:30-13:30PM	Lunch Break	
Session: Laser II Chair: Massimo Bottini		
13:30-13:55PM	D18: Noiselike pulses from modelocked fiber lasers: recent advances and applications	**Olivier Pottiez** Center for Research in Optics (CIO) Mexico Page 60
13:55 -14:20PM	D19: Optical properties of type II quantum wells predicted for active region in Interband Cascade Lasers	**Marcin Motyka** Wroclaw University of Technology Poland Page 61
14:20 -14:45PM	D20: Er:Yb double clad single mode fiber laser configurations	**Baldemar Ibarra-Escamilla** National Institute of Astrophysics, Optics and Electronics Mexico Page 62
14:45 -15:10PM	D21: High energy high frequency P-P lasers	**Victor V. Apollonov** Prokhorov General Physics Institute of RAS Russia Page 63
15:10-15:55PM	Poster Session	
15:55-16:00PM	**Welcome to the Workshop of Nanomedicine** **Chair: Massimo Bottini**	
Session: Nanomedicine I Chair: Olivier Pottiez		
16:00-16:25PM	D22: Intra-articular carbon nanotubes in the treatment of osteoarthritis	**Massimo Bottini** University of Rome Tor Vergata and Sanford Burnham Medical Research Institute Italy Page 63
16:25-16:50PM	D23: Interactions between carbon-based nanomaterials and the immune system: focus on inflammation	**Bengt Fadeel** Karolinska Institutet, Sweden Sweden Page 64
16:50-17:15PM	D24: Dendrimer Nanomedicine for Targeted Cancer Gene Therapy	**Hu Yang** Virginia Commonwealth University, USA Page 65
17:15-17:40PM	D25: Self-assembling zwitterionic nanogels for pancreatic islet immunoisolation	**Omid Veiseh** MIT, USA Page 65
18:00PM	Dinner Social	

Wednesday Jun. 10 Room B		
7:00-8:00AM	Breakfast	
Session: Process and Device III Chair: Juejun Hu		
8:10-8:35AM	B15: Trapping and Breakdown in GaN devices: A simulation study	**Kazushige Horio** Shibaura Institute of Technology Japan Page 65
8:35-9:00AM	B16: Layered (InxGa1-x)2Se3 (III2-VI3) Compounds as Novel Buffer Layers for GaAs on Si System	**Nobuaki Kojima** Toyota Technological Institute Japan Page 67
9:00-9:15AM	B17: Pathways for lowering the Interface Trap Density in Ge based MOS devices	**Ole Bethge** Vienna University of Technology Austria Page 68
9:15-9:40AM	B18: Control of the surface chemistry during Inductively-coupled plasma etching of InP and related compounds for the fabrication of photonic devices	**Sophie Bouchoule** CNRS-LPN France Page 68
9:40-10:05AM	B19: Modeling of the Space-charge Region in Nanowire Junctions	**Shreepad Karmalkar** Indian Institute of Technology India Page 69
10:05-10:20AM	Session Break	
Session: Photonics and Optoelectronics IV Chair: Nobuaki Kojima		
10:20 -10:45AM	B20: Monolithic Platforms for Mid-Wave Infrared (MWIR) Sensing	**Juejun Hu** MIT USA Page 70
10:45-11:00AM	B21: Properties of PbTe mid-infrared imaging devices of focal plane arrays	**Arata Yasuda** National Institute of Technology, Tsuruoka College Japan Page 71
11:00-11:25AM	B22: Cavity Quantum Electrodynamics in a Quantum Dot Molecule - Photonic Crystal Architecture	**Patrick Vora** George Mason University USA Page 72

11:25-11:50PM	B23: Replication of large-area nanostructures for optical devices	**Keisuke Nagato** The University of Tokyo Japan Page 73
12:30-13:30PM	Lunch Break	
Session: Laser III Chair: Jifeng Liu		
14:00-14:25PM	B24: Ultrabright terahertz-wave generation using nonlinear wavelength conversion at room temperature	**Shin'ichiro Hayashi** RIKEN Japan Page 74
14:25 -14:50PM	B25: The uniformity investigations of type II InAs/GaInSb W-shaped quantum wells wafers by means of mid-infrared photoluminescence spectroscopy	**Mateusz Dyksik** Wrocław University of Technology Poland Page 75
14:50 -15:15PM	B26: Improved relations for shock ignition hot-spot condition	**Seyed Abolfazl Ghasemi** Science and Technology Research Institute Iran Page 76
15:15 -15:40PM	B27: Integrated micro-ring photonics: principles and applications for soliton generation, mode-locked lasers and optical communications	**IS Amiri** University of Malaya, Malaysia Page 77
15:40-15:55PM	Session Break	
Session: Photonics and Optoelectronics V Chair: Mateusz Dyksik		
15:55-16:20PM	B28: Nanomaterials for light management and solar energy harvesting	**Jifeng Liu** Dartmouth College USA Page 77
16:20-16:45PM	B29: Nano-photonic and nano-plasmonic structures to harvest photons in thin film solar architectures	**Rana Biswas** Ames Laboratory and Iowa State University USA Page78
16:45-17:10PM	B30: Tunable multiwavelength fiber lasers based on a Mach-Zehnder interferometer and photonic crystal fiber	**Juan M. Sierra-Hernandez** Universidad de Guanajuato Mexico Page 79
17:10-17:35PM	B31: Self-organized structuring of light bullets, dissipationless vortices, and lightning	**Vladimir Skarka** University of Angers France Page 79
17:35-17:50PM	B32: Self-energy function of quantum-dot and non-radiative transition	**Mohammad Reza Mohebbifar** Kazan Federal University, Russia Russia Page 80
18:00PM	Dinner Social	

Wednesday Jun. 10 Room C		
7:00-8:00AM	Breakfast	
Session: Materials III Chair: Nate Newman		
8:00-8:25AM	C26: Optical properties of novel semiconductor compounds: Dilute bismides	**Robert Kudrawiec** Wroclaw University of Technology Poland Page 80
8:25-8:50AM	C27: Self-organized vicinal surfaces used for nanostructure growth	**Elsa Thune** Ecole Nationale Supérieure de Céramique Industrielle France Page 81
8:50-9:15AM	C28: Femtosecond laser-induced micro and nanostructured metallic oxides	**Santiago Camacho-Lopez** CICESE Mexico Page 82
9:15-9:40AM	C29: TiO2 nanomaterials: synthesis, properties, modifications, and photocatalytic applications	**Giuliana Impellizzeri** University of Catania Italy Page 83
9:40-10:05AM	C30: Nonlinear optical properties of Au-nanoparticles in water, lipodic acid, and NaCl	**Monica Trejo Duran** University of Guanajuato Mexico Page 84
10:05-10:20AM	Session Break	
Session: Materials IV Chair: Robert Kudrawiec		
10:20 -10:35AM	C31: Mechanism of Microwave Loss in Commercial Dielectric Materials	**Nate Newman** Arizona State University USA Page 85
10:35-11:00AM	C32: Field-effect surface chemistry: Gate-controlled photo-oxidation of graphene	**Ryo Nouchi** Osaka Prefecture University Japan Page 85
11:00-11:25AM	C33: Bulk Photovoltaic Effects in BiFeO3 Thin Films	**Seiji Nakashima** University of Hyogo Japan Page 86
11:25-11:50PM	C34: Silicon Nanostructures for Nanoelectronics and Photovoltaics	**Kunji Chen** Nanjing University China Page 88

12:30-13:30PM	Lunch Break	
Session: Nanomedicine II Chair: Takashi Goto		
14:00-14:25PM	C35: Engineered Soft Bionanocomposites	**Vladimir V. Tsukruk** Georgia Institute of Technology and Molecular Science&Engineering USA Page 88
14:25 -14:50PM	C36: Understanding the formation of lipid-polymeric patchy particles	**Carolina Salvador-Morales** George Mason University, USA Page 89
14:50 -15:15PM	C37: Metal Nanoantimicrobials: a smart electrochemical solution to the quest for novel antibacterial agents, or just another toxic chemical?	**Nicola Cioffi** Università degli Studi di Bari "Aldo Moro" Italy Page 89
Session: General II Chair: Vladimir V. Tsukruk		
15:15 -15:40PM	C38: High speed and low temperature deposition of SiC film by laser CVD	**Takashi Goto** Tohoku University Japan Page 90
15:40-15:55PM	Session Break	
15:55-16:20PM	C39: In-situ TEM observation of Li battery reactions at electrolyte/electrode interface using liquid cell	**Akihiro Kushima** MIT, USA Page 92
16:20-16:35PM	C40: Planar chiral nanostructures for biosensing	**Lingling Huang** Beijing Institute of Technology China Page 92
16:35-16:50PM	C41: Jahn-Teller Cu(II) ion induced mm wave energy levels in ferroelectric crystals of Cu(II):Cd2(NH4)2(SO4)3	**Dilip K. De** Covenant University Nigeria Page 93
18:00PM	Dinner Social	

Wednesday Jun. 10 Room D		
7:00-8:00AM	Breakfast	
Session: General III Chair: Randy Jalem		
8:20-8:45AM	D26: Electromagnetic Coupling in Regular Arrays of Plasmonic Nanostructures	**Anatoliy Pinchuk** University of Colorado Colorado Springs USA Page 93

8:45-9:10AM	D27: Organic polariton condensates in all-dielectric microcavities: Polariton interactions and coherence properties	**Raymond Murray** Imperial College London, UK UK Page 94
9:10-9:35AM	D28: Thermoelectronic Solar Power Conversion with Parabolic Concentrato	**Dilip K. De** Covenant University Nigeria Page 95
9:35-9:50AM	D29: Innovative therapeutic and diagnostic tools based on delivery and imaging of miRNAs by multifunctional carbon nanotubes	**Silvia Bistarelli** National Laboratory of Frascati, Italy Page 96
Session: Physics II Chair: Anatoliy Pinchuk		
9:50-10:05AM	D30: An efficient rule-based screening approach for discovering fast ion conductors using density functional theory and informatics	**Randy Jalem** Global Research Center for Environment and Energy Based on Nanomaterials Science (GREEN) –National Institute for Materials Science (NIMS) Japan Page 96
10:05-10:20AM	Session Break	
10:20-10:45AM	D31: Ultrafast Spectroscopic Study of Acoustic Transport and Phonon Interactions in Nanoscale Materials	**Masashi Yamaguchi** Rensselaer Polytechnic Institute USA Page 97
10:45-11:10AM	D32: Mechanical manipulation of Skyrmion crystal	**Yoichi Nii** RIKEN Japan Page 98
11:10-11:35AM	D33: Control of mesoscale phenomena in strongly correlated oxides	**T.Zac Ward** Oak Ridge National Laboratory USA Page 98
11:35-12:00PM	D34: Huge spin-driven polarizations and optical-diode effect at room temperature in $BiFeO_3$	**Jun Hee Lee** Oak Ridge National Laboratory USA Page 99
12:30-13:30PM	Lunch Break	
Session: Nanomedicine III Chair: Luis Felipe Jiménez García		
14:00-14:25PM	D35: Immunotoxicity of nanomaterials	**Andrij Holian** University of Montana, USA Page 99
14:25 -14:50PM	D36: Multifunctional rare-earth based nanoparticles for reactive oxygen species sensing and magnetic resonance imaging	**Antigoni Alexandrou** Ecole polytechnique France Page 100

14:50 -15:15PM	D37: Tumor penetrating pH-sensitive polymersomes for intraperitoneal tumor theranostics	**Lorena Simon Gracia** University of Tartu Estonia Page 101
15:15 -15:40PM	D38: Molecular imaging and nanotechnology to study biology of tumor microenvironment	**Jamal Zweit** Virginia Commonwealth University USA Page 102
15:40-15:55PM	Session Break	
Session: Nanomedicine IV Chair: Andrij Holian		
15:55-16:20PM	D39: Cerium oxide nanoparticles for normal tissue protection during radiation therapy: combining molecular imaging and nanotechnology approaches	**Philip Reed McDonagh** Virginia Commonwealth University, USA Page 102
16:20-16:45PM	D40:Nanotherapeutic approaches for the management of arthritis	**Christine Pham** Washington University School of Medicine USA Page 104
16:45-17:10PM	D41: Probing cell structure by atomic force microscopy	**Luis Felipe Jiménez García** Universidad Nacional Autónoma de Mexico Mexico 104
17:10-17:35PM	D42: How functional genomics informs nano-drug design for precision cancer medicine	**Alexander H. Stegh** Robert H. Lurie Cancer Center USA 105
17:35-17:40PM	**Concluding remarks** **Chair: Massimo Bottini**	
18:00PM	Dinner Social	

Tuesday Jun. 9 15:10-15:55PM		
Poster Session		
P1	Solvent-Free Functionalization of Multiwalled Carbon Nanotube-Based Buckypaper with Amines	**E. V. Basiuk** Universidad Nacional Autónoma de México Mexico 106
P2	Interaction of a Ni(II) Tetraazaannulene Complex with Spherical Fullerenes and Short Carbon Nanotube Models: A DFT Study	**Vladimir A. Basiuk** Universidad Nacional Autónoma de México Mexico 106

P3	In Situ Functionalization of Multiwalled Carbon Nanotube Buckypaper with a Long-Chain Aliphatic Amine Polyethyleneimine	**V. Meza-Laguna** Universidad Nacional Autónoma de México Mexico 107
P4	Advances in Pd/Pt Nanoparticle Size decoration of mesoporous carbon spheres for energy application	**Ryszard Kaleńczuk** West Pomeranian University of Technology Poland 108
P5	Hig Brightness diode-pumped organic solid-state laser	**Sébastien Forget** PARIS 13 University and CNRS France 109
P6	Simulations of Polyelectrolytes	**Filip Uhlik** Charles University in Prague Czech Republic 110
P7	Coordination Functionalization of Graphene Oxide and Nanodiamond with Tetraazamacrocyclic Complexes of Nickel(II)	**E. V. Basiuk** Universidad Nacional Autónoma de México Mexico 110
P8	Noncovalent Complexes of Phthalocyanines with Spherical Fullerenes and Short Nanotube Models: A DFT Study	**Vladimir A. Basiuk** Universidad Nacional Autónoma de México Mexico 111
P9	Non-Covalent Functionalization of Multiwalled Carbon Nanotube Buckypaper with a Ni(II) Tetraazaannulene Complex	**V. Meza-Laguna** Universidad Nacional Autónoma de México Mexico 112

Invited Talk Session

A01: High-performance, low-cost, single-crystal-like device layers and controlled self-assembly of nanostructures within device layers for wide-ranging energy and electronic applications

Amit Goyal

Fellow NAI, MRS, AAAS, APS, WIF, ASM, ACERS, IOP, WTN
Director, RENEW (Research & Education in eNergy, Environment and Water) @ SUNY-Buffalo
Empire Innovation Professor @ UB in CBE, EE, Physics, and Materials Design & Innovation
Emeritus Corporate Fellow & Distinguished Scientist, Oak Ridge National Laboratory
Emeritus Battelle Distinguished Inventor
Ph.: (865) 300-4202
Email: agoyal@buffalo.edu
Email: goyala@ornl.gov

Abstract

For many energy and electronic applications, single-crystal-like materials offer the best performance. However, in almost all cases, the single-crystal form of the relevant material is too expensive. In addition, for many applications, very long or wide materials are required, a regime not accessible by conventional single-crystal growth. This necessitates the use of flexible, large-area, long, single-crystal-like substrates for heteroepitaxial growth of the relevant advanced material for the electronic or energy application in question. Since the factor determining suitability for applications is price/performance, the process used for fabrication of the artificial substrate needs to be very scalable and low-cost. Details of such large-area, single-crystal substrate fabrication and the range of materials that can be epitaxially grown on such substrates will be discussed. Heteroepitaxial buffer layers of various materials (of rock salt, flourite, perovskite and pyrochlore crystal structures) can be deposited in a roll-to-roll configuration using web-coating employing electron-beam evaporation, sputtering or chemical solution deposition. In addition, for many applications, controlled incorporation of a 3D network of nanodots or nanorods within a matrix is desired for optimization of physical properties or for enabling novel properties or phenomena. It will be shown that controlled incorporation of 3D self-assembled nanodots and/or nanorods of a multicomponent material can be achieved within another multicomponent device layer using a simultaneous phase separation and strain ordering process. As an example of a material for energy and electronic applications, detailed results will be presented for growth of high-temperature superconductors on such substrates. For both of these platform technologies (single-crystal-like substrates and 3D self-assembly of nanomaterials), wide ranging applications exist in electronic and energy sectors including applications in photovoltaics, ferroelectrics, multiferroics, and ultra-high density storage. The talk will give examples for each of these applications using these platform technologies.

A02: Graphene layer as surface transparent electrode, advantages and drawbacks

Anna Kozłowska[1], G. Gawlik[1], A. Piątkowska[1], Roman Szewczyk[2]

[1]Institute of Electronic Materials Technology, 133 Wólczyńska St., 01-919 Warsaw, Poland Email: Anna.Kozlowska@itme.edu.pl, web site: http://www.itme.edu.pl

[2] Warsaw University of Technology, Institute of Metrology and Biomedical Engineering, Św. A. Boboli 8 St., 02-525 Warsaw, Poland

Graphene is promising material for energetic applications because of its ability to conduct electric current of high density. Its absorption is as low as 2.3%, and is almost uniform from the visible range to infrared. High optical transparency is especially desirable for such applications as transparent screens or transparent joule heaters integrated with glass windows. Because of its transparency graphene may be applied also in photovoltaics or in elastic displays. Another potential application is energy storage. In a battery it can be used as a cathode together with traditional lithium anode. The

advantage of such a battery is its flexibility and energy density in the range of supercapacitors, higher than thin lithium batteries. The specific features of graphene make this material interesting candidate for surface electrodes.

In a nanoscale, graphene is a robust material with a high fracture strength reaching 130 GPa [1]. However, in practical technical applications, single layer graphene is rather fragile and easy to get damaged. Macroscopic discontinuities of the graphene layer may affect proper operation of device. The current flow through the structure usually is affected by such changes of the electrode shape. This can cause serious problems, especially in applications where high current densities are encountered. High current flow generates joule heating of the resistor which is the layer of graphene. Inhomogeneity of the layer resistivity may result inhomogeneous temperature of the graphene and combined substrate.

Manufacturing, assembly, maintenance or accidental events can cause local damage to the graphene sheet. In the paper, the influence of the mechanical injury to the joule heating of the graphene layer was investigated. Graphene mechanical strength was examined by using nanoscratch method at incremental load and ball on flat surface tribological test at different constant loads. The one stroke mode was applied in tribological tests for better observation of the graphene wear phenomena. Different destruction mechanisms of the graphene layer were observed depending on the applied load and depending on the adhesion of the graphene to the glass substrate, such as cohesive cracks, wrinkles formation under shear stress, delamination of the large graphene areas, destruction on folds and tearing stripes. All of the mentioned phenomena lead to the formation of more or less extended nonconductive areas mostly in the form of scratches and modify current flow in the graphene layer.

Graphene was synthesized by chemical vapor deposition (CVD) on Cu foil and then transferred onto the glass substrate. Ohmic contacts to graphene were formed by using silver conductive paste or by vacuum deposition of Cr/Au layers. An Auriga cross beam workstation from Carl Zeiss has been used for SEM characterization of the graphene surface. Infrared imaging has been performed using InSb 640 M camera (Thermosensorik / DCG Systems). The sample was placed on the heated table in order to register the calibration maps in the controlled temperature.

Modelling of the Joule heating distribution in the graphene layer was performed using finite element method. The static current approximation Maxwell's equations was used [2] and object mesh was generated using top down strategy. Partial differential equations describing Maxwell's equations were solved using conjugate gradient oriented strategy. The model was implemented using open-source software. Mesh was created using NETGEN 5.1, whereas partial differential equations describing Maxwell's equations were solved using ELMER FEM software. The modelling results were compared with experimental infrared imaging results of Joule heated graphene samples and a good agreement was found.

The presented results give a new insight into the role of mechanical defects such as cracks or discontinuities in the overall performance of graphene transparent electrodes.

1. C. Lee, X. Wei, J. W. Kysar, and J. Hone, *Science* **321**, 385 (2008).
2. P. Raback, M. Malinen, J. Ruokolainen, A. Pursula, T. Zwinger, *Elmer Models Manual* (CSC – IT Center for Science) (2014).
This work was supported by the Polish National Center for Research and Development under the project no GRAF-TECH/NCBiR/06/30/2012.

A03: Microelectrochemical capillary experiments in energy material research

U. Langklotz[1], M. Schneider[2], A. Michaelis[1,2]
[1] TU Dresden, Institute of Materials Science, Dresden, Germany
Email:ulrike.langklotz@ikts.fraunhofer.de
[2] Fraunhofer Institute for Ceramic Technologies and Systems, Dresden, Germany

The electrochemical microcapillary technique is a powerful tool to examine the electrochemical properties of various materials with a high lateral resolution. This technique is used for more than 25 years to investigate surfaces and material particles, respective. The microcapillary cell design used in our group (Fig.1) enables the combination with complementary investigation methods, e.g. microscopy and spectroscopy. The benefits of the microcapillary technique will be presented, using the examples of two energy storage material systems.

The first example describes the investigation of ultra-thin dielectric titanium oxide films. Due to their relatively high permittivity, such dielectric films are prospective candidates in capacitor applications. However, it is reported in literature (e.g. Kudelka et al. [1]) that the oxide film growth on titanium is strongly dependent on the crystallographic grain orientation. The examination of this effect by micro-capillary as well as approaches to overcome this drawback are presented [2, 3].

In a second example the electrochemical microcapillary technique is applied to investigate individual active material particles for lithium ion batteries. In contrast to oxide films, this issue is accompanied by a number of new challenges. The microelectrochemical experiments have to be carried out under inert atmosphere, using organic electrolytes and non-standard counter and reference electrodes. Furthermore, individual particles of the size of few microns have to be handled. Different approaches to ply with these conditions are compared. Moreover, first experimental results will be presented and the potentialities of this technique in battery science will be discussed.

Fig1. Electrochemical microcapillary cell in bend geometry.

1. S. Kudelka, J. W. Schultze, *Electrochimica Acta* **42**, 2817 (1997).
2. M. Schneider, S. Schroth, J. Schilm and A. Michaelis, *Electrochimica Acta* **54**, 2663 (2009)
3. S. Schroth, M. Schneider, T. Mayer-Uhma, U. Klemm and A. Michaelis, *Surface & Interface Analysis*, **40**, 850 (2008)

A04: Multi-Dye-Stacked Light-Harvesting Antennas Grown by Liquid-Phase Molecular Layer Deposition for Sensitization of ZnO

Tetsuzo Yoshimura
School of Computer Science, Tokyo University of Technology, Hachioji, Tokyo, Japan
Email: tetsu @cs.teu.ac.jp

Light-harvesting antennas in the photo-synthesize systems of plants have been known as high-efficiency photon collectors. We propose to apply them to dye sensitization of semiconductors for solar cells. The proposed light-harvesting antenna has a multi-dye-stacked structure grown by Liquid-Phase Molecular Layer Deposition (LP-MLD) [1-4], in which different kinds of molecules are sequentially provided onto a surface to grow tailored materials with designated molecular arrangements. Requirements for the source molecules in MLD are that different kinds of molecules can be connected and the same kind of molecules cannot be connected.

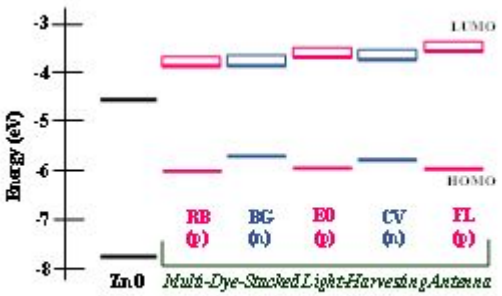

Fig1. Energy-level scheme of a multi-dye-stacked light-harvesting antenna for sensitization of ZnO.

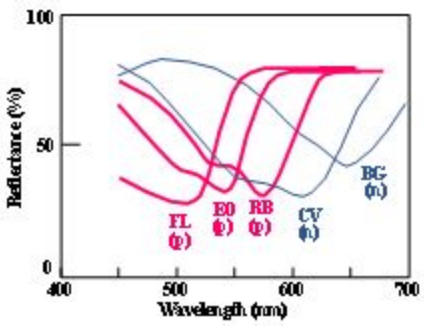

Fig2. Reflection spectra of dyed ZnO powder layers.

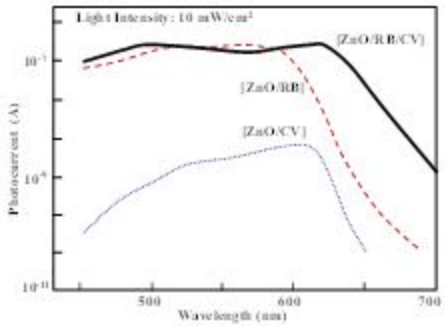

Fig3. Photocurrent spectra of [ZnO/RB], [ZnO/CV], and [ZnO/RB/CV].

Fig. 1 shows an energy-level scheme of a multi-dye-stacked light-harvesting antenna for sensitization of ZnO. The energy levels were determined using the Photoemission Yield Spectroscopy in Air (PYSA) [5]. Fluorescein (FL), eosine (EO), and rose bengal (RB) are p-type dyes that tend to accept electrons, and crystal violet (CV) and brilliant green (BG) are n-type dyes that tend to donate electrons [6]. A p-type dye molecule and an n-type dye molecule can be connected while the same type of dye molecules cannot be connected, satisfying the MLD requirements.

When RB is provided onto an n-type ZnO surface, a monomolecular layer of RB is formed. Once the surface is covered with RB, the deposition of RB is automatically terminated. After removing RB, BG is provided to connect BG to RB. By repeating the process in an order of RB-BG-EO-CV-FL, the light-harvesting antenna shown in Fig. 1 would be formed with monomolecular steps in principle. The antenna is expected to have a broad absorption spectrum of a superposition of the five dyes' absorption bands (Fig. 2).

Fig. 3 shows a typical result of sensitization for ZnO by a two-dye-stacked structure of RB/CV [7]. The photocurrent spectrum of [ZnO/RB/CV] extends to a longer wavelength region comparing to the spectrum of [ZnO/RB]. This suggests that by inserting p-type RB between n-type CV and n-type ZnO, an n/p/n structure is constructed to enhance the electron injection from CV to ZnO.

In order to obtain a guideline to optimize the dye molecule sequences in the light-harvesting antennas, effects of energy-level schemes on the sensitization is under investigation for multi-dye-stacked structures.

1. T. Yoshimura, H. Watanabe, C. Yoshino, *J. Electrochem. Soc.* **51**, 158 (2011).
2. T. Yoshimura, *Thin-Film Organic Photonics: Molecular Layer Deposition and Applications* (CRC Press/Taylor & Francis, Boca Raton, 2011).
3. T. Yoshimura, Japanese Patent, Tokukai Hei3-60487 (1991) [in Japanese].
4. T. Yoshimura, Japanese Patent, Tokukai 2009-60487 (2009) [in Japanese].
5. Y. Nakajima, D. Yamashita, A. Ishizaki, B. Pellissier, and M. Uda, *Mater.Res. Symp. Proc.* **1029**, 1029-F04-02 (2008).
6. H. Meier: J. Phys. Chem. **69**, 719 (1965).
7. T. Yoshimura, K. Kiyota, H. Ueda, and M. Tanaka, *Jpn. J. Appl. Phys.* **20**, 1671 (1981).

A05: Surface characterization and optical properties of phosphor materials

Hendrik C Swart, Vinod Kumar, OM Ntwaeaborwa, RE Kroon, E Coetsee and JJ Terblans

Department of Physics, University of the Free State, Bloemfontein, ZA9300, South Africa Email:swarthc@ufs.ac.za, web site: http://natagri.ufs.ac.za/content.aspx?id=989

Luminescent compounds and materials have numerous uses in devices of various sorts such as displays, light emitting diode (LED) lighting and watches. The emission properties are

defined by the chemical composition and the physical structure of the luminescent material. Auger electron spectroscopy (AES) and cathodoluminescence (CL) both excited by the same electron beam, were used to monitor changes in surface composition and luminous efficiency during electron bombardment of different phosphor materials. Degradation was manifested by a non-luminescent ZnO layer that formed on the surface of ZnS phosphors according to electron stimulated surface chemical reactions (ESSCRs).

The high electron mobility, high thermal conductivity, wide and direct band gap and large excitation binding energy make ZnO stable for a wide range of applications. Knowledge of the composition, optical, structural properties and impurity effects of ZnO nanocrystalline films and powders is very important for the engineering and design of devices. The crystallinity and growth orientation play a very important role in the optoelectronic properties of the ZnO. Surface characterization techniques play a vital role in the complete understanding of the luminescent properties of phosphor materials. ZnO nanophosphors were synthesized (undoped and doped with rare earth elements) with different techniques for UV, blue, green, red and near white light emission applications. X-ray photo electron spectroscopy (XPS) indicated that the O1s peak consists of three different components, figure 1. These were O1 (oxide) and O2 (deficient oxygen; OH groups) and O3 (chemisorbed species). All samples showed near band edge (NBE) and defect level emission (DLE). The DLE enhancement was due to the increase in oxygen related defects such as oxygen vacancies/interstitials. Different defect level emissions that varied from the blue to red visible range were observed. Due to the combination of the NBE and DLE, near white light emission was observed in some cases. The emission could be tuned by varying preparation parameters such as different ultrasonic times, combustion temperatures, dopant concentration and different precursors. Luminescent ZnO thin films were also obtained with pulsed laser deposition and spin coating. The defect emission wavelengths were successfully changed as well as the colour for both the nanoparticles and thin films.

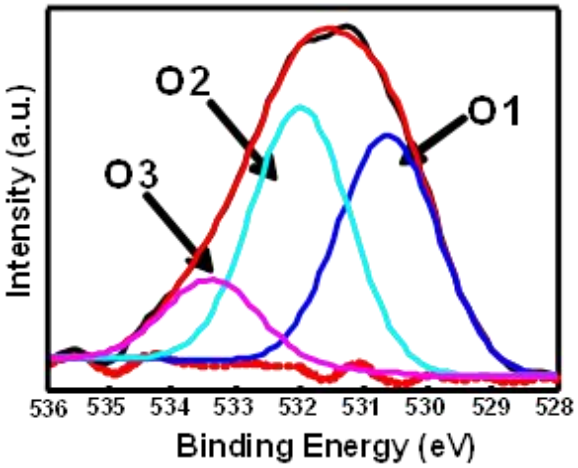

Fig1. O 1s XPS spectrum.

1. Vinod Kumar, Vijay Kumar, S. Som, Jannie Neethling, E.J. Olivier, O.M. Ntwaeaborwa, H.C. Swart, Nanotechnology, *Nanotechnology* **25**, 9pp (2014).

A06: Excited state dynamics in nanomaterials for solar energy applications

Oleg V. Prezhdo

Department of Chemistry, University of Southern California, Los Angeles, CA 90089, USA

Photovoltaic and photo-catalytic processes are initiated by a light-driven charge separation at an interface of two complementary materials. The separation competes with electron-vibrational energy losses, energy transfer, charge recombination and other processes. Our group has developed [1-4] and implemented [5,6] a suite of theoretical and simulation approaches, aimed at modeling these events in the time domain and at the atomistic level of detail, as they occur in experiment. The approaches combine time-dependent density functional theory with non-adiabatic molecular dynamics [1]. They treat electrons quantum-mechanically and nuclei semi-classically [2,3,6,7].

We show how the asymmetry of electron and hole transfer at a polymer/nanotube interface can

be used to optimize solar cell performance [8]; that the mechanism of electron injection from a CdSe nanoparticle into nanoscale TiO2 depends on the dimensionality of the latter [9]; that plasmon-driven charge separation on TiO2 sensitized with plasmonic nanoparticles has a 50% chance to occur already during light absorption [10]; that optically dark states govern the rates and yields of singlet fission and charge transfer at a pentacene/C60 interface [11]; that nanoscale materials exhibit a new, Auger-assisted type of electron transfer [12]; that the low efficiency of photo-catalytic water splitting by GaN is due to unfavorable competition of charge relaxation and transfer [13]; that atomic defects can be both detrimental and beneficial for the charge separation [14]; how a long, insulating bridge can accelerate charge separation [15]; why graphene, a metal, can be used as a TiO2 sensitizer [16]; and how excited electrons can be extracted from quantum dots prior to relaxation [17].

The software [5,6] is available free of charge at http://gdriv.es/pyxaid.

1. C. F. Craig, W. R. Duncan, O. V. Prezhdo, Phys. Rev. Lett., 95 163001 (2005).
2. B. F. Habenicht, O. V. Prezhdo, Phys. Rev. Lett., 100, 197402 (2008).
3. S. R. Fischer, B. F. Habenicht, A. B. Madrid, W. R. Duncan, O. V. Prezhdo, J. Chem. Phys., 134, 024102 (2011).
4. H. M. Jaeger, S. Fisher, O. V. Prezhdo J. Chem. Phys., 137, 22A545 (2012).
5. A. V. Akimov, O. V. Prezhdo, J. Chem. Theor. Comp., 9, 4959 (2013).
6. A. V. Akimov, O. V. Prezhdo, J. Chem. Theor. Comp., 10, 789 (2014).
7. O. V. Prezhdo, Theor. Chem. Acc., 116, 206 (2006).
8. R. Long, O. V. Prezhdo, Nano Lett., **14**, 3335 (2014)..
9. D. N. Tafen, R. Long, O. V. Prezhdo, Nano Lett., 14, 1790 (2014).
10. R. Long, O. V. Prezhdo, J. Am. Chem. Soc., 136, 4343 (2014).
11. A. V. Akimov, O. V. Prezhdo, J. Am. Chem. Soc., 136, 1599 (2014).
12. H. Zhu, Y. Yang, K. Hyeon-Deuk, M. Califano, N. Song, Y. Wang, W. Zhang, O. V. Prezhdo, T. Lian, Nano Lett., **14**, 1263 (2014).
13. A. V. Akimov, J. T. Muckerman, O. V. Prezhdo, J. Am. Chem. Soc., 135, 8682 (2013).
14. R. Long, N. J. English, O. V. Prezhdo, J. Am. Chem. Soc., 135, 18892 (2013).
15. V. V. Chaban, V. V. Prezhdo, O. V. Prezhdo, J. Chem. Phys. Lett., 4, 1 (2013).
16. R. Long, N. English, O. V. Prezhdo, J. Am. Chem. Soc., 134, 14238 (2012).
17. R. Long, O. V. Prezhdo, J. Am. Chem. Soc., 133, 19240 (2011).

A07: Multiphoton microscopy for investigation of optical nonlinearities in layered materials

Lasse Karvonen[1]

[1]Aalto University, Department of Micro and Nanosciences, Tietotie 3, FI-02150 Espoo, Finland
lasse.karvonen@aalto.fi

Due to the ever increasing demand for high speed data transfer, optical telecommunication is one of the key fields pursuing novel applications by exploiting second- and third-order optical nonlinearities. 2D nanomaterials have shown to be suitable materials for integration to silicon waveguides. Specifically, graphene was used to demonstrate waveguide-based modulators and detector devices [1, 2]. We have shown that graphene is a highly nonlinear material with the $\chi^{(3)}$ of ~$3*10^{-7}$ esu at the telecommunication wavelengths [3]. We have also observed broadband fluorescence from graphene under the femtosecond laser excitation [3] (Fig. 1a shows RGB composite image generated from the fluorescence and THG signals from few-layer graphene flakes and Fig. 1d presents the spectra of generated light from graphene on SiO_2/Si substrate with different excitation powers). However, in the guided-wave devices, the high absorption of graphene causes high propagation losses hindering its practical use. Therefore, the highly nonlinear layered semiconductors (with a band-gap) would be more suitable for real guided-wave applications.

We have studied the nonlinear optical properties of different layered semiconductors (including GaSe, WS_2, etc.) using multiphoton microscopy. Strong second- and third-harmonic generations were observed in few-layer gallium selenide flakes. Figure 1b shows an RGB composite SHG-THG micrograph of the GaSe flake with different thicknesses. The red color in the RGB image represents the SHG signal, and the green color represents the THG signal. The areas that simultaneously show a high intensity for both SHG and THG appear yellow in the composite image. Even the peak around 390 nm wavelength, corresponding to the four photon process, was observed from a ~40 nm thick flake (as seen in Fig. 1c). Figure 1e and 1f show the optical and THG image of few-layer WS_2 flake. We will compare the nonlinear optical properties of graphene with other 2D layered materials, such as GaSe, WS_2, etc.. We discuss the generated nonlinear signal as the function of the number of layers, the excitation power, and the excitation wavelength. In addition, we also discuss the spectral properties of the graphene fluorescence on different substrates.

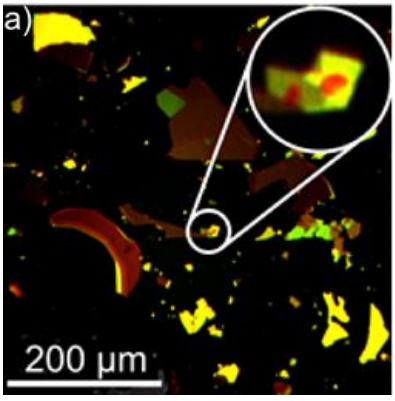

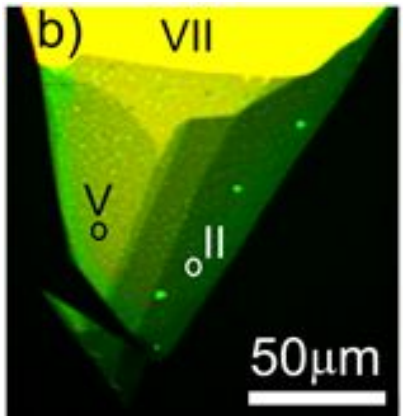

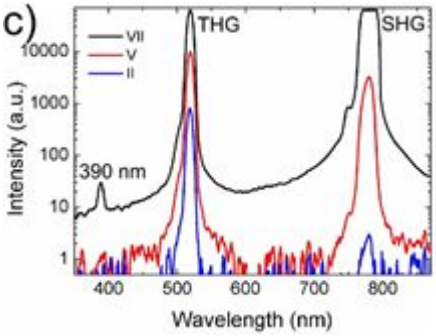

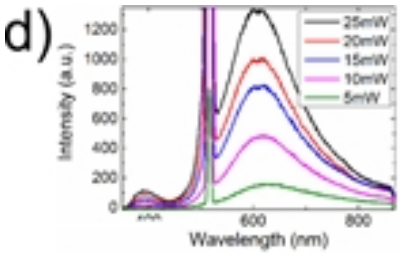

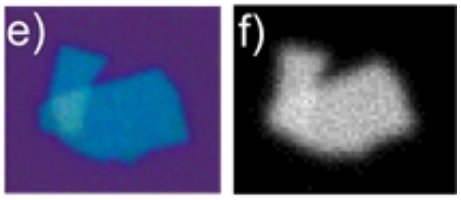

Fig. 1: a) RGB composite image generated from fluorescence (red) and THG (green) signals of few-layer graphene, b) RGB composite image generated from SHG (red) and THG (green) images of few-layer GaSe, c) generated light spectra from GaSe (the locations shown in b)), d) generated light spectra from graphene on SiO_2/Si substrate with different powers, e) optical image of few-layer WS_2 and f) THG image of few-layer WS_2.

[1] M. Liu *et al., Nature* **474**, 64 (2011).

[2] X. Gan *et al., Nature Photonics* **7**, 883-887 (2013).
[3] A. Säynätjoki *et al.*, *ACS Nano* **7**, 8441 (2013).
[4] L. Karvonen *et al.,* Nanocarbon Photonics and Optoelectronics 2014, Polvijärvi, Finland, July 28 - August 1 2014.

A08: Phase camera for observing nanoscale aberrations of an optical cavity

Kazuhiro Agatsuma[1], Martin van Beuzekom[1], Mesfin Gebyehu[1], Laura van der Schaaf[1], Jo van den Brand[1,2]

[1]*National Institute for Subatomic Physics (Nikhef), Amsterdam, The Netherlands*
Email: agatsuma@nikhef.nl

[2] *VU University, Amsterdam, The Netherlands*

Worldwide studies have been performed to detect gravitational waves (GWs). However, GWs have not been observed directly yet. Advanced Virgo (AdV), which is a laser interferometer located in Pisa, is one of the next generation detectors that are expected to detect GWs. AdV has a marginally stable configuration in the power recycling cavity. This configuration merits in the reduced number of mirrors, which makes the control easier in comparison with the stable folding mirror configuration. On the other hand, the cavity becomes sensitive against the aberrations of the compound mirrors. To overcome these aberrations will be an essential part of AdV.

The so-called sidebands that are produced by the modulation/demodulation method are used to control each mirror position and alignment. Especially low-frequency sidebands can be affected greatly by aberrations and phase cameras allow tracking any such changes. A map of aberrations can be created via a phase map survey using the phase camera that observes the laser wave front of sidebands. In order to make a phase map, the phase camera utilizes heterodyne detection and beam scanning with a pin-hole photo detector (see Fig.1). This technique can resolve every sideband and focus on a specific sideband that is used for controlling the power recycling cavity.

We have developed a prototype of this phase camera. [1] The expected sensitivity is 1 nm within an area of about 60% of the beam spot. The maximum operation speed is 20 images per second due to the scanner performance. A total of 5 different sidebands (10 signals) and one heterodyne signal are demodulated at the same time by a digital demodulation. Low noise PDs with a pin-hole and digital boards have been made. Tests of the performance by the prototype experiment are almost completed. Also, we have just started to install the optics to the AdV site. After the installation and commissioning, the phase camera will be combined to CO_2 laser and compensation plates as the thermal compensation system. We will report the latest results on the phase camera including the prototype experiment and the installation.

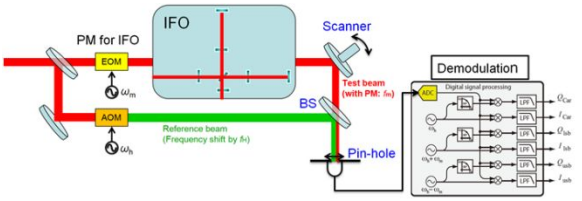

Fig1. Principle of the phase camera. The abbreviations show PM, phase modulation; EOM, electro-optic modulator; AOM, acousto-optic Modulator; IFO, interferometer; and BS, beam splitter.

1. Kazuhiro Agatsuma, David Rabeling, Martin van Beuzekom, Jo van den Brand, "Phase camera development for gravitational wave detectors", *Proceedings of Science* PoS(TIPP2014)228 (2014)

A09: Enhanced Nonlinear Optical Response in Plasmonic Nanomaterials

Tiziana Cesca[1], N. Michieli[1], B. Kalinic[1], H. Sanchez Esquivel[2], C. Scian[1], P. Mazzoldi[1] and G. Mattei[1]

[1]*Physics and Astronomy Department, University of Padova, Padova, Italy*

Email: tiziana.cesca@unipd.it, web site: http://materia.fisica.unipd.it/NSG01/

[2]*Departemento de Óptica, Centro de Investigación Científica y de Educación Superior de Ensenada, Ensenada, Mexico*

Nonlinear optical (NLO) phenomena in nanomaterials play a key role for the realization of advanced nanophotonic devices with applications in many different fields, as ultra-fast all-optical switching, optical limiting or harmonic generation, and much research effort has been done in recent years to overcome the intrinsic weakness of nonlinear processes. To this aim, an efficient strategy is to exploit plasmonic effects (coherent oscillations of conduction electrons) in noble metal nanostructures. [1] The coupling of light to surface plasmons induces intense enhancements of the local electromagnetic field at the nanostructures that can be further increased by exploiting the interaction among the plasmonic nano-building blocks, thus allowing to design plasmonic nanosystems with properly tuned and amplified nonlinear optical response. In this presentation we will report on the third-order NLO properties, investigated by means of the single beam z-scan technique, of two peculiar classes of interacting nanosystems: (i) nanoplanets (NPLs) and (ii) bidimensional ordered arrays of triangular nanoprisms (NPAs). The NLO response was excited by a ps single pulse Nd:YAG laser coupled to an optical parametric amplifier for tuning the excitation wavelength onto the linear absorption resonances. The plasmonic properties were theoretically investigated in the framework of a full-interaction electromagnetic approach. The characteristic topological configuration of the investigated nanostructures makes them very promising for NLO applications. The results proved that the intense local-field enhancements theoretically demonstrated for these systems, arising from the strong electromagnetic coupling among the nano-building blocks, give rise to a significant boost of their nonlinear optical response. [2] This enables to activate and observe phenomena otherwise not accessible in the intensity range that can be employed to investigate the response of these materials without damaging the matrix. Particularly, this has a dramatic impact on their nonlinear absorption behavior and a tunable changeover from reverse saturable absorption to saturable absorption can be obtained in these nanosystems by acting on the pump intensity, the laser wavelength, or by controlling the nanoprims composition.

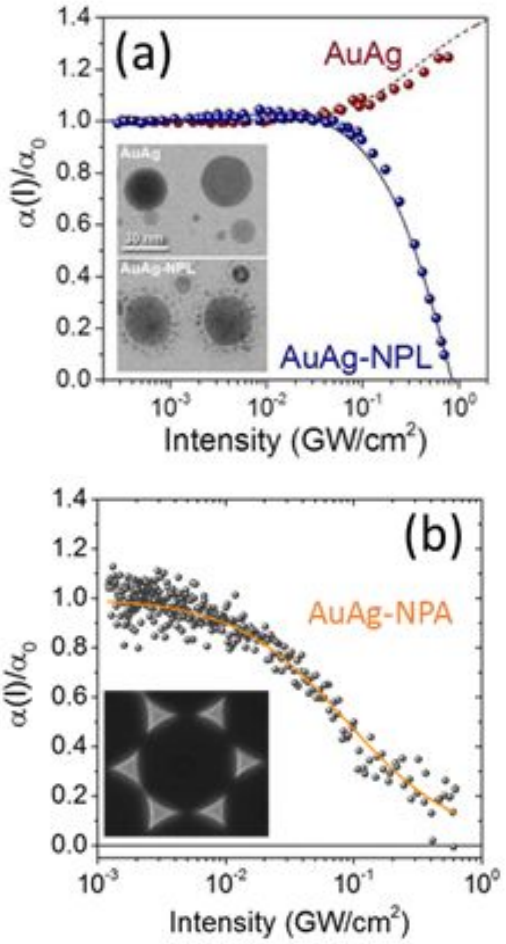

Fig1. Normalized absorption coefficient of (a) Au-Ag nanoplanets compared to the AuAg nanoparticle configuration and of (b) Au-Ag nanoprims array. The insets show the TEM (a) or SEM (b) micrographs of the obtained nanostructures.

1. M. Kauranen and A. V. Zayats, *Nature Photonics* **6**, 373 (2012).
2. T. Cesca, P. Calvelli, G. Battaglin, P. Mazzoldi and G. Mattei, *Optics Express* **20**, 4537 (2012).

A10: Property-controlled III-N quantum dots for quantum photonics

Hui Deng[1], Lei Zhang[1], Tyler Hill[1], Chu-hsaing Teng[2], Brandon Demory[2], Pei-cheng Ku[2]

[1]*Physics Department, University of Michigan, Ann Arbor, MI USA Email:dengh@umich.edu, web site: http://sites.lsa.umich.edu/deng-lab/*

[2]*Department of Electrical Engineering and Computer Science, University of Michigan, Ann Arbor, MI USA*

Semiconductor quantum dots (QDs) provide an on-chip platform to isolate single charges or single excitations. Single charges furthermore can be manipulated optically via the excitonic transitions, while single excitations can be used to create single photon or entangled states. Hence, semiconductor QDs have been a fertile testbed for coherence spectroscopy and quantum information science. However, self-assembled III-Asnide QDs not only suffer from random positioning but also are limited to cryogenic operation temperatures due to relatively small bandgap and exciton binding energies. To overcome these limitations, site-control of QDs have been developed to enable scalability, and wide bandgap materials have been explored to allow high operation temperatures. Site-control of the QDs has also been developed. Single photon emission has been reported in site-controlled III-N QDs from 90~K up to the room temperature. Yet charge tuning has not been achieved, and electrical excitation has been challenging with many site-controlled structures.

In this talk, we will present site-controlled InGaN/GaN QDs made by a top-down fashion that allows not only precise control over the position and dimensions of the QDs but also efficient electrical tuning and injection. We demonstrate single-photon emission up to 90 K in these QDs via optical pumping, which is the highest temperature among all InGaN/GaN QDs. Furthermore, we achieve electrically pumped single photon emission, which for the first time combines electrical injection and site-control, two critical requirements for scalable single-photon sources, in a wide bandgap material. Finally, we demonstrate quantized electron charging in the QDs, which lays the ground for coherent control of the single charge or spin in III-N QDs, opening a door to III-Nitride based spintronics and spin-qubit quantum information processing.

B01: Short-Range and Long-Range Excitonic Coupling in Molecular Aggregates: Introducing a New Design Paradigm for Organic Materials

N.J. Hestand*, R. Tempelaar**, H. Yamagata*, T.L.C. Jansen**, J. Knoester** and F. C. Spano*

**Department of Chemistry, Temple University, Philadelphia, PA 19122*

***Zernike Institute for Advanced Materials, University of Groningen, Nijenborgh 4, 9747 AG Groningen, The Netherlands*

Solid phases of π-conjugated molecules and polymers continue to receive widespread attention as semiconducting materials in field effect transistors, light emitting diodes and solar cells. However, despite the more than five decades of intensive experimental and theoretical research following Kasha's pioneering work on H- and J-aggregates[1] there are still a great many questions regarding the nature of the photo- excitations in molecular assemblies and how their spectral signatures are related to crystal packing and morphology. The theory of Kasha is based on the long-range Coulombic coupling between chromophores. However, in packing morphologies such as the commonly occurring π-stacking motif, the intimate contact between nearest neighbors allows for charge transfer and the creation of a short-range excitonic coupling mechanism due to wave function overlap. In this talk, it is shown how the simultaneous presence of long-range and short-range intermolecular couplings impact photophysical and transport properties in molecular π-stacks. The effect is similar to that recently described in polymer π-stacks.[2] The analysis is based on a Holstein-style Hamiltonian which includes Coulombic coupling and charge transfer. The interference between short-range and long-range couplings

defines four aggregate types: HH, HJ, JH and JJ, based on the sign of the couplings. Each of the four aggregate types possess unique photophysical and transport properties. For example, HH-aggregates have constructively enhanced exciton mobilities and small radiative decay rates, making them excellent candidates for solar cell absorbers. JJ-aggregates can be superradiant at room temperature and therefore serve as good light emitting materials. The photophysical signatures of the four aggregate types include aggregation-induced changes to the vibronic progressions in the absorption and photoluminescence spectra.[3] The vibronic progression, sourced primarily by the ubiquitous vinyl-stretching mode common to virtually all π-conjugated molecules, therefore serves as a direct probe of the nature of the excitonic coupling, as well as the exciton coherence length and mobility. Specific applications will be made to rylene π-stacks which have been intensively investigated as dye pigments and electron-transporting materials.[4, 5] A new design paradigm for organic electronic materials is presented based on the extreme sensitivity of the short-range coupling to small (sub Angstrom) intermolecular displacements transverse to the stacking axis.[6, 7]

References

1. M. Kasha, Radiation Research **20** (1), 55- 70 (1963).
2. F. C. Spano and C. Silva, Ann. Rev. Phys. Chem. **65** (2014).
3. F. C. Spano, Acc. Chem. Res. **43** (3), 429-439 (2010).
4. F. Wurthner and M. Stolte, Chem. Comm. **47** (18), 5109-5115 (2011).
5. B. A. Jones, A. Facchetti, M. R. Wasielewski and T. J. Marks, J. Am. Chem. Soc. **129** (49), 15259-15278 (2007).
6. H. Yamagata, D. S. Maxwell, J. Fan, K. R. Kittilstved, A. L. Briseno, M. D. Barnes and F. C.Spano, J. Phys. Chem. C **118** (49), 28842 28854 (2014).
7. N. J. Hestand, R. Tempelaar, J. Knoester, T. L. C. Jansen and F. C. Spano, Phys. Rev. B submitted.

B02: Soft Supra-Molecular Nanotubes for Robust Light Harvesting?

Dorthe M. Eisele[1]

[1]*Chemistry Department, City College of New York (CCNY) of City University of New York (CUNY)*
Email: Eisele@Eiselegroup.com

The most remarkable materials that demonstrate the ability to capture solar energy are natural photosynthetic systems such as found in rather primitive marine algae and bacteria. Their light-harvesting (LH) antennae are crucial components, as they absorb the light and direct the resulting excitation energy efficiently to a reaction center, which then converts these excitations (excitons) into charge-separated states. Nature's highly efficient light-harvesting antennae, like those found in Green Sulfur Bacteria [1], consist of supra-molecular building blocks that self-assemble into a hierarchy of close-packed structures.

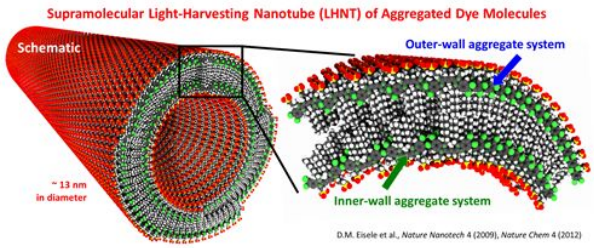

In an effort to mimic the fundamental processes that govern nature's efficient systems, it is important to elucidate the role of each level of hierarchy: from molecule, to supra-molecular building block, to close-packed building blocks. Here, I will discuss the impact of hierarchical structure. I will present a model system [1, 2, 3] that mirrors nature's complexity: cylinders self-assembled from cyanine-dye molecules (as illustrated in the figure). I will show that even though close-packing may alter the cylinders' soft mesoscopic structure, robust delocalized excitons are retained: internal order and strong excitation-transfer interactions—prerequisites for efficient energy transport—are both

maintained.[4] These results suggest that the cylindrical geometry strongly favors robust excitons; it presents a rational design that is potentially key to Nature's high efficiency, allowing construction of efficient light-harvesting devices even from soft supra-molecular materials.

References:

[1] Orf, G. S. & Blankenship, R. E. "Chlorosome antenna complexes from green photosynthetic bacteria." ***Photosynth. Res.*** (2014).

[2] Eisele, D.M., Knoester, J., Kirstein, S., Rabe, J.P., and Vanden Bout, D.A.: "Uniform exciton fluorescence from individual molecular nanotubes immobilized on solid Substrates." *Nature Nanotech.* 4, **(2009)** 658-663.

[3] Eisele, D.M., Cone, C.W., Bloemsma, E.A., Vlaming, C.G.F. van der Kwaak, S.M., Silbey, R.J., Bawendi, M.G., Knoester, J., Rabe, J.P., and Vanden Bout, D.A.: "Utilizing Redox-Chemistry to Elucidate the Nature of Exciton Transitions in Supramolecular Dye Nanotubes." *Nature Chem.* 4, **(2012)** 655–662.

[4] Eisele, D.M., Arias, D.H., Fu, X., Bloemsma, Steiner, C.P., E., Jensen, R., Rebentrost, P., Eisele, H., Llyod, S., Tokmakoff, A., Knoester, J., Nicastro, D., Nelson, K.A., and Bawendi, M.G.:
"Robust Excitons in Soft Supramolecular Nanotubes."
PNAS, 111 **(2014)** E3367-E3375.

B03: Benchmarking calculations of excitonic couplings between chlorophylls

Elise Kenny, Ivan Kassal

School of Mathematics and Physics, University of Queensland, Brisbane, Australia Email:i.kassal@uq.edu.au, web site: http://www.quantum.bio

Excitonic couplings between (bacterio)chlorophyll molecules are fundamental ingredients for any simulation of excitonic dynamics in photosynthetic complexes. A number of techniques for calculating the couplings have been developed, from the simple point-dipole approximation to fully quantum-chemical methods. We perform a detailed comparison of the performance of the different methods to determine whether the additional computational expense of quantum-chemical methods is justified in practical circumstances [1]. An important consideration, previously neglected, is the propagation of errors in these calculations. In particular, calculations based on crystal structures are affected by the uncertainty in the positions of the atoms. We show that for recent high-resolution structures, the errors in the positions of the atoms translate to an uncertainty of about 10% in the estimated couplings. Because the quantum-chemical corrections (due to exchange and overlap) are generally much smaller than 10% in the vast majority of cases, we conclude that the additional computational expense is rarely justified. At the same time, the widely used point-dipole approximation incurs gross errors even at moderate separations. Consequently, we recommend the TrEsp method of Renger and coworkers [2] across the whole range of separations and orientations between the two molecules, because its cost premium over point-dipole is minimal, while its accuracy compared to quantum-chemical calculations is better than the 10% uncertainty. We also caution against the common practice of computationally optimising a crystal structure before calculating energies and couplings, as it can lead to large and uncontrollable errors.

1. E. Kenny and I. Kassal, *in preparation* (2015).
2. M.E. Madjet, A. Abdurahman, and T. Renger, *J. Phys. Chem. B* **110**, 17268 (2006).

B04: Elucidation of the Mechanisms of Photoprotection in Single LHCII Complexes

Gabriela Schlau-Cohen[1], Hsiang-Yu Yang[2], W.E. Moerner[2]

[1]*Department of Chemistry, Massachusetts Institute of Technology, USA*

Email:gssc@mit.edu, web site: http://SchlauCohenLab.com

[2]*Department of Chemistry, Stanford University, USA*

In photosynthetic light harvesting, absorbed energy migrates through a protein network to reach a dedicated location for conversion to chemical energy. In higher plants, this energy flow is efficient, directional, and regulated. The regulatory response involves complex and complicated multi-timescale processes that safely dissipate excess energy, thus protecting the system against deleterious photoproducts. We explore the mechanisms behind this photoprotective process in the major light-harvesting protein from green plants (LHCII). By characterizing the conformational states and dynamics of individual proteins, we identify the extent of energy dissipation in single LHCII proteins and how the extent of dissipation changes in response to pH and carotenoid composition, two components known to play a role in photoprotection. From this information, we explore how individual complexes contribute to the balance between efficiency and adaptability in photosynthetic light harvesting.

B05: Conformational Memory of Single Photosynthetic Pigment-Protein Complexes. A Precursor of Non-Photochemical Quenching?

Mario Schörner[1], Sebastian Beyer[1], June Southall[2], Richard J. Cogdell[2], Jürgen Köhler[1]

[1]*Physics Department, Experimental Physics IV and Bayreuth Institute for Macromolecular Research (BIMF), University of Bayreuth, Germany Email:juergen.koehler@uni-bayreuth.de, web site: http://www.ep4.phy.uni-bayreuth.de*
[2]*Institute of Molecular, Cell & Systems Biology, College of Medical Veterinary and Life Sciences, University of Glasgow, United Kingdom*

Proteins are supramolecular machines that carry out a wide range of different functions many of which require flexibility. The current picture is that proteins can assume many different conformations or conformational substates in order to fulfill their tasks. Generally these structural fluctuations can be made visible by optical spectroscopy of chromophores that are embedded in the protein matrix. Since the energies of the electronic energy levels of a chromophore are very sensitive to its interactions with the local surrounding, conformational fluctuations of the protein lead to changes in the chromophore-protein interactions that show up as spectral fluctuations (spectral diffusion) of the probe molecule. However, as a consequence of the conformational heterogeneity, protein ensembles exist in a broad variety of structures, which manifests itself as a dramatic increase in dynamic heterogeneity reflecting the distribution of the associated barriers that separate the various structures. In order to elucidate information that is commonly washed out by ensemble averaging single-molecule techniques have been exploited. This allows these dynamic processes to be observed that are usually obscured by the lack of synchronization within an ensemble, because a single protein that undergoes conformational fluctuations is at any time in a distinct, well-defined substate.

In order to learn more about the conformational fluctuations of a protein we exploit the phenomenon of fluorescence intermittency, also termed blinking. Up untill now spontaneous conformational fluctuations of proteins have always been assumed to reflect a stochastic random process. The present single-molecule study shows a system where a protein, the LH2 complex from a purple photosynthetic bacterium, displays clear conformational memory. We argue that such a behaviour is exactly the process that can facilitate the evolution of control of switching between two conformational states that can then be used to regulate protein function. If changing between different conformational states was random than it would be much more difficult to understand how conformational control of protein function could have evolved. For the LH2 complexes the conformational memory behaviour seen could provide a pathway by which non-photochemical quenching evolved.

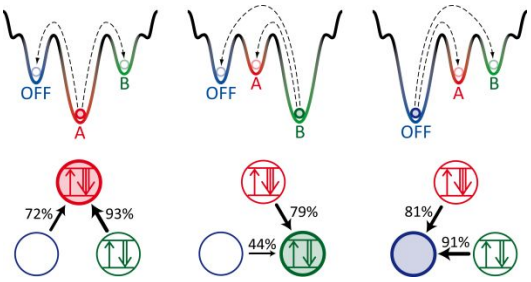

Fig1. Schematic sketch of the observed memory in the intensity fluctuations of LH2. At the top a schematic energy landscape with minima at A, B, and OFF, respectively, is displayed. The minima are associated with the initial intensity levels of the emitted fluorescence of the protein. The numbers next to the arrows at the bottom correspond to the probability to return within two consecutive intensity jumps back to the initial state. The probability for a stochastically independent random event amounts to 50% and is observed only for the transition from OFF → B if B is the initial state (bottom centre), whereas all other probabilities exceed this value clearly.

C01: Coherent control of a molecular ionization process by using Fourier-synthesized laser fields

Hideki Ohmura[1]

[1]*National Institute of Science and Technology (AIST), Tsukuba, Ibaraki 305-8565, Japan*
Email:hideki-ohmura@aist.go.jp

The manipulation of atoms and molecules by laser fields has progressed rapidly due to the recent advent of techniques to generate intense ultrafast laser pulses. Tunneling ionization (TI) by laser fields is one of the most fundamental phenomena induced by intense laser fields. TI occurs when the laser field suppresses the binding potential of the electron so strongly that the wavefunction of the outermost electron penetrates and escapes the tunneling barrier [1]. Recent studies have revealed that TI occurs mainly in the attosecond (1 attosecond [as] = 10^{-18} s) time region, when the electric field of the laser reaches its maximum values owing to a highly nonlinear optical response [2]. Such highly nonlinear processes depending on the amplitude of the electric fields are strongly affected by the laser's phase. Therefore, so-called coherent or quantum control, which is the direct manipulation of the wavefunction and its quantum dynamics through the coherent nature of a laser field, is expected to be a powerful tool to control the coherent motion of electrons. Recently, we have investigated intense phase-controlled two-color laser fields consisting of a fundamental light and a second harmonic light to achieve quantum control of molecular TI in the space domain and the resultant orientation-selective molecular TI (OSMTI) in simple molecules (Fig.1) [3-11].

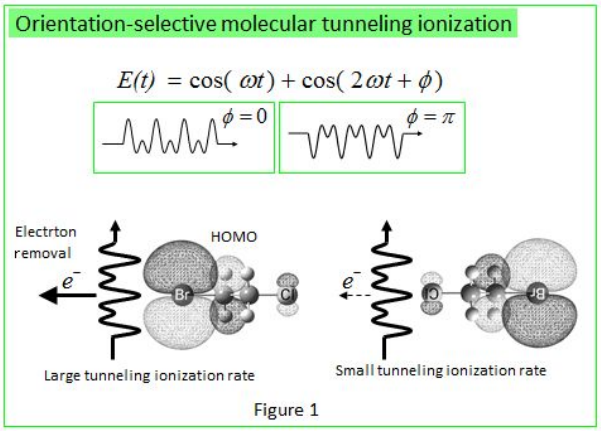

Figure 1

Here, we have extended the quantum control of molecular tunneling ionization by using four-color Fourier-synthesized laser fields. The directionally asymmetric molecular TI induced by intense ($\sim 10^{13}$ W/cm^2) Fourier-synthesized laser fields consisting of fundamental, second-, third-, and fourth-harmonic light achieves the OSMTI. We show that the OSMTI is very effective for measurement of the relative phase differences between the fundamental and each harmonic light. Our results promise not only lightwave engineering but also the control of matter, triggering the creation and establishment of usage of Fourier-synthesized laser fields.

1. L. V. Keldysh, *Sov. Phys. JETP* **20**, 1307 (1965).

2. M. Uiberacker et. al., *Nature* **446**, 627 (2007).

3. H. Ohmura, T. Nakanaga and M. Tachiya, *Phys. Rev. Lett.* **92**, 113002(2004).

4. H. Ohmura, N. Saito, and M. Tachiya, *Phys. Rev. Lett.* **96**, 173001 (2006).

5. H. Ohmura, F. Ito, M. Tachiya, *Phys. Rev.* A **74**, 043410(2006)

6. H. Ohmura, M. Tachiya, *Phys. Rev.* A **77**, 023408(2008)

7. H. Ohmura, N. Saito, H. Nonaka, and S. Ichimura, *Phys. Rev.* A **77**, 053405(2008)

8. H. Ohmura, N. Saito, and T. Morishita, *Phys. Rev.* A **83**, 063407(2011)

9. H. Ohmura, N. Saito, and T. Morishita, *Phys. Rev.* A **89**, 013405(2014).

10. H. Ohmura and N. Saito, *J. Phys. B: At. Mol. Opt. Phys.* **47**, 204007(2014) .

11. H. Ohmura "Orientation-Selective Molecular Tunneling Ionization by Phase-Controlled Laser Fields"

Advances in Multi-Photon Processes and Spectroscopy (Volume 21) , Chapter 2 (p55-103), ISBN:978-981-4518-33-8)

C02: Material gain in dilute nitrides materials using 8-band and 10-band models

M. Gladysiewicz

Faculty of Fundamental Problems of Technology, Wroclaw University of Technology,
Wybrzeże Wyspiańskiego 27, 50-370 Wrocław, Poland
Email: marta.gladysiewicz@pwr.edu.pl

With the fabrication of novel III-V-N semiconductor materials like GaNAsSb/GaAs(InP) or GaNPSb/GaAs(InP) and creation of quantum well structures involving those materials there is a need for theoretical analysis and numerical simulations of their optical properties. Typical simulations are performed by applying 10-band model. However, input parameters for numerical simulations in this model, mostly based on experimental data are limited or not available. For example, reliable optical gain calculations with BAC (i.e., 10-band ***kp*** model calculations) have been rather impossible to perform at present for such QWs, despite the fact that the band structure parameters like energy gaps, effective masses, band offsets are known from experimental studies. In such situation, the usual 8-band ***kp*** model can be applied, but it is unclear how accurate such an approach can be.

In an effort to eliminate, at least partially, the parameter's problem we have compared 10-band and 8-band models for GaInNAs/GaAs QWs to high indium concentration (In~35%) where BAC parameters are parameterized by simple formulas. We go to the conclusion that suitably fixed 8-band model gives virtually similar results. Therefore, for the o type GaNAsSb and GaNPSb quantum wells we use 8-band model to calculate the band structure. We investigate two kinds substrate: GaAs and InP. We analyze band structure and optical gain for this kinds of quantum wells to find material for 1, 55 1, 3 m laser.

C03: Multiple optical injection in semiconductor laser

Najm M. Al-Hosiny

Physics Department, Aljouf University, KSA
Email:nalhosiny@yahoo.co.uk

Semiconductor lasers are crucial components in many modern technological applications due to their distinct features, which include small size, integrability, low cost and high efficiency [1]. They are also considered as ideal nonlinear dynamical systems as they exhibit rich dynamics when injected by external single [2] or multiple [3] beams. The driving force behind this huge interest is to generate broad chaos for the use in crypto graphical communications. The investigation of nonlinear dynamics in these oscillators provides also deep insight to the physics of chaotic and nonlinear behaviors.

In this study, we theoretically investigate the sensitivity of two different routes to chaos, namely period doubling and quasi-periodic routes, to the injection of an additional optical signal using bifurcation diagrams. Bifurcation means qualitative change in the dynamic of the system when a parameter of the system is varied. The routes are chosen by careful investigation in

stability map (frequency detuning vs injection power shown in Fig.1) of the injected laser.

Period-doubling route to chaos is found to be less sensitive to the injection of an additional signal. On the other hand, the quasi-periodic route to chaos seems to be more sensitive to such perturbation. This is mainly due to the relatively wide frequency bandwidth of the quasi-periodic route compared to the period-doubling route. A wide systematic approach can provide good examination of the routes' sensitivity and will surely contribute to the development of ultra stable nonlinear resonators.

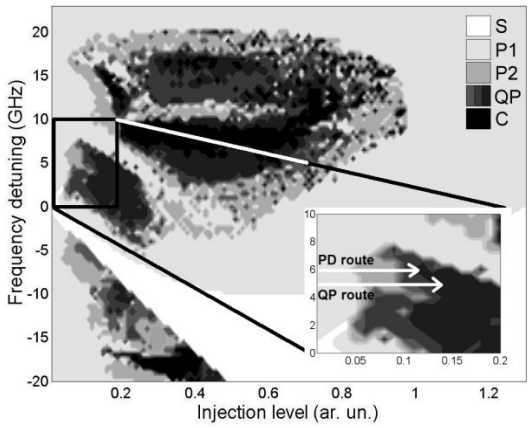

Fig1. The Old Main, University of Arkansas.

1. F . Mogensen. et al., IEEE J. Quantum Electron., **21**, 784-793, (1985).
2. N. Al-Hosiny, et al., IEEE J. Quantum Electron., **42**, 570 - 580, (2006)
3. N. Al-Hosiny, et al., Optics commun., **269**, 166 - 173, (2007).
4. J. Doe and R. U. Hu, *Journal title* **1**, 246 (2007).
5. A.B. Green, C.D. Black, *Book title* (Publisher), 135 (2006).

C04: Organic thin-film solid-state lasers: towards applications

Sébastien Chénais

Université Paris 13, Sorbonne Paris Cité, Laboratoire de Physique des Lasers, CNRS, F-93430, Villetaneuse, France
Email:sebastien.chenais@univ-paris13.fr, web site: http://www-lpl.univ-paris13.fr:8088/lumen/

Lasers based on solution-processed thin-film gain media have recently emerged as low-cost, broadly tunable and versatile active photonics components that can fit to any substrate, and are useful for e.g. chemo or biosensing, or visible spectroscopy. Many materials can act as gain media: dye-doped polymer films, dye-doped liquid crystals, organic semiconductors[1], colloidal quantum dots and recently hybrid perovskites[2]. We have recently demonstrated a novel device architecture for this kind of lasers, called Vertical External Cavity Surface Emitting Organic Lasers (VECSOLs)[3], since they are the counterparts of VECSELs with organic thin-film gain materials. VECSOLs enable combining in a single device the advantages of thin-film organic lasers (low cost, ease of fabrication, broad emission spectra, easy chemical tuning and high gain) with those of inorganic semiconductor VECSELs, i.e., high conversion efficiency, diffraction-limited beam quality, power scaling capability, and a high versatility offered by the open cavity, which includes the possibility to easily tune the laser wavelength or to achieve frequency conversion to reach new spectral domains.
In this talk, we will expose our recent works on VECSOLs that aim at developing new laser sources in the context of making them ready for practical applications. The discussion will be focused on three achievements:
- a diode-pumped high-brightness VECSOL, that enables obtaining a very high brightness laser beam, of the order of ~ 10 TW/m²/sr, in a truly low-cost system (see figure). This is typically ~2 orders of magnitude higher than the usual brightness obtained in classical organic laser geometries [4]; - an ultra-narrow linewidth (< picometer) organic laser with a Volume Bragg grating: in typical thin-film laser schemes, the linewidth is fundamentally limited by short photon cavity lifetimes, and coherence lengths are at most a few mm. Thanks to the use of a Volume Bragg Grating acting both as a spectral filter and an output coupler, a coherence length

of 1 m can be obtained in a near-Fourier-Transform-limited pulse. - a VECSOL based on an inkjet-printed active array of laser pixels. An active ink has been formulated based on a transparent dielectric with optimized jetting properties, and results are comparable with those obtained with a highly transparent polymer (PMMA) that is not easily directly printable.

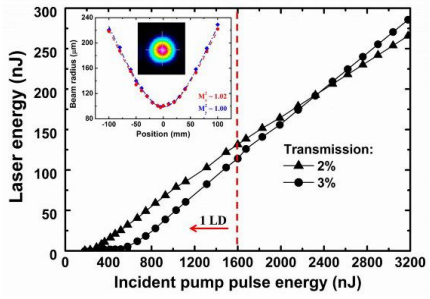

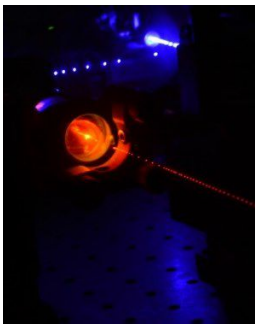

Fig1. A diode-pumped vertical external cavity surface-emitting Organic laser. Left : laser input/output characteristics. Right : long-exposure photo of the laser (dots are due to the pulsed nature of lasing)

References

1. Wang, Y. *et al.* LED pumped polymer laser sensor for explosives. *Laser Photonics Rev.* **7,** 71–76 (2013).

2. Xing, G. *et al.* Low-temperature solution-processed wavelength-tunable perovskites for lasing. *Nat. Mater.* **13,** 476–80 (2014).

3. Rabbani-Haghighi, H., Forget, S., Chénais, S. & Siove, A. Highly efficient, diffraction-limited laser emission from a vertical external-cavity surface-emitting organic laser. *Opt. Lett.* **35,** 1968–1970 (2010).

4. Zhao, Z., Mhibik, O., Nafa, M., Chénais, S. & Forget, S. High brightness diode-pumped organic solid-state laser. *Appl. Phys. Lett.* **106,** 051112 (2015).

C05: Real-Time Laser Based Diagnostics for Complex Thin Films Thermo-physical and Thermo-electrical Properties Characterization

N. Semmar, A. Melhem, A. Stolz, A. Talbi, C. Tchiffo, G. Savriama, D.T.T. Huynh, T. Lecas, A. Petit, S. Kaya-Boussougou, E. Millon, C. Boulmer-Leborgne

GREMI-UMR 7344-CNRS/University of Orléans, BP 6744, 45067 Orléans Cedex 2, France Email: Nadjib.Semmar@univ-orleans.fr, web site: http://www.univ-orleans.fr/gremi/

Fast optical methods were successfully used for the thermo-physical characterization of various samples, from metallic films to complex films such as vertically aligned carbon nanotube (CNT) carpets and mesoporous silicon (MeSi) substrates. Contribution of real-time reflectometry (RTR) to laser induced processes is highlighted through several applications with Excimer and Nd:YAG laser beams processing a high number of materials (sc-Si, sc-ZnO, etc.) related to sensors fabrication [1-2]. The pulsed photo-thermal technique (PPT, with less than 2ns response time, see Fig.1) allows the evaluation of thermal properties of a wide range of thin film materials. Due to their promising microelectronic applications in design and packaging, thermo-physical properties of AlN, CNT and MeSi films will be discussed leading to predict the best materials fabrication process for a targeted application. As reducing the size of active surfaces, laser-based nanostructuration of copper thin films was also successfully monitored using RTR at picosecond time scale [3]. This last topic is also illustrated in this paper and connected to the enhancement of the thermo-electric properties of thin films, particularly in the case of oxides and polymers. The detailed description of the measurement setup (Fig.2) and the instrumental concept behind will also be illustrated. The complete

characterization of selected materials (polymer based, MeSi, etc.) will be discussed [4] namely on their figure of merit and efficiency.

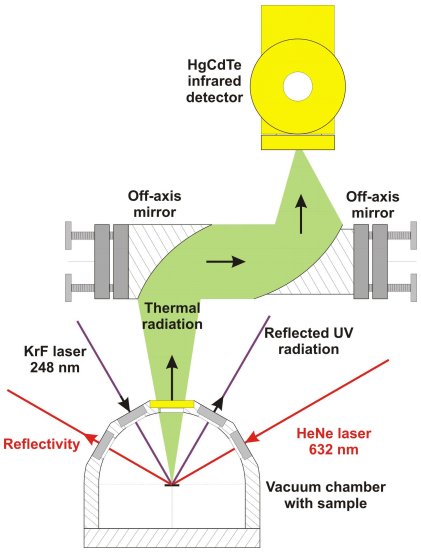

Fig.1: Pulsed Photo-Thermal (PPT) setup for thermo-physical characterisation of thin films.

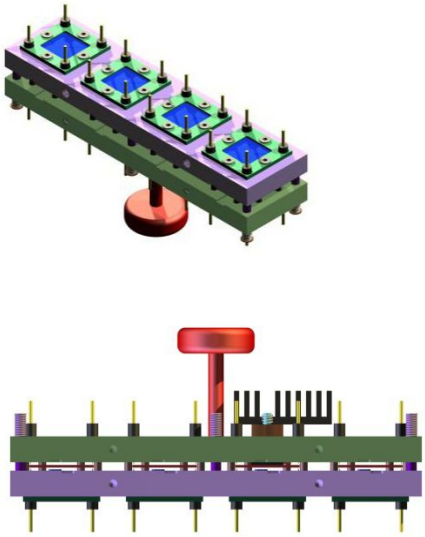

Fig.2: Schematic of the sample holder for the thermo-electrical characterization of thin films.

1. J. Martan, N. Semmar, C. Boulmer-Leborgne, P. Plantin, E. Le Menn, Nanosc. Microsc. Therm. **10** (4) 333-344 (2006).
2. N. Semmar, M. Tebib, J. Tesar, N.N. Puscas, E. Amin-Chalhoub, Appl. Surf. Sci. **255** (10), 5549-5552 (2009).
3. T.T. Dai Huynh, N. Semmar, Applied Physics A **116** (3), 1429-1435 (2014).
4. O. Abbes, A. Melhem, C. Boulmer-Leborgne, N. Semmar, Adv. Mater. Lett. *in press* (2015).

Acknowledgements: Authors are grateful to the 'Région Centre' and 'Agence Nationale de la Recherche' French institutions for supporting this work.

C06: Principle of innovative laser-dicing of silicon wafer -Stealth Dicing

Etsuji Ohmura

Graduate School of Engineering, Osaka University, Suita, Osaka, Japan
Email: ohmura@mit.eng.osaka-u.ac.jp

Blade dicing is used conventionally for dicing of a semiconductor wafer. Stealth dicing (SD) was developed as an innovative dicing method by Hamamatsu Photonics K.K. The SD method includes two processes. One is a "laser process" to form a belt-shaped modified-layer (SD layer) into the interior of a silicon wafer for separating it into chips. The other is a "separation process" to divide the wafer into small chips. When a permeable nanosecond laser is focused into the interior of a silicon wafer and scanned in the horizontal direction, a high dislocation density layer and internal cracks are formed in the wafer. The internal cracks progress to the surfaces by applying tensile stress due to tape expansion without cutting loss. As the SD is a noncontact processing method, high speed processing is possible. In the SD, there is no chipping and no cutting loss, so there is no pollution caused by the debris. The advantage of using the SD method is clear. A complete dry process of dicing technology has been realized and problems due to wet processing have been solved. In our previous studies, heat conduction analysis by considering the temperature dependence of the absorption coefficient and crack propagation analysis were performed for the SD method.
An example of the time variation of temperature distribution is shown in Fig. 1. Figure 2 shows the maximum temperature distribution and a

schematic of SD layer formation. SD layer looks like an exclamation mark "!". As a result, a train of the high dislocation density layer and void is generated as a belt in the laser scanning direction. Figure 3 shows an inside modified-layer observed by a confocal scanning infrared laser microscope before division. It is confirmed that a train of the high dislocation density layer and void is generated as a belt as estimated in the previous studies. The validity of the analytical results were confirmed. As a result the principle of the SD was clarified and the characteristic processing phenomena in the SD became predictable based on this principle.

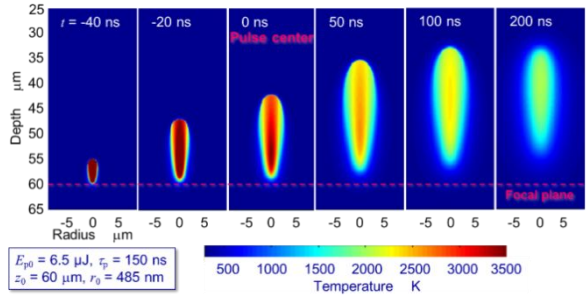

Fig. 1 Time variation of temperature distribution obtained by heat conduction analysis.

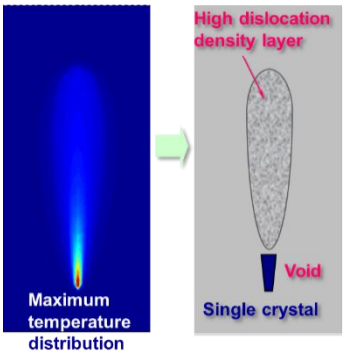

Fig. 2 The maximum temperature distribution (left) and a schematic of SD layer formation (right).

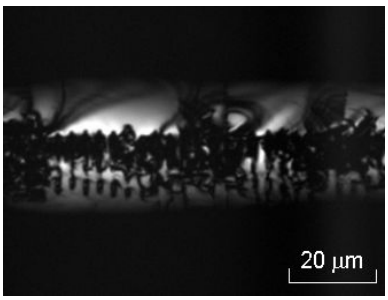

Fig. 3 IR laser microscopy image before division

1. E. Ohmura, *Heat Transfer* (InTech), 29 (2011).
2. E. Ohmura, Y. Kawahito, K. Fukumitsu, J. Okuma and H. Morita, *J. Mat. Sci. Eng.*, A, **1**, 46 (2011).

C07: Gate-bias dependent carrier distribution visualization in SiC power-MOSFET using super-higher-order SNDM

Norimichi Chinone, Yasuo Cho

Research Institute of Electrical Communication, Tohoku University, Japan
Email:yasuocho@riec.tohoku.ac.jp, web site: http://www.d-nanodev.riec.tohoku.ac.jp

Visualization of gate-bias dependent carrier distribution using super-higher-order (SHO) SNDM was demonstrated. SHO-SNDM, one of the scanning probe microscopies, measures tip-sample capacitance response to the tip-sample voltage[1,2], which has strong correlation with the density and polarity of carrier under the tip. When ac voltage $V_S(t)=V_{S,0}\cos\omega_S t$ was applied between tip and sample, the tip-sample capacitance variation $\Delta C_s(t)$ is given by following Fourier expression[1,2]

$$\Delta C_s(t)=\sum_{n=1}^{\infty}\left(C_n^{\cos}\cos\omega_S t+C_n^{\sin}\sin\omega_S t\right). \qquad (1)$$

In Eq. (1), $C_1^{\cos}$ is proportional to $\partial C_s/\partial V$, which is measured in conventional SNDM. Acquisition of Fourier coefficients at once (SHO-SNDM measurement) allows us to local capacitance-voltage (CV) curve reconstruction by plotting the locus of $(V_S(t),\Delta C_s(t))$. When the Fourier coefficients are two-dimensionally obtained, local CV curves can be mapped. One of the easy translations of the map of CV curve is depletion layer distribution analysis, which categorizes every pixel to p-type, n-type, or depletion region focusing on the shape of reconstructed CV curves[2,3]. Next, let's consider the case that ac voltage $V_{GS}(t)=V_{GS,0}\cos\omega_{GS}t$ is applied to gate. In this case, carrier distribution changes periodically, which periodically

modulates under the tip. The $\partial C_s/\partial V$ can be expressed by a function of time as follows

$$\partial C_s/\partial V(t) = \alpha_0 + \sum_{n=1}^{\infty}(\alpha_n \cos\omega_{GS}t + \beta_n \sin\omega_{GS}t) \quad (2)$$

where α_0 is time-averaged $\partial C_s/\partial V$ and $\alpha_n, \beta_n (n \geq 1)$ are the Fourier coefficients. After measuring the coefficients in Eq. (2), the relationship between $\partial C_s/\partial V$ and V_{GS} is obtained by drawing the locus of $(V_{GS}(t), \partial C_s/\partial V(t))$, which enables us to get $\partial C_s/\partial V$ at arbitrary V_{GS}. During the measurements, gate-bias-induced tip-sample voltage was cancelled in order to avoid artifact coming from the tip-sample voltage.

At first, "off" and "on"-states were imaged. Figures 1(a) and 1(b) are C_1^{cos} images (i.e., $\partial C_s/\partial V$ images) for "off" and "on" state, respectively. The area beneath the gate most strongly depends on gate-bias. Fig. 1(b) exhibits strong negative signals unlike Fig. 1(a), which indicates the electron accumulation and channel formation under the gate. Moreover, depletion distributions in "off"-state and "on"-state were analyzed using SHO-SNDM images. Figures 1(c) and 1(d) show the analytical results. Second, visualization of detailed gate-bias-induced carrier redistribution was demonstrated. In this measurement, ac voltage was applied to gate and $\partial C_s/\partial V(V_{GS})$ was two-dimensionally mapped in the area illustrated in Fig. 2(a). Figures 2(b)–(d) are the reconstructed $\partial C_s/\partial V$ images at given V_{GS}. The carrier redistribution (accumulation and channel formation) was visualized. These results show that SHO-SNDM is useful technique for analysis of device operation.

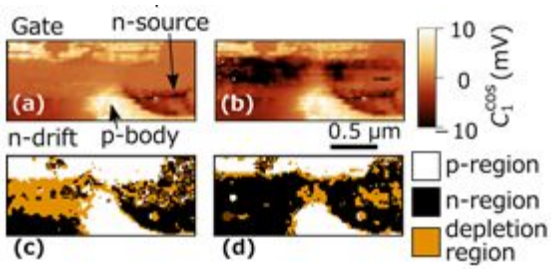

Fig 1. Visualization of "on" and "off" state.

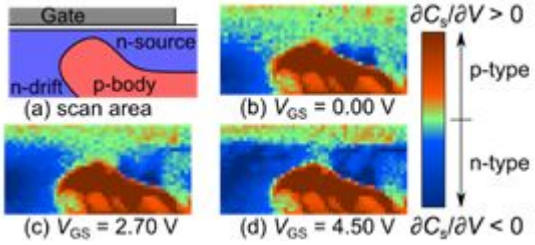

Fig 2. Detailed gate-bias dependent carrier profiling

Acknowledgements: This work is partially supported by Research Fellowships of Japan Society for Promotion of Science for Young Scientists (No. 268084) and Grant-in-Aid for Scientific Research S (No. 23226008) from the Japan Society for Promotion of Science.

1. Y. Cho, A. Kirihara, and T. Saeki, Rev. Sci. Instrum. **67**, 2297 (1996).
2. N. Chinon, T. Nakamura, and Y. Cho, J. Appl. Phys. **116**, 084509 (2014).
3. H. Edward *et al.*, Appl. Phys. Lett. **72**, 698 (1998).

C08: Charge modulation spectroscopy and electric field induced optical second harmonic generation measurement for analyzing organic device

Eunju Lim[1,2]*, Y. S. Song[3], D. Taguchi[4], M. Bok[1], S. Jo[2], C. Lee[2], M. Kim[2], M. Iwamoto[4]

[1]*Department of Applied Physics/Science Education, Dankook University, Gyunggigo, Korea*
Email:elim@dankook.ac.kr
[2]*Department of Creative Convergent Manufacturing & Engineering, Dankook University, Gyunggigo, Korea*
[3]*Department of Fiber System Engineering, Dankook University, Gyunggigo, Korea*

[4]Department of Physical Electronics, Tokyo Institute of Technology, Tokyo, Japan

There are many reports on thin film transistors using organic and polymeric semiconductors because of their potential applications such as low-cost memory cards, smart price tags and labels [1,2]. These materials developments and device processing techniques are accomplished by improvements in their mobility, stability and so on, and these are utilized in fabrication technologies of organic field effect transistors, organic light emitting diodes, organic solar cells, and so forth. Therefore many theoretical and experimental studies on carrier mechanisms are necessary [3]. However, understanding of the driving mechanism, device degradation, and carrier motions is still not sufficient for the use of organic semiconductors in actual organic devices. We here studied the electric field distribution change induced in ITO/PI/TIPS-pentacene/Au diodes by carrier injection [4]. Upon application of a step voltage to the diodes, the electric field change across the TIPS-pentacene layer was measured. Significant electric field distribution change was suggested due to the carrier injection, and a simple model that accounts for the current voltage and capacitance-voltage characteristics of the diodes was proposed, on the basis of the Maxwell-Wagner effect model analysis. By using charge modulation spectroscopy (CMS) and time-resolved electric field induced optical second harmonic generation (TR-EFISHG) measurement, we further studied the carrier transport and trapping mechanism in ITO/PI/TIPS-pentacene/Au diodes [5-7]. Under stress-biasing of TIPS-pentacene diodes, accumulation of interfacial charge was observed. TR-EFISHG is very effective to directly measure electric field distributions and potential distributions in these devices under operational conditions. That is, it allows us to study the device performance in terms of carrier injection and behavior.

1. G. Gelinck, P. Heremans, K. Nomoto, T. D. Anthopoulos, Adv. Mater. 22, 3778 (2010).
2. T. Sekitani, T. Someya, Mater. Today 14, 398 (2011).
3. R.Tamura, E.Lim, T.Manaka, M.Iwamoto,J. Appl. Phys. 100, 114515 (2006).
4. E. Lim, D. Taguchi, M. Iwamoto, Org. Elec. 14, 1903 (2013).
5. T. Manaka, E. Lim, R. Tamura, M. Iwamoto, Nat. Photo. 1, 581 (2007).
6. E. Lim, D. Taguchi, M. Iwamoto, Org. Elec. 15, 3590 (2014).
7. E. Lim, D. Taguchi, M. Iwamoto, Appl. Phys. Lett. 105, 073301 (2014).

C09: Towards the fabrication of 3D-$LiNbO_3$ nanostructures

G. Ulliac, C. Guyot, N. Courjal, B. Guichardaz and M-P Bernal

Optics Department, FEMTO-ST Institute, Franche-Comté University, Besançon, FRANCE Email:gwenn.ulliac@femto-st.fr

Structuring lithium niobate ($LiNbO_3$, LN) for photonic applications has been attracting much attention over the last decade owing to the potentialities offered by this material in terms of electro-optical, acousto-optical or nonlinear interactions. However, achieving LN photonic crystal (PhC) represents a challenging task due to the well-known resistance of this material to standard machining methods [1]. Previously, we have reported the fabrication of 1D-PhCs by direct FIB milling on standard optical waveguides [2]. However the etching profile exhibits angles close to 85°, an aspect ratio AR≈6 and a conical shape, due to the re-deposition of LN on sidewalls during the FIB milling process (figure 1). Alternatively, we propose a method based on the possibility to etch laterally PhC structures by FIB milling (Focused Ion Beam) on very thin optical ridge waveguides. For that purpose, we reported a fast and easy method based on “optical grade dicing” for the fabrication of low-loss optical ridge

waveguides [3]. These optical ridges are subsequently processed by lateral FIB milling in order to optimize the aspect ratios of 1D-PhCs. If the width of the ridge is smaller than 7µm, it is possible to etch the hole through the whole width of the ridge. Fig. 2 shows a side view of a 4µm-wide, 5µm-deep, 10µm-long and 1086nm-period 1D-PhC with angles close to verticality and a AR>9. Moreover, this new strategy of etching is less time consuming and offers a better interaction between the optical waveguide and the 1D-PhC structure. An experimental reflectivity of 53% at 1550nm has been measured with an ultra-short 8µm-long Bragg grating on Ti-diffused LN ridge waveguide with this new method [4]. Additionally, this new approach gives promising perspectives towards the fabrication of LN 3D-PhCs, as illustrated in Fig. 3. This structure has been achieved by firstly etching different windows on the ridge waveguide to define a 3D dice of 27µm3 and by secondly milling each side of this dice by FIB. This new strategy of etching constitutes a significant step towards micro and nanoscale integrated optics devices in lithium niobate.

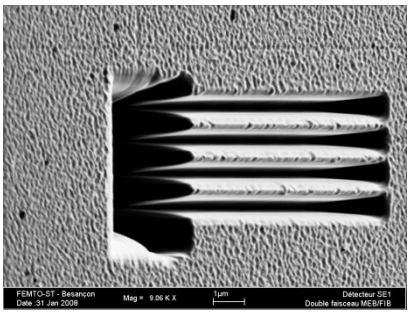

Fig.1. FIB cross-section on 1D-PhC top etched by FIB

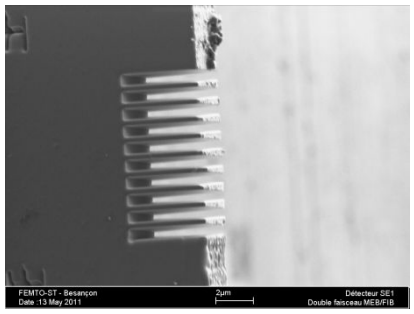

Fig.2. SEM view of a 1D-PhC laterally etched by FIB

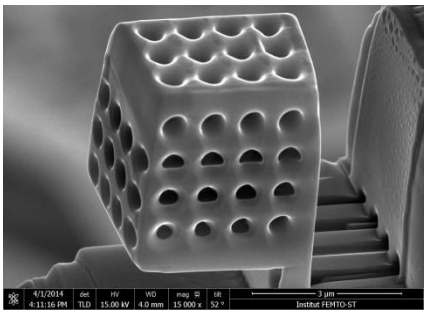

Fig.3. SEM view of a 3D-PhC performed on an optical ridge

This work was supported by the French ANR under Charades project and partly by the french RENATECH network and its FEMTO-ST technological facility.

[1] G. Ulliac and al, Optical Materials, 31, 196-200, 2008
[2] K. Ghoumid and al, JLT, Vol.28, n°23, 3488-3493, 2010
[3] N. Courjal and al, Journal of Physics D: Applied Physics 44, 30 (2011) 305101
[4] C. Guyot and al, Optics Letters, Vol. 39 Issue 2, pp.371-374 (2014)

D01: TiO_2-based nanostructures for photocatalytic applications synthesized by vapor-phase pulsed laser ablation

Takehito Yoshida[1], Ikurou Umezu[2]

[1]Course of Chemical Engineering, National Institute of Technology, Anan College, Anan, Tokushima, Japan

Email: takehito@anan-nct.ac.jp, web site: http://www01.anan-nct.ac.jp/souran/takehito
[2]Department of Physics, Konan University, Kobe, Japan

Focusing on photocatalysis particles, first of all, nanometer-sizing is significant because of increasing specific surface areas. Secondary, agglomeration structures of the photocatalysis nanoparticles have particular interests to realize novel functions. Pulsed laser ablation (PLA) in vapor-phase is a candidate process to synthesize nanocrystallites with controlling not only their crystal structures but also agglomeration structures. In this study, we prepared TiO_2 nanocrystallites agglomerated in self-organized web-structures by the PLA in O_2 background gas, and characterized the photocatalytic actvities.

The TiO_2 nanocrystallites were formed by the PLA of a TiO_2 high density target in O_2 background gases. The third harmonics beam of a Nd:YAG laser (wavelength: 355 nm, pulse width: 6 ns, energy density: 2.7 J/(cm^2 · pulse)) was focused onto the TiO_2 target. The O_2 background gas pressure (PO_2) was varied from 100 to 550 Pa. Distance from the target to unheated deposition substrate (T/S) was 20 mm. The rapid thermal annealig (RTA) was carried out at 600 ºC, for 60 sec, aiming at recovering the surface disordered layers, suppressing the sintering diffusions.

Concerning the TiO_2 nanocrystallites formed by the vapor-phase PLA, we have clarified so far[1,2], as follows: 1) Primary particles are nanometer-sized single-crystalline, and their mean diameter was 5 nm, 2) Crystal structures of the as-deposited TiO_2 nanocrystallites can be controlled to anatase or rutile varying PO_2 or T/S, 3) Agglomeration structures of the as-deposited TiO_2 nanocrystallites transferred from columnar film to cauliflower-like and web-like structures with increasing PO_2 (Fig. 2), 4) In the self-organized cauliflower-like and web-like structures, we obtained autocorrelation functions to find the periodic structures indicated by characteristic lengths. The characteristic lengths dispersed from 5 to 10 m. Above phenomenon 2) can be explained by cooling processes in the vapor-phase PLA.

Paying attention to influence of the self-organized agglomeration structures on photocatalytic activities (PCA), we adapted a methylene blue decomposition method. Si substrates on which the TiO_2 nanocrystallites deposited, in methylene blue aqueous solution, were irradiated by an excitation light (band-pass-filtered Xe lump: 360 nm). These results are shown in Fig. 2. The PCA means decrease of main absorbance peak (664 nm). It was confirmed that introducing "normalized PCA" defined as (raw PCA)/(apparent volume of the deposited species), the web-like structures were about three times higher than the cauliflower-like structures. We can infer the web-like structures had high porous relating larger specific surface area, in comparison with the cauliflower structures.

Consequently, the agglomerated structures of the primary photocatalytic nanocrystallites cause strong influence on the specific surface areas leading increase of PCA. Basically, as the single-nanometer-sized nanocrystallites are smaller than the diffusion lengths of minority carriers in TiO_2 (tipycally 10 nm), effective electron-hole charge separation can be realized. Furthermore, the self-organized web-like structures having high specific area, namely high pours, are presumably suitable for high performance photocatalysis.

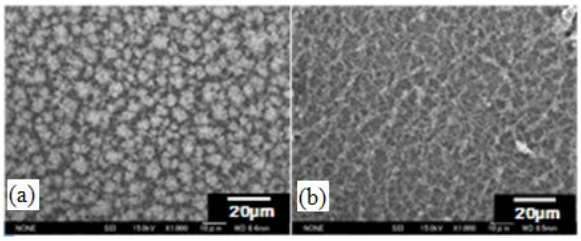

Figure 1 : Plane-view by FESEM of TiO_2 nanocrystallites deposited in O_2 background gas at 100 Pa (a), 400 Pa (b).

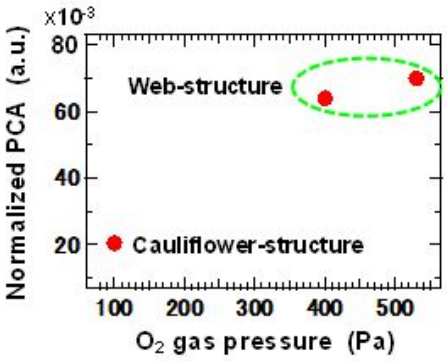

Figure 2 : Normalized photocatalytic activities as a functon of background gas (O_2) pressure.

1. T. Yoshida et al., Appl. Phys. A, **117**, 223 (2014).
2. I. Umezu et al., Proc. of Conf. on Lasers and Electro-Optics Pacific Rim, TuE3 (2013).

D02: Nanoparticles and Nanostructures Produced by Ultra-short Laser Ablation in Liquid

R.Teghil[1], A. De Bonis[1], M. Sansone[1], A. Galasso[1], A. Santagata[2]

[1]*Dipartimento di Scienze, Università della Basilicata, Potenza, Italy*
Email:roberto.teghil@unibas.it
[2] *UOS Potenza, CNR-ISM, Tito Scalo (PZ), Italy*

Laser ablation in liquid (LAL) technique, performed both with short and ultra-short laser sources, has been widely used in the last years to produce nanoparticles (NPs) and nanostructures (NSs) with a wide range of applications, in particular in the field of material science [1,2]. This technique presents several advantages in the production of NPs with respect to the most commonly used chemical methods. In fact, by varying in a simple way the experimental conditions and without the use of chemical agents and stabilizers, it is possible to control NPs size, shape and crystallinity and to obtain nano- and micro-structured materials [2-5].

In this paper several examples of NPs and NSs produced by LAL in different solvents are presented. In all cases a frequency doubled Nd:glass laser with a pulse duration of 250 fs has been used. The use of a fs laser as laser source can offer different possibilities in respect to those obtainable by longer pulse durations, due to the creation of high temperature an pressure conditions that are highly favorable for the formation and stabilization of metastable phases [5,6]. Among the presented systems, the ablation of graphite in water and of palladium in tetraethyl orthosilicate (Fig. 1) are reported and discussed in detail.

The produced materials have been characterized by conventional techniques such as Scanning and Transmission Electron Microscopies, Atomic Force Microscopy, Raman Spectroscopy, X Ray Photoelectron Spectroscopy and X Ray Diffraction.

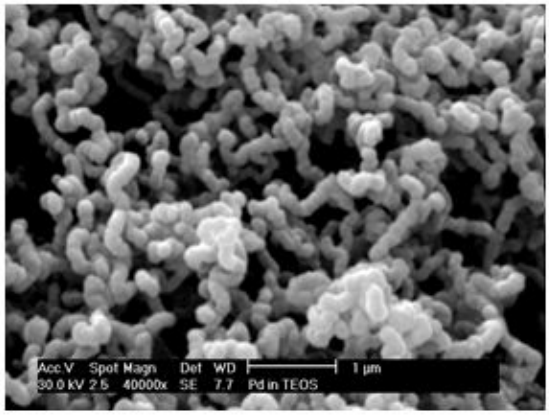

Fig1. Xerogel obtained by LAL of Pd in tetraethyl orthosilicate.

1. Z. Yan, D.B. Chrisey, *J. Photochem. Photobiol. C* 13, 204 (2012).
2. V. Amendola, M. Meneghetti, *Phys. Chem. Chem. Phys.* **15**, 3027 (2013).
3. T. Tsuji, M. Tsuji, S. Hashimoto, *J. Photoch. Photobio. A* **221**, 224 (2011).
4. A. Nath, S.S. Laha, A. Khara, *Appl. Surf. Sci.* **257**, 3118 (2011).
5. A. De Bonis, A. Galasso, N. Ibris, A. Laurita, A. Santagata, R. Teghil, *Appl. Surf. Sci.* **268**, 571 (2013).
6. A. Santagata, A. De Bonis, A. De Giacomo, M. Dell'Aglio, A. Laurita, G.S. Senesi, R. Gaudiuso, S. Orlando, R. Teghil, G.P. Parisi, *J. Chem. Phys. C* **115**, 5160 (2011).

D03: Deposition and Characterization of Silicon/Nitrogen-Doped Diamond-Like Carbon Films

Hideki Nakazawa

Graduate School of Science and Technology, Hirosaki University, Hirosaki, Aomori 036-8561, Japan
Email:hnaka@eit.hirosaki-u.ac.jp

Doping of Si into diamond-like carbon (DLC) films has been intensively studied because of the reduction of internal stress and the resultant improvement of friction performance in air or in aqueous conditions.[1,2] However, it has a drawback that the wear protection is lowered by the incorporation of Si. On the other hand, carbon nitride films has been reported to exhibit extreme hardness values [3], whereas the incorporation of N degraded the friction performance in air and the adhesion strength to a substrate.[4] In this study, we have deposited silicon/nitrogen-doped DLC (Si-N-DLC) films by radio-frequency plasma-enhanced chemical vapor deposition using methane (CH_4) and hexamethyldisilazane {$[(CH_3)_3Si]_2NH$} as the Si and N source, and systematically investigated the structure and the mechanical and tribological properties of the films.

DLC films were deposited in an rf (13.56 MHz)-PECVD chamber, whose base pressure was 8.0×10^{-5} Pa. The substrate used was a Si wafer. A negative dc bias (-500 V) or a negative pulse bias (-500 V, 20 kHz) was applied to the substrate. HMDS and monomethylsilane (CH_3SiH_3; MMS) flow ratios [HMDS(MMS)/(HMDS(MMS)+CH_4] were changed from 0 to 5%. Ar or H_2 flow rate was 22 sccm and the total flow rate was kept at 44 sccm.

We investigated the properties of the Si-N-DLC films and the Si-DLC films prepared by PECVD using MMS as the Si source. We also compared the Si-N-DLC films deposited using the pulse bias applied to the substrate with those prepared using the dc bias. Ar was used as the dilution gas. Many particles were observed on the film surfaces when the deposition with Ar was carried out. It was found that the use of the pulse bias was effective in suppressing the formation of particles. The Si content in DLC films estimated by EPMA increased with increasing HMDS or MMS flow ratio. There was little difference in Si content between the HMDS and MMS films. We confirmed that the N content increased with the HMDS flow ratio, and the pulse-biased films were found to contain higher N concentrations than the dc-biased films. XPS analysis revealed that the use of the pulse bias increased Si-N bonds in the films.

The internal stress decreased as the Si content increased. It was found that the internal stress values of the Si-N-DLC films are lower than those of the Si-DLC films. Raman, FTIR, and PES using synchrotron radiation light measurements suggested that the decrease in internal stress is predominantly due to the increase in sp^2 carbon atoms and the ordering of those. Meanwhile, the internal stress values of the pulse-biased films are lower than those of the dc-biased films. The adhesion strength to the substrate evaluated by scratch tests increased with increasing Si content. We found that the use of the pulse bias was effective in further increasing the adhesion strength. The Si-N-DLC films deposited using the pulse bias exhibited the highest adhesion strength, which is due to the sufficient reduction of the internal stress in the films.

The tribological properties were investigated by ball-on-plate reciprocating friction tests in air. The friction coefficient of the films decreased with increasing Si content. It was found that the Si-N-DLC films had as a low friction coefficient as the Si- DLC films in ambient air, and the friction coefficients of the films prepared with the pulse bias were lower than the dc-biased films. We also found that there was an optimum HMDS ratio where the Si-N-DLC films had a lower wear rate than the Si-DLC films. Meanwhile, the pulse-biased films had a higher wear resistance than the dc-biased films.

We compared the properties between the Si-N-DLC films deposited with H_2 and those with Ar, which were used as the dilution gases. A negative dc bias was applied to the substrate during the deposition. As the HMDS flow ratio increased, internal stress decreased and, at the same time, adhesion strength determined by scratch tests increased. It was found that the use of H_2 was effective in suppressing the formation of particles and further increasing adhesion strength. Friction coefficient, as evaluated by ball-on-plate reciprocating friction tests, decreased with increasing HMDS flow ratio. We found that employing H_2 as the dilution gas reduced the friction coefficient and wear rate of the films.

1. K. Oguri, T. Arai, Surf. Coat. Technol. **47**, 710 (1991).
2. T. Ohana, T. Nakamura, M. Suzuki, A. Tanaka, Y. Koga, Diamond Relat. Mater. **13**, 1500 (2004).
3. H. Sjostrom, S. Stafstrom, M. Boman, J. E. Sundgren, Phys. Rev. Lett. **75**, 1336 (1995).
4. H. Nakazawa, A. Sudoh, M. Suemitsu, K. Yasui, T. Itoh, T. Endoh, Y. Narita, M. Mashita, Diamond Relat. Mater. **19**, 503 (2010).

D04: Avalanche amorphous Selenium (a-Se) for optical and x-ray imaging

Alla Reznik*, [1,2]

[1] *Department of Physics, Lakehead University, Thunder Bay, P7B 5E1, Canada*
[2] *Thunder Bay Regional Research Institute, Thunder Bay, P7B 6V4, Canada*
**e-mail: areznik@lakeheadu.ca*

The avalanche multiplication in amorphous selenium (a-Se) is of outstanding significance to the field of optical and radiation medical imaging as it promises to reproduce the internal gain previously the exclusive domain of bulky, low quantum efficiency electro-optical devices. It was found empirically, and demonstrated theoretically, that a-Se is the only amorphous photoconductor where charge, while drifting in high electric field, can avoid energy dissipation and hence can acquire enough energy to initiate impact ionization and secondary charge creation leading to avalanche multiplication [1,2]. This results in a stable and essentially noiseless [1,3] multiplication gain of up to 1000 depending on a-Se layer thickness and applied electric field.

While the discovery of impact ionization in a-Se was initially greeted with skepticism over the years avalanche multiplication has been not only confirmed by numerous experiments, but has been also utilized in commercial a-Se photoconductive targets used in ultra-sensitive HARP (High-gain Avalanche Rushing Photoconductor) TV camera tubes. [4] It has been proposed that, due to their ultra-high sensitivity, provided by avalanche gain a-Se HARP photosensors is a promising approach for low dose x-ray imaging detectors and a viable alternative to photomultiplier tubes for functional medical imaging (i.e. Positron Emission Tomography). [5-7] In a-Se-based PET detectors, the combination of high gain with high quantum efficiency for scintillation light (almost unity for all scintillators used in x-ray and PET) significantly improves low dose detector performance. Furthermore, a-Se avalanche photodetectors are magnetic field insensitive and can be used in dual modality imaging where radiation detectors are used in conjunction with Magnetic Resonance Imaging.

Avalanche multiplication is also of great importance to direct conversion a-Se based detectors, as it promises to increase a-Se's x-ray to charge conversion efficiency and lead to a-Se detectors that are effectively quantum noise limited in operation at all exposure levels. A further often overlooked advantage of avalanche multiplication is to increase the dynamic range of a system by permitting the maximum signal capacity to be adjusted by changing the effective multiplication gain.

Although the high potential of avalanche multiplication in a-Se was well recognized, the development of commercial avalanche a-Se detectors has been a long journey in both fundamental and applied research. From the first demonstrational a-Se insulating structures which were used to prove the existence of avalanche

multiplication phenomenon in a-Se, - to the first practical a-Se High-gain Avalanche Rushing Photoconductor (HARP) blocking structures used in ultra-high sensitive TV camera tubes and recently to the first prototype of solid-state a-Se avalanche photosensor with metal electrodes. The present talk discusses the technological peculiarities of these structures and recent advances in avalanche a-Se technology addressing the particular requirements for use in optical and radiation medical imaging detectors for a variety of clinical and biomedical applications.

References

1. A. Reznik, S. D. Baranovskii, O. Rubel, G. Juska, S. O. Kasap, Y. Ohkawa, K. Tanioka, and J. A. Rowlands, Journal Appl. Phys. 102, 053711 (2007).
2. S. Kasap, J.A. Rowlands, S.D. Baranovskii, K. Tanioka, Journal Appl. Physics 96, 2037 (2004)
3. D.C Hunt, K. Tanioka, J.A. Rowlands, Medical Physics, 34, 976 (2007)
4. Kubota, M., Kato, T., Suzuki, S., Maruyama, H., Shidara, K., Tanioka, K., Sameshima, K., Makishima, T., ‍ Tsuji, K., Hirai, T., Yoshida, T., IEEE Trans. Broadcasting, ‍ ‍ 42(3), 251 (1996).‍ .
5. A. Reznik , S.D. Baranovskii, O. Rubel, K. Jandieri, S.O. Kasap, Y. Ohkawa, M. Kubota, K. Tanioka, J.A. Rowlands, Journal of Non-Crystalline Solids 354 2691 (2008).
6. A. Reznik , S.D. Baranovskii, O. Rubel, K. Jandieri, S.O. Kasap, Y. Ohkawa, M. Kubota, K. Tanioka, J.A. Rowlands, Journal of Non-Crystalline Solids 354 2691 (2008).
7. M. Wronski, W. Zhao, A. Reznik, K. Tanioka, G. Decscenzo, J. A. Rowlands, Med. Phys. 37 9 (2010).

D05: Photovoltaic cells and modules towards terrawatt era

Vitezslav Benda

Departmment of Electrotechnology, Czech Technical University in Prague, Czech Republic
Email: benda@fel.cvut.cz, web site: http://www.fel.cvut.cz

In the last decade, photovoltaics has been one of the most dynamically growing industries [1]. Impressive progress in PV technology over the past years is evident from the lower costs, the rising efficiency and the great improvements in system reliability and yield., Cumulative installed power yearly growths were on an average more than 40% in the period from 2000 to 2013, and in 2014, the global cumulative PV power installed has reached a level over 180 GW_p. The level 0.5 TW_p could be reached before 2020.

The production processes in the solar industry still have great potential for optimisation both wafer based and thin film technologies. This is reached by the combination of increased cell and module performance in conjunction with significantly reduced manufacturing cost especially at the cell and module level, by the efficient use of Si and non-Si materials. The wafer based crystalline silicon technologies have the role of workhorse of present PV power generation, representing nearly 90% of total module production. A decrease of crystalline-Si PV module cost below 0.4 €/W_p before 2017 can be expected.

In future, further progress can be achieved by new processes, new tools based on this processes, new materials and new designs of products. .

In order to create huge PV markets, the following criterion must be used in the selection of appropriate photovoltaic module manufacturing technology
- No material supply constrains
- Low cost of ownership
- Low production cost
- Prospects for further cost reduction
- High durability, low degradation rate (both LID and PID)
- Environmental safety and easy recycling

Technology improvements have to be implemented without significantly increasing costs per unit, despite the necessarily more complex manufacturing processes involved.

Very promising may be tandems of crystalline silicon and thin film cells, where efficiency over

30% might be reached [2],. Crystalline silicone proven technology could serve as a very good bottom cell in tandem and in combination with perovskit top cell is very promising for future development [3], using advantages of wafer based technology. Durability may be a limiting factor of this technology.

1. EPIA Global Market Outlook for Photovoltaics 2014 -2018, EPIA report, June 2014
2. Green, M. A., Hao1, X; Bremner, S;et al,: Silicon Wafer-Based Tandem Cells: The Ultimate Photovoltaic Solution?, Proc. 28th European Photovoltaic Solar Energy Conference, 2013, pp.7-
3. P. Loper, B. Niesen, S.-J. Moon, et al., Organic-Inorganic Halide Perovskites: Perspectives for Silicon-Based Tandem Solar Cells, IEEE J. Photovolt. 4 (2014) 1545–1551

D06: Quantitative Analysis of Coal Using Laser Induced Breakdown Spectroscopy

Zhe Wang[1], Zongyu Hou[1]

[1]State Key Lab of Power Systems, Department of Thermal Engineering, Tsinghua-BP Clean Energy Center, Tsinghua University, Beijing, 100084, China Email: zhewang@tsinghua.edu.cn

Fast or online coal analysis is extremely important for combustion optimization, energy saving and emission control in power plant. Laser-induced breakdown spectroscopy (LIBS) has a great potential in online coal analysis due to its advantages such as fast measurement and multi-elements analysis. Currently, LIBS is under through a critical time before successful commercialization in quantitative analysis, while the main obstacles are the low signal repeatability and prediction accuracy.

Averaging the spectra from multi-pulse was a commonly used method to improve the signal repeatability of LIBS. While partial least square (PLS) was a popular multivariate model to improve the accuracy of LIBS analysis. In this work, it was illustrated that the averaged spectrum can eliminate only the random noise but has no effect for nonrandom noise, and the traditional PLS model will accumulate the variations of different spectral lines so as to reduce the repeatability of the predicted value. Thus, using PLS and averaged intensity will results in low repeatability of the predicted results. The dominant factor based PLS model with spectral line standardization was proposed to improve the repeatability and accuracy. The spectral line intensities from a single pulse were corrected by the unique property of the plasma so as to get standard line intensities with standard plasma parameters. With the standardized line intensities, the lines of major elements were then used to construct the dominant factor because they are more reliable and repeatable. The lines of minor and trace elements were used to compensate the residue of the dominant factor. Comparing to traditional PLS model, the relative standard deviation (RSD) of the predicted carbon content in coal was reduced from 2.11% to 0.89%, and the error of the calibration was reduced from 1.87% to 1.26%. The precision and accuracy of the results were very close to the national standard of coal chemical analysis. Besides the carbon content analysis, the hydrogen content analysis and proximate analysis of coal such as volatile content, heat value, and ash content were also demonstrated in laboratory and onsite. The results of LIBS are all very close to the national standard of coal chemical analysis, indicating the feasibility and prospect of LIBS on quantitative and online coal analysis.

D07: Catalyst-free growth of ZnO nanowires on sapphire substrates by various steps of laser processing

Tetsuya Shimogaki[1], Masahiro Takahashi[1], Mitsuhiro Higashihata[1], Hiroshi Ikenoue[1], Daisuke Nakamura[1], Yoshiki Nakata[2], Tatsuo Okada[1]

[1]Department of Information Science and Electrical Engineering, Kyushu University, Fukuoka, Japan Email:Shimogaki@laserlab.ees.kyushu-u.ac.jp
[2] Institute of Laser Engineering, Osaka University, Osaka, Japan

Zinc oxide (ZnO) has attracted the attention for the reasonable material for piezoelectric devices, sensing devices, field emitting devices, and ultraviolet light emitting diodes (UV-LED). We have been trying to realize ZnO-based electric devices using ZnO nanowires. ZnO nanowires, which are characterized by their unique configurations and fine structures, can be synthesized by various methods. In our study, ZnO nanocrystals have been synthesized on sapphire substrates using nanoparticle assisted pulsed laser deposition (NAPLD) [1]. Since it can be achieved without catalyst or etching process, more simple and reasonable fabrication than hydrothermal than MOCVD can be expected. The configuration of ZnO nanocrystals could be controlled by experimental conditions. ZnO nanowires were fabricated in relatively higher pressure (> 100 torr) and at high temperature (> 700 °C). In this report, the overview of ZnO nanowire growth is discussed such as the dependence on orientation of sapphire substrates and the effect of surface laser treatment of ZnO buffer layers.

ZnO buffer layer has a big role when ZnO nanowires are grown on substrates with large lattice mismatches. Basically, the ZnO buffer layer relaxes lattice mismatches. In NAPLD, thin buffer layer is firstly grown on substrates, then ZnO nanowires are grown on it. In this study, we deposited the ZnO buffer layer in advance by pulsed laser deposition. Then, we investigated morphological and optical variations due to orientations of sapphire substrates. It was resulted that ZnO buffer layer was grown along <001> direction on *a*-cut and *c*-cut sapphire substrates. They had high in-plane orientation, but it was found by electron back scattering diffraction measurement that their directions were varied. These results are in good agreement with Melton's report about growth theory of GaN crystal on sapphires, which has similar crystalline structure as ZnO. [2] On the other hand, ZnO buffer layer deposited on *m*-cut sapphire was grown along <100> direction.

ZnO nanowires were grown on the ZnO buffer layers by NAPLD. Figure 1 shows the images observed by a scanning electron microscopy (SEM). In the case of using ZnO buffer layer deposited on the *a*-cut sapphire substrate, most of nanowires were grown perpendicularly to the normal line of the buffer layer. In the case of *c*-cut, nanowires were grown densely and the growth direction was not uniformed. In the case of m-cut, few nanowires were grown with tilt to normal line of the substrate. Number densities of nanowires differed as $N_c > N_a > N_m$. In addition, it was achieved that periodic micro-patterned ZnO nanowires were fabricated on ZnO buffer layers by four-beam interference laser-patterning. The talk will describe our experiments and evaluations, then future prospects of applications of ZnO nanowires will be discussed.

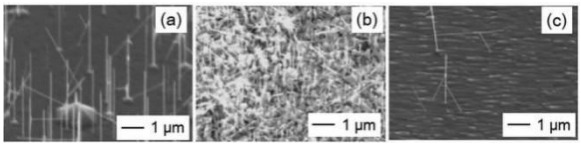

Fig1. SEM images of ZnO nanowires grown on ZnO buffer layers deposited on (a) *a*-cut, (b) *c*-cut, and (c) *m*-cut sapphire substrates.

1. R. Q. Guo, J. Nishimura, M. Matsumoto, D. Nakamura, and T. Okada, *Applied Physics A* **93**, 843 (2008).
2. W. A. Melton and J. I. Pankove, *Journal of Crystal Growth* **178**, 168 (1997).

D08: Integrated Circuits for Analog Optical Applications

Vincent J. Urick

Applied RF Photonics Section, U.S. Naval Research Laboratory, Washington, DC, USA
Email: vincent.urick@nrl.navy.mil

The field of microwave photonics continues to provide niche solutions for a variety of problems despite extraordinary advances in digital electronics and signal processing. Application opportunities for analog photonics include the generation, distribution and processing of signals in both public and military sectors, boasting advantages such as wide bandwidth, low propagation loss, invulnerability to electromagnetic interference, low latency, small size and weight, and good radio-frequency (RF) phase stability [1]. Lacking in high-volume

applications, microwave photonics has always leveraged technology stemming from commercial telecommunications. Decades of industrial development on photonic integrated circuits (PICs) has now resulted in an infrastructure to help fuel the emerging area of integrated microwave photonics [2]. Microwave PICs offer numerous advantages over traditional photonic approaches while retaining most of the attractive features offered by fiber optics. For example, the environmental stability of a PIC will typically exceed that of the same circuit when implemented in fiber-based components. This can allow for feasible implementations of coherent optical structures, which have great potential for microwave photonics. There are a variety of materials to consider for implementing PICs with two of the leading candidates being InP and Si. Full-scale integration including lasers, modulators and photodetectors is more practical in InP [3,4] although significant steps have been made to that end in Si [5,6]. Both have additional advantages and downfalls but the decision of which to pursue relies on the desired functionality. However, other materials should not be discounted to fill niche applications in the field of analog photonics.

This presentation will review the present application opportunities for PICs in analog photonics including a summary of the often unique requirements in the field. A few examples of PICs designed to leverage optically coherent techniques will be described, such as shown in Fig. 1. Finally, an outlook on the uncertain future of integrated microwave photonics will be offered.

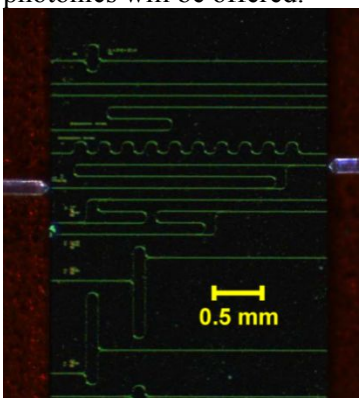

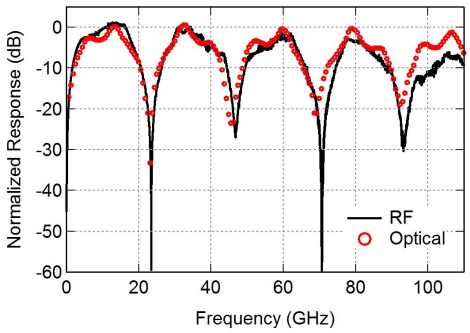

Fig. 1. (Left) Image of a fiber-coupled chip containing numerous silicon-on-insulator Mach-Zehnder interferometers for analog signal processing. (Right) Measured results demonstrating a radio-frequency (RF) filter function.

1. V. J. Urick, J. D. McKinney, and K. J. Williams, *Fundamentals of Microwave Photonics*, Wiley (2015).
2. D. Marpaung, et al., "Integrated microwave photonics," *Laser & Photonics Review* **7**, 506-538 (2013).
3. R. Nagarajan, et al., "InP photonic integrated circuits," *IEEE J. Sel. Top. Quant. Electron.* **16**, 1113-1125 (2010).
4. L. A. Coldren, et al., "High performance InP-based photonic ICs—a tutorial," *J. Lightwave Technol.* **29**, 554-570 (2011).
5. M. J. R. Heck, et al., "Hybrid silicon photonic integrated circuit technology," *IEEE J. Sel. Top. Quant. Electron.* **19**, 6100117 (2013).
6. G. Fish, "Heterogeneous photonic integration for microwave photonic applications," in *OFC Tech. Dig.*, OW3D.5 (2013).

B06: Singlet Fission in Polyene-type Materials

Andrew J. Musser[2], Jenny Clark[1]

[1]*Department of Physics and Astronomy, University of Sheffield, Sheffield, S3 7RH, UK. Email:jenny.clark@sheffield.ac.uk, web site: http://www.jennyclark.staff.shef.ac.uk*

[2]*Cavendish Laboratory, University of Cambridge, J J Thomson Avenue, Cambridge, CB3 0HE, UK.*

Singlet fission (see Fig.1) is a process by which the bright singlet (spin-0) exciton spontaneously

splits into two triplet (spin-1) excitons. The triplets are initially coupled into an overall singlet state, conserving spin. Our recent work shows that singlet fission in polyenes is ultrafast (<90 fs) and surprisingly robust to changes in intermolecular structure [1, 2]. Fig.1 shows a schematic of the main photophysical processes in polyenes. In isolated short-chains ('monomer'), excitation to the bright exciton (1Bu) is followed by internal conversion (~100 fs) to the first excited singlet state (2Ag). In aggregates or long polymer chains, singlet fission occurs on a time-scale faster than or comparable to internal conversion directly from the bright 1Bu exciton. This last finding contradicts the currently accepted polyene model [3-5].

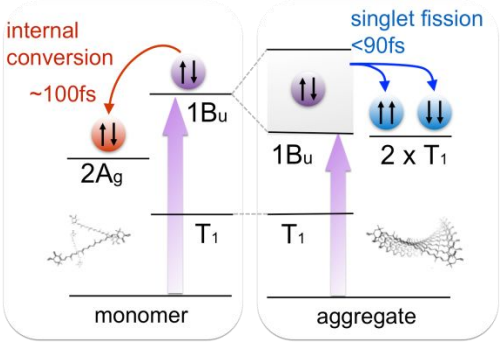

Fig. 1. Energy Level Schematic for Polyenes.

We have studied both intra- and inter-chain singlet fission, most recently in a series of five distinct carotenoid (naturally occurring small polyene) aggregates whose absorption spectra are shown in Fig.2. Singlet fission occurs with a similar time-constant (65-90 fs) in all aggregates: whether strongly (aggregates I,V) or weakly (II, III) coupled or with large (I) or small (V) energetic driving force (energy difference between singlet and triplet pair state). Comparison with the more established polyacenes, which show adiabatic (coupling-independent) fission rates only for the most strongly coupled systems (pentacene and TIPS) [6], suggests that singlet fission remains in the adiabatic regime in all of the carotenoid aggregates studied and may reflect a unique property of singlet fission in polyenes.

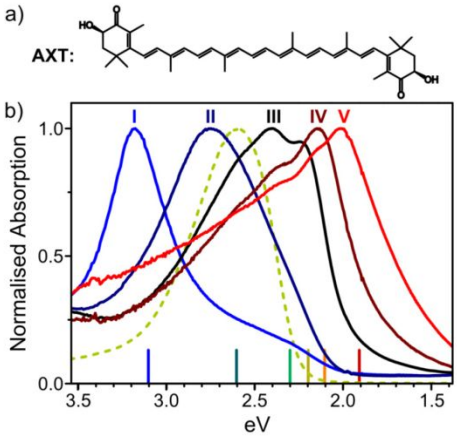

Fig. 2. (a) Astaxanthin structure,(b) Normalised absorption spectra of astaxanthin monomer (green dashed) and five aggregates (I-V).

[1] A.J. Musser, M. Al-Hashimi, M. Mauri, D. Brida, M. Heeney, G. Cerullo, R.H. Friend, J. Clark*J Am Chem Soc*, *135*, 12747 (2013).
[2] A. J. Musser, M. Mauri, D. Brida, G. Cerullo, R. H. Friend and J. Clark *J. Am. Clem. Soc.*, 137, 5130 (2015).
[3] B. Kraabel, D. Hulin, C. Aslangul, C. Lapersonne-Meyer, M. Schott, *Chem Phys* 227, 83 (1998).
[4] G. Lanzani, S. Stagira, G. Cerullo, S. De Silvestri, D. Comoretto, I. Moggio, C. Cuniberti, G.F. Musso, G. Dellepiane, *Chem Phys Lett 313,* 525 (1999).
[5] C. Wang, M.J. Tauber *J Am Chem Soc 132*, 13988 (2010).
[6] S.R. Yost, et al., *Nature Chemistry 6*, 492 (2014).

B07: Uncovering Structure-Function Relationships for Singlet Exciton Fission

Aaron K. Le,[1] Jon Bender,[1] & Sean T. Roberts[1]

[1]*Department of Chemistry, University of Texas at Austin, Austin, TX, USA Email: roberts@cm.utexas.edu, web site: http://www.cm.utexas.edu/sean_t_roberts*

Singlet exciton fission is a process that occurs in select organic chromophores wherein a photoexcited molecule in a spin singlet state uses approximately half of its excess energy to

excite a second electron on a neighboring molecule. As a process that effectively excites two electrons from a single photon absorption event, singlet fission dyes can provide a path towards the inexpensive design of multijunction photovoltaic cells that mitigate thermalization losses by using high energy photons to excite more than one electron-hole pair. Achieving such a system requires the design of materials that undergo singlet fission in high yield and the ability to pair these materials with a complimentary absorber that can both harvest low energy photons and accept triplet excitons that are generated by the singlet fission material. To date, the bulk of the experimental work investigating singlet fission has focused on the family acene dyes as these materials have been demonstrated to undergo fission in high quantum yield. However, incorporating acenes into photoharvesting systems remains a challenge due to their modest absorption cross-sections and low degree of photostability relative to other organic dyes. In contrast, the family of perylene diimide (PDI) dyes have long been used as synthetic pigments due to their strong absorption features and high degree of photostability. Like the acenes, PDIs possess a low lying triplet energy that makes them well situated to undergo singlet fission. Here, we report the results of transient absorption and photoluminescence studies carried out on a series of polycrystalline PDI thin films whose crystalline packing arrangements have been systematically varied by tuning the chemical functionalization of the central PDI chromophore. We find that introducing some degree of slip along both the transverse and longitudinal directions of the PDI core correlates with the production of triplet excitons. In contrast, slippage along only the longitudinal direction appears to promote excimer formation, likely due to a reduction of the singlet energy relative to the triplet due to excitonic coupling. Our results demonstrate that achieving the proper intermolecular arrangement of molecules in thin films is critical to achieving a high SF yield.

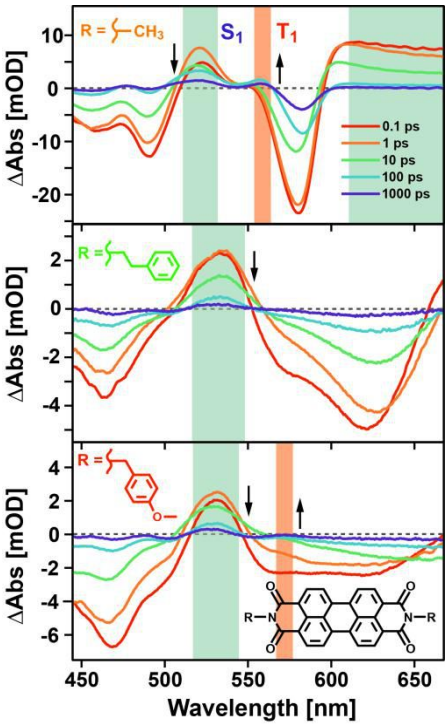

Figure 1: Transient absorption spectra measured for three different PDI thin films wherein the central PDI chromophore has been functionalized with different alkyl groups (λ_{Ex} = 560 nm). Each film is polycrystalline, but differs in the degree of slippage between cofacial PDI planes, with the phenyl substituted films experiencing slip primarily along the long PDI axis while the methyl substituted film is slipped along both the short and long PDI axis. Only the methyl substituted film shows strong evidence of triplet formation (red band).

Once formed, triplets produced by singlet fission need to be extracted from a film. As triplets primarily transfer via Dexter energy transfer, the density of states formed at an interface between a singlet fission material and a complimentary red absorber has a critical impact on the rate of energy transfer between them. While many beautiful techniques exist for characterizing the electronic properties of exposed surfaces, accessing the density of states of buried interfaces still presents a large experimental challenge. To address this issue, our lab has developed a broadband electronic sum frequency generation (ESFG) spectrometer that can be used to directly characterize the density of states at organic-inorganic interfaces. As an even order nonlinear spectroscopy, ESFG is only generated from portions of a sample that experience a

breakage of inversion symmetry, which naturally occurs at material interfaces. In addition to our work on PDI films, we will discuss the implementation of our ESFG spectrometer and show preliminary data measured for thin films of organic aggregates.

B08: Extended Charge Carrier Lifetimes in Hierarchical Donor-Acceptor Supramolecular Polymer Films

Amy M. Scott

Chemistry Department, University of Miami, 1301 Memorial Drive, Coral Gables, FL 33146 Email:amscott@miami.edu, web site: http://www.as.miami.edu/chemistrylabs/ScottGroup/

Supramolecular polymers are a promising class of materials that could potentially be used for preparing organized films that undergo photoinduced charge separation. Supramolecular polymers are macromolecules whose monomers repeat noncovalent bonds hold units together, and their noteworthy characteristics include assembly from easy-to-prepare small molecules, hierarchical structure, and stimuli responsiveness. Several systems have been explored in the context of photoinduced charge separation in solution and the solid-state, including a system we developed composed of a mono-diamidopyridine diketopyrrolopyrrole (mDPP) electron donor and a perylene bisimide (PDI) electron acceptor that assembles into 2:1 mDPP:PDI helical supramolecular polymers as the result of cooperative hierarchical assembly involving π•••π stacking and H-bonding. In solution, this mDPP-PDI supramolecular polymer undergoes ultrafast photoinduced charge separation into $mDPP^{\bullet+}$- $PDI^{\bullet-}$ followed by a recombination τ_{CR} = 33 ps. Thus we sought to investigate whether this emergent photophysical property – photoinduced charge separation – observed when the donor-acceptor superstructures formed in solution could be translated to the solid state. The challenge however is that the structures of supramolecular polymers that arise in solution and that produce the desirable emergent properties are not always maintained in thin films, and the effect of the condensed phase on photophysical properties are difficult to anticipate. Herein we report how mDPP:PDI supramolecular polymer structure is maintained in the solid state with order at the molecular and micrometer length scales, leading to photoinduced charge separated states that persist a thousand fold longer in the solid-state than in solution. This finding is significant because charge carrier lifetime is directly related to the ability to collect and use the resulting charges.

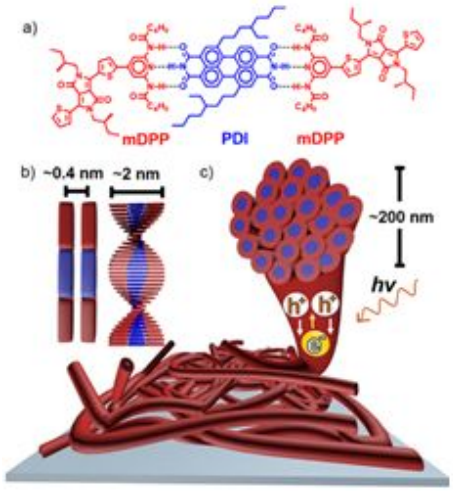

Figure 1. a) Chiral mDPP donor (red) and the PDI acceptor (blue) form 2:1 aggregates as a results of H-bonding. b) π-stacking orthogonal to the H-bonding creates donor-acceptor superstructures with helical chirality. c) Drop-casting of a 2:1 mDPP:PDI solution results in films comprised of hierarchical ropes whose fibers are the chiral superstructures that contain π-channels for transport following photoinduced charge separation.

B09: Signatures of charge transfer in the fifth-order nonlinear response

Arend G. Dijkstra

Max Planck Institute for the Structure and Dynamics of Matter, Hamburg, Germany Email:arend.dijkstra@mpsd.mpg.de

Charge transfer is essential for the function of natural and artificial light harvesting systems. In biological photosynthetic systems energy in the form of excitons is transported to the reaction center, while in bulk heterojunction photo-

voltaic cells it moves to an interface between different materials. Subsequently, the exciton decays into a charge transfer state, where electron and hole are spatially separated. It is clear that the charge transfer process is of fundamental interest. However, it has so far been difficult to observe it directly, because the charge transfer states are dark and therefore not directly visible in optical experiments. Furthermore, it is not clear how the signature of charge transfer can be separated from signal originating in vibrational motion.

Here, we have performed a rigorous study of a charge transfer system coupled to an underdamped vibration. We find that it is difficult to extract information on the charge transfer from linear or third-order spectroscopies. In fact, waiting time traces in the two-dimensional spectrum are dominated by vibronic coherence. Vibrations also affect the exciton dynamics. We find, however, that the fifth-order nonlinear spectrum is very sensitive to the charge transfer. We propose an experiment called 'two-dimensional population spectroscopy'. We find that, in this technique, the presence of charge transfer can qualitatively change the spectrum.

The figure shows our calculated fifth-order response function without charge transfer (panel iii) and with charge transfer (panel iv). A different sign of the response is observed, as is plotted in blue and red/green/yellow colors.

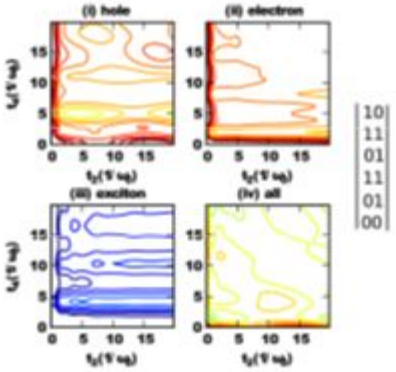

1. A. G. Dijkstra and Y. Tanimura, J. Chem. Phys. **142**, 212423 (2015).
2. A. G. Dijkstra, C. Wang, J. Cao and G. R. Fleming, J. Phys. Chem. Lett. **6**, 627 (2015).

B10: Energy Transport in Nanotubular Supramolecular Cyanine Aggregate Systems

Emma Leigh Kreuger[1], Katie Ann Clark[1], David A. Vanden Bout[1]
[1]*Chemistry Department, University of Texas, Austin,TX, USA*
dvandenbout@cm.utexas.edu

Exciton transport lengths in well separated and bundled cylindrical 3,3'-bis- (2-sulfopropyl)-5,5',6,6'-tetrachloro-1,1'-dioctylbenzimida-carbocyanine (C8S3) J-aggregates were measured using direct imaging of fluorescence emission with highly localized excitation. Fluorescence confocal images of the aggregates, deposited on a glass substrate, were collected and regions of interest within the sample were identified. These regions were probed with a focused laser spot, and the resulting emission was imaged onto an electron multiplying charged coupled device camera. A two dimensional Gaussian fitting scheme was used to quantitatively compare the excitation beam profile to the broadened aggregate emission profiles. We report one-dimensional average energy transport lengths of 60 nm along well-separated cylindrical C8S3 J-aggregates. Energy migration in bundled samples was found to span much longer length scales (hundreds of nm). Additionally, exciton delocalization both along and across bundles indicates that energy transport is two dimensional in the bundled J-

aggregate samples.[1] Further results will be discussed on efforts to stabilize the aggregate systems in polymer matrixes as well as accelerating bundle formation by controlling the ionic strength of solutions.

1. K. A. Clark, E. L. Krueger, and D. A. Vanden Bout, *J. Phys. Chem. Lett.*, ***5***(13), 2274-2282 (2014).

B11: Direct imaging of long-range exciton transport in porphyrin aggregates by ultrafast microscopy

Yan Wan,[1] Anna Stradomska,[2] Jasper Knoester, [3] and Libai Huang[1]

[1]*Department of Chemistry, Purdue University, West Lafayette, IN 47907, USA*
libai-huang@purdue.edu,
www.chem.purdue.edu/huang
[2]*School of Chemistry, University of Glasgow, Glasgow, G12 8QQ, Scotland, UK.*
[3]*Zernike Institute for Advanced Materials, University of Groningen, Nijenborgh 4, 9747AG Groningen, The Netherlands*

Molecular aggregates formed by self-assembled dye molecules represent one of the most promising constructs for efficient exciton transport materials that mimic photosynthetic antennas. Because the intermolecular coupling can be tuned by both synthetic chemistry and self-assembly tools, exciton transport in these assemblies provides model systems in the intermediate coupling regime to understand the interplay between coupling and disorder, coherent and incoherent pathways. We employ tubular molecular aggregates derived from meso-tetra(4-sulfonatophenyl) porphyrin (TPPS4) as a model system for long-range biomimetic energy transport. Here we present our recent work on direct imaging of excitons transport in porphyrin nanotubes by mapping exciton population with ~ 200 fs temporal resolution and ~ 50 nm spatial precision using transient absorption microscopy (TAM).

An example of TAM imaging of exciton transport are shown in Figure 1. The probe wavelength is in resonance with the lowest Q exciton transition measuring ground state bleaching, and the signal intensity is proportional to exciton population. As shown in Figure 1, exciton transport is remarkably fast with transport length up to ~ 50 nm in 3 ps as deduced from the population profiles at 0 and 3 ps. We have directly measured a diffusion constant of ~ 10 cm^2/s, more than three orders of magnitude larger than exciton diffusion in disordered organic materials such as conjugated polymer thin films. Theoretical modeling of exciton transport will also be discussed.

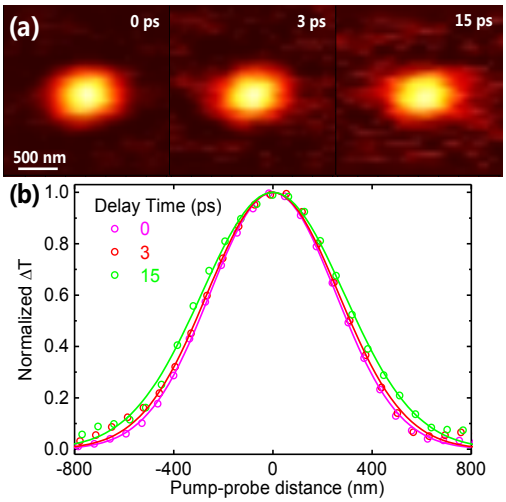

Figure 1. (a) Transient absorption microscopy (TAM) imaging of exciton population of a porphyrin nanorod at different delay pump-probe times. The images show the spatial distribution of the Δ T signal measured at pump-probe delay time as labeled. (b) Cross-sections of the TAM images fitted with Gaussian functions at different time points along the long axis of the nanorod, with the maximum ΔT signal normalized.

B12: Exciton dynamics in tubular porphyrin aggregates

Anna Stradomska[1]
[1]*School of Chemistry, University of Glasgow, Glasgow, United Kingdom*
Email:anna.stradomska-szymczak@glasgow.ac.uk

Self-assembled tubular aggregates, such as those formed by TPPS4 porphyrin ([1], see figure 1), are a novel class of materials that mimics the structure of photosynthetic antenna system of

green sulphur bacteria (the chlorosomes). They exhibit unique linear and non-linear optical properties as well as effective excitation energy transport. Therefore they are of fundamental interest as a model for understanding the photophysical processes occurring in natural light harvesting complexes, and as systems to study the nature and dynamics of excited states in molecular assemblies of low dimensionality. Potential applications for optoelectronics, energy transport, and artificial light harvesting make them attractive from the practical perspective.

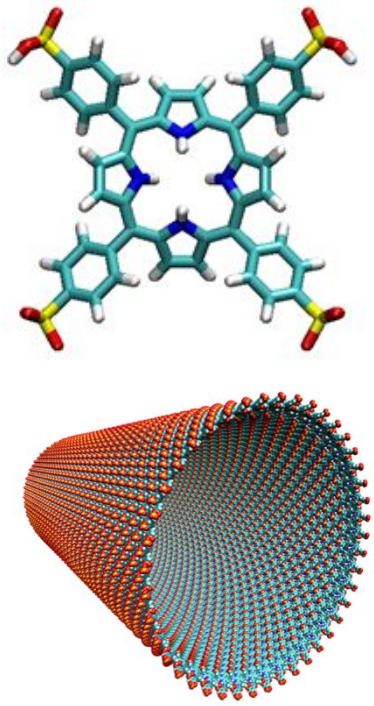

Fig1. Structure of the monomer and the aggregate of TPPS4 porphyrine.

In this contribution I will present results on theoretical modelling of the excited state dynamics in single-walled TPPS4 porphyrin nanotubes. In order to account for all the relevant interactions operative in the studied system, our approach combines several methods rooted in exciton theory. In particular, we account for (i) the intermolecular resonance interactions between the molecules in the aggregate, (ii) the influence of the static disorder, and (iii) the interactions with the continuum degrees of freedom in the environment (the thermal bath). We obtain a good agreement between the theory and experimental spectroscopic data, and are able to explain the mechanism responsible for the lack of temperature dependence of absorption linewidths, as well as very low fluorescence quantum yield reported in the experiments on TPPS4 nanotubes. Finally, we study the exciton diffusion in porphyrin nanotubes and find a good agreement with recent experiments.

1. S.M. Vlaming, R. Augulis, M.C.A. Stuart, J. Knoester, and P.H.M. van Loosdrecht, *J. Phys. Chem. B* **113**, 2273 (2009).
2. A. Stradomska and J. Knoester, *J. Chem. Phys.* **133**, 094701 (2010).
3. Y. Wan, A. Stradomska, S. Fong, Z. Guo, R.D. Schaller, G.P. Wiederrecht, J. Knoester, and L. Huang, *J. Phys. Chem. C* **43**, 24854 (2014).

B13: Coherent Transport in Light-harvesting and Nano-scale Systems

Jianshu Cao

Department of Chemistry, MIT, Cambridge, MA 02139, USA

Email: Jianshu@mit.edu

The focus of the talk is quantum coherence, which plays a key role in exciton transfer of light-harvesting systems, charge mobility of organic semi-conductors, and heat transfer in nano-systems.

(1) The transfer process in between LH2 rings is dramatically enhanced by the coherence resulting from the 9-fold ring symmetry, which will be explained by the minimal frustration consideration. Further, we have developed a numerically exact method based on stochastic path integrals (sPI) to predict emission spectra and generalized Forster rate of molecular aggregates and found that the enhanced rate in LH2 is 9ps without disorder and around 20ps with disorder, consistent with experimental measurements.

(2) We have studied coherent quantum transport in disordered systems and showed an optimal diffusion constant at an intermediate level of noise/temperature. Detailed calculations indicate the crucial role of coherence length and predict charge mobility in organic semi-conductors close to experimental values. Further, we have explored 1D-2D transition in the diffusion of nanotubes and the possibility of ballistic dynamics in 2-D dipolar lattices.

(3) Classical Fourier law of heat transfer is based on the diffusion picture. Exact calculations indicate ballistic dynamics in harmonic lattices and in one-dimensional spin chains. However, in spin ladders, quantum transport can be diffusive. We have developed a theoretical framework to explain the ballistic-diffusive transition in quantum lattices.

B14: Modeling Excitation Energy Transport in Supramolecular Systems

Jasper Knoester[1]

[1]*Zernike Institute for Advanced Materials, University of Groningen, Groningen, The Netherlands*
Email: j.knoester@rug.nl

Transport and other dynamical properties of electronic and vibrational excitations in molecular systems are crucial for their functional properties, which may include light emission, light harvesting, energy transduction, etc. In systems that contain many chemically identical building blocks, such as molecules in light-harvesting aggregates or amide groups in polypeptides, the excitations are (partially) delocalized, which potentially leads to fast, coherent transport. Interactions with static and dynamic degrees of freedom in the environment, will lead to disorder and dephasing and strongly influence transport properties. The two normally considered extreme situations are ballistic and diffusive transport. Modeling dynamic and transport properties in the type of systems mentioned is hard, due to the complex interplay of degrees of freedom that play a role.

In this presentation, I will discuss theoretical methods that we have developed over the past decade to model the dynamics and transport properties of collective excitations in supramolecular systems and address examples of systems that we have studied this way. Our methods range from perturbatively treated (Redfield theory) phenomenological models to ab initio QM/MD calculations. Examples of systems investigated by us are: (i) Linear molecular aggregates with an energy gradient, where we have shown the competition between downward exciton transport and Bloch localization of the excitons to lead to nonmonotonic dependence of transport speed on the energy gradient [1]; (ii) Linear molecular aggregates with Lévy disorder, where we have shown the occurrence of exchange broadening, nonuniversal exciton localization, and subdiffusive motion [2,3]; (iii) Light-harvesting system 2 (LH2) of purple bacteria, where we have used ab initio modeling to show that transport from the B800 ring to the B850 ring takes place via states that are partially delocalized over both rings [4]; (iv) Energy transport along amide I and II vibrations in alpha helices, where we have shown the possibility to experimentally probe various intra- and inter-band components of these dynamics by using polarization resolved two-dimensional infrared spectroscopy [5].

1. S.M. Vlaming, V.A. Malyshev, and J. Knoester, *J. Chem. Phys.* **127**, 154719 (2007).
2. A. Eisfeld, S.M. Vlaming, V.A. Malyshev, and J. Knoester, *Phys. Rev. Lett.* **105**, 137402 (2010).
3. S.M. Vlaming. V.A. Malyshev, A. Eisfeld, and J. Knoester, J. Chem. Phys. **138**, 214316 (2013).
4. N. van der Vegte, J. Prajapati, U. Kleinekathoefer, J. Knoester, and T.L.C. Jansen, *J. Phys. Chem. B* **119**, 1302 (2015).
5. A.G. Dijkstra, T.L.C. Jansen, and J. Knoester, *J. Phys. Chem. B* **115**, 5392 (2011).

C10: Physics of Metal/Ge Interfaces; Fermi-level Unpinning and Interface Disorders

Takashi Nakayama

Department of Physics, Chiba University, 1-33 Yayoi, Inage, Chiba 263-9522, Japan
Email:nakayama@physics.s.chiba-u.ac.jp, web site: http://phys8.s.chiba-u.ac.jp/nakayamal/index.html

Germanium (Ge) has high carrier mobility compared to Si and is expected to work as a promising key material in next-generation high-speed devices. With respect to metal/Ge interfaces, however, there exist two serious issues to be overcome for applications; one is the control of Schottky-barrier height (SBH) and the other is the control of interface disorders. In this work, we discuss these issues based on fundamental properties of metal/Ge interfaces.

It is well known that a variety of metal/Ge interfaces show a strong Fermi-level pinning (FLP); the Fermi energies of various metals are located at similar energy positions around the valence-band edge of Ge irrespective of the kind of metal, which induces the difficulty in controlling the SBH by simply changing the kind of metal. By the first-principles calculations, we found that this FLP is caused by the small band gap of Ge and the long penetration depth of metal-induced gap states (MIGS) into Ge layers even at clean interfaces.[1] Moreover, by evaluating the formation energies of various defects and dynamical atom motions around the interface, we showed that the MIGS are well hybridized with electronic states of defects and become the leading actors to increase the interface disorders, as displayed in Fig.1(a) for the case of vacancy defect in Ge layers. Correspondingly, even at weakly FL-unpinned Fe_3Si/Ge interface, the interface defects also promote the FLP.[2]

One of recipes to release the FLP is to insert the third materials into the interfaces by the segregation of dopant atoms such as S and P and the transition layers made of semiconductor/oxide, similar to the cases of metal/Si interfaces. [3] As shown in Fig. 1(b), for example, we found that the appearance of ultrathin semiconducting α-Sn layers between metallic β-Sn and Ge layers works to increase the SBH for hole carriers, in agreement with the experiments. Similarly, when GeO_2 oxide is present between metal and Ge layers, the MIGS penetration into Ge layers is prohibited and the SBH increases to the original position.

These results are discussed in details, together with showing recent observations and focusing on the fundamental physics at metal/Ge interfaces

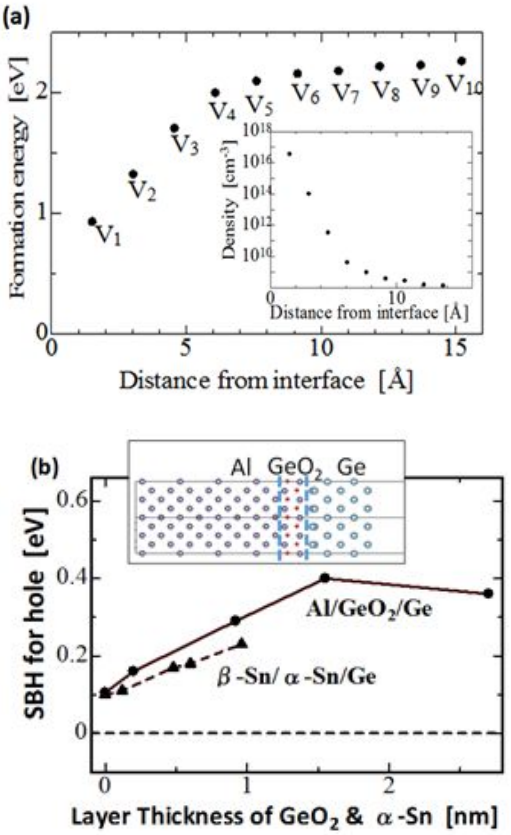

Fig1. (a) Calculated formation energy of Ge vacancy and its density (inset) around Al/Ge(100) interface, as a function of the distance of vacancy from the interface. (b) Calculated SBH for hole carriers at β-Sn/α-Sn/Ge(111) and Al/GeO_2/Ge(100) interfaces as functions of thicknesses of interfacial α-Sn and GeO_2 layers.

1. T. Hiramatsu et al., Jpn. J. Appl. Phys. **53**, 058006 (2014).
2. K. Kobinata and T. Nakayama, Jpn. J. Appl. Phys. **53**, 035701 (2014).
3. T. Nakayama and K. Kobinata, Thin Solid Films **520**, 3374 (2012).

C11: Synthesis and Characterization of Cd-free Buffer layers to be used in thin films solar Cells

[1]W. Vallejo, [1]C. Diaz-Uribe, [1]C. Fajardo

[1]Chemistry Program, Sciences School, Universidad del Atlántico, Barranquilla, Colombia. Email: williamvallejo@mail.uniatlantico.edu.co

Although thin film solar cells have lower industrial production costs and great stability, this technology has a limitation from the environmental point of view because they incorporate into their structure a thin layer of CdS (50nm); a highly toxic material, which is dangerous for man and the environment when devices are manufactured, and besides, they are potentially dangerous during the time that solar cell is in operation. Besides due to its band gap energy (2.4 eV), part of the incident radiation in the solar cell is absorbed in the buffer layer causing losses photocurrent [1]. Currently, manufacturing alternative Cd free buffer layers with optimal properties is a research topic in the field.

Buffer layers can be manufactured through out different methods such as thermal evaporation, atomic layer deposition (ALD), sulfurization, spputering, metal organic chemical vapor deposition (MOCVD), electrodeposition and CBD [2, 3]; currently the CBD process is the most commonly used synthesis method for synthesizing buffer layers; This method allows depositing thin films of different semiconductors with high adhesion, reproducibility and uniformity coverings, plus the equipment required for their synthesis are inexpensive. CBD method relies in strict precipitation (homogeneous and heterogeneous) of a chalcogenide (S, Se, Te i.e.) and a metal (Cd, Zn, In, Pb, Mg, i.e.); a complexing agent and buffer solution control pH and chemical species content into solution.

Figure 1 shows optical transmittance of buffer thin films based on Zn, In, and Cd. this spectra shows Cd free buffer layers have optical transmission higher than 80% in the visible range, this result is typical to buffer layers and it is higher than typical transmittance of CdS thin films layers. Table 1 listed the band gap to buffer layers synthesized; table 1 indicates Cd-free buffer layer shift the band gap to blue energies; this shift is very positive because of the blue response of solar cells is improvement. Finally, optical results suggest that both materials have adequate optical properties to be use as buffer layer because they have a bad gap bigger than CdS [5].

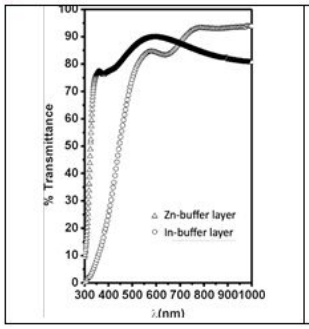

Buffer layer	Band Gap (eV)
Zn	3,68
In	2,64

Fig1. (a) Optical transmittance to buffer layers deposited by CBD (b) list of band gap value to buffer layers deposited by CBD

1. T. Klinkert, T. Hildebrandt, M. Jubault, F. Donsanti, J. Guillemoles, N. Naghavi, *Thin Solid films*, 582 (2015) 295-299.
2. M. Kriisa, R. Sáez-Araoz, C. Fischer, T. Kóhler, E. Kärber, Y. Fu, F Hergert, M. C. Lux-Steiner, M. Krunks, *Solar Energy,* 115 (2015) 562-568
3. M.A. Islam, M.S. Hossain, M.M. Aliyu, P. Chelvanathan, Q. Huda, M.R. Karim, K. Sopian, N. Amin, *Energy Procedia*, 33 (2013) 203-21
4. A.B. Green, C.D. Black, *Book title* (Publisher), 135 (2006).
5. A. Goudarzi, G. M. Aval, R. Sahraei, H. Ahmadpoor, Thin Solid Films 516 (2008) 4953–4957

C12: Growth and doping control of diamond semiconductor for junction device applications

Hiromitsu Kato*, Masahiko Ogura, Toshiharu Makino, Daisuke Takeuchi, Satoshi Yamasaki

Advanced Power Electronics Research Center, AIST, Tsukuba, Ibaraki 305-8568, Japan. CREST, JST, Chiyoda, Tokyo 102-0081, Japan.
**hiromitsu.kato@aist.go.jp*

P- and n-type doped diamonds underlay the design of virtually all electronic and optoelectronic applications. To achieve the valency control, comprehensive knowledge of the fundamental processes that control impurity doping is required. For *p*-type, the impurity boron is easily incorporated into both natural and synthesis diamonds, whereas n-type diamond, which is not present in nature, has been recently established by phosphorus doping [1,2]. The progresses in p- and n-type doping in diamond semiconductor have stimulated much research on the various types of p-n junction devices [3-6].

Diamond has been identified as a potential candidate for use in high-power and high-frequency devices owing to its superior physical and electric properties. The highest breakdown voltage among wide-band-gap semiconductors with high thermal conductivity and high saturation velocity potentially lead to a higher attainable power density. In addition, exciton-related devices [4], electron emitters with negative electron affinity [5], and single photon source [6] with excellent spin characteristics including long coherence time are also considered to be future applications utilizing the unique properties of diamond semiconductors.

Figure 1 shows the relationship between resistivity at room temperature and impurity concentrations. The acceptor and donor levels of diamond semiconductor are 370 meV by boron and 570 meV by phosphorus doping, respectively. Owing to these deep dopant levels, only a low free-carrier concentration is thermally generated from the dopants at room temperature. But, in the case of deep dopants, when the doping concentration increases, the carrier transport is changed from “band conduction” to “hopping conduction” through the impurity band states, and this hopping conduction can easily achieve lower resistivity. The combination of such low resistive hopping layer and the pure band conduction layer strongly support the recent diamond device fabrications, which can drive at room temperature.

Detailed aspects of doping control of diamond semiconductor and the electrical properties of fabricated unique diamond devices will be discussed.

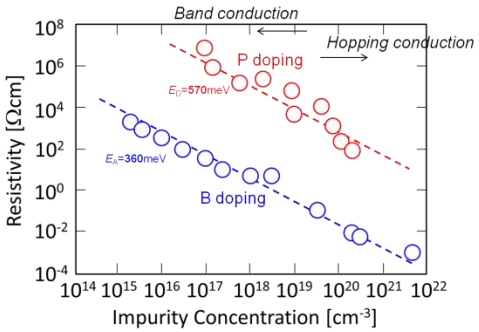

Figure 1. Relation between the resistivity at room temperature and impurity concentrations. Red and blue circles indicate the data for n-type phosphorus doping and p-type boron doping, respectively.

1. H. Kato, T. Makino, S. Yamasaki, and H. Okushi, J. Phys. D **40** (2007) 6189.
2. H. Kato, T. Makino, M. Ogura, N. Tokuda, H. Okushi, and S. Yamasaki, Appl. Phys. Express **2** (2009) 055502.
3. H. Kato, T. Makino, M. Ogura, D. Takeuchi, and S. Yamasaki, Diamond Relat. Mater. 27-28 (2012) 19.
4. T. Makino, K. Yoshino, N. Sakai, K. Uchida, S. Koizumi, H. Kato, D. Takeuchi, M. Ogura, K. Oyama, T. Matsumoto, H. Okushi, and S. Yamasaki, Appl. Phys. Lett. **99** (2011) 061110.
5. D. Takeuchi, et.al, Phys. Status Solidi A **210** (2013) 1961.
6. N. Mizuochi, T. Makino, H. Kato, D. Takeuchi, M. Ogura, H. Okushi, M. Nothaft, P. Neumann, A. Gali, F. Jelezko, J. Wrachtrup, and S. Yamasaki: Nat. Photonics **6** (2012) 299.

C13: Interferometric imaging for the detection of nanoparticles and for airborne instrumentation

S. Saengkaew, S. Coetmellec, D. Pejchang, D. Lebrun, G. Grehan and M. Brunel.

UMR CNRS 6614/CORIA, Université et INSA de Rouen, Avenue de l’Université,

76 800, Saint Etienne du Rouvray, France, Sawitree_s@coria.fr

Optical diagnostic techniques have a huge number of applications in the domains of energy, materials and nanotechnologies. Among the different possibilities, we demonstrate that the optical techniques based on interferences can be the sources of innovative and powerful approaches. In this talk, we will present innovative instruments devoted to two specifics applications: the characterization of nanoparticles suspension at low concentration and the characterization of atmospheric cloud composed of droplets and ice crystals.

To optically characterize low concentration nanoparticle suspensions, the main difficulty is the dependence of the signal intensity on the power 6 of the particle diameter (d^6). We introduced two alternative approaches to overpass this constraint. In air, the counting of nanoparticles is achieved by using condensation particle counters where an increasing of the nanoparticle size is obtained by the condensation of oil vapor. Similarly, we propose to increase the effective size of the nanoparticles in liquid by warming them enough to produce a liquid vapor bubble around them. The size of the bubble is a measurement of the nanoparticle size. Accordingly, we use a powerful pulse laser to warm the nanoparticle located in a droplet.
The difficulties are to be able to accurately measure the bubble size [1] and to find the relationship between the bubble size and the nanoparticle size [2]. In our presentation at Cancun, the accurate measurement of the bubble 3D location and size in a water droplet using in-line Holography technique will be described. Another approach called Fourier Interferometry Imaging (FII) has been introduced. This approach is based on the recording of the interference field created by the scattered light and its processing in the associated 2DFFT domain. The main advantage of this approach is the fact that the signal intensity does not depend anymore on d^6. The measurement of a temporal series of the location of traces in the 2DFFT domain is a characterization of the Brownian motion [3].

The characterization of clouds in the close vicinity of a plane is also a challenge where the interference approaches can be applied. By including the generalized Huygens-Fresnel integrals combined to optical transfer matrices, a powerful description of out-of-focus devices has been carried out permitting to design an airborne instrument and to extend is range of application from spherical droplets to irregular ice crystals [4, 5]. The airborne instrument can simultaneously measure spherical droplets and irregular ice crystals. The software is able to detect the contribution of water droplets and solid ice crystals from the recorded out-of-focus image. Then the appropriated processing strategy is applied to the different part of images permitting to measure the droplet diameter and the size of ice crystal.

[1] S. Coetmellec, D. Pejchang, D. Allano, G. Grehan, D. Lebrun and M. Brunel, Digital in-line holography in a droplet with cavitation air bubbles, Journal of European Optical Society-Rapid publications, 2014[2]
[2] A. Chaari, T. Grosges, L. Giraud-Moreau, D. Barchiesi, Numerical modeling of the photo-thermal processing for bubble forming around nanowire in a liquid. Sci. World J. 2014, 8.
[3] S. Saengkaew, A. Garo, S. Meunier-Guttin-Cluzel and G. Grehan, Counting and measuring nano particles by using Fourier Interferometric Imaging, NanoTech, Washingtong D.C., May, 2014
[4] M. Brunel, H.H. Shen, S. Coetmellec, G. Grehan and T. Delobel, Determination of the size of irregular particles using interferometric out-of-focus imaging, International Journal of optics, 2014, ID 143904, 8 pages
[5] M. Brunel, W. Wichitwong, S. Coetmellec, A. Masselot, D. Lebrun, G. Grehan and G. Edouard, Numerical models for the exact description of in-situ digital in-line holography experiments with irreglarly-shaped arbitrarily-located particles, Applied Sciences, 2015

C14: 2-D Materials for strong light-matter-interaction and photo conversion devices

Volker J. Sorger[1]

[1]*Department of Electrical & Computer Engineering, The George Washington University, 801 22nd Street NW, Washington, DC 20052, USA*
Email: sorger@gwu.edu

Recent investigations of semiconducting two-dimensional (2D) transition metal dichalcogenides have provided evidence for strong light absorption relative to its thickness attributed to high density of states. Stacking a combination of metallic, insulating, and semiconducting 2D materials enables functional devices with atomic thicknesses. While photovoltaic cells based on 2D materials have been demonstrated, the reported absorption is still just a few percent of the incident light due to their sub-wavelength thickness leading to low cell efficiencies. Here we show that taking advantage of the mechanical flexibility of 2D materials by rolling a molybdenum disulfide (MoS_2)/graphene (Gr)/hexagonal boron nitride (hBN) stack to a spiral solar cell allows for solar absorption up to 90%. The optical absorption of a 1 μm-long hetero-material spiral cell consisting of the aforementioned hetero stack is about 50% stronger compared to a planar MoS_2 cell of the same thickness; although the volumetric absorbing material ratio is only 6%. A core-shell structure exhibits enhanced absorption and pronounced absorption peaks with respect to a spiral structure without metallic contacts.

Strong light-matter-interactions (LMI) are achieved and investigated in cylindrical nanocavities comprised of 2D materials as the active absorber (Fig. 1). Stacking a combination of metallic, insulating, and semiconducting 2D materials enables functional devices with atomic thicknesses. Here we show that taking advantage of the mechanical flexibility of 2D materials by rolling a molybdenum disulfide (MoS_2)/graphene (Gr)/hexagonal boron nitride (hBN) stack to a spiral nanocavity, which allows for absorption up to 90% (here we tested solar radiation). A core-shell structure exhibits enhanced absorption and pronounced absorption peaks with respect to a spiral structure without metallic contacts. The resonances themselves suggest the cylinder spiral structure resembling a nanowire, and hence exhibiting Fabry-Perot cavity behavior. We confirm the latter via (i) investigating the modal features of this cavity (Fig. 1c), where the transverse (x-y direction, i.e. *x* in Fig. 1a) mode profile indicates a dipole for larger wavelength, which turns into quadruples and doubled-quadruples for blue shifting the resonance wavelength (6 to 1 in Fig. 1c). In addition the cavities' standing waves can be seen in the cross-sectional-longitudinal modal profile (i.e. *x'* Fig. 1a), where the mode spacing decreases with wavelength. The higher Q-factors observed of the core-shell cell relative to the spiral cell are visible in the crossectional mode profiles as distinct power density lopes (Fig. 1b). Interestingly, the absorbing materials (graphene and MoS_2) occupy only 6% of the total volume of spiral cells. This suggests that the ratio of solar energy absorption to volume of photoactive material was ~8:1 compared to a bulk MoS_2 photovoltaic cell of the same size. We name this ratio "enhancement" and define it as

$$\frac{\alpha_{spiral\ cell} - \alpha_{bulk\ cell}}{\alpha_{bulk\ cell}} \div \frac{t_{MoS2} + t_{Gr}}{t_{MoS2} + t_{Gr} + t_{hBN}} \quad (4)$$

where α denotes absorption and *t* refers to the respective physical layer thickness. This enhancement is proportional to the absorption efficiency and thickness of the hBN layer (Fig. 1d).

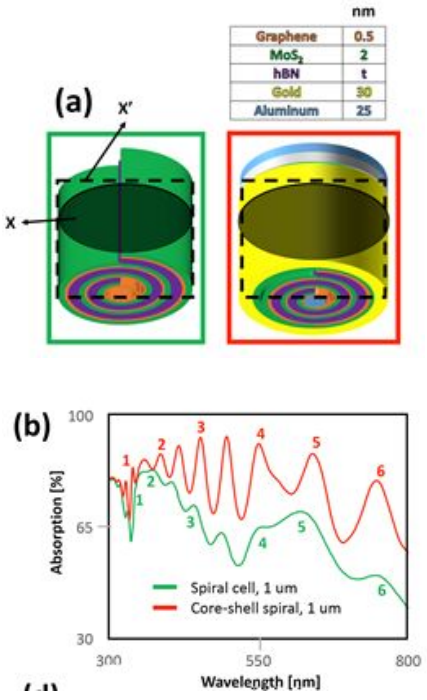

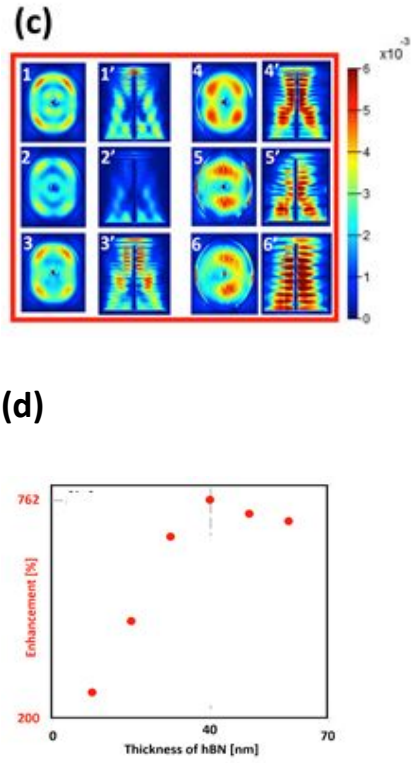

Fig1. (a) Schematic of spiral (left) and core-shell cavities (right). Horizontal (vertical) cross sections labeled by X(X') are power monitors recording profiles shown in (c). (b) Absorption efficiency of spiral cell and core-shell structure. (c) Wavelengths correspond to absorption peaks of the core-shell structure. (d) Optimization of hBN thickness to achieve highest LMI (Eqn 4) enhancement.

1. We acknowledge AFOSR financial support under award numbers FA9559-14-1-0215 and FA9559-14 1-037, and the National Science Foundation under award number NSF 1436330 and the Materials Genome Initiative (MGI).

C15: Sensitive Terahertz-wave detection and imaging by nonlinear frequency up-conversion

Hiroaki Minamide[1]

[1]*RIKEN Center for Advanced Photonics, Sendai, Miyagi, JAPAN*
Email: minamide@riken .jp, web site: http://www.riken.go.jp/lab-www/tera/

Development of laser-based sources and detection in the terahertz (THz) region has attracted much attention over the past 20 years. Furthermore, technologies available in the THz frequency range have shown great progress with those developed sources and detectors. Using nonlinear optical crystal, wavelength conversion between THz wave and infrared light was examined in earlier frontier studies. To achieve more efficient conversion, we have examined potential optical methods and have investigated conversion mechanisms in nonlinear optical crystals.

Recently, a remarkable breakthrough related to radiation peak-power over ten kilowatt or broad-band frequency-tunability covering tens of THz frequency were achieved using nonlinear optical wavelength-conversion [1-4]. Moreover, highly sensitive detection of terahertz-waves with wide dynamic range using frequency up-conversion at room temperature was obtained [5-11].

In nondestructive sensing applications, THz imaging has attracted a lot of interests for more than 10 years. But real time, high sensitive, low cost THz imaging in room temperature, which is widely needed by fields such as biology, biomedicine and homeland security, has not been fully developed yet. A lot of approaches have been reported on the raster scanning imaging technologies or using THz cameras with photoconductive antenna or microbolometer integrated. But they still have much limitation.
Our current research has proved that THz detection by nonlinear frequency up-conversion offers fast response up to nanosecond scale, and very high sensitivity with orders higher than Bolometer, attributed to the high nonlinear coefficient of the 4-Dimethylamino-N-Methyl-4-Stilbazolium Tosylate (DAST) crystal.

In this paper, we would like to introduce high-peak-power THz-wave generation, sensitive THz-wave detection at room temperature, and a real-time THz-wave imaging using nonlinear optical wavelength-conversion.

Acknowledgements

I'd like to thank all of previous and present team members for excellent research activities and thank Prof. Hiromasa Ito and Prof. Masafumi Kumano for research advices. This work was partially supported by Collaborative Research Based on Industrial Demand of the Japan Science and Technology Agency (JST), and JSPS KAKENHI Grant Numbers 26246046, 26620162, 15K18080, 25220606, 26287067, 26390106, 15K18079.

References

1. H. Minamide, S. Hayashi, K. Nawata, T. Taira, J. Shikata, and K. Kawase, Journal of Infrared, Millimeter, and Terahertz Waves 35, 25 (2014).
2. S. Hayashi, K. Nawata, T. Taira, J. Shikata, K. Kawase, and H. Minamide, Scientific Reports 4, 05045 (2014).
3. H. Minamide and H. Ito, Comptes Rendus Physique 11, 457 (2010).
4. H. Minamide, T. Ikari, and H. Ito, REVIEW OF SCIENTIFIC INSTRUMENTS 80, 123104 (2009).
5. H. Minamide, J. Zhang, R. X. Guo, K. Miyamoto, S. Ohno, and H. Ito, Appl. Phys. Lett. 97, 121106 (2010).
6. S. Fan, F. Qi, T. Notake, K. Nawata, Y. Takida, T. Matsukawa, and H. Minamide, Opt Express 23, 7611 (2015).
7. S. Fan, F. Qi, T. Notake, K. Nawata, T. Matsukawa, Y. Takida, and H. Minamide, Appl. Phys. Lett. 104, 101106 (2014).
8. F. Qi, S. Fan, T. Notake, K. Nawata, T. Matsukawa, Y. Takida, and H. Minamide, Opt. Lett. 39, 1294 (2014).
9. F. Qi, S. Z. Fan, T. Notake, K. Nawata, T. Matsukawa, Y. Takida, and H. Minamide, Laser Phys Lett 11, 085403 (2014).
10. F. Qi, K. Nawata, S. Hayashi, T. Notake, T. Matsukawa, and H. Minamide, Appl. Phys. Lett. 104, 031110 (2014).
11. K. Nawata, T. Notake, H. Ishizuki, F. Qi, Y. Takida, S. Fan, S. Hayashi, T. Taira, and H. Minamide, Appl. Phys. Lett. 104, 091125 (2014).

C16: New developments in guided-mode resonance nanophotonics

Robert Magnusson

Department of Electrical Engineering, University of Texas - Arlington, Arlington, Texas 76019, USA Email: magnusson@uta.edu, web site: http://www.leakymoderesonance.com/

Nanostructured surfaces and films are widely applied in nanoplasmonics and nanophotonics. Under the right conditions, as incident light couples to the film, attendant resonance effects impose diverse spectral signatures on the output light. The guided-mode resonance (GMR) concept refers to quasi-guided, or leaky, waveguide modes induced in periodic layers. Whereas the fundamental GMR occurs in any diffraction regime, subwavelength architectures often enable the most useful spectra. Even though these effects have been known for a long time, new attributes and application possibilities continue to appear. Wide parametric design spaces allow precise control of light amplitude, phase, polarization, near-field intensity, and light distribution on surfaces as well as within the device volume. The output spectra can be retrieved in either transmission or reflection. Applications such as laser mirrors, multiparametric biosensors, solar-cell absorption enhancement, tunable filters, narrowband nanoelectromechanical display pixels, nonlinear conversion, surface-enhanced Raman spectroscopy, slow-light control, leaky-mode nanoplasmonics, resonant Rayleigh reflectors, and many others have been suggested in the past.

In this paper, we review the physics of GMR device operation, illustrate their design with rigorous methods, discuss fabrication processes, and present results of physical and spectral characterization. We indicate the application potential of this field, discuss some past device examples, and provide new and emerging aspects. In particular, we present new wideband resonant reflectors designed with gratings in which the grating ridges are matched to an identical material thereby eliminating local reflections and phase changes. This critical interface therefore possesses zero refractive-index contrast; hence we call them “zero-contrast gratings.” For simple gratings with two-part periods, we show that zero-contrast grating reflectors outperform comparable high-contrast grating reflectors with nearly 700-nm bandwidth

achieved at 99% reflectance. We introduce a new class of reflectors and polarizers fashioned with dielectric nanowire grids that are mostly empty space. We provide computed results predicting high reflection and attendant polarization extinction in multiple spectral regions. Experimental results with Si nanowire grids yield ~200-nm-wide band of total reflection for one polarization state and free transmission of the orthogonal state. Finally, resonance elements functioning as simultaneous spatial and spectral filters are introduced and substantiated with computed and experimental results that are in excellent agreement.

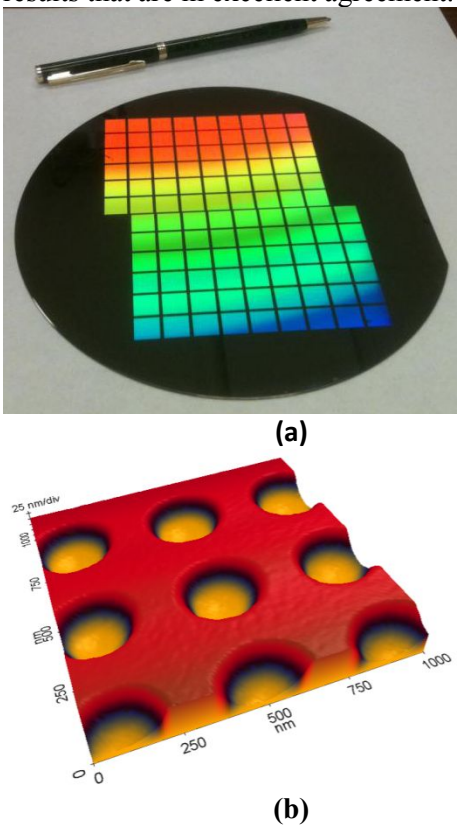

(a)

(b)

Fig.1. Examples of nanostructured surfaces. (a) A silicon wafer with numerous periodic devices. (b) An array of gold nanocups.

C17: An Optimized Spectral Response the HBT InP/InGaAs as an Optoelectronic Mixer mm-wave Radio over Fiber

S.M Idrus[1], N.A Shaharuddin[2], S. Isaak[3].

[1]*Lightwave Communication Research Group, Faculty of Electrical Engineering, Universiti Teknologi Malaysia, 81310, UTM Johor Bahru, Johor, Malaysia.*
Email:sevia@fke.utm.my, web site: http://sevia.fke.utm.my/

[2]*Faculty of Electrical Engineering, Universiti Teknologi MARA (UiTM), Shah Alam, Selangor.*
[3] *Department of Electronic and Computer Engineering, Faculty of Electrical Engineering (FKE), Universiti Teknologi Malaysia, 81310, UTM Johor Bahru, Johor, Malaysia.*

The optoelectronic mixing is an attractive approach for high frequency in millimeter wave band due to an advantages of low loss and modulate high frequency signal for up and down conversion. Due to this advantage, it is practical implementation of RoF whereby it performs the detection and frequency conversion simultaneously that are required at antenna BS. Heterojunction Bipolar Transistor (HBT) enable to photodetects and optoelectronic converters for radio over fiber communication systems [1, 2]. Hence, HBT has been identified as a suitable candidate of an OEM by simultaneously photodetecting an intensity modulated wavelength frequency translating the detected signal to a higher or lower frequency which can provide high mixing efficiency up to 30GHz. In this work, analysis of the spectral model of HBT in lattice-matched InP/InGaAs as an optoelectronic mixer in millimeter-wave radio over fiber (RoF) has been done thoroughly. The proposed HBT was analysed by considering the wavelength of 1310nm and 1550nm for an up-conversion frequency of 20GHz. It was found that the optimum device parameters and characteristics of spectral response were determined based on the influenced of optical window $5x6\mu m^2$ and $8x8\mu m^2$ and responsivity of the device. The responsivity of the HBT obtained is 0.2 A/W at 1550nm wavelength and 0.3A/W at 1300nm. The characteristics was further investigated to develop the appropriate structure device for OEM application. The proposed HBT InP/InGaAs is for heterodyne RoF transceiver system to perform photodetection and frequency up-conversion in millimeter wave RoF.

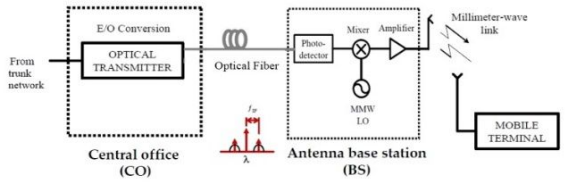

1. Mohamed, N., et al. *Nonlinear analysis for performance characterization of heterojunction bipolar transistor optoelectronic mixer*. in *Lasers & Electro Optics & The Pacific Rim Conference on Lasers and Electro-Optics, 2009. CLEO/PACIFIC RIM '09. Conference on*. 2009.
2. Liu, C.P., et al. *Two-tone third-order intermodulation distortion characteristics of an HBT optoelectronic mixer using a two-laser approach*. in *Microwave Photonics, 1999. MWP '99. International Topical Meeting on*. 1999.

C18: Cu2O-based solar cells using oxide semiconductors

Tadatsugu Minami, Yuki Nishi and Toshihiro Miyata

Optoelectronic Device System R&D Center. Kanazawa Institute of Technology, Japan Email:minami@neptune.kanazawa-it.ac.jp

Recently, we reported that the Al-doped ZnO (AZO)/n-type oxide semiconductor/p-type Cu_2O heterojunction solar cells with high conversion efficiency were fabricated by depositing AZO and n-type oxide thin films on room temperature (non-intentionally heated) Cu_2O sheets prepared by thermally oxidizing Cu sheets. In this paper, we describe the present status and prospects for further development of the n-oxide semiconductor/p-Cu_2O heterojunction solar cells fabricated using Cu_2O sheets with a thickness of approximately 0.2 mm. The influence of the inserted n-oxide semiconductor thin film on the obtainable photovoltaic properties in the Cu_2O-based heterojunction solar cells was investigated by inserting n-various multi-component oxide thin films prepared under various deposition conditions. AZO thin films and $(Ga_2O_3)_X$-$(MO)_{1-X}$ multi-component oxide thin films such as Ga_2O_3-ZnO, Ga_2O_3-Al_2O_3 Ga_2O_3-In_2O_3 and Ga_2O_3-SnO_2 systems were prepared by using a pulsed laser deposition (PLD) method. The obtained photovoltaic properties in Cu_2O-based heterojunction solar cells were strongly affected by material system used and chemical composition in $(Ga_2O_3)_X$-$(MO)_{1-X}$ thin films as well as deposition conditions. In heterojunction solar cells with $(Ga_2O_3)_X$-$(ZnO)_{1-X}$ and $(Ga_2O_3)_X$-$(Al_2O_3)_{1-X}$ multicomponent oxide thin films, the highest efficiency was obtained by adding an amount of MO that was small relative to that of Ga_2O_3, *i.e.*, an $(Ga_2O_3)_{0.9}$-$(ZnO)_{0.1}$ and $(Ga_2O_3)_{0.975}$-$(Al_2O_3)_{0.025}$, respectively. However, the obtained photovoltaic properties in AZO/$(Ga_2O_3)_X$-$(In_2O_3)_{1-X}$/Cu_2O heterojunction solar cells gradually degraded as the chemical composition (X) of $(Ga_2O_3)_X$-$(In_2O_3)_{1-X}$ multi-component oxide thin films was decreased from 1 (Ga_2O_3) to 0 (In_2O_3). In addition, we found that an improvement of obtainable photovoltaic properties in n-oxide semiconductor/p-Cu_2O heterojunction solar cells could also be achieved by both decreasing the resistivity of Cu_2O sheets without changing the Hall mobility of 90-110cm^2/Vs as well as optimizing preparation conditions of multi-component oxides such as $(Ga_2O_3)_{0.9}$-$(ZnO)_{0.1}$ and $(Ga_2O_3)_{0.975}$-$(Al_2O_3)_{0.025}$, used as the n-oxide thin-film layer. The former was achieved by incorporating Na into the Cu_2O sheets by post-annealing, in an Ar gas atmosphere with various sodium compounds, as recently reported by us [1]. The hole concentration in Na-doped Cu_2O (Cu_2O:Na) sheets was controlled in the range of 10^{13}-10^{19} cm^{-3} by varying the annealing temperature and duration. Consequently, a maximum efficiency of 6.25% was obtained in a MgF_2/AZO/$(Ga_{0.975}Al_{0.025})_2O_3$/$Cu_2O$:Na heterojunction solar cell fabricated using a Cu_2O:Na sheet with a resistivity on the order of 10 Ωcm and a $(Ga_{0.975}Al_{0.025})_2O_3$ thin film with a thickness of approximately 60 nm.

[1] T. Minami, Y. Nishi, and T. Miyata, Appl. Phys. Lett. **105** (2014) 212104.

C19: Recent progress in fabrication process for highly efficient GaN LEDs

Joon Seop Kwak

Department of printed Electronics Engineering, Sunchon National University, Jeonnam 540-742, Korea
Email:jskwak@sunchon.ac.kr

Highly efficient, high power LEDs have attracted great attention as light sources for general lightings and back-light unit (BLU) of LCD displays, as well. One of the main concerns in the fabrication of high power LEDs is the improvement of light extraction efficiency (LEE). This presentation discusses new approaches in fabrication process to improve the LEE of flip chip LEDs (FC-LEDs), since FC-LEDs draw great attention recently for light sources of head lamps and BLU of LCD displays. We will focus on recent progress in fabrication process for FC-LEDs with indium tin oxide (ITO)/distributed Bragg reflector (DBR). The FC-LEDs with ITO/DBR showed better reliability and relatively simple fabrication process than the conventional FC-LEDs with Ag reflectors. For this purpose, damage-free sputtered ITO ohmic contact to p-GaN, optimization of the DBR structure, and forming a current blocking layer (CBL) by ion implantation will be presented.

First, based upon the carrier transport phenomena in metal contacts to p-GaN, we will focus on ITO ohmic contact to p-GaN since ITO is commonly used as a transparent electrode on p-type GaN in LEDs. Because transmittance and specific resistance of ITO film have a significant impact on the LEE of FC- LEDs with ITO/DBR, various vacuum deposition methods have been studied to grow a high quality ITO film on p-type GaN. However, due to the plasma damage in ITO sputtering process, e-beam evaporated ITO is widely used in spite of its relatively low film quality. Although a sputtering process is well known to obtain the best quality of ITO films, it cannot be applied due to the degradation of p-type GaN through the impact of high energy ion or electron in plasma. In this study, the properties of sputtered ITO films grown by plasma damage-free condition will be shown, and the mechanism for forming a low resistance sputtered ITO ohmic contact to p-GaN will also be discussed.

Second, a method of for forming a CBL by ion implantation in will be demonstrated. The LEE and radiant intensity of the lateral LEDs with a nitrogen implanted CBL was increased greatly compared to that of a conventional LED due to an increase in the effective current path, which reduces light absorption at the thick p-pad electrode.

Finally, for optimization of the DBR in FC-LEDs with ITO/DBR, we fabricated two-type of DBR structures; 12 pair (A-type) and 24 pair (B-type) of dielectric reflector layers. Both the DBRs showed near 100 % reflection in the wavelength range emitted from the quantum wells in FC-LEDs. However, although both the FC-LEDs with ITO/DBR yielded same operating voltage of 3.2 V, the output power of FC-LEDs with B-type DBR was greatly higher than that of the FC-LEDs with A-type DBR. The mechanism for this behavior will be discussed in the presentation.

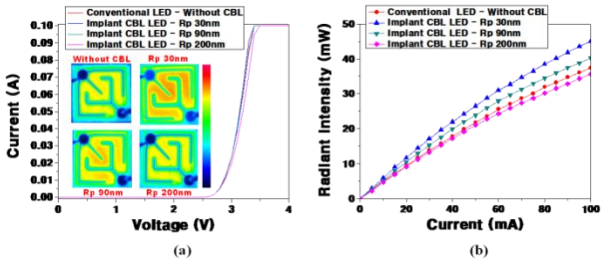

Fig.1. (a) *I-V* curves of the LEDs and (b) *L-I* characteristics with nitrogen implanted CBL, which has different Rp. Shown in the inset are beam-profiles at an applied current 80mA of the LEDs.

C20: Is electron accumulation in InN intrinsic or may it be a material for photovoltaic applications?

Holger Eisele[1]

[1]*Institut für Festkörperphysik, Technische Universität berlin, 10623 Berlin, Berlin, Germany*
Email:holger.eisele@physik.tu-berlin.de

In recent years an intrinsic electron accumulation at different InN surfaces is broadly discussed as a general aspect of this material [1,2]. Such an electron accumulation would be hindering any *p*-doping in InN — or at least

making the formation of sharp interfaces with *p*-doped InN electronically impossible. Hence, also photovoltaic applications would not be able to benefit from InN and its material properties, especially not from its useful bandgap in the near infrared wavelength region.

In this contribution new experiments on non-polar InN surfaces will be presented, showing no electron accumulation [3,4,5]. Here, the InN was prepared from high-quality grown thick layers on different substrate materials by *in situ* cleavage under UHV conditions. This preparation method leads to as-cut stoichiometric *m*- and *a*-planes, on which no electron accumulation was found as long as they remain clean. Different scanning tunneling spectroscopy measurements and also photoelectron spectroscopy measurements show the Fermi level being energetically located within the fundamental bulk band gap. From this result, an intrinsic electron accumulation can be negated and *p*-doping, in general, should be possible. Furthermore, also the intrinsic electronic surface states are both energetically located outside the bulk band gap [6].

In contrast, grown, non-polar surfaces still show electron accumulation [7]. On the one hand, this leads to the question how to improve or modify growth conditions in a way to receive also stoichiometric clean surfaces without electron accumulation. On the other hand, it demonstrates that electron accumulation is not an intrinsic property of InN material, but rather more a question of surface preparation.

1. P.D.C. King *et al.*, *Appl. Phys. Lett.* **91**, 092101 (2007).
2. H. Eisele and Ph. Ebert, *Phys. Stat. Solidi RRL* **6**, 359 (2012).
3. Ph. Ebert *et al.*, *Appl. Phys. Lett.* **98**, 062103 (2011).
4. H. Eisele *et al.*, in preparation (2015).
5. C.-L. Wu *et al.*, *Phys. Rev. Lett.* **101**, 106803 (2008).
6. D. Segev and C.G. van de Walle, *Europhys. Lett.* **76**, 305 (2006).
7. C.L. Wu *et al.*, *Appl. Phys. Lett.* **92**, 162106 (2008).

C21: Surface modification of III-Nitride epilayers by Chemical Mechanical Planarization (CMP)

Dibakar Das

School of Engineering Sciences and Technology, University of Hyderabad, Hyderabad 500046, India

Chemical Mechanical Planarization (CMP) is a process by which the surface of the material, which requires finishing, is chemically altered to a soft layer, which is subsequently removed by the mechanical abrasion of the polishing slurry. Polishing slurry is essentially a mixture of suitable chemicals and abrasive material. The process is extremely sensitive to the polishing parameters, such as suitable oxidizers/chemicals, its concentration, slurry pH, its flow rate, polishing pressure, abrasive medium, its size, size-distribution, shape, and concentration, polishing pad etc. The process is an integral part of the integrated circuits (ICs) fabrication technology. Nitride electronics are becoming increasingly popular in high power and high frequency micro- and optoelectronics devices. One of the major technical challenges in developing these novel electronics is the non-availability of large size epi-ready substrates. This talk will mostly focus on the CMP process, its difference with the conventional mechanical polishing, the influence of CMP processing parameters on the material removal rate (MRR) and surface finish of polar (0001), non-polar (11-20), and semi-polar (11-22) GaN/AlN/AlGaN surfaces.

C22: Organic semiconductor light sources for visible light communications

G.A. Turnbull,[1] P. Manousiadis,[1] S Zhang,[1] H. Chun,[2] S. Rajbhandari,[2] M.T. Sajjad,[1] D. Amarasinghe,[1] G.E. Faulkner,[2] C. Orofino,[3] D. Cortizo-Lacalle,[3] A.L. Kanibolotsky,[3] P.J. Skabara,[3] D.C. O'Brien,[2] I.D.W. Samuel,1

[1]*Organic Semiconductor Centre, SUPA, School of Physics and Astronomy, University of St Andrews, UK*

[2]*Department of Engineering Science, University of Oxford, Oxford, UK*
[3]*WestCHEM, Department of Pure and Applied Chemistry, University of Strathclyde, UK*

Visible light communications (VLC) is an emerging area of wireless data communications, which aims to take advantage of solid-state lighting infrastructure to provide both illumination and high speed data links. Gallium nitride LEDs are suitable for high bandwidth modulation, and have achieved data transfer rates as high as 3 Gb/s with blue light [1]. The conventional phosphors used in LED lighting to achieve white light emission are, however, not well suited to fast modulation due to their luminescence lifetimes in the microsecond range, limiting the system bandwidth to a few MHz. The complementary properties of nitride and organic semiconductors open new directions for addressing challenges in visible light communications. Attractive features of organic semiconductors relevant to VLC are their visible band gaps, radiative lifetimes of 1 ns and below, their high photoluminescence quantum yields, and their scope for simple fabrication including integration with nitride semiconductors.

In this talk we present the use of organic semiconductor materials as fast colour convertors for VLC. We report the design and performance of hybrid nitride-organic emitters which generate white, green and red light with data transfer rates in the 100s MHz to Ghz range [2-4]. We also report the demonstration of directional light emission using organic and hybrid LEDs with imprinted photonic crystals.

The organic colour convertors used include poly(paraphenylene-vinylene) based conjugated polymers [2,3] and boron dipyromethene star-shaped molecules [4], and were optically pumped by nitride LEDs or laser diodes. The transmitters were configured either to emit a single colour (green, yellow or red), or to transmit also a portion of the blue LED light to give a combined white emission. The organic colour convertors exhibit modulation bandwidths (3 dB) from 40 MHz to >300 MHz. We measured data transfer rates over short free-space links of up to 300 Mb/s using on-off keying, and at the Gb/s level with high-level encoding.

We also report the development of directional light sources for VLC, using both organic light emitting diodes (OLEDs) and hybrid LEDs, which include imprinted photonic crystal structures [5,6]. The photonic crystal is either used internally to an OLED to extract waveguided modes into a directional beam, or is used to extract the substrate modes in an OLED or fast colour converter layer. The directional beam may be steered in angle by bending a flexible substrate.

In summary, we have shown that organic semiconductors are attractive new materials for fast LED colour conversion, with potential applications for high-bandwidth visible light communications.

1. D. Tsonev, H. Chun, S. Rajbhandari, J. McKendry, S. Videv, E. Gu, M. Haji, S. Watson, A. Kelly, G. Faulkner, M. Dawson, H. Haas, and D. O'Brien, *IEEE Phot. Tech. Lett.* **26**, 637 (2014)
2. H. Chun, P. Manousiadis, S. Rajbhandari, D.A. Vithanage, G. Faulkner, D. Tsonev, J.J.D. McKendry, S. Videv, E. Xie, E. Gu, M.D. Dawson, H. Haas, G.A. Turnbull, I.D.W. Samuel, D.C. O'Brien *IEEE Phot. Tech. Lett.* **26**, 2035 (2014)
3. M.T. Sajjad, P.P. Manousiadis, H. Chun, D.A. Vithanage, S. Rajbhandari, A.L. Kanibolotsky, G. Faulkner, D. Obrien, P.J. Skabara, I.D.W. Samuel, G.A.Turnbull, *ACS Photonics* **2**, 194 (2015)
4. M.T. Sajjad, P. Manousiadis, C. Orofino, D. Cortizo-Lacalle, A.L. Kanibolotsky, S. Rajbhandari, D.A. Vithanage, H. Chun, G. Faulkner, D.C. O'Brien, G.A. Turnbull, I.D.W. Samuel, Adv. Opt. Mater. **3**. 536 (2015)
5. S. Zhang, G.A. Turnbull and I.D.W. Samuel,
Appl. Phys. Lett. **103**, 213302 (2013).
6. S. Zhang, G.A. Turnbull and I.D.W. Samuel, *Adv. Opt. Mat.* **2**, 343 (2014).

C23: Optical cavity spectroscopy for environment, military and medicine applications

Jacek Wojtas[1], Zbigniew Bielecki[1], Tadeusz Stacewicz[2], Janusz Mikolajczyk[1], Dariusz Szabra[1], Mirosław Nowakowski[1], Marek Helman[3]

[1] Institute of Optoelectronics, Military University of Technology, Warsaw, Poland Email:jwojtas@wat.edu.pl, web site: http://www.ioe.wat.edu.pl/
[2] Institute of Experimental Physics, Faculty of Physics, University of Warsaw, Poland
[3]Faculty of Technical Physics, Poznan University of Technology, Poland

The paper presents an application of the laser absorption spectroscopy (LAS) to trace matter detection. This technique ensures both low detection limits and high selectivity. Such performances were achieved using e.g. cavity enhanced absorption spectroscopy (CEAS). In this method, an optical cavity of a high quality factor is applied. That results in a long effective optical path, even up to a few kilometers [1].

To reach high sensitivity of the sensor, the appropriate spectral adjustment of cavity characteristic, and laser beam to the test gas absorption lines should be done. Three experimental setups were built. Our sensors were designed for nitrogen oxides. These compounds as well as sulfur dioxide are the main pollutants of air. They cause strong acidification of precipitation, the formation of photochemical smog and highly toxic secondary pollutants (ozone, aromatic hydrocarbons). They strongly raise the corrosion of stone buildings and metal structures as well. Moreover, they threaten human health, irritate the respiratory system and generally weaken the body's resistance to infectious diseases.

Our portable NO_2 sensor was build using blue-violet semiconductor laser working at 414 nm wavelength. The instrument was tested in outdoor experiment consisting in determination its applicability for measuring nitrogen dioxide concentrations in the atmosphere. For detection of other nitrogen oxides (e.g. NO and N_2O) the ro-vibronic molecular transitions from mid-infrared range were exploit [2]. In this case quantum cascade (QC) lasers from Alpes Laser SA and from the Institute of Electron Technology were applied as the radiation sources [3]. The optical signals were registered with low noise detection modules developed by VIGO System SA.

In practice, the designed nitrogen oxides sensors provide opportunity to observe trace gas concentration with the limit up to 1 ppb. Due to high sensitivity, besides atmospheric investigation use the sensors might be applied to the detection of some high vapor-pressure explosives, like nitro-glycerin (NG), nitrocellulose and TNT. For explosives with lower vapors pressure, special gas concentrator was developed. The device provides to collect the particles of the explosives from a high air volume and to perform their thermal decomposition. As a result, the increase of nitrogen oxides concentration was achieved and detection of other explosives such as PETN, RDX and HMX was also demonstrated [2].

Our CEAS sensors can be also used as the effective tools for monitoring of certain molecules in the human breath. These molecules are used as the markers of specific diseases. The experiments showed that in this way the detection of pathogenic changes is possible. Such type of diagnosis would significantly increase the chances for effective therapy due to screening for early detection of some diseases. Recent progress in optoelectronics provides opportunity to construct compact, low costs and user-friendly breath sensors based on laser absorption spectroscopy which might lead to high accessibility of such screening [4].

Acknowledgement
The presented works were supported by The National Centre for Research and Development and National Science Centre in the scope of Projects: ID: 179616, ID: 151673 and ID: 179900.

References
1. T. Stacewicz, et al. *Opto−Electron. Rev.* **20**(1). pp. 34-41, (2012).

2. J. Wojtas, J. Mikolajczyk, Z. Bielecki. *Sensors*, **13**(6), 7570-7598, doi:10.3390/s130607570, (2013).
3. K. Pierscinski, et al. *J. Appl. Phys*., **112**(4), 043112, (2012).
4. B. Buszewski, et al. *Bioanalysis*, **5**(18):2287-306, (2013).

C24: Enhancing the luminescent properties of Si nanoparticles by applying the additional continuous laser during ablation in liquid

Dusan M. Popovic[1], A. A. Zekic[1], B. Kasalica[1], M. Trtica[2], J. Stasic[2], M. Bogdanovic[1]

[1]University of Belgrade-Faculty of Physics, Studentski trg 12, 11001 Belgrade, Serbia Email:drdmpopovic@gmail.com
[2]Vinca Institute of Nuclear Science, University of Belgrade, P.O. Box 522, 11001 Belgrade, Serbia

The interest in research of silicon and silicon based nanoparticles (NPs) is present in literature for numerous reasons. For instance, the authors has been analyzed the bioapplications of these NPs [1]. Also, the photoluminescence properties of Si-NPs make them a candidate for biomaging applications [2]. The extremely small silicon NPs are used in optoelectronic devices. As far as the theoretical investigations are concern, silicon and silicon-based NPs are important in the study of fundamental quantum effects. Related with the research on the biomedical application and effects, some authors analyze the toxicities of silicon and silicon-based NPs.

Laser ablation of solid targets in liquids (LAL) is a promising technique for producing NPs. It provides an important advantage against the contamination risk in the produced NPs.

Recently, we analyzed the effect of the laser pulse energies and repetition rate of applied pulse laser on the LAL process [3], as well as the effect of the applying the additional continuous laser (CW) during the LAL process [4]. In this work, we focused our attention at the photoluminescence (PL) properties on NPs produced by LAL. We demonstrated that that the applying of the additional CW laser during LAL process induces the change of shape and ***intensity*** of the PL ***spectra (Fig. 1).***

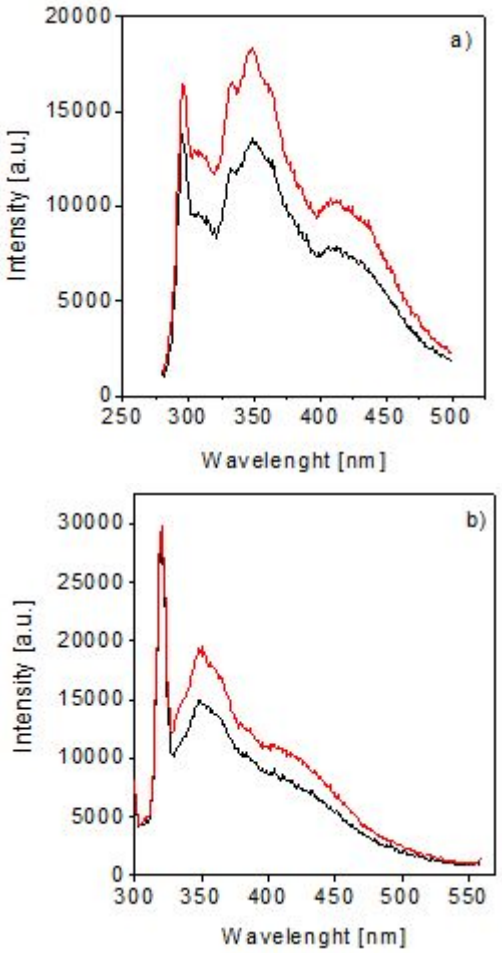

Fig1. Photoluminescence spectra of silicon nanoparticles produce by laser ablation in de-ionized water for excitation at (a) 270 nm and (b) 290nm, without (black line) and with (red line) applying the additional continuous laser.

1. Y. He, C. Fan, and S.-T. Lee, *Nano Today* 5.4 282, (2010)
2. J.-H. Park, L. Gu, G. von Maltzahn, E. Ruoslahti, S.N. Bhatia, and M. J. Sailor, *Nat. Mater.* 8 (4), 331 (2009)
3. D.M. Popovic, J.S. Chai, A.A. Zekic, M. Trtica, M. Momcilovic, S. Maletic, *Laser Phys. Lett.* 10, 026001 (2013)
4. D.M. Popovic, J.S. Chai, A.A. Zekic, M. Trtica, J. Stasic, M.Z. Sarvan, *Laser Phys. Lett.* 11, 116101 (2014).

C25: Newly Developed Soft Magnetic NANOMET® Powder Cores with High Magnetic Flux Density

Yan Zhang[1], Parmanand Sharma[1] and Akihiro Makino[2]

[1]Institute for Materials Research, Tohoku University, Sendai, Japan
[2]Tohoku University, Sendai, Japan
Email:zy-jp@imr.tohoku.ac.jp

With the development of human society, there is an increasingly urgent requirement for reduction in electrical losses (mainly the core losses) of equipments. Key to success is to develop new soft magnetic materials (which are used as a core) with high saturation magnetization ($M_s \approx B_s$), low coercivity (H_c) and low core loss (W). It is well known that Fe-based amorphous and nanocrystalline materials exhibit good soft magnetic properties, such as low H_c and high permeability (μ) than their crystalline alloys. Soft magnetic materials using powder metallurgical techniques are gaining widespread use in motors, sensors, actuators, filters, power transformers, relays, inductors, power circuits, communication devices, microelectronics, power electronics and AC power devices operating at high frequencies. Recently, it is reported that a new energy-saving material named as NANOMET shows high magnetic flux density and excellent soft magnetic properties. NANOMET presents a crystalline micro-structure with nano-size α-Fe crystals evenly spread throughout the amorphous matrix [1],[2].

We have made attempts on developing new soft magnetic amorphous or nano-crystalline powder core materials with high magnetic flux density. Various metallurgical techniques were used in present research, such as cutting and crushing of ribbons to flake forms, conventional gas atomization process and new spinning water atomization process (SWAP). After being coated or mixed with different insulations, powders were consolidated by cold-pressing (CP) and spark plasma sintering processes (SPS). The structure and morphology of powder core materials were examined by X-ray diffractometer (XRD), transmission electron microscopy (TEM) and scanning electron microscope (SEM). Magnetization (M), coercivity (H_c), permeability (μ) and core loss (W) were measured by VSM, DC B-H loop tracer, impedance analyzer and AC B-H analyzer, respectively.

Fe-rich amorphous and nano-crystalline FeSiBP(Cu) powder cores exhibit high magnetic flux density. Amorphous powder have high $M_s \sim$ 1.5 T, which can further increase to 1.72 T by annealing treatment. High density can be obtained in the bulk amorphous alloys compacted with the glassy powder by SPS. The lamellar micro-structure in the core can contribute to obtain high μ, high B_s and low H_c. Meanwhile, it can also result in significantly lower W in the frequency range of kilohertz. Small powder particles insulated with resin can increase the operating frequency and decrease the W in a wide frequency range (from kilohertz to megahertz range). To meet the needs of industrial applications of low W at different frequency range and necessary B_s, it is possible to accurately adjust the parameters, e.g., initial and final structure, metallurgical techniques, consolidation processes and annealing conditions. The details about the influence of alloy composition, fabrication process, thermal, structural and magnetic properties including magnetic core loss will be presented.

1. A. Makino, T. Kubota, K. Yubuta, A. Inoue, A. Urata, H. Matsumoto, and S. Yoshida, *J. Appl. Phys.*, **109**, 07A302, 2011.
2. Y. Zhang, P. Sharma, and A. Makino, **50**, 2003004, 2014.

D09: Graphene and graphene based nanostructures as molecular transporters

E. Mijowska[1], K. Cendrowski, K. Urbas[1], M. Barylak[1], M. Perużyńska[2], M. Droździk[2], M. Jedrzejczak[3], R.J. Kalenczuk[1]

[1]Institute of Chemical and Environment Engineering, West Pomeranian University of Technology Szczecin, Szczecin, Poland

Email:emijowska@zut.edu.pl

[2]*Department of Pharmacology, Pomeranian Medical University, Szczecin, Poland*

[3]*Laboratory of Cytogenetics, West Pomeranian University of Technology, Dra Judyma 6, 71-466 Szczecin, Poland*

Recently, the researchers focused on graphene oxide (GO) as a promising material due to its two- dimensional structure with many oxygen containing functional groups. Oxidized graphene sheets show strong hydrophilic performance with easy surface modification, good biocompatibility, and low cytotoxicity. Also GO can be functionalized by many guest molecules, which makes it good platform for the nanoparticles or molecules being covalently and non-covalently attached (see Fig.1). Furthermore, GO can serve as a template for the formation new molecular systems e.g. mesoporous silica flakes. Therefore, in this presentation the overview of the potential of graphene as a molecular transporter will be presented. The main focus will be on the graphene platform used for drug molecules and metal nanoparticles transport. The possibility to perform the multifunctional functionalization of graphene allows to verify the potential application of the prepared nanostructures in several fields.

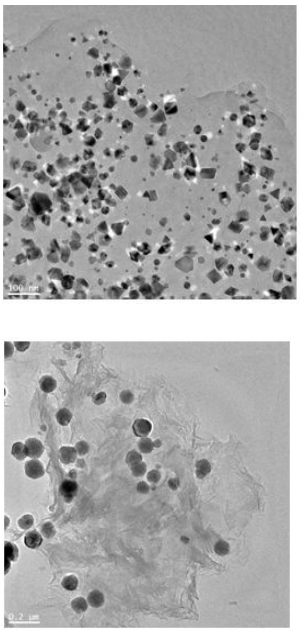

Fig1. TEM images of palladium (left panel) and iron oxide (right panel) decorated graphene.

Acknowledgements: The authors are grateful for the financial support of National Science Centre within OPUS program (Project No. DEC/2011/03/B/ST5/03239

D10: Plasmonic nanostructure instability by surface diffusion

James W. M. Chon and Adam B. Taylor

Centre for Micro-Photonics, Dept. of Physics, Faculty of Science, Engineering and Technology, Swinburne University of Technology, Hawthorn, 3122, VIC, Australia Email:jchon@swin.edu.au

Plasmonic gold nanorod instability and reshaping behaviour at below melting points are important for many future applications but are yet to be fully understood, with existing nanoparticle melting theories unable to explain the observations.

We report here the photothermal reshaping behaviour of gold nanorods irradiated with femtosecond laser pulses, and that the instability is driven by curvature induced surface diffusion rather than threshold melting process, and that the stability dramatically decreases with increasing aspect ratio. We successfully utilized surface diffusion model to explain the observations and found that the activation energy for surface diffusion was dependent on the aspect ratio of the rods, from 0.6 *eV* for aspect ratio of 5, to 1.5 *eV* for aspect ratio less than 3. This result indicates that the surface atoms are much easier to diffuse around in larger aspect ratio rods than shorter rods, and can induce reshaping at any given temperature.

These findings will be especially important for the field of gold nanorod photothermal therapy and two-photon biolabelling, plasmonic circuitry, solar cells using plasmonic structure, where increased laser power, and sharper geometric features are often seen as a mechanism for greater field enhancement. This work shows that surface diffusion based reshaping must be considered for plasmonic nanostructures for

their stable operations, even at temperatures well below melting points.

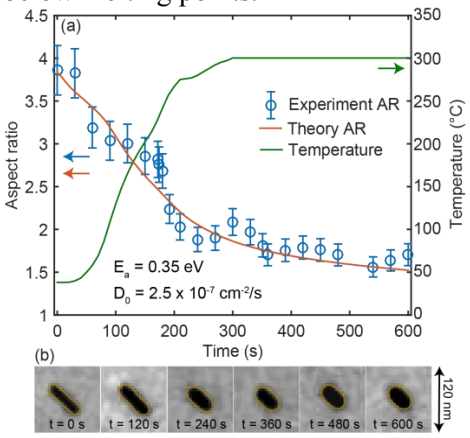

Fig1. Surface diffusion model fitting with reshaping of a gold nanorod.

1. Taylor, A., Siddique, M., and Chon, J. W. M., 'Below melting point photothermal reshaping of single gold nanorods driven by surface diffusion', ACS Nano, Vol 8, No. 12, 12071-12079, 2014

D11: Effects of kosmotrope and chaotrope interactions at the micelle surfaces on the formation of lyotropic biaxial nematic phases: Intrinsically Biaxial Micelle Model

Erol AKPINAR

Abant Izzet Baysal University, Arts and Sciences Faculty, Department of Chemistry, 14280, Bolu, TURKEY
e-mail: akpinar_e@ibu.edu.tr

Since lyotropic mixture potassium laurate (KL)/decanol (DeOH)/water, presenting the biaxial nematic phase (N_B), was reported in the literature for the first time in 1980 [1], various hypotheses and models on the evidence of N_B phases were suggested. Due to this N_B phase being an intermediate phase between uniaxial discotic nematic phase (N_D) and uniaxial calamitic nematic phase (N_C), at the beginning, it was asserted that N_B phase arises from the co-existence of N_D and N_C phases. However, from subsequent theoretical and experimental studies, N_B phase could not be a mixture of these two uniaxial phases and then it was proved that N_B phase is a distinct and a stable phase from other two nematic phases. We believe that the most reliable and important model to explain the formation of all three nematic phases was proposed by Neto [2] and Galerne [3], so-called "intrinsically biaxial micelles model, IBM". This model is mainly based on two parameters: (a) micelle symmetry and (b) orientational fluctuations. The IBM model states that the micelles have orthorhombic symmetry in all three different nematic phases and the driving force for occurrence of these phases is different orientational fluctuations around different symmetry axes.

Because N_B phases have two optical axes, they exhibit the advantage in terms of optics with respect to other two uniaxial phases; by this way, one of the optical axes can be aligned in the magnetic field instead of other. Therefore, finding new lyotropic mixtures exhibiting stable N_B phase and large biaxial phase domain on the phase diagrams is important in terms of both science and applications based on biotechnology. By this way, information obtained from these new mixtures will cause important scientific and biotechnological improvements. Furthermore, finding new factors that affect the preparation of the lyotropic mixtures, which present N_B phases, is another important point.

In this presentation, we will show how kosmotrope and chaotrope interactions between head groups of surfactant molecules and their counterions at the micelle surfaces play a role on the formation of the nematic phases from our recent experimental studies. For this purpose, we have studied on two series of novel lyotropic mixtures, KL/alkali salt/DeOH/water and sodium dodecylsulfate/alkali salt/DeOH/water, whose phase compositions were different than the mixtures already given in the literature. The main experimental technique was laser conoscopy (see Figure for interference patterns) which is a very useful technique to determine the second order uniaxial-to-biaxial phase transitions [4] from the temperature dependence of the birefringences of each nematic phases.

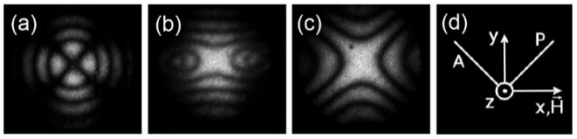

Figure. Characteristic conoscopic patterns of three nematic phases from laser conoscopy: (a) N_D; (b) N_B (near the N_D to N_B phase transition); (c) N_C. (d) Geometry of the experiment with the laboratory frame axes, polarizer (P), and analyzer (A) directions, and the direction of the applied magnetic field, H.

References

[1] L. J. Yu and A. Saupe, *Phys. Rev. Lett.* **45**, 1000-1003, **1980**.
[2] A. M. Figueiredo Neto, Y. Galerne, A. M. Levelut and L. Liebert, *J. Phys. (Paris) Lett.*, **46**, L-409-506, **1985**.
[3] Y. Galerne, A. M. Figueiredo Neto and L. Liebert, *J. Chem. Phys.*, **87**, 1851-1856, **1987**.
[4] Y. Galerne and J. P. Marcerou, *J. Physique* ,**46**, 589-594, **1985**

**The study subjected to this presentation was financially supported by TUBITAK (grant no: 113Z469).*

D12: Studying the effect of zeolite inclusion in aluminum alloy on measurement of its hardness using electron density measurement

Osama Khalil [1] and M. A. Harith [2]

[1] *Faculty of Engineering, MTI University, Cairo, Egypt.*
Email: okhalil@eng.mti.edu.eg, dr.osamakhalil@gmail.com

[2] *National Institute of Laser Enhanced Science (NILES), Cairo University, Giza, Egypt*
Email: mharithm@niles.edu.eg

Abstract

Laser-induced breakdown spectroscopy (LIBS) has been used to study the surface hardness of special aluminum alloys containing zeolite. The aluminum alloy has acquired pronounced changes in its metallurgical properties due to the zeolite inclusion. The surface hardness of the samples under investigation was determined by measuring the spectral intensity ratios of the ionic to atomic spectral lines in the LIBS spectra of samples having different surface hardness values that have been conventionally measured before for comparison. The presence of aluminum silicate mineral in the studied alloys enabled material volume to expand under compression. This feature gave new results in the measurement of hardness via LIBS. It has been proven that the trend of the alloy density change complies with the increase of ionic to atomic spectral line intensity ratio. The relation between the plasma electron density and the hardness/density confirm the previous results and assure that the electron density measurement could be used as a hardness measuring technique.

D13: Ferromagnetic semiconductors and heterostructures for semiconductor spintronics: New n-type electron-induced ferromagnetic semiconductor and its quantum wells

Masaaki Tanaka[1,2], Le Duc Anh[1], Pham Nam Hai[1,3]

[1] *Department of Electrical Engineering & Information Systems, The University of Tokyo*
[2] *Institute for Nano-Quantum Information Electronics, The University of Tokyo*
[3] *Department of Physical Electronics, Tokyo Institute of Technology*

Ferromagnetic semiconductors (FMSs) have been intensively studied for decades as they have novel functionalities that cannot be achieved with conventional metallic materials, such as the ability to control magnetism by electrical gating or light irradiation [1][2]. Prototype FMSs such as (Ga,Mn)As, however, are always p-type, making it difficult to be used in real spin devices. Here, we demonstrate that by introducing iron (Fe) to InAs, it is possible to fabricate a new n-type electron-induced FMS with the ability to control ferromagnetism by both Fe and independent carrier doping. The studied $(In_{1-x},Fe_x)As$ layers were grown by low-temperature molecular beam epitaxy on semi-insulating GaAs substrates. Electron carriers in these layers are generated by independent chemical doping of donors. The ferromagnetism

was investigated by magnetic circular dichroism (MCD), superconducting quantum interference device (SQUID), and anomalous Hall effect (AHE) measurements. With increasing the electron density concentration (n = 1.8×10^{18} cm^{-3} to 2.7×10^{19} cm^{-3}) and Fe concentration (x = 5 - 8%), the MCD intensity shows strong enhancement at optical critical point energies E_1 (2.61 eV), $E_1 + \Delta_1$ (2.88 eV), E_0' (4.39 eV) and E_2 (4.74 eV) of InAs, indicating that the band structure of (In,Fe)As is spin-split due to sp-d exchange interaction between the localized d states of Fe and the electron sea. SQUID and AHE measurements are also consistent with the MCD results. The Hall and Seebeck effects confirm the n-type conductivity of our (In,Fe)As samples. The electron effective mass is estimated to be as small as 0.03-0.175m_0, depending on the electron concentration. These reveal that the electrons are in the InAs conduction band rather than in the impurity band, making it easy to understand (In,Fe)As by conventional Zener-model of carrier-induced ferromagnetism [3]. This band picture is different from that of GaMnAs [4][5]. Our results open the way to implement novel spin-devices such as spin light-emitting diodes or spin field-effect transistors, as well as help understand the mechanism of carrier-mediated ferromagnetism in FMSs [6-11].

Furthermore, we demonstrate new phenomena in (In,Fe)As and its hetrerostructures: Novel crystalline anisotropic magnetoresistance with two fold and eight fold symmetry [7], and control of ferromagnetism by strain, quantum confinement, and wavefunction engineering in quantum heterostructures with a (In,Fe)As quantum well [9,10].

This work was partly supported by Grant-in-Aids for Scientific Research including Specially Promoted Research and Project for Developing Innovation Systems of MEXT.

References

[1] S. Koshihara, A. Oiwa, M. Hirasawa, S. Katsumoto, Y. Iye, C. Urano, H. Takagi and H. Munekata, Phys. Rev. Lett. **78**, 4617 (1997).
[2] H. Ohno, D. Chiba, F. Matsukura, T. Ohmiya, E. Abe, T. Dietl, Y. Ohno and K. Ohtani, Nature **408**, 944 (2000).
[3] T. Dietl, H. Ohno, F. Matsukura, J. Cibert and D. Ferrand, Science **287**, 1019 (2000).
[4] S. Ohya, I. Muneta, P. N. Hai, and M. Tanaka, Phys. Rev. Lett. **104**, 167204 (2010).
[5] S. Ohya, K. Takata, and M. Tanaka, Nature Phys. **7**, 342 (2011).
[6] P. N. Hai, L. D. Anh and M. Tanaka, cond-mat, arXiv:1106.0561v3 (2011); P. N. Hai, L. D. Anh, S. Mohan, T. Tamegai, M. Kodzuka, T. Ohkubo, K. Hono, and M. Tanaka, Appl. Phys. Lett. **101**, 182403 (2012).
[7] P. N. Hai, D. Sasaki, L. D. Anh, and M. Tanaka, Appl. Phys. Lett. **100**, 262409 (2012).
[8] P. N. Hai, L. D. Anh, and M. Tanaka, Appl. Phys. Lett. **101**, 252410 (2012).
[9] L. D. Anh, P. N. Hai, and M. Tanaka, Appl. Phys. Lett. **104**, 042404 (2014).
[10] D. Sasaki, L. D. Anh, P. N. Hai, and M. Tanaka, Appl. Phys. Lett. **104**, 142406 (2014).
[11] M. Tanaka, S. Ohya, and P. N. Hai (invited), Appl. Phy. Rev., **1**, 011102 (2014).

D14: Switchable Photo-induced Current of Strongly Correlated Ferroelectric Thin Films

Norifumi Fujimura, Hiroshi Uga, Lejun Zhang, Atsushi Ashida, Takeshi Yoshimura

Department of Physics and Electronics, Graduate School of Eng. Osaka Prefecture Univ. Osaka,Japan

fujim@pe.osakafu-u.ac.jp

Optical response of ferroelectric materials is attracting great attention nowadays, because switchable photocurrent by ferroelectric polarization and photo-voltage above-bandgap is observed in $BiFeO_3$ suggesting that the ferroelectric films can be utilized as the semiconductors [1,2]. Therefore, we have been interested in a photo-induced phenomena of strongly correlated ferroelectric $YMnO_3$ which has a ferroelectric phase transition at 1000 K and an antiferromagnetic phase transition at 80 K. In this study, the wavelength and temperature dependence of fundamental optical property of multiferroic $YMnO_3$ films and discuss the relationship between electron transfer process to

the Mn^{3+} excited state from the conduction band and the photo-induced current.

The temperature dependence of the optical absorption and the photoluminescence of the stoichiometric $YMnO_3$ films by pulsed laser deposition on (111) MgO was investigated. Broad absorption peaks and PL sharp peak are recognized at around 1.7 eV and the absorption peak has temperature dependence, but PL does not show any temperature dependence. Therefore, the absorption and PL at 1.7eV correspond to different electron transfer. The transfer energy of the intra-atomic Mn^{3+} PL bands at 1.7eV are independent of temperature, therefore the transition should be related to Mn $3d$(xz,yz) (e_{1g} state) and Mn $3d(3z^2\text{-}r^2)$ orbital (a_{1g} state) because these orbital spreads to the out-of plane, <0001> direction not to the in-plane, because antiferromagnetic spin ordering occurs through in-plane superexchange interaction. Regarding the intra-atomic Mn^{3+} PL, the wavelength and the decay time do not change at Néel temperature (80K), however, the intensity drastically decreases at Néel temperature indicating that a considerable decrease of the electron-transfer efficiency to the a_{1g} state of Mn^{3+} occurs at Néel temperature [3].

$YMnO_3$/Pt structured samples with a transparent top electrode, Al doped ZnO, were fabricated for measuring wavelength dependence of the photo-induced current at zero bias. Fig.1 shows the poling bias voltage dependence of the photo-induced current of the films. After applying the poling voltages, which are described at the top of the figure, the photo-induced current was measured without the bias voltage. The schematics indicate the polarization states that measured by capacitance-voltage properties. Photo-induced current, switchable photo-induced current of $YMnO_3$ films along the polarization axis are successfully observed under the illumination of white-light. The wavelength dependence of the photo-induced current was also measured. The photo current at 2.52 eV increases than 2.42eV suggesting that increase of the electron-transfer efficiency to the a_{1g} state of Mn^{3+} effects of photo-induced current of YMO films because the electron transfer predominantly originates from carriers generated in the energy region from 2.5 to 3.0 eV by measuring PLE.

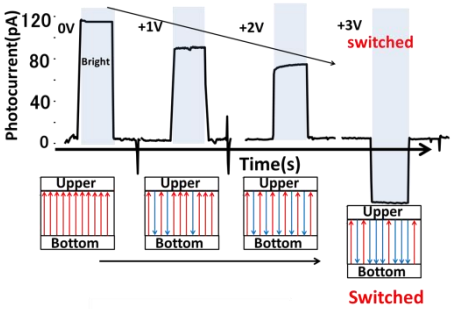

Fig.1 Poling bias voltage dependence of the photo-induced current of the $YMnO_3$ film. After applying the poling voltages, the photo-induced current was measured without the bias voltage under the illumination of white light.

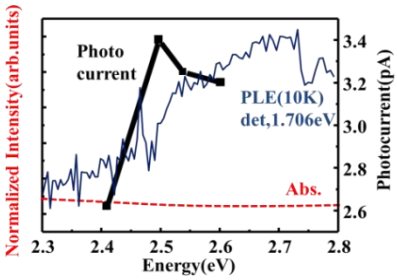

Fig.2 Absorption coefficient(dotted line), PLE (solid line) and photo-induced current (■)of $YMnO_3$ thin films against the photon energy

The talk focuses on the switchable photo-induced current of $YMnO_3$ films and the origin of it.

1. S.Y.Yang *et al*, Nat. Nanotechnol ,451.143 (2010)
2. D. Lee *et al*, Phys. Rev. B 84, 125305(2011)
3. M. Nakayama, Y. Furukawa, K. Maeda, T. Yoshimura, H. Uga, and N. Fujimura, Applied Physics Express, 7 (2014) 023002

D15: Dynamic Modeling and Control of Membrane Filtration Process

Zakariah Yusuf[1], Norhaliza Abdul Wahab[2], Shafishuhaza Sahlan[3]

[1,2,3]*Control and Mechatronics Engineering Department, Faculty of Electrical Engineering, Universiti Teknologi*
Malaysia, 81310, Skudai, Johor, Malaysia
Email:aliza@fke.utm.my, web site: http://norhaliza.fke.utm.my/

Membrane filtration process is promising technology in separation process. However, this technology involves many interactions from biological and physical operation behavior. Membrane fouling in filtration process is another complex problem that needs to be understood to ensure energy efficiency from the filtration process [1]. The aim of this paper is to study the potential of neural network based dynamic model for submerged membrane filtration process as shown Figure 1. The purpose of the model is to represent the dynamic behavior of the filtration process therefore suitable control strategy and tuning of the controller can be developed to control the filtration process more effectively. Several works had been done to control the filtration process especially in SMBR filtration system such as in [2],[3],[4].

In this work, a feed-forward neural network (FFNN) and radial basis function neural network (RBFNN) were employed with recurrent structure to perform the dynamic model of the filtration process. The random step was applied to the suction pump to obtained the permeate flux and trans-membrane pressure (TMP) dynamic models. The models were evaluated in term of %*R2*, root mean square error (RMSE,) and mean absolute deviation (MAD). The result of proposed models showed that the RNN structure is able to model the dynamic behavior of the filtration process. The developed model also can be a reliable aid for the control strategy development in the membrane filtration process. In this work, different control strategies were tested to see the effectiveness of filtration control system.

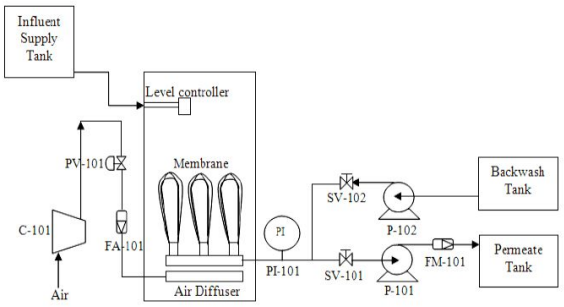

Fig1. Schematic Diagram of the Submerged MBR.

1. S. Judd, *The MBR Book Principles and Applications of Membrane Bioreactors in Water and Wastewater Treatment*, Second Edi. Elsevier, (2010).
2. A. Robles, M. V Ruano, J. Ribes, and J. Ferrer, "Advanced control system for optimal filtration in submerged anaerobic MBRs (SAnMBRs)," *J. Memb. Sci.*, vol. 430, pp. 330–341 (2013).
3. S. Curcio, V. Calabrò, and G. Iorio, "Design and tuning of feedback controllers: effects on proteins ultrafiltration process modeled by a hybrid system," *Desalin. Water Treat.*, vol. 34, no. 1–3, pp. 295–303 (2011).
4. H.-G. Han, J.-F. Qiao, and Q.-L. Chen, "Model predictive control of dissolved oxygen concentration based on a self-organizing RBF neural network," *Control Eng. Pract.*, vol. 20, no. 4, pp. 465–476 (2012).

D16: Quantum spin dynamics and spin-orbit coupling at terahertz frequencies in strained germanium quantum wells

M. Failla, M. Myronov, C. Morrison, D. R. Leadley and J. Lloyd-Hughes

Department of Physics, University of Warwick, Coventry, United Kingdom.
Email:j.lloyd-hughes@warwick.ac.uk, web site: go.warwick.ac.uk/ultrafast

The high hole mobility μ of Ge among the most studied semiconductors offers an attractive and compatible alternative to improve the current Si CMOS technology. Two dimensional hole gases

(2DHGs) in strained Ge quantum wells (sGe-QWs) experience, because of the lifting of hole band degeneracy by the strain at k=0, a further decrease of the hole effective mass as well as a low interband scattering, leading to even higher μ. Furthermore, structural inversion asymmetry in 2D systems also lifts the spin degeneracy through the Rashba spin-orbit interaction. [1] The chance to split spin-up and spin-down energy states makes those systems excellent candidates to realize field effect transitstors with an electric field controlled spin transport.

Here we use THz time-domain spectroscopy (THz-TDS) to investigate two sGe-QWs with a thickness of 11 (SiGe1) and 22 nm (SiGe2) enclosed between buffer layers of relaxed $Si_{0.2}Ge_{0.8}$ acting as source of strain because the lattice mismatch with the Ge-QWs. THz-TDS, as a powerful variant of CR spectroscopy, has the further advantage to examine, in a contactless method, the cyclotron dynamics, Fig1(a). Interference beats in the time-domain, with spin dephasing times exceeding 10 ps, clearly show split cyclotron resonances (CRs) in the frequency domain, Fig1(b), for magnetic fields higher than 3 T.

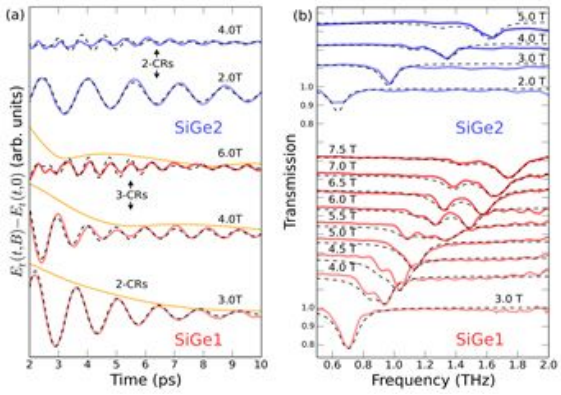

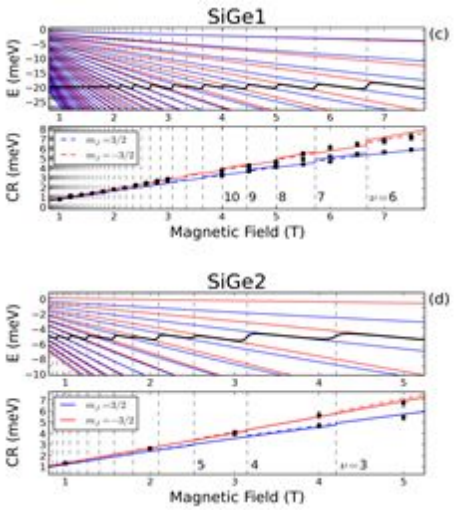

Fig1. (a) Time-domain; **(b)** Frequency-domain ; **(c,d)** Calculated subband levels/transitions for SiGe1 and SiGe2.

The CR's energy difference is linked to the cubic Rahsba interaction, typical for heavy-holes. [1] The cubic Rashba coefficient β, which quantifies the density and energy difference between spin-up and spin-down hole states, is determined via two methods. The first method evaluates the hole density for spin-up and spin-down states by fitting time and frequency domain data, black lines in Fig1(a,b), while the second exploits the dependence of CR energy transitons with respect to the magnetic field due to the energy split $\Delta=2\beta k_F^3$, Fig1 (c,d).

We obtain, a Rashba splitting energy of ~ 2.0 meV which is about one order of magnitude higher than previous studies on Ge-QWs, [2] as a consequence of a reduced strain. [3] Remarkably, our results are in line with magneto-transport measurements, [4] but obtained with a technique unaffected by device fabrication issues.

1. R. Winkler, *Spin-Orbit Coupling Effects in Two-Dimensional Electron and Hole Systems*, (Springer-
Verlag Berlin Heidelberg, 2003).
2. R. Moriya *et al.*, Phys. Rev. Lett. **113,** 086601 (2014).
3. M. V. Fischetti and S. E. Laux, Journal of Applied Physics **80**, 2234 (1996).

4. C . Morrison *et al.*, Applied Physics Letters, **105,** p. 182401, (2014).

D17: First-principle Vs Experimental design of Diluted Magnetic Semiconductor

Omar Mounkachi[1]

[1]*Moroccan Foundation for Advanced Science, Innovation and Reseach*

**o.mounkachi@mascir.com; kachiomar@gmail.com*

Semiconductors that exhibit room-temperature ferromagnetism are central to find ways to manipulate and use electronic spin to the same degree that electronic charge is used in silicon-based electronics. Diluted magnetic semiconductors (DMS) are a promising class of such materials to the development of semiconductor spintronics, but their success will depend on our ability to understand and optimize their behavior. The interface between first principle and experimental materials design could provide a way to achieve these goals.

The purpose of talk is to propose some ideas to answer the most important question in material science for semiconductor spintronics, namely, how we can realize room-temperature ferromagnetism in DMS? And I will discuss the correlation between first principle and experimental design to see how we can predict the properties of yet-to-be-synthesized materials. Based on experimental design I will discuss structural and magnetic properties of same DMS materials. Based on first-principles spin-density functional calculations, the half-metallic ferromagnetic properties of same DMS materials with magnetic impurity have been investigated.

New magnetic behaviors will be discussed in DMSs recently observed as spin glass, super paramagnetic, this creates new opportunities for development and construction a new spintronics devises.

D18: Noiselike pulses from modelocked fiber lasers: recent advances and applications

Olivier Pottiez[1], J. P. Lauterio-Cruz[1], J. C. Hernandez-Garcia[2], H. Santiago-Hernandez[1], M. Duran-Sanchez[3], B. Ibarra-Escamilla [3], E. A. Kuzin[3]

[1]*Centro de Investigaciones en Óptica, León, Guanajuato, Mexico*
Email:pottiez@cio.mx, web site: http://www.cio.mx/investigacion/cvs/e_olivierj.html
[2]*División de Ingenierías Campus Irapuato-Salamanca, Universidad de Guanajuato, Salamanca, Guanajuato, Mexico*
[3]*Instituto Nacional de Astrofísica, Óptica y Electrónica, Puebla, Puebla, Mexico*

Passively mode-locked fiber lasers are versatile low-cost sources whose ability to produce a wide variety of optical pulses, including conventional solitons, dispersion-managed solitons and dissipative solitons, has been demonstrated over the years. A quite distinct regime of these sources, called noiselike pulsing, which was first thoroughly described in the late 1990's [1] and attracted moderate attention over the following decade, is now becoming the focus of many researchers [2]. A noiselike pulse (NLP) [Fig. 1(a)] is a long (~ns) and compact waveform with a fine inner structure formed by many thousands or even millions of sub-ps sub-pulses presenting strong and fast fluctuations. In spite of this inner variability, the global parameters of NLPs (e.g., duration, average spectral width) are usually quite stable on the long term, so that this regime is sometimes described as partial (or incomplete) mode-locking. Considering their high energy, wide optical bandwidth [Fig. 1(b)] and short coherence time, NLPs are attractive for applications like supercontinuum generation [3], sensing or micromachining [4], among others. Recently, these complex pulses also attracted the attention of physicists engaged in the quest for optical rogue waves [5].

In this work we will present the recent advances of our group in the study of NLPs generated from passively mode-locked lasers in both figure-eight [Fig. 1(c)] and ring [Fig. 1(d)] configurations [6,7]. Diverse aspects will be tackled, including the understanding of the

mechanisms of formation of NLPs, the adjustability of their parameters, the existence of single- or multiple-pulsing regimes (including harmonic mode locking) and the challenging task of characterizing precisely these pulses. Next, potential applications of NLPs will be discussed. Finally, an intriguing NLP dynamics, which was recently discovered and bears some analogy with the so-called soliton rain/release of solitons dynamics [8], will be presented.

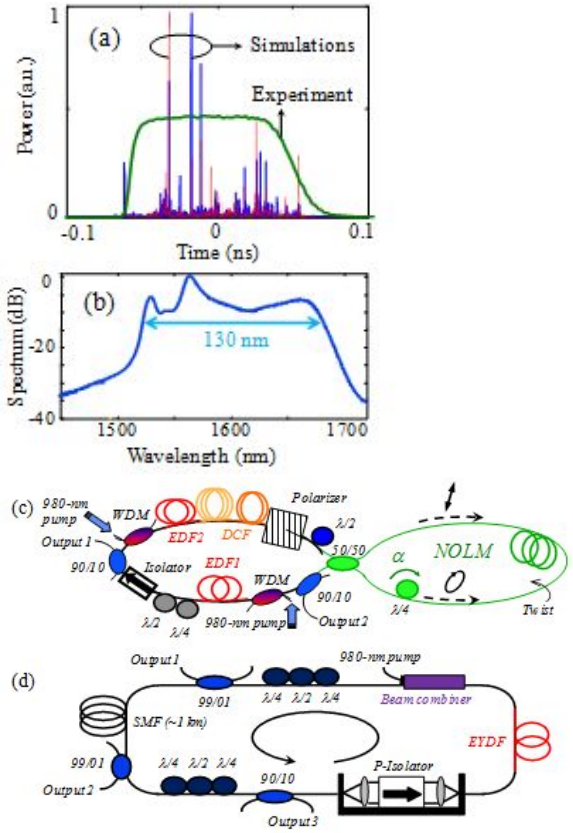

Fig1. (a) Temporal profiles of NLPs (2 simulated waveforms separated by one cavity round-trip and their envelope measured using 25-GHz photodetector and sampling scope), (b) typical optical spectrum (measured using an optical spectrum analyzer) and (c) figure-eight and (d) ring laser schemes used for NLP generation.

1. M. Horowitz and Y. Silberberg, *IEEE Photonics Technology Letters* **10**, 1389 (1998).
2. Y. Jeong at al., *Optical Fiber Technology* **20**, 575 (2014).
3. A. Zaytsev et al., *Optics Express* **21**, 16056 (2013).
4. K. Özgören et al., *Optics Express* **19**, 17647 (2011).
5. C. Lecaplain and Ph. Grelu, *Physical Review A* **90**, 13805 (2014).
6. O. Pottiez et al., *Applied Optics* **50**, E24 (2011).
7. O. Pottiez et al., *Laser Physics* **24**, 115103 (2014).
8. S. Chouli and Ph. Grelu, *Physical Review A* **81**, 63829 (2010).

D19: Optical properties of type II quantum wells predicted for active region in Interband Cascade Lasers

Marcin Motyka

Laboratory for Optical Spectroscopy of Nanostructures, Department of Experimental Physics,Wrocław University of Technology, Wybrzeże Wyspiańskiego 27, Wrocław, Poland Email:marcin.motyka@pwr.edu.pl, web site: http:// http://www.osn.if.pwr.wroc.pl

The Applications related to the detection of hazardous and environmentally-relevant gasses drive the growing demands with respect to all the sensor system components, requiring cheap and compact laser sources. This can be well fulfilled by semiconductor lasers, where one of the efficient solutions is interband cascade laser (ICL[1-3]). Such devices have already been proven to emit at some wavelengths of the mid-infrared (even beyond 10 μm), i.e. in ranges characteristic for maximal absorption of many gasses, and shown to offer continuous wave single mode operation at room temperature between 3 and 5 μm, and additionally significantly lower power consumption [2] than the more common quantum cascade lasers. However, ICLs still need further developments regarding especially the demanded performances at longer wavelengths, broad bandwidth or widely tunable devices.

It has been investigated, both experimentally and theoretically, several modifications in the active region of the ICLs. The considered type II quantum wells are based on InAs/(Ga,In)(As,Sb) materials combinations (see Fig1.), forming a broken gap system, confining electrons and

holes in spatially separate layers, typically grown on either GaSb or InAs substrates. These studies were aimed to maximizing the optical transition oscillator strength (OS) via tailoring the electronic structure, the related strain and wave function engineering. The OS is the most critical parameter of the type II system because it can allow for compensating the intrinsic losses while extending the emission wavelength or the gain bandwidth.

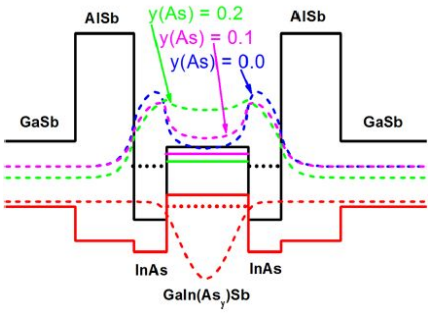

Fig.1. Band structure diagram together with electron and holes wave functions for layers with different Arsenic content.

A combination of two spectroscopic techniques were used, emission-like (photoluminescence) and absorption-like (modulated reflectivity) supported by the energy level calculations employing multiband k•p modeling. It was demonstrated, that addition of arsenic into the commonly used ternary layer of GaInSb for the holes confinement can significantly enhance the transition OS, while decreasing the overall strain and keeping still the type II design [4,5]. Moreover, it was also shown, that use of a triple type II quantum well structure instead of a typically used double well "W-design" allows for simultaneous red shift of the transition energy and increase of the oscillator strength [6]. Eventually, further structure optimizations utilizing uncommon material combinations will be discussed. In this part, application of the GaAsSb layers instead of typically used GaInSb will be consider as a new way for holes confinement. Performed calculation includes strain engineering, will be finally supported by their experimental verification.

1. R. Q. Yang, Superlattices and Microstructures **17**, 77 (1995).
2. I. Vurgaftman et al., Nature Commun. **2**, 585 (2011).
3. A. Bauer et al., Appl. Phys. Lett. **95**, 251103 (2009)
4. F. Janiak et al., Appl. Phys. Lett. **100**, 231908 (2012).
5. K. Ryczko et al., J. Appl. Phys. **114**, 223519 (2013).
6. Motyka et al., J. Appl. Phys. **117**, 084312 (2015)

D20: Er:Yb double clad single mode fiber laser configurations

Baldemar Ibarra-Escamilla*[1], Evgeny A. Kuzin[1], M. Duran-Sanchez[1], Ricardo I. Alvarez-Tamayo[1], Olivier Pottiez[2] and Andrés González-García[3]

[1]*Instituto Nacional de Astrofísica, Optica y Electrónica, Luis Enrique Erro No. 1, Puebla Pue 72000, Mexico.*
**Email: baldemar@inaoep.mx*
[2]*Centro de Investigaciones en Optica, Loma del Bosque No. 115, León, Gto 37150, Mexico.*
[3]*Instituto Tecnológico Superior de Guanajuato, Carretera Estatal Guanajuato-Puentecillas, km., 10.5, C. P. 36262, Guanajuato, Gto., México.*

During the last years we have been working with different fiber configurations like mode-locked fiber lasers and Q-Switched fiber laser. For the first one configuration, we are considering the passive mode-locked fiber laser as a simple and effective setup to generate ultrashort pulses. Many mode-locking techniques have been reported to implement a passive mode-locked laser including semiconductor saturable absorber, nonlinear amplifier loop mirror (NALM), Nonlinear Optical Loop Mirror (NOLM) and nonlinear polarization rotation with a polarizer. Configurations that include a NOLM or a NALM are called Figure-Eight fiber Lasers (F8L). For the second one configuration, we have reported an efficient and stable operation at the wavelength 1549 nm of an actively Q-switched fiber laser base on Er:Yb doped, double-clad, single mode fiber. It operates with a repetition rate from 45 to 120 kHz and pulse duration from 34 to 80 ns, the output pulse shape and peak pulse intensity are stable over hours

operation. For a repetition rate of 120 kHz and a maximum pump power of 8.1 W we obtained an average output power of 4.0 W with an overall efficiency of 50% and with minimum pulse duration of 34 ns. [1] In other configuration, we reported a double-clad Er/Yb doped fiber tunable laser in continuous wave (*cw*) and actively Q-switched fiber laser using a fiber Bragg grating (FBG) as wavelength selective in a linear cavity resonator. The laser was tuned in a range from 1532 to 1542 nm for both *cw* and pulsed mode. The minimum pulses duration were obtained with 420 ns at a repetition rate of 120 kHz and ~0.7 W average output power in *cw* (slope efficiency of ~8%) and 1.03 W average output power in pulsed mode (slope efficiency of ~12%). [2]

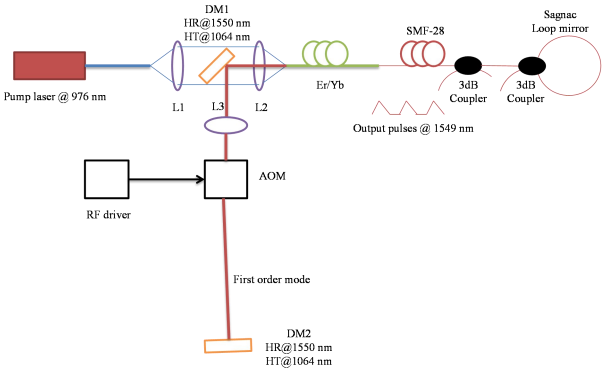

Fig1. Schematic diagram of the actively Q-switched Er/Yb doped double clad fiber laser. [1]

1. A. González-García, B. Ibarra-Escamilla, E. A. Kuzin, F. Maya-Ordoñez, M. Durán-Sánchez, O. Pottiez, C. Deng, J. W. Haus, and P. E. Powers, Optics and Laser Technology **48** 182 (2013).
2. A. González-García, B. Ibarra-Escamilla, O. Pottiez, E. A. Kuzin, F. M. Maya-Ordoñez, and M. Duran-Sánchez, Laser Physics **25** 045104 (2015).

D21: High energy high frequency P-P lasers

V.V. Apollonov

Prokhorov General Physics Institute, Vavilov str.38, Moscow, Russia, 119991

The goal of the talk is to present the high-energy high-frequency pulse periodic (P-P) laser systems, which in the nearest time will find a lot of applications in the field of ecology, machinery, space engineering, nuclear technologies and many others. A laser-plasma generator of multiply charged ions produces a large number of heavy ions in the regime of short periodic pulses, which is of interest for ion accelerators operating in the P-P regime as well is the topic of high interests. The source of this type is also promising for effective use in the field of heavy-ion fusion, brittle materials figure cutting, oil films elimination from the water surface and so on. Paper has considered in details a new approach to the problem of a laser jet engine creation, which is based on the resonance merging of shock waves generated by an optical pulsating discharge, produced by such a P-P laser. To obtain an optical pulsating discharge, we suggested the usage of high-energy P-P laser radiation, which can be generated by wide aperture carbon dioxide, chemical and mono-module disk type solid-state laser systems. Future developments of the disk laser technology as the most effective and scalable to the level of many hundreds of kW as well are under consideration in the paper.

D22: Intra-articular carbon nanotubes in the treatment of osteoarthritis

Massimo Bottini[1,2], C. Sacchetti[1,3], R. Liu-Bryan[4], A. Magrini[5], N. Rosato[2], N. Bottini[3]

[1] *Inflammatory and Infectious Disease Center, Sanford Burnham Medical Research Institute, La Jolla, CA 92037, USA.*
Email: mbottini@sanfordburnham.org
Web site: http://labs.sanfordburnham.org/centerandlabs/infectiousdisease/bottinilab

[2] *Department of Experimental Medicine and Surgery, University of Rome Tor Vergata, Rome, Italy.*

[3] *Division of Cellular Biology, La Jolla Institute for Allergy and Immunology, La Jolla, CA 92037, USA.*

[4] *Department of Medicine, VA Medical Center, University of California San Diego, San Diego, CA, USA.*

[5] *Department of Biopathology and Imaging Diagnostics, University of Rome Tor Vergata, Rome, Italy.*

Osteoarthritis (OA) is the most common form of arthritis and leads to irreversible cartilage damage. Currently, there is no disease-modifying OA drugs (DMOADs) approved by the Food and Drug Administration and blocking OA progression is an unfulfilled challenge in Rheumatology. The recent discovery that OA progression is governed by the transition of chondrocytes from a cartilage-producing anabolic state to a cartilage-degrading catabolic state led to the identification of several biochemical pathways that are ideal targets for OA therapy. Nevertheless, the delivery of compounds into chondrocytes is still a limiting factor to translate these findings into innovative OA therapies. Intra-articular (IA) administration is theoretically an effective way to ensure delivery of DMOADs into chondrocytes, however success using this route is currently hampered by the fast clearance of compounds from the synovial cavity through the loose synovial lining and lack of compound penetration through the cartilage extra-cellular matrix.

We recently found that IA-administered PEG-modified carbon nanotubes (IA-PNTs) had a long joint half-life (2 weeks) and efficiently accumulated into chondrocytes of OA mice, without eliciting local side-effects in mice. IA-PNTs carrying anti-green fluorescent protein (GFP) morpholino anti-sense oligonucleotides (GFP-ASOs) enabled the inhibition of GFP expression in chondrocytes of OA GFP-transgenic mice [1]. We also found that neutrophils degraded PNTs *ex vivo* through the combined action of proteases and myeloperoxidase, which are present in OA joints [2]. These data suggest that IA-PNTs might be used for efficient and safe delivery of DMOADs into OA chondrocytes.

1. C. Sacchetti, R. Liu-Bryan, A. Magrini, N. Rosato, N. Bottini, M. Bottini, *ACS Nano* **8**, 12280 (2014).

2. K. Bhattacharya, C. Sacchetti, R. El-Sayed, A. Fornara, G.P. Kotchey, J.A. Gaugler, A. Star, M. Bottini, B. Fadeel, *Nanoscale* **6**, 14686 (2014).

D23: Interactions between carbon-based nanomaterials and the immune system: focus on inflammation

Bengt Fadeel[1]

[1]*Nanosafety & Nanomedicine Laboratory, Institute of Environmental Medicine, Karolinska Institutet, Stockholm, Sweden*
E-mail: bengt.fadeel@ki.se, web site: http://ki.se/en/imm/unit-of-molecular-toxicology

Inflammation is a complex protective response to harmful stimuli including pathogens, damaged or dying cells, and other irritants. However, inflammation is a double-edged sword insofar as chronic inflammation can lead to destruction of tissues thus compromising the homeostasis of the organism. Recent studies from several laboratories have shown that engineered nanomaterials can trigger activation of the inflammasome complex in phagocytes resulting in secretion of pro-inflammatory cytokines [1]. On the other hand, neutrophils and eosinophils, key cells of the innate immune system, have been shown to be capable of peroxidase-mediated degradation of carbon nanotubes (CNTs), with mitigation of the pro-inflammatory effects. Moreover, neutrophils produce so-called neutrophil extracellular traps (NETs) consisting of chromatin fibers plus neutrophil granule proteins to capture bacteria and fungi and recent work has revealed that NETs can also capture CNTs leading to acellular degradation. Recent studies from our laboratory have shown that graphene oxide (GO) also triggers IL-1β secretion production in lipopolysaccharide (LPS)-primed macrophages, and we also found that GO can undergo peroxidase-mediated degradation. This presentation will focus on the reciprocal interactions between carbon-based nanomaterials and cells of the immune system.

1. C. Farrera and B. Fadeel. It takes two to tango: Understanding the interactions between engineered nanomaterials and the

immune system. *Eur J Pharm Biopharm*. 2015 Mar 11. [Epub ahead of print].

D24: Dendrimer Nanomedicine for Targeted Cancer Gene Therapy

Leyuan Xu[1], W. Andrew Yeudall[2,3], Hu Yang[2,3]

[1]*Department of Biomedical Engineering, Virginia Commonwealth University, Richmond, Virginia 23284, USA*

[2]*Philips Institute of Oral and Craniofacial Molecular Biology, Virginia Commonwealth University, Richmond, Virginia 23298, USA*

[3]*Massey Cancer Center, Virginia Commonwealth University, Richmond, Virginia 23298, USA*
Email:hyang2@vcu.edu

Head and neck squamous cell carcinoma (HNSCC) is the sixth most common cancer worldwide. Improvements in clinical outcome have not mirrored the major advances in chemotherapeutic and surgical protocols that have been made in recent decades. To treat HNSCC more effectively, we are exploring unconventional modalities with the aid of nanotechnology. One of our research projects is development of an efficient nanostructured nonviral vector for gene therapy of HNSCC. Nonviral vectors can be engineered to avoid toxicity and immunogenicity, achieve high gene carrying capacity and tumor specificity, and allow low-cost manufacturing. Nonetheless, existing nonviral vectors are far less efficient than viral vectors in gene transfection due to the lack of adequate functions to overcome extra- and intra-cellular barriers and, as a result, have limited clinical utility in treating HNSCC and many other cancers. To develop a nonviral vector meeting both safety and clinical acceptable transfection efficiency in gene therapy of HNSCC, we utilized highly branched nanoscale polyamidoamine (PAMAM) dendrimers as a platform and explored RNA interference technology as a therapeutic tool. Our recent in vitro and in vivo studies have demonstrated that functionalized dendrimer nanoparticles resulted in enhanced delivery, improved transfection, or tumor-specific targeting and imaging. Furthermore, nanoparticle-mediated delivery of nucleic acid therapeutics such as siRNA effectively inhibited cancer cell growth, proliferation, and metastasis through gene knockdown.

D25: Self-assembling zwitterionic nanogels for pancreatic islet immunoisolation

Omid Veiseh

Massachusetts Institute of Technology, USA , veiseho@mit.edu

Abstract
The concept of pancreatic islet transplantation to patients with diabetes to restore normoglycemia is viable clinical strategy. However, widespread clinical application of islet transplantation remains limited because of the deleterious side effects of immunosuppressive therapy necessary to prevent host rejection of transplanted cells. Here we report the fabrication of an MRI detectable superbiocompatible nanogel and a novel coating strategy for the protection of pancreatic islet cells against host rejection in vivo. Superparamagentic Iron Oxide nanoparticle loaded Zwitterionic nanogels (100-300nm in size) where fabricated using an emulsion polymerization synthesis scheme and further surface modified with CLICK reactive functional groups. Pancreatic islet cells where engineered to express azide functionalities on their cell membranes and used as chemical handles to control assembly of nanogels onto cell surfaces. Confocal fluorescence microscopy was used to verify covalent reaction and assembly of nanogel coating on to engineered islet cell clusters. Cytocompatibility of coating and islet cell functionality where examined using a combination of in vitro glucose tolerance tests and live/dead staining. Our results indicate that developed nanogel formulation and encapsulation strategy provides a viable strategy for prolonged protection and enable non-invasive MRI based tracking of transplanted islets.

B15: Trapping and Breakdown in GaN Devices: A Simulation Study

Kazushige Horio
Faculty of Systems Engineering, Shibaura Institute of Technology, Saitama 337-8570, Japan
Email:horio@sic.shibaura-it.ac.jp

AlGaN/GaN HEMTs are now receiving great attention for applications to microwave power devices and high-power switching devices [1, 2]. However, slow current transient due to traps are often observed even if the gate voltage or the drain voltage is changed abruptly. This is called gate lag or drain lag. The slow transient means that the RF current-voltage (*I*-*V*) curves and dc *I*-*V* curves become quite different, resulting in lower RF power available than that expected from the dc operation. This is called current collapse. This phenomenon also appears as an increase in the dynamic on resistance when the switching device is concerned. It is also recognized that the breakdown voltage of AlGaN/GaN HEMT is usually lower than that expected from the critical electric field (~ 3 MV/cm). To improve the breakdown voltage, the introduction of field plate [3] and the introduction of a high-*k* passivation layer [4] are considered.

In this talk, we will present our simulation works on AlGaN/GaN HEMTs. It is shown that the lag phenomena and current collapse are reproduced by considering deep levels in the semi-insulating GaN buffer layer [5]. The lags and current collapse are shown to be reduced by introducing a field plate, because the electric field at the drain edge of the gate is reduced, and the electron injection into the buffer layer and the resulting trapping effects are reduced [6]. We will next discuss the breakdown voltage. The off-state breakdown of AlGaN/GaN HEMTs is shown to increase by introducing a field plate, because the electric field at the drain edge of the gate is reduced, but an optimum field-plate length exists when a small-gate-to-drain device is considered [7]. It is also shown that the introduction of high-*k* passivation layer is effective to improve the off-state breakdown voltage because the electric field at the drain edge of the gate is reduced [4].

Next, we will describe an example of calculated results [4]. Fig.1 shows an example of device structure analyzed here. Fig.2 shows the calculated off-state drain current – drain voltage characteristics of AlGaN/GaN HEMTs as a parameter of relative permittivity of passivation layer ε_r. The solid lines show the case with impact ionization, and the dashed lines shows the case without impact ionization. The drain current in this case corresponds to the buffer leakage current, which is clearly seen to be lower for higher ε_r. When ε_r is relatively low ($\leq$ 20), an abrupt increase in the drain current due to impact ionization of determines the breakdown voltage because the electric field at the drain edge of the gate becomes very high. (Here, the breakdown voltage is defined as a drain voltage when the drain current becomes 1 mA/mm.) However, when ε_r is relatively high ($\geq$ 30), the electric filed at the drain edge is weakened, and the buffer leakage current reaches 1mA/mm before the abrupt increase in the drain current, and it determine the breakdown voltage. Therefore, the breakdown voltage becomes higher when the high-*k* layer is used.

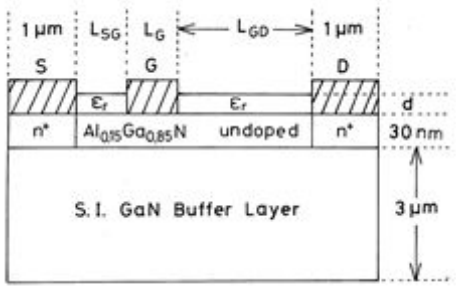

Fig1. Device structure analyzed here.

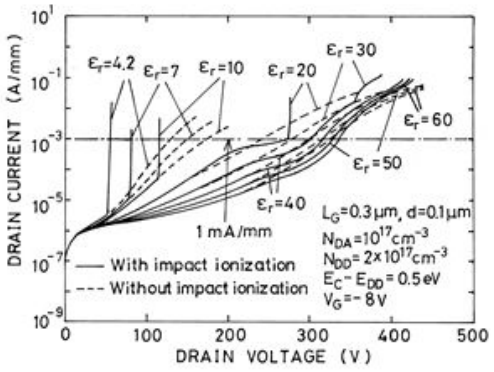

Fig.2. Calculated $I_D - V_D$ curves as a parameter of ε_r. L_{GD} = 1.5 μm and d = 0.1 μm.

1. U. K. Mishra, L. Shen, T. E. Kazior, and Y.-F. Wu, *Proc. IEEE* **96**, 287 (2008).
2. N. Ikeda et al., *Proc. IEEE* **98**, 1151 (2010).
3. S. Karmalkar and U. K. Mishra, *IEEE Trans. Electron Devices* **48**, 1515 (2001).
4. H. Hanawa, H. Onodera, A. Nakajima and K. Horio, *IEEE Trans. Electron Devices* **61**, 769 (2014).
5. K. Horio and A. Nakajima, *Jpn. J. Appl. Phys*. **47**, 3428 (2008).
6. K. Horio, A. Nakajima, and K. Itagaki, *Semicond. Sci. Technol*. **24**, 085022 (2009).
7. H. Onodera and K. Horio, *Semicond. Sci. Technol*. **27**, 085016 (2012).

B16: Layered $(In_xGa_{1-x})_2Se_3$ (III_2-VI_3) Compounds as Novel Buffer Layers for GaAs on Si System

Nobuaki Kojima, Yoshio Ohshita, and Masafumi Yamaguchi

Toyota Technological Institute, Nagoya, JAPAN
Email: nkojima@toyota-ti.ac.jp

III-V compound solar cells on Si have been investigated extensively with expectations of the significant cost reduction of high efficiency multi-junction solar cells. Si substrate is more inexpensive and abundant than Ge substrate, which is the usual substrate material for multi-junction cells. In addition, the band gap energy of Si is suitable to realize high efficient dual and triple-junction solar cells. However, the large lattice mismatch and thermal expansion coefficient difference between GaAs and Si generate a high density of threading dislocations in III-V overlayers grown on Si, which severely reduce GaAs material quality, minority carrier lifetimes, and ultimately solar cell performance. To overcome such difficulties, numerous approaches have been investigated for more than two decades, including the two-step growth, the thermal cycle annealing, the graded buffer layers, and the strained superlattice interlayers. In spite of these approaches, the threading dislocation densities in GaAs on Si system have not been reduced below 10^6 cm^{-2}. A further improvement in conversion efficiency can be obtained by reducing the dislocations densities to less than 10^5 cm^{-2}, in the GaAs/Si system.

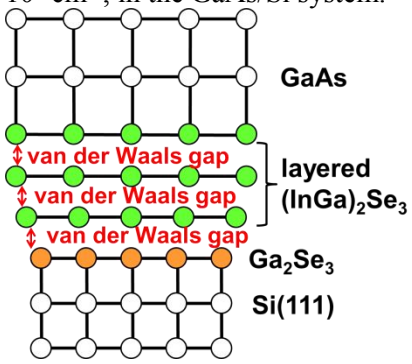

Fig. 1 Schematic drawing of proposed $(In_xGa_{1-x})_2Se_3$ buffer layers for the GaAs on Si(111) system.

We proposed novel buffer layers consisting of defect zincblende structured $(In_xGa_{1-x})_2Se_3$ (III_2-VI_3) compounds for the GaAs on Si(111) system, as shown in Fig. 1. $(In_xGa_{1-x})_2Se_3$ has the lattice constant between that of Si and GaAs, depending on In content, and can have layered structure with loose van der Waals gaps. In this crystallographic orientation, the layered defect zincblende $(In_xGa_{1-x})_2Se_3$ can be grown on Si epitaxially with the van der Waals gaps aligned parallel with the Si(111) substrate surface. The van der Waals interface of the layered structure should absorb any strain caused by lattice mismatch and thermal expansion coefficient difference between Si and GaAs.

However, III-VI compounds have several stable compositions and polytype structures other than the defect zincblende structure. In the case of In-Se system, In_4Se_3, InSe, In_4Se_7 and In_2Se_3 are known as the stable compositions, and α-, β-, γ-, δ-type In_2Se_3 are known as the polytype structures. The layered defect zincblende In_2Se_3 is classified as α-type. Furthermore, weak van der Waals bonding may cause twin crystal domain formation during the crystal growth. Such twin defects should be eliminated from the epi-layer for use of the buffer layer between GaAs and Si.

In this paper, we will report the GaAs(111) vicinal substrates are effective for the both of the preferential growth of α-type In_2Se_3 and the

suppression of twin formation by predominating the step-flow growth at the surface step edge.

B17: Pathways for lowering the Interface Trap Density in Ge based MOS devices

O. Bethge[1], C. Zimmermann[1], B. Lutzer[1], J. Kauer[1], E. Bertagnolli[1]

[1]Institute for Solid State Electronics, Vienna University of Technology, Vienna, Austria Email:ole.bethge@tuwien.ac.at, web site: http://fke.tuwien.ac.at

The continuously downscaling of the device dimensions in Metal Oxide Semiconductor Field-Effect Transistors (MOSFET) in the Complementary (CMOS) technology gave birth of several outstanding innovations. One of the most important invention was the high-*k* metal gate stack introduced for lowering exceeding gate leakage currents caused by ultra-scaled SiO2 gate oxide, which ran out of atoms [1]. The next important change in CMOS technology is expected to be the replacement of the silicon channel by alternative semiconductor materials with demanded higher charge carrier mobility. The most promising candidate for pMOS transistors is germanium, offering 4 times higher hole mobility compared to Si. However, the implementation of the high-*k* metal gate stack in Ge based MOSFET is challenging due to a restive Ge surface.

Due to an outstanding step coverage, homogeneity, and thickness control, Atomic Layer Deposition (ALD) is the most applicable deposition technique for the growth of the high-*k* gate oxide on various semiconductors [2]. Main issues to solve are the finding of a suited high-k oxide which can be grown by ALD offering a stable interface layer on Ge with a low interface trap density and a low equivalent oxide thickness (EOT) at the same time.

In this presentation, processing pathways are shown how the interface trap density (Dit) in Ge based MOS devices can be effectively lowered. By means of ALD-grown ZrO2, HfO2, and Y2O3 on (100)-Ge substrates, the impact of several annealing techniques will be discussed in terms of electrical, physical, and chemical properties. By using X-ray Photoelectron Spectroscopy, High Resolution Transmission Electron Microscopy, Electron Energy-loss Spectroscopy, and several electrical characterization techniques, a stable interface layer is identified able to lower down the Dit to values which are comparable to well established High-*k*/SiO2/Si gate stacks.

1. K. Mistry *et al.*, *Electron Devices Meeting, 2007. IEDM 2007. IEEE International*, 247 (2007).
2. T. Suntola, *Applied Surface Science* **100-101**, 391 (1996).
3. O. Bethge *et al.*, *Journal of Applied Physics* **116,** 214111 (2014).

B18: Control of the surface chemistry during inductively-coupled plasma etching of InP and related compounds for the fabrication of photonic devices

Sophie Bouchoule[1]

[1]Laboratoire de Photonique et de Nanostructures LPN, CNRS, Route de Nozay, 91 460 Marcoussis, France Email:sophie.bouchoule@lpn.cnrs.fr, web site: http://www.lpn.cnrs.fr

III-V semiconductors are important materials for the development of efficient optical emitters. Among them InP and related compounds are required for the fabrication of laser diodes and photonic integrated circuits operating in the 1.3 µm-1.5 µm wavelength range for optical communications. The need for larger device integration and tighter photonic confinement has pushed forward the development of highly anisotropic plasma etching processes for making deeply etched high-reflectivity mirrors, nano-ridge waveguides, micro-ring, or photonic-crystal cavities. A dry-etching process that can vertical and smooth sidewalls free from undercuts or notches is crucial in order to minimize the optical scattering losses in such devices. Inductively coupled plasma (ICP) etching has been used widely for this purpose, and various chlorine-containing chemistries have

been proposed for the patterning of InP-based heterostructures. However the etching mechanisms are generally poorly understood. In this talk we will present an experimental study of the passivation mechanisms taking place during anisotropic ICP etching of InP with chlorine- or HBr-containing chemistries. We will show that anisotropic etching of InP-based heterostructures is possible owing to the controlled deposition of a SiO_x passivation layer on the etched sidewalls.[1] The important plasma parameters promoting this passivation mechanism will be identified.[2] Several etching chemistries allowing for such a passivation mechanism will be proposed, leading to an aspect ratio as high as 1:20.[3,4] Finally it will be shown that the smoothness of the etched surface depends on temperature, and that in the temperature range where smooth InP etching occurs, the etched surface is P-rich, and not In-rich as it is generally expected considering the low volatility of the InClx reaction products. The phosphorous top-layer is formed at the plasma/InP interface both on the bottom etched surface and the etched sidewalls.[5,6] The surface P-enrichment is very strong for chlorine-containing chemistries, and may be reduced when using HBr as an etching gas.

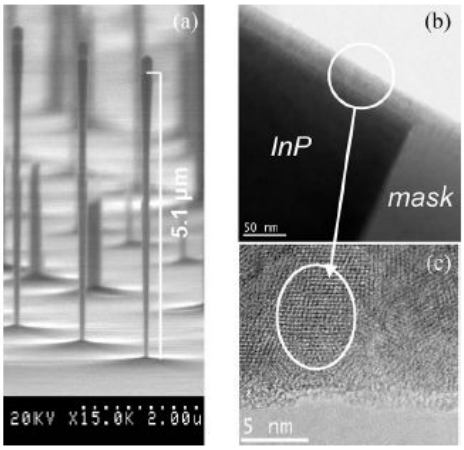

Fig1. (a) :Ansisotropic ICP etching of InP obtained with SiH_4/Cl_2 plasma chemistry showing a record aspect ratio higher than 1:20 (SEM image).

(b)-(c) : STEM image of the etched sidewall showing the Si-rich SiOx passivation layer deposited on the etched sidewalls with this chemistry.

1. S. Bouchoule, G. Patriarche, S. Guilet, L. Gatilova, L. Largeau, and P. Chabert, J. Vac. Sci. Technol., B 26, 666 (2008).
2. L. Gatilova, S. Bouchoule, S. Guilet, and P. Chabert, , J. Vac. Sci. Technol., B 27, 262 (2009)
3. L. Gatilova, S. Bouchoule, S. Guilet, and G. Patriarche, J. Vac. Sci. Technol. B 29, 020601 (2011).
4. S. Bouchoule, L. Vallier, G. Patriarche, T. Chevolleau, C. Cardinaud, J. Vac. Sci. Technol. A 30, 031301 (2012).
5. R. Chanson, S. Bouchoule, C. Cardinaud, C. Petit-Etienne, E. Cambril, A. Rhallabi, S. Guilet, and E. Blanquet, J. Vac. Sci. Technol. B 32, 011219 (2014).
6. S. Bouchoule, R. Chanson, A. Pageau, E. Cambril, S. Guilet, A. Rhallabi, and C. Cardinaud, *submitted* to J. Vac. Sci. Technol. A (2015)

B19: Modeling of the Space-charge Region in Nanowire Junctions

Shreepad Karmalkar, V. K. Gurugubelli

Department of Electrical Engineering, Indian Institute of Technology Madras, Chennai 600036, India
Email:karmal@ee.iitm.ac.in, web site:http://www.ee.iitm.ac.in/~karmal/

Today, intense efforts are on [1, 2] to fabricate conventional semiconductor devices in semiconductor nanowires (NWs) (see Fig. 1(a)) to harness the unique properties of materials in the nano-scale. Junctions form an essential part of these NW devices (see Fig. 1(b)). Hence, modeling of their space-charge region (see Fig. 1(c)) is indispensable for NW device design. Unlike in bulk junction, the surrounding field plays an important role in a NW junction (see Fig. 1(c)). Hence, the depletion width W of a NW junction depends on the radius R, the effective separation $2S$ and ambient permittivity ε_a, apart from the parameters which affect a bulk junction, namely - semiconductor doping N_A, semiconductor permittivity ε_s, and the potential drop V_d across the junction. We present the derivation of the following simple text-book like formula for W on the lightly doped p-side of a

one-sided p-n junction in a semiconductor NW array [3], and discuss it's application to device design.

$$W \approx W_B\sqrt{1+\frac{\varepsilon_a}{\varepsilon_s}\left[\left(\frac{S}{R}\right)^2-1\right]} \quad \text{for } W \quad R,S; \qquad W_B=\sqrt{\frac{2\varepsilon_s V_d}{qN_A}}$$

Here, W_B is the depletion width on the lightly doped side of the corresponding bulk junction and q is the electronic charge. As shown in Fig.2 the results of the above formula agree with numerical simulations.

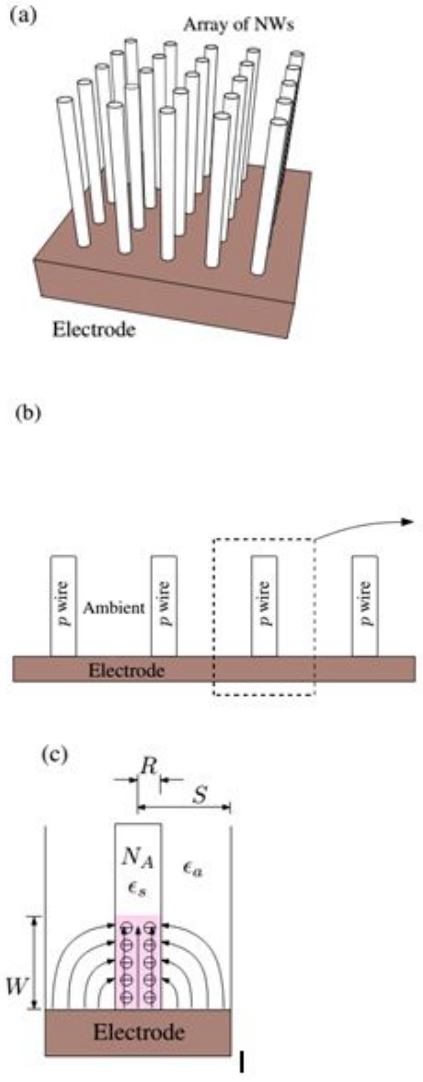

Fig.1. (a) 3D view of a junction between an array of semiconductor NWs and an electrode layer, which could be a heavily doped semiconductor of opposite polarity or metal. (b) A cross-section of the junction showing a few wires. (c) Space-charge region, field lines and parameters associated with a wire of the array.

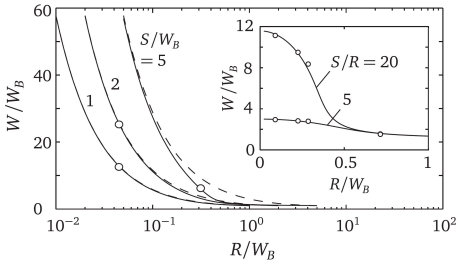

Fig. 2. Depletion width of a Si NW array versus NW radius for different values of S and S/R (inset). The ambient is SiO_2 so that $\varepsilon_s/\varepsilon_a = 3$, and the electrode is metal. Legend: dashed lines – simple Eq. (1); solid lines – infinite series solution; circles – numerical simulations for $N_A = 10^{16}$, 10^{17} cm^{-3}, $V_d = 0.4$ V, $R =$ 10, 20, 50, 70 nm.

1. J.Goldberger, A. I. Hochbaum, R. Fan, and P.Yang, *Nano Lett.* **6**, 973 (2006).
2. A. D. Franklin and Z. Chen, *Nat. Nanotechnol.* **5**, 858 (2010).
3. V. K. Gurugubelli and Shreepad Karmalkar, *Appl. Phys. Lett.* **104**, 203502 (2014)

B20: Monolithic Platforms for Mid-Wave Infrared (MWIR) Sensing

Hongtao Lin, Jianfei Wang, Pao-Tai Lin, Vivek Singh, Timothy Zens, Anu Agarwal, Lionel C. Kimerling, Juejun Hu

Department of Materials Science & Engineering, MIT, Cambridge, MA, USA Email:hujuejun@mit.edu, web site: http://web.mit.edu/hujuejun/www/

Mid-wave infrared (MWIR, 3-6 μm in wavelength) is a strategically important wave band for imaging and sensing. Unfortunately, development photonic devices operating in these wavelength regime have been hampered by exacerbated thermal noise as well as high cost due to complicated hybrid integration. In this talk we will discuss two monolithic photonic platforms to enhance MWIR device performance: on-chip resonator chemical sensors based on chalcogenide glasses, and cavity-enhanced MWIR detectors based on polycrystalline lead chalcogenides.

1. J. Hu, L. Li, H. Lin, Y. Zou, Q. Du, C. Smith, S. Novak, K. Richardson, and J. D. Musgraves, "Chalcogenide glass microphotonics: Stepping into the spotlight," *Am. Ceram. Soc. Bull.* **94**, 24-29 (2015).
2. H. Lin, L. Li, Y. Zou, S. Danto, J. D. Musgraves, K. Richardson, S. Kozacik, M. Murakowski, D. Prather, P. Lin, V. Singh, A. Agarwal, L. C. Kimerling and J. Hu, "Demonstration of high-Q mid-infrared chalcogenide glass-on-silicon resonators," *Opt. Lett.* **38**, 1470-1472 (2013).
3. J. Wang, T. Zens, J. Hu, P. Becla, L. C. Kimerling, and Anuradha M. Agarwal, "Monolithically integrated, resonant-cavity-enhanced dual-band mid-infrared photodetector on silicon," *Appl. Phys. Lett.* **100**, 211106 (2012).
4. J. Wang, J. Hu, P. Becla, A. Agarwal, and L. C. Kimerling, "Room-temperature oxygen sensitization in highly textured, nanocrystalline PbTe films: A mechanistic study," *J. Appl. Phys.* **110**, 083719 (2011).

B21: Properties of PbTe mid-infrared imaging devices of focal plane arrays

Arata Yasuda[1], Toru Kurabayashi[2, 3], Ken Suto[3], Jun-ichi Nishizawa[3]

[1] Department of Control and Information Systems Engineering, National Institute of Technology, Tsuruoka College, Sawada 104, Inooka, Tsuruoka, Japan
Email:y-arata@tsuruoka-nct.ac.jp, web site: http://www.tsuruoka-nct.ac.jp/en/
[2] Department of Mathematical Science and Electrical-Electronic-Computer Engineering, Akita University, Tegata gakuen-machi, Akita, Japan
[3] Semiconductor Research Institute of Semiconductor Research Foundation, Aramaki-aza-Aoba, Japan

We fabricated p–n-junction-type and Schottky barrier (SB)-type lead telluride (PbTe) mid-infrared focal plane arrays (FPAs) using a flip-chip bonder. Fig.1 shows the typical FPA image. Fig.2 shows the detection wavelength peak of the SB-type FPA shifted from 6.10 μm to 4.95 μm as the ambient temperature was increased from −258.15 °C to −148.15 °C. The detection wavelength peak and cut-off wavelength of the SB-type FPA at −196.15 °C were 5.68 μm and 6.16 μm, respectively. The photoconductivity spectrum of the p–n-junction-type FPA was the sharpest among the spectra of the investigated devices, which was assumed to be a consequence of the Tl-related deep levels in the *p*-type PbTe epitaxial layer in the p–n-junction-type FPA.[1] These deep levels absorb the mid-infrared light and cut-off the detection wavelength range. Thus, the p–n-junction-type FPAs are assumed to be suitable for use in mid-infrared wavelength selectable vision cameras and sensors. The SB-type FPA has a wide depletion layer that can detect a wider mid-infrared range of wavelengths compared to the p–n-junction type because of its high dielectric constant. On the basis of the results obtained in this study, we propose that the fabrication of simple, highly sensitive, mid-infrared imaging devices with a wide scan range is feasible using FPAs based on the PbTe system.

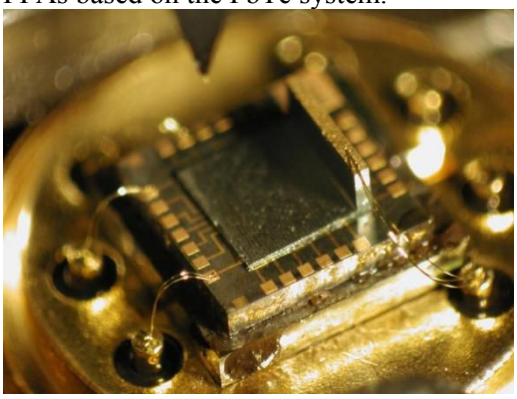

Fig1. Image of a PbTe focal plane array

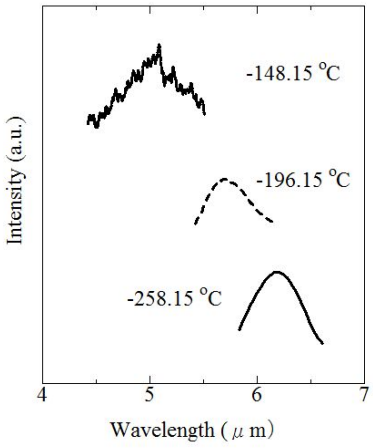

Fig2. Temperature dependence of the infrared detection spectra of a Schottky-barrier-type focal plane

1. A. Yasuda, K. Suto, Y. Takahashi, and J. Nishizawa. Mid-infrared Photoconductive Properties of Heavily Bi-doped PbTe p-n Homojunction Diode Grown by Liquid-phase Epitaxy. Infrared Phys. Technol. vol. 67, 609 (2014)

B22: Cavity Quantum Electrodynamics in a Quantum Dot Molecule – Photonic Crystal Architecture

P. M. Vora[1], A. S. Bracker[2], S. G. Carter[2], T. M. Sweeney[3], M. Kim[4], C. Kim[2], L. Yang[3], P. G. Brereton[5], S. E. Economou[2], and D. Gammon[2]

[1]George Mason University, Fairfax, VA 22030, USA
E-mail: pvora@gmu.edu, Website: http://physics.gmu.edu/~pvora/
[2]Naval Research Laboratory, Washington, DC 20375, USA
[3]NRC research associate residing at the Naval Research Laboratory, Washington, DC 20375, USA
[4]Sotera Defense Solutions, Inc., Columbia, MD 21046, USA
[5]US Naval Academy, Annapolis, MD 21402, USA

Quantum information based on optical cavities often utilizes an atomic Λ-system consisting of two Zeeman split levels coupled to common excited states. In solid state systems, however, the exploration of Λ-systems coupled to cavities is only now beginning. Long-lived spin states in charged InAs quantum dots (QDs) are known to form a Λ-system and have been demonstrated as an optically addressable spin qubit [1]. Recently, our team incorporated charged InAs QDs within a doped GaAs photonic crystal cavity (Fig. 1a,b) where we demonstrated qubit operations in the engineered photonic environment [2] and cavity-stimulated Raman emission [3]. However, the Zeeman splitting in QDs is comparable to the cavity linewidth which makes it difficult to selectively enhance different branches of the QD Λ-system and achieve spin-cavity interactions.

We have overcome this limitation by developing a cavity-coupled quantum dot molecule (QDM) (Fig. 1c). The properties of QDMs (two QDs connected by a coherent tunnel barrier) can be finely tuned during growth [4] and the QDM can be charged with two electrons that hybridize to form a singlet-triplet Λ-system (Fig. 1d). The singlet-triplet splitting is determined by the kinetic exchange interaction which can be controlled by the tunnel barrier. We design our structure so that the singlet-triplet splitting is 1.45 meV, almost an order of magnitude larger than the 0.19 meV cavity linewidth. This is a new spectroscopic regime for cavity-coupled QDs, where the cavity can be coupled exclusively to either the excitation branch or the emission branch of the Λ-system. Tuning the cavity to the excitation branch, we drive the QDM system strongly into the nonlinear regime to investigate the Autler-Townes state dressing (Fig. 1e) and laser-induced control of the spin exchange energy. Incorporation of a highly engineerable QDM into the photonic crystal architecture advances prospects for an all-optical quantum network.

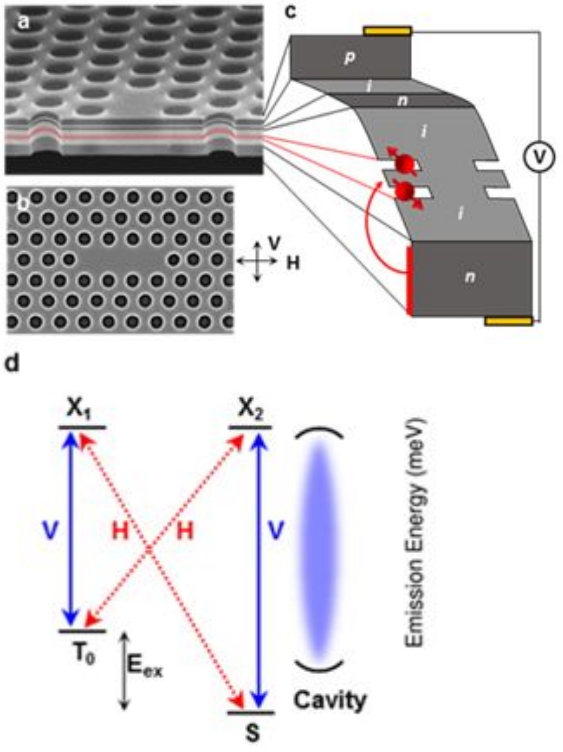

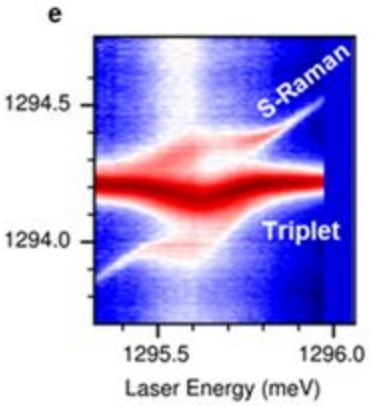

Figure 1: (a) Cross-sectional SEM image of the doped GaAs photonic crystal membrane. (b) Top-down SEM image of the GaAs photonic crystal L3 defect cavity. (c) Band diagram of the doped photonic crystal membrane illustrating the two-electron QDM. d) Level diagram of the two electron QDM. e) Cavity-enhanced Autler-Townes splitting.

1. A. J. Ramsay, *Semiconductor Science and Technology* **25**, 103001 (2010).
2. S. G. Carter, T. M. Sweeney, M. Kim, C. S. Kim, D. Solenov, S. E. Economou, T. L. Reinecke, L. Yang, A. S. Bracker, and D. Gammon, *Nature Photonics* **7**, 329–334 (2013).
3. T. M. Sweeney, S. G. Carter, A. S. Bracker, M. Kim, C. S. Kim, L. Yang, P. M. Vora, P. G. Brereton, E. R. Cleveland, and D. Gammon, *Nature Photonics* **8**, 442–447 (2014).
4. M. Scheibner, A. Bracker, D. Kim, and D. Gammon, *Solid State Communications* **149**, 1427–1435 (2009).

B23: Replication of large-area nanostructures for optical devices

Keisuke Nagato[1,2]

[1]*Department of Mechanical Engineering, The University of Tokyo, Tokyo, Japan Email:nagato@hnl.t.u-tokyo.ac.jp, web site: http://www.nmpl.jp*
[2]*PRESTO, JST, Saitama, Japan*

Optical films with nano- or microstructures are expected to be used in various optical devices such as displays, illuminations, and the lights of traffic signals to increase their performance. For example, antireflection structure [1], light-extraction structure [2], polarization structure [3], photonic crystals [4], light-diffusion structure [5] are the next-generation large-area nano- or microstructures. Furthermore, flexible displays/sensors, or bioplates are also expected to be nanostructured films.

Since nanoimprint lithography (NIL) was developed [6], NIL has been increasingly investigated as a candidate to replace UV and EB lithography. Among NIL, thermal nanoimprinting requires no expensive optical equipment, furthermore, roller thermal nanoimprinting [7] has advantages such as high-throughput and continuity. However, in thermal roller nanoimprinting, the surface of polymer film should be heated, filled into the mold, cooled, solidified, and demolded, by turn at the short contact area for a short time. Meanwhile, the local surface-heating technique was developed and high-speed thermal replication of nanostructures was demonstrated by using a direct Joule heating [8] or a laser irradiation [9]. Our group apply this technique to the roller imprinting. This study introduces the demonstration of diffraction grating, antireflection structure, light-extraction structure, and bioplates by using laser-assisted roller imprinting.

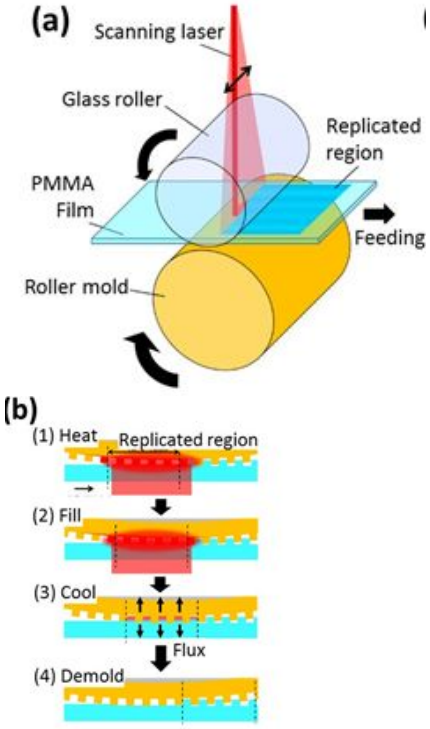

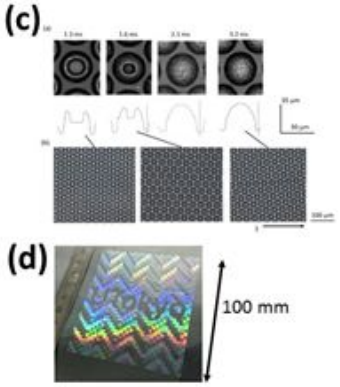

Fig. 1. (a) Schematic of laser-assisted replication system, (b) process of replication, (c) laser microscopy results of replicated microlens array, and (d) a photo of sheet with submicron grating pattern replicated by laser-assisted replication.

1. K. Nagato, H. Moritani, T. Hamaguchi, M. Nakao, *J. Vac. Sci. Technol. B* **28**, L39 (2010).
2. K. Takahashi, K. Nagato, T. Hamaguchi, M. Nakao, *Microelectron. Eng.* in press.
3. A. Leither, Z. Zhao, H. Brunner, F. Aussenegg, A. Wokaun, *Appl. Opt.* **32**, 102 (1993).
4. H. Schift, S. Park, B. Jung, C.-G. Choi, S.-P. Han, K.-B. Yoon, J. Gobrecht, *Nanotechnology* **16**, S261 (2005)
5. T. Thurn-Albrecht, R. Steiner, J. DeRouchey, C.M. Stafford, E. Huang, M. Bal, M. Tuominen, C.J. Hawker, T.P. Russell, *Adv. Mater.* **2**, 787 (2000).
6. S.Y. Chou, P. R. Krauss, P. J. Renstrom, *Appl. Phys. Lett.* **67**, 3114 (1995).
7. K. Nagato, S. Sugimoto, T. Hamaguchi, M. Nakao, *Microelectron. Eng.* **87**, 1543 (2010).
8. K. Nagato, S. Hattori, T. Hamaguchi, M. Nakao, *J. Vac. Sci. Technol. B* **28**, C6M122 (2010).
9. K. Nagato, K. Takahashi, T. Sato, J. Choi, T. Hamaguchi, M. Nakao, *J. Mater. Proc. Technol.* **214**, 2444 (2014).

B24: Ultrabright terahertz-wave generation using nonlinear wavelength conversion at room temperature

Shin'ichiro Hayashi[1], Kouji Nawata[1], Kodo Kawase[1,2], and Hiroaki Minamide[1]

[1]RIKEN Center for Advanced Photonics, 519-1399 Aramakiaoba, Aoba, Sendai, 980-0845 Japan
Email: shayashi@riken.jp, web site: http://www.riken.go.jp/lab-www/tera/index_en.html
[2]Graduate School of Engineering, Nagoya University, Furocho, Chikusa, Nagoya, 464-8603, Japan

The hottest frequency region in terms of research currently lies in the 'frequency gap' region between microwaves and infrared: terahertz waves. Although new methods for generating terahertz radiation have been developed, most sources cannot generate high-brightness terahertz beams. Over the past decade, there has been remarkable growth in the field of terahertz frequency science and engineering, which has become a vibrant, international, cross-disciplinary research activity. Wavelength conversion in nonlinear optical materials is an effective method for generating and detecting coherent terahertz wave radiation owing to the high conversion efficiency, bandwidth, wide tunability, and room-temperature operation.

Here we demonstrate the generation of ultrabright terahertz waves (brightness ~0.2 GW/sr·cm^2, brightness temperature of ~10^{18} K, peak power of >50 kW)[1,2] using parametric wavelength conversion in a nonlinear crystal[3]; this is brighter than many specialized sources such as far-infrared free-electron lasers (~10^{16} K, ~2 kW)[4]. We revealed novel parametric wavelength conversion using stimulated Raman scattering in $LiNbO_3$ without stimulated Brillouin scattering using recently-developed microchip Nd:YAG laser[5]. Furthermore, nonlinear up-conversion techniques allow the intense terahertz waves to be visualized and their frequency determined.

A number of applications require intense, narrowband terahertz waves such as observing multi-photon absorption to specific excitation states. The generation of narrowband mega-watts peak power monochromatic terahertz-wave (sub-nanoseconds duration, several hundreds cycles) pulses with field levels in the megavolt per centimeter range will enable novel applications in terahertz nonlinear optics. We also demonstrated the visualization of generated

terahertz waves using nonlinear up-conversion, which is similar to a wavelength dispersive spectrometer. Additionally, this method also provides phase information of the terahertz wave through the interaction with a simultaneously generated terahertz wave and the idler beam, and furthermore, works as a terahertz-wave amplifier by extracting the terahertz waves generated in a detection crystal. We speculate that the ultrabright terahertz-wave and its visualization could be powerful tools not only for solving real world problems but also fundamental physics, such as real-time spectroscopic imaging, remote sensing, 3D-fabrication, and manipulation or alteration of atoms, molecules, chemical materials, proteins, cells, chemical reactions, and biological processes. We expect that these methods will open up new fields and tune up killer applications.

Acknowledgements
The authors would like to thank Prof. T. Taira of IMS, Dr. Sakai of Hamamatsu Photonics, all of previous and present team members, Prof. H. Ito of RIKEN and Prof. M. Kumano of Tohoku University for useful discussions. This work was partially supported by Collaborative Research Based on Industrial Demand of the Japan Science and Technology Agency (JST), and JSPS KAKENHI Grant Numbers 25220606.

References

1. S. Hayashi, K. Nawata, T. Taira, J. Shikata, K. Kawase, and H. Minamide, *Scientific Reports*, **4**, 05045 (2014).
2. H. Minamide, S. Hayashi, K. Nawata, T. Taira, J. Shikata, and K. Kawase, *Journal of Infrared, Millimeter, and Terahertz Waves*, **35**, 25 (2014).
3. M. A. Piestrup, R. N. Fleming, and R. H. Pantell, *Applied Physics Letters*, **26**, 418 (1975).
4. G. Rarnian, *Nucl. Instrum. Methods Phys. Res.*, Sect. A **318**, 225 (1992).
5. H. Sakai, H. Kan, and T. Taira, *Optics Express*, **16**, 19891 (2008).

B25: The uniformity investigations of type II InAs/GaInSb W-shaped quantum wells wafers by means of mid-infrared photoluminescence spectroscopy

Mateusz Dyksik[1], Marcin Motyka[1], Grzegorz Sęk[1], Jan Misiewicz[1], Mathias Dallner[2], Robert Weih[2],
Martin Kamp[2], Sven Höfling[2,3]

[1] *Laboratory for Optical Spectroscopy of Nanostructures, Department of Experimental Physics, Wrocław University of Technology, Wrocław 50-370, Poland*
Email: mateusz.dyksik@pwr.edu.pl
[2] *Technische Physik, University of Würzburg, Wilhelm-Conrad-Röntgen-Research Center for Complex Material Systems, Am Hubland, Würzburg D-97074, Germany*
[3] *School of Physics and Astronomy, University of St. Andrews, North Haugh, St. Andrews KY16 9SS, United Kingdom*

During the last years mid-infrared semiconductor lasers have continuously increased their application range to include gas sensing for detection and control of the presence and concentration of environmentally-relevant gases like hydrocarbons, CO_2, SO_x and NH_3. One of the efficient solutions is the interband cascade laser (ICL) employing a broken gap material system to separately confine various carriers, and utilizing the interband transition in a cascade scheme. The natural candidate for the active region of ICLs is the so-called "W"-shaped type II quantum well made of InAs and GaInSb to confine electrons and holes, respectively. Such approach provides the effective band gap reduction and reduces the non-radiative processes i.e. Auger recombination.

Several approaches have been studied in order to spectrally cover the region of mid-infrared involving the ICL's substrate variation of GaSb and InAs. The GaSb based interband cascade lasers are able to cover the spectral range from 2 to 6 μm. In order to extend the emission to longer wavelengths the cladding region based on so-called index-guiding method (InAs/AlSb superlattices) has to be replaced due to too strong absorption in mid and far-infrared. This limitation may be overcome by an application of a plasmon-enhanced waveguide composed of highly doped indium arsenide layers. The plasmon-enhanced waveguide approach reduces

cladding thickness that leads to enhanced heat dissipation and shorter growth time [1].

This work presents the results of uniformity investigations of full two-inch wafers containing five stages of type-II InAs/InGaSb W-shaped quantum wells grown on GaSb and InAs substrate, predicted for emission at 3 – 5 μm and 5 – 7 μm, respectively. The photoluminescence large scale spatial mapping has been performed in Fourier-based spectrometer (FTIR) with an evacuated external chamber for emission measurements in a step-scan mode [2]. InSb and MCT detectors have been used in order to cover the broad spectra range of interest. The laser was focused to the spot of 0.5 mm^2 on wafer, which was placed on an x-y stage, and which determines the spatial resolution.

The obtained results show high uniformity of the emitted wavelength deviating across the wafer's diameter within the range of 390±5 meV (3180±40 nm). This corresponds to the InAs layer thickness variation of below one monolayer. The full width at half maximum map also shows high regularity of 40±5 meV in the scale of the full wafer.

1. Z. Tian et al., *Proc. of SPIE* **7616**, 76161B (2010)
2. M. Motyka et al., *Appl. Phys. Express*. **2,** 126505 (2009)

B26: Improved relations for shock ignition hot-spot condition

S. A. Ghasemi[1], A. H. Farahbod[1], S. Sobhanian[2]

[1] Plasma Physics Research Department, NSTRI, End of North Kargar Avenue, Tehran, Iran
[2] Department of Physics, University of Tabriz, Tabriz, Iran

In this paper, improved relations of the main parameters of ignition in shock ignition approach such as total fuel energy, fuel gain, hot-spot radius and total areal density considering areal density of hot-spot in a non-isobaric model of the fuel assembly have been analytically derived, revised and compared with the numerical results of simulations have been done by Ref. [1]

Our calculations indicate that the approximations made by Refs. [1] and [2] for the calculation of burn-up fraction are not accurate enough to give results consistent with the numerical simulations. Therefore, we have introduced more appropriate approximations for the burn-up fraction and total areal density of the fuel considering the term of areal density of the hot-spot which are in more agreement with the previous simulation results of shock ignition. Meanwhile, it is shown that the related formulas of the non-isobaric model for total fuel energy, fuel gain and also hot-spot radius cannot determine the model parameters independently, but the improved model choose a better selection with less restrictions on determination of the parameters for the non-isobaric model. Such derivations can be used in theoretical studies of the ignition conditions and burn-up fraction of the fuel in shock ignition scenario. Figure 1 typically shows the rms (root mean squares) for total areal density of the fuel. The blue column indicates the difference between the improved relations with Ref. [1] code simulations and the red one shows the difference between non-isobaric relations of Ref. [1] with the simulation code data. Here, E, Rh and G refers to three different approaches of fuel energy, hot-spot radius and target gain.

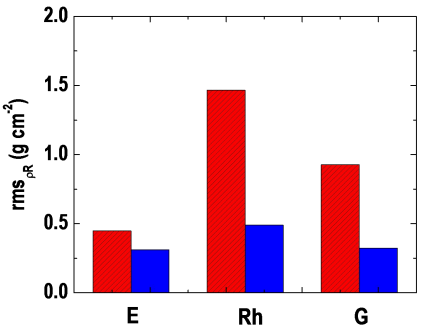

Fig1. The rms difference between the improved and Ref. [1] non-isobaric relations with code results.

1. A. J. Schmitt, J. W. Bates, S. P. Obenschain, S. T. Zalesak, and D. E. Fyfe, *Phys. Plasmas* **17,**042701 (2010).

2. M. D. Rosen, J. D. Lindl, and A. R. Thiessen, LLNL Laser Program Annual Report, UCRL-50021-83, 3-5 (1983).

B27: Integrated micro-ring photonics: principles and applications for soliton generation, mode-locked lasers and optical communications

ABSTRACT: Add-drop filters using microring resonators (MRRs) have shown great promise for practical applications. A wavelength-selective optical add-drop filter is a requirement for adding and dropping a particular wavelength division multiplexing (WDM). The system of multiple mode lock soliton generation containing an add-drop filter MRR connected to a smaller ring on the right side holding a saturable absorber (SA) is presented. Semiconductors, have been well demonstrated as the SA for mode-locking. The III/V semiconductors (InGaAsP/InP) on the basis of InP with a direct bandgap is used to fabricate the ring resonator. The photonic circuits simulator PICW based on the time-domain travelling wave (TDTW) method, is capable of modelling passive photonic circuits. The generated multi wavelength mode lock solitons have a bandwidth (FWHM) and free spectral range (FSR) of 1.1 and 30.24 nm correspond to 0.13 and 3.77 THz respectively. The drop port output signals have bandwidth and FSR of 1.5 and 31.13 nm respectively, correspond to 0.187 and 3.88 THz in frequency domain, where the pulse duration and repetition of the train mode lock pulses are 4 ps and 100 GHz respectively. The finesse obtained is approximately 20.7, where the Q-factor is ~1×10^3. The side band soliton mode locks have FSR=0.86 nm.

Keywords: Microring resonators (MRRs), Add-drop filters, mode lock soliton, saturable absorber (SA), InGaAsP/InP

B28: Nanomaterials for Light Management and Solar Energy Harvesting

Jifeng Liu

[1]Dartmouth College, Thayer School of Engineering, Hanover, NH 03755, USA Email:Jifeng.Liu@dartmouth.edu, web site: http://engineering.dartmouth.edu/people/faculty/jifeng-liu/

Light-matter interactions on nanoscale lead to interesting applications in optical sensing and energy harvesting. In this talk, we discuss two examples of such applications: (1) Self-assembled, nano-needle structured conductive SnO_x (x<2) for high-efficiency, low-loss light trapping in infrared photonics and 2D materials; and (2) Interfacially engineered plasmonic metal nanoparticles for cermet solar selective absorbers in concentrated solar thermal power (CSP) systems.

Light trapping in thin film photonic devices (e.g. thin film solar cells) is an important factor to increase the optical absorption and boost the efficiency. Conventionally, textured transparent conductive oxides (TCOs) are applied for this application. However, the high-roughness surface textures increase the surface area and correspondingly, the surface leakage. In addition, their light trapping effect diminishes for sub-micron thin film absorbers and atomically thin 2D materials. To overcome these issues, we have investigated nano-needle structured conductive SnO_x (x<2) (Fig. 1a) [1,2] as a low-temperature (<250 °C) self-assembled electrode for efficient light trapping in thin film and 2D photonic devices without increasing the surface area of the active absorber. Remarkably, when the SnO_x nano-needle light-trapping nanostructure is applied to a single layer graphene (SLG) on a quartz substrate, the absorption in graphene is greatly enhanced from 2% to >12% in a broad wavelength range of 750-1600 nm, and the maximum absorption reaches 14% at 800 nm (Fig. 1c). In fact, the light trapping is so effective that it allows the observation of SLG with naked eyes (Fig. 1b). These results indicate promising applications in thin film and 2D materials IR photonic devices.

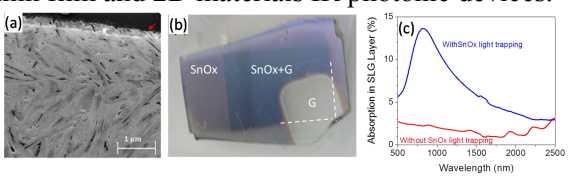

Fig.1 (a) SEM image of high-density, randomly oriented nano-needles formed in a $SnO_{0.85}$ thin film. Fig1. (a) Photo of graphene (G), nano-needled SnO_x(SnO_x), and SnO_x on graphene(SnO_x+G) on the quartz substrate. The SnO_x+G part appears much darker than SnO_x. (b) Absorption in SLG on silica vs. wavelength with and without SnO_x light-trapping nanostructure.

CSP and solar photovoltaics (PV) are two major approaches to harvest solar energy. Compared to PV, CSP can be more easily integrated with conventional power plants. In addition, it offers great advantages in low-cost energy storage since the heated working fluid (e.g. molten salt) can be stored and kept at a high temperature for an extended period of time. Selective solar thermal absorber coatings for CSP systems have been an important research area in solar energy materials. They convert solar energy efficiently into heat with minimal thermal radiation losses in the infrared (IR) regime. Conventional solar thermal absorbers are based on interference effect, requiring stringent control of film thicknesses and vacuum deposition. Typically they also need to operate under vacuum to prevent oxidation, which increases the cost of CSP systems. We employ two major innovations to address these challenges [3,4]: (1) A novel plasmonic Ni nanochain cermet solar thermal coating whose spectral selectivity is inherent to the nanochain optical properties, with performance comparable to vacuum-deposited counterparts. Stringent film thickness control is no longer required, greatly facilitating large-scale, low-cost solution-chemical fabrication. (2) Interfacial engineering of metal nanostructure-SiO_x ($x<2$) systems for long-term antioxidation behavior at >550 ºC in air without using noble metal. Oxidation termination is demonstrated at 580 ºC in air for Ni-SiO_x cermets, with potentials for >95% solar absorptance and <10% thermal emittance in vacuum-free operations.

1. A. Wong, X. X. Wang, and J. Liu, *J. Appl. Phys* **117**, 103109 (2015)
2. X. X. Wang, A. Wong, S. Malek, Y. Cai, and J. Liu, to be published in *Opt. Lett.*
3. X. X. Wang, H. F. Li, X. B. Yu, X. L. Shi, and J. F. Liu, *Appl. Phys. Lett.* 101, 213109 (2012)
X. Yu, **X. Wang**, Q. Zhang, J. C. Li, and J. F. Liu, *J. Appl. Phys* **116** 073508 (2014)

B29: Nano-photonic and nano-plasmonic structures to harvest photons in thin film solar architectures

Rana Biswas
Ames Laboratory; Iowa State University

Recent advances in periodic structures such as photonic crystals have offered unique ways to control and manipulate light. This talk will highlight how periodic nano-photonic and nano-plasmonic structures can harvest photons in thin film solar cells.

A common feature of many thin solar cells including organic and thin silicon based solar cells is that they absorb very weakly in the red and near infrared wavelengths, since the photon absorption length exceeds the absorber layer thickness. A novel way to enhance the path length of photons in thin film solar architectures is to utilize periodically patterned substrates on which a fully conformal solar cell can be grown[1]. For thin silicon solar cells this has led to enhanced short circuit current of exceeding 30%, with even higher simulated enhancements. The basic mechanism is a generation of wave-guided modes in the plane of the solar cell, accompanied by propagating surface plasmon modes at the corrugated metal-semiconductor interface. Due to difficulties in spin coating organic layers on corrugated substrates, a particularly fruitful architecture consists of a polymer microlens at the air-glass interface, coupled with a photonic-plasmonic crystal at the metal cathode on the back of the cell [2]. The micro-lens focuses light on the periodic nanostructure that in turn generates strong diffraction of light. The optimal architecture has a period of 500 nm for both arrays, resulting in absorption enhancement of 49% and photocurrent enhancement of 58% relative to the flat cell, for nearly lossless metal cathodes.
We discuss the parasitic losses due to the metal electrodes, and strategies for minimizing these losses.

[1] R. Biswas, E. Timmons, Optics Express **21** Iss. S5, pp. A841–A846 (2013).
[2] A. Peer, R. Biswas, ACS Photonics 1 (9), 840–847 (2014).

B30: Tunable multiwavelength fiber lasers based on a Mach-Zehnder interferometer and photonic crystal fiber

Juan M. Sierra-Hernandez

Universidad de Guanajuato, jm.sierrahernandez@ugtomx.onmicrosoft.com

In this talk a tunable multi-wavelength erbium doped fiber laser, based on a Mach–Zehnder interferometer, is presented. Here the interferometer is achieved by splicing a piece of photonic crystal fiber (PCF) between two segments of a single-mode fiber. The laser can emit a single, double, triple or quadruple line, which can be tuned from 1530 to 1556 nm by controlling the polarization state. Finally it is shown, by experimental results, that the laser has high stability at room temperature.

B31: Self-organized structuring of light bullets, dissipationless vortices, and lightning

Vladimir Skarka

Photonic Laboratory of Angers, EA 4464, University of Angers, 2 Boulevard Lavoisier, 49045 Angers Cedex 01, France.

In general, external energy and/or matter supply in a nonlinear system provides for the emergence of the self-organized dissipative structures far from the thermodynamic equilibrium. The solitonic structures self-organization involves the balance of antagonistic effects: loss versus gain, diffusion against nonlinearity-induced self-contraction. Complex Ginzburg-Landau equations (CGLEs) describe well the dissipative solitonic structures generation in nanophotonics, plasmonics, fluids, plasmas, and electromagnetism, through superconductivity, superfluidity, elementary particles, and biological systems. The soliton acting as an ***attractor*** is a stable self-generated localized structure. The soliton morphogenesis is the result of the balance between the diffraction, cubic nonlinearity induced self-focusing, and competing defocusing provided by the quintic nonlinearity that prevents the system collapse, as it was recently demonstrated experimentally. In the synergy with that, the dynamical equilibrium between the omnipresent losses and the gain leads to the generation of structures that can be called ***dissipationless solitons***, which may be supported by many varieties of CGLEs.

Lightning seems to be of solitonic nature. It can be seen as a machinegun of ***light bullets*** shining through atmosphere. A dissipationless light bullet is a stable self-organized soliton completely localized in space and in time due to the simultaneous compensation of dispersion and diffraction by saturating nonlinearity together with a concomitant loss-gain balance.

In particular, the dissipationless "volcano-shaped" solitons with embedded vorticity $\boldsymbol{S}$ (the topological charge) feature zero intensity at the centre. They are maintained by the intrinsic angular momentum, $\boldsymbol{M = SP}$, where $\boldsymbol{P}$ is their power. Such a morphogenesis of rotating solitonic structures, having counterparts in nature (e.g., tornados), can be implemented experimentally in diverse settings. Recently we found that "volcano-shaped" vortices spontaneously break axial symmetry due to modulational instability, evolving into stably rotating ellipsoidal or crescent vortices. In the experiment, the loss modulation may be induced by a localized gain which partly compensates the uniform loss (an "iceberg of gain" submerged into the "sea of loss").

Here, we demonstrate, using the synergy of analytical methods and parallelized numerical simulations, the morphogenesis of a much broader class of novel robust solitons, shaped as a variety of four- to ten-pointed stars. They can be adequately modeled by the two-dimensional cubic-quintic CGLE that governs the evolution of envelope of electromagnetic waves in photonic or plasmonic media with a "gain iceberg" *protruding above* the surface of the "loss sea". Self-generation of spontaneous

symmetry breaking followed by the emergence of a novel solitonic structure with reduced symmetry establishes CGLE as an adequate model for ubiquitous morphogenesis in nature.

We established theoretically and numerically for the first time the stability of vortex solitons up to the topological charge ***S=20***. We demonstrated the possibility to imbed into the vortex soliton of highest vorticity solitons with lower vorticity allowing selective dynamic optical tweezing of microparticles and nanoparticles. Possible applications would be to engineer reconfigurable guides in metal-dielectric nanocomposites as well as to characterize forces exerted by molecular motors such as myosin, kinesin, and ribosomes.

B32: Self-energy function of quantum-dot and non-radiative transition

R. Kh. Gainutdinov, M. A. Khamadeev, M. R. Mohebbifar and A. A. Mutygullina

Optics and Nanophotonics Department, Institute of Physics, Kazan Federal University, 18 Kremlevskaya St, Kazan 420008, Russia
Email: mmohebifar@gmail.com

Abstract
Semiconductor quantum dots are nanometer-sized three-dimensional structures which confine electrons in all three directions. This confinement gives rise to a discrete energy spectrum. The self-interaction of a quantum dot tunnel with Coulomb interaction coupled to two non-interacting leads is investigated. The self-energy function describing this interaction is added to a bare energy of a dot state. In the standard way of determining the self-interaction (tunneling-induced) corrections to bare energies of emitters (atoms, quantum dots, etc) the variations of the self-energy functions with energy are ignored, and these corrections are considered to be equal to the values of the self-energy functions for bare energies of states. We show that actually in the case of quantum dots the variations of the self-energy functions in the energy interval between the bare and true energies can be strong, and this can have a significant effect on the values of the tunneling-induced shifts of energy levels of quantum dots.

In our investigation we use the method [1] that allows one to solve the problem nonperturbatively. This method is based on the generalized dynamical equation (GDE) that has been derived in [1] as the most general dynamical equation consistent with the current concepts of quantum physics. Being equivalent to the Schrödinger equation in the case when the interaction in a quantum system is instantaneous, GDE allows one to extend dynamics to the case of nonlocal-in-time interactions.

Reference
[1] Gainutdinov R Kh 1999 J. Phys. A 32 5657

C26: Optical properties of novel semiconductor compounds: Dilute bismides

Robert Kudrawiec

Faculty of Fundamental Problems of Technology, Wroclaw University of Technology, Wybrzeze Wyspianskiego 27, 50-370 Wroclaw, Poland
Email: robert.kudrawiec@pwr.edu.pl

Dilute bismides (i.e., zincblende III-V-Bi alloys with low bismuth concentration) have received much attention in the past few years due to their unusual physical properties and promising applications in optoelectronic devices including laser diodes and solar cells. Despite a significant progress in understanding III-V-Bi materials, many fundamental properties of dilute bismides are still unclear and/or controversial. One of them is the unusual electronic band structure of III-V-Bi materials as well as the application of valence band anticrossing (VBAC) model [1] to describe the electronic band structure in these compounds. The other issue is the formation of Bi-related defects in this material system, their evolution with Bi concentration and their change/annihilation upon annealing. In this presentation I am going to show a review of our recent studies of this material system. I will present examples of application of such optical techniques like photoreflectance, contactless electroreflectance, photoluminescence and time

resolved photoluminescence to study various material issues in dilute bismides and their low dimensional heterostructures [2-7]. In addition, I am going to review our recent studies of Bi-induced changes in the band structure of Ga-V-Bi and In-V-Bi alloys obtained within the density functional theory (DFT) for alloys with Bi ≤ 3.7 % [8]. The observed chemical trends will be discussed in the context of the virtual crystal approximation (VCA) and the VBAC model. It will be clearly shown that the incorporation of Bi atoms into III-V host modifies both the conduction and the valence band. The Bi-induced reduction of the band gap is very consistent with the available experimental data. The chemical trends observed in our calculations as well as in experimental data are very clear: in a sequence of alloys from III-P-Bi to III-Sb-Bi the Bi-induced changes in the band structure weaken. For dilute $GaSb_{1-x}Bi_x$ and $InSb_{1-x}Bi_x$ alloys the band structure modification, in the first approximation, can be described within the VCA, while for Ga-V-Bi and In-V-Bi alloys with V = As or P another phenomenological approach is needed to predict the Bi-induced changes in their band structure. We have found that a combination of the VCA with the VBAC model, which is widely applied for highly mismatched alloys, is suitable for this purpose. The chemical trends for III-V-Bi alloys observed in our DFT calculations are also exhibited by the VBAC coupling parameter, which describes the magnitude of interaction between Bi-induced levels and VB states in the valence BAC model. This coupling parameter monotonously decreases along the sequence of alloys from III-P-Bi to III-Sb-Bi.

1. K. Alberi, J. Wu, W. Walukiewicz, K. M. Yu, O.D. Dubon, S. P. Watkins, C. X. Wang, X. Liu, Y. –J. Cho, and J. Furdyna, Phys. Rev. B **75**, 045203 (2007).
2. J. Kopaczek, R. Kudrawiec, W. M. Linhart, M. K. Rajpalke, K. M. Yu, T. J. Jones, M. J. Ashwin, J. Misiewicz, and T. D. Veal, Appl. Phys. Lett. **103**, 261907 (2013).
3. M. P. Polak, P. Scharoch, R. Kudrawiec, J. Kopaczek, M. J. Winiarski, W. M. Linhart, M. K. Rajpalke, K. M. Yu, T. J. Jones T J, Ashwin M J and T. D. Veal, J. Phys. D: Appl. Phys. **47**, 355107 (2014).
4. J. Kopaczek, R. Kudrawiec, W. Linhart, M. Rajpalke, T. Jones, M. Ashwin, and T. Veal, Appl. Phys. Express **7**, 111202 (2014).
5. J. Kopaczek, M. K. Rajpalke, M. W. Linhart, T. S. Jones, M. J. Ashwin, R. Kudrawiec, and T. D. Veal, Appl. Phys. Lett. **105**, 112102 (2014).
6. R. Kudrawiec, J. Kopaczek, M. P. Polak, P. Scharoch, M. Gladysiewicz, J. Misiewicz, D. Richards, F. Bastiman, and J. P. R. David, J. Appl. Phys. **116**, 233508 (2014).
7. Kopaczek J, Kudrawiec R, Polak M P, Scharoch P, Birkett M, Veal T D, Wang K, Gu Y, Gong Q and Wang S 2014 Appl. Phys. Lett. **105**, 222104 (2014).
8. M. P. Polak, P. Scharoch, and R. Kudrawiec, Semcond. Sci. Technol. in press (2015).

C27: Self-organized vicinal surfaces used for nanostructure growth

Elsa Thune[1], Caroline Matringe[1], David Babonneau[2], René Guinebretière[1]

[1]*Laboratoire Science des Procédés Céramiques et de Traitement de Surface (SPCTS, UMR CNRS 7315), ENSCI, Limoges, France*
Email : elsa.thune@unilim.fr, web site: http://www.unilim.fr/spcts/

[2]*Institut PPRIME (UPR CNRS 3346), Université de Poitiers, Futuroscope Chasseneuil, France*

The final properties of nanostructured systems made of islands surfaces depend on the shape and the size of nanoparticles but also on their organization. On this general framework, we aim at producing self-organized nanostructures using sapphire vicinal surfaces. Such vicinal surfaces are obtained by cutting a single crystal with a small deviation of the surface normal with respect to a crystallographic plane leading to a surface with terraces separated by steps. Suitable templates are created thanks to the re-arrangement of the steps during thermal treatment (step bunching) [1-2]. Different types of nanostructured surfaces can be elaborated and exhibit a 1D- or 2D periodic pattern (see Fig. 1). The surface morphology and the wavelength of the obtained periodic patterns, which can be tuned with the thermal treatment parameters (i.e. temperature, duration, and atmosphere) and also

with the sample parameters (i.e. miscut and azimuthal angles), are first characterized ex-situ after each treatment on a laboratory scale by Atomic Force Microscopy (AFM), which provides a direct image of the surface morphology (step height, step curvature, terrace width...). The measurements of the evolution of the small angle scattering signal recorded under grazing incidence (GISAXS) and as a function of the azimuthal angle allow us to determine the shape of the steps and the main characteristics of the patterns. Those GISAXS experiments were performed at the BM02 beamline at the ESRF (Grenoble, France).

Such templates are chemically and structurally stable over long periods of time and in various environments so as to be compatible with various deposition processes. Few examples of nanostructured thin films (ZrO_2, SnO_2, AlN) produced by different methods on such templates will be shown.

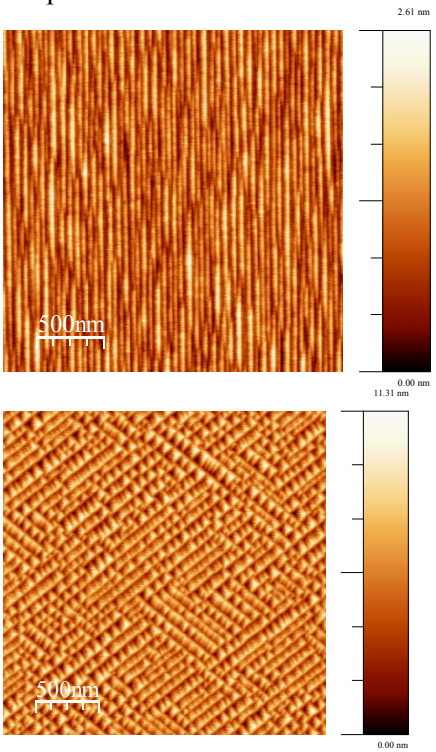

Fig1. AFM images of (a) 1D and (b) 2D periodic patterns obtained after thermal treatment of a sapphire vicinal surface

1. R. Bachelet, S. Cottrino, G. Nahélou, V. Coudert, A. Boulle, B. Soulestin, F. Rossignol, R. Guinebretière and A. Dauger, *Nanotechnology* **18**, 015301 (2007)

2. E. Thune, A. Boulle, D. Babonneau, F. Pailloux, W. Hamd, O. Preziosa and R. Guinebretière, *Appl. Surf. Science* **256**, 924-928 (2009)

C28: Femtosecond laser-induced micro and nanostructured metallic oxides

Santiago Camacho-Lopez[1], M. A. Camacho-Lopez[2], Y. Esqueda-Barron[1], M. Cano-Lara[1], Jon Redenius[3], Guillermo Aguilar[3]

[1]Departamento de Optica, CICESE, Ensenada, Baja California, Mexico Email:camachol@cicese.mx, web site: www.cicese.edu
[2]Facultad de Quimica, UAEMex, Estado de Mexico, Mexico
[3]Department of Mechanical Engineering, UCR, California, US

In this work, we will be presenting our findings on the formation of metallic oxides when a transition metal thin film is irradiated using a femtosecond laser. We have demonstrated that a series of metallic oxides can be rapidly synthesized by the use of MHz repetition rate femtosecond laser pulses of very low fluence [1]. The laser processing of materials offers significant advantages over other processing techniques. When using a laser high spatial resolution patterning is possible and fast processing is also achievable. Our results show that as compared to conventional thermal synthesis of metallic oxides, femtosecond laser processing is very fast; in addition fine patterning (micron spatial resolution) of distinct oxides with specific stoichiometry, crystalline structure and morphology can be obtained [2]. Depending on the laser irradiation parameters micro or nanocrystalline metallic oxide structures can be synthesized in a matter of a few seconds or a few minutes. We have characterized these oxides using SEM, EDS, XRD and micro-Raman spectroscopy.

Figure 1 shows results of femtosecond laser-induced molybdenum oxides. On the left hand side an optical micrograph is shown of a

molybdenum thin (500 nm) film irradiated for a 30 seconds period of time, using 60 fs duration laser pulses of 1.5 mJ/cm^2 fluence per pulse delivered at a repetition rate of 70 MHz. The laser source is a typical Ti:sapphire femtosecond laser oscillator emitting at 800 nm. On the right, SEM micrographs of different regions within the transformed region are shown.

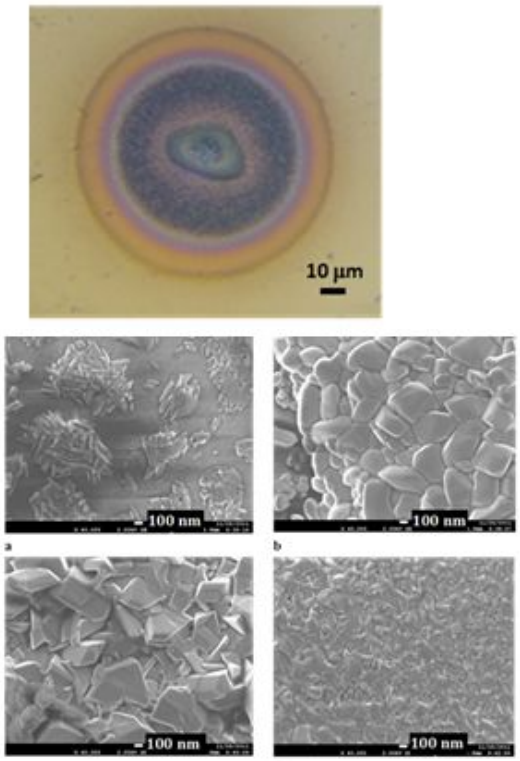

Fig 1. MoO_x induced by means of femtosecond laser irradiation.

For the case shown in figure 1, we can observe how nanobars or microsized crystals form as a result of the laser irradiation, the nanobars synthesize right at the center of the laser irradiated region, while larger crystals form in the surrounding concentric colored rings. Micro-Raman revealed that different crystalline phases correspond to each colored ring on the pattern. We found the formation of the following molybdenum oxides *m*-MoO_2, -MoO_3, *o*-Mo_4O_{11}, *m*-Mo_8O_{23}, *o*-$Mo_{18}O_{52}$.

1. M. Cano-Lara, S. Camacho-Lopez, A. Esparza-Garcia. M. A. Camacho-Lopez. *Opt. Mat.* **33**, 1648 (2011).

2. M. Cano-Lara "Óxidos de molibdeno inducidos por irradiación láser de pulsos ultracortos" PhD. Thesis (CICESE), November 2013.

C29: TiO_2 nanomaterials: synthesis, properties, modifications, and photocatalytic applications

Giuliana Impellizzeri

CNR-IMM, Department of Physics and Astronomy, University of Catania, Catania, Italy Email:giuliana.impellizzeri@ct.infn.it, web site:http://www.dfa.unict.it/matis/index.php?option=com_jresearch&view=member&task=show&id=70&Itemid=61

One of the most pervasive problems afflicting people is inadequate access to clean water and sanitation. Titanium dioxide (TiO_2) is an oxide semiconductor with excellent photocatalytic performances in the degradation of organic pollutants and in killing microorganisms in water. In addition it has many unique properties: non-toxicity, good chemical stability, strong mechanical properties, and low cost.

Recently, extensive efforts have been made to improve the photocatalytic performance in terms of electron/hole recombination rate and visible-light absorption [1]. In order to reduce the electron/hole recombination, we coupled Au nanoclusters with thin layers of TiO_2 (Fig. 1a) [2], and we combined TiO_2 nanoparticles with C nanotubes. On the other hand, with the aim of enhancing the efficiency in the visible spectral range, we synthesized hydrogenated TiO_2 nanoplumes (Fig. 1b), and doped TiO_2 thin films by ion implantation of Fe^+ and C^+, to narrow the TiO_2 bang-gap energy [3,4]. In addition, we integrated TiO_2 nanoparticles into low-cost polymers (PMMA), functionalized with porphyrins, so to make the nanocomposites sensitive to the visible light. All the materials were deeply characterized and tested for applications in water purification.

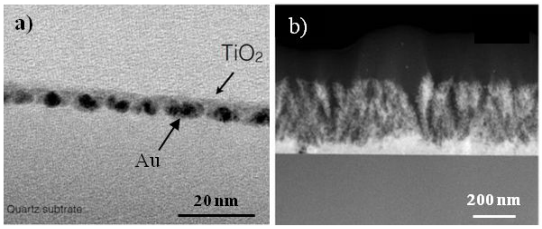

Fig. 1 a) Au nanoclusters embedded in TiO_2 thin layer, b) TiO_2 nanoplumes, d) TiO_2 nanoparticles into PMMA.

1. S. Malato, P. Fernàndez-Ibáñez, M. I. Maldonado, J. Blanco, and W.Gernjak, *Catalysis Today* **147**, 1 (2009).
2. V. Scuderi, G. Impellizzeri, L. Romano, M. Scuderi, M. V. Brundo, K. Bergum, M. Zimbone, R. Sanz, M. A. Buccheri, F. Simone, G. Nicotra, B. G. Svensson, M. G. Grimaldi, and V. Privitera, *Nanoscale* **6**, 11189 (2014).
3. G. Impellizzeri, V. Scuderi, L. Romano, P. M. Sberna, E. Arcadipane, R. Sanz, M. Scuderi, G. Nicotra, M. Bayle, R. Carles, F. Simone, and V. Privitera, *J. Appl. Phys.* **116**, 173507 (2014).
4. G. Impellizzeri, V. Scuderi, L. Romano, E. Napolitani, R. Sanz, R. Carles, and V. Privitera, *J. Appl. Phys.* **117**, 105308 (2015).

C30: Nonlinear optical properties of Au-nanoparticles in water, lipoic acid, and NaCl

M. Trejo-Durán[1], I.Severiano-Carrillo[2], M. Cano-Lara[2], E. Alvarado-Mendez[3]

[1] Multidisciplinary Department DICIS-Guanajuato University, Guanajuato, Mexico email:mtrejo@ugto.mx,
[2] Postdoctoral position DICIS-Guanajuato University, Guanajuato, Mexico
[3] Electronic Department DICIS-Guanajuato University, Guanajuato, Mexico

Au nanoparticles (AuNPs) have had relevant application in different areas. In optics, their nonlinear optical properties (NLO) are important to design optoelectronic devices. In this work, a NLO study of Au NPs in different solutions is presented. A thermal model is used for analyzing the thermo-optical coefficient and degree of nonlocality.

AuNPs were prepared using a Brust´s method [1], the samples were prepared using a 5:1 molar ratio between $NaBH_4$ and $HAuCl_4$, respectively. The size of the obtained NPs (less of 5 nm) was estimated according the method proposed by W. Haiss et al. [2]. Once the AuNPs were synthesized, lipoic acid (LA) or reduced lipoic acid (DHLA) was used to stabilize these colloids, and NaCl was add too. Five different solutions were prepared at AuNPs concentration of 300 nM/L: (a) in water, (b)with reduced lipoic acid in water, (c) with reduced lipoic acid and sodium chloride in water, (d) with lipoic acid in water, and (e) with lipoic acid and sodium chloride in water.

Transmittance of samples were obtained using the z-scan technique, using an argon laser at 514 nm with 10mW, 16mW and 25mW power which waist beam was 29 μm, and the obtained data were analyzed with a thermal model. The transmittance outcome is shown in Figure 1.

Behavior of nonlinearity degree is discussed; even though, all of them are from thermal origin, result show that there are some differences.

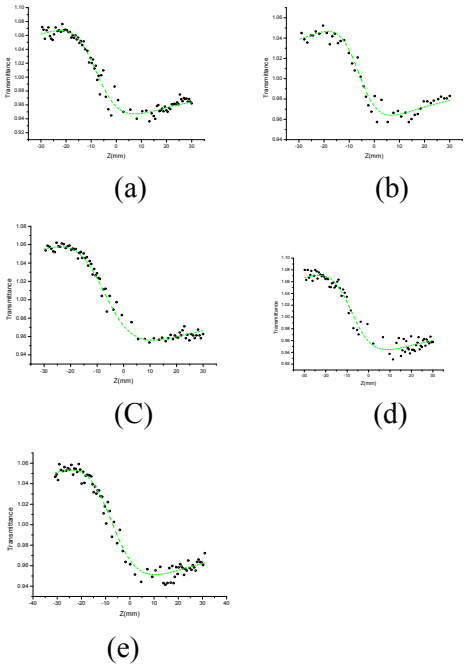

Fig. 1. Transmittance normalized to close aperture with z-scan technique. a) in water, b)with reduced

lipoic acid in water, c) with reduced lipoic acid and sodium chloride in water, d) with lipoic acid in water, and e) with lipoic acid and sodium chloride in water.

1. M. Brust, M. Walker, D. Bethell, D.J. Schiffrin and R. Whyman, *J. Chem. Soc., Chem. Commun.*, **7**, 801-802 (1994).
2. W. Haiss, N.T.K. Thanh, J. Aveyard and D. G. Fernig, *Anal. Chem.* **79**, 4215-4221 (2007).

C31: Mechanism of Microwave Loss in Commercial Dielectric Materials

Nathan Newman[1] and Shengke Zhang[1]

[1]*Materials Department, Arizona State University, Tempe, AZ, USA*
Email: Nate.Newman@asu.edu, web site: https://webapp4.asu.edu/directory/person/267342

Miniaturization of satellite communication and cellular systems requires low-loss temperature-compensated microwave materials with enhanced dielectric constants. Despite the practical importance of achieving a small loss tangent a fundamental understanding of what physical mechanism determines this important parameter has not been firmly established.

In this talk, I review my group's work using modern experimental and theoretical condensed matter methods to understand the intrinsic and extrinsic factors involved in optimizing the performance of high-performance dielectrics; with a focus on identifying the mechanism of microwave loss in these materials. We will focus our discussions on Ni-doped $BaZn_{1/3}Ta_{2/3}O_3$ since it is the highest performer at room temperature, but also show that the conclusions are general for other commonly-used materials.

$Ba(Zn_{1/3}Ta_{2/3})O_3$ exhibits the unusual combination of a large dielectric constant, $_r$, and a small loss tangent at microwave frequencies. Ab-initio electronic structure calculations showed this desirable property arises because of charge transfer between the cation *d*-orbitals (from Ta 5*d*-levels at the CBM to Zn 3*d*-levels at the VBM); providing a degree of covalent directional bonding that resists angular distortions between atoms.[1] The *d*-electron bonding in BZT and BCT is responsible for producing a more rigid lattice with higher melting points, enhanced phonon energies than comparable ionic materials and thus inherently low microwave loss.[1]

The properties of commercial materials are optimized by adding dopants or alloying agents, such as Ni or Co to adjust the temperature coefficient, $_F$ to zero. This occurs as a result of the temperature dependence of e_r offseting the thermal expansion. At low temperatures, we show that the dominant loss mechanism in these commercial materials comes from spin excitations of unpaired transition-metal d electrons in isolated atoms (light doping) or exchange coupled clusters (moderate to high doping), a mechanism differing from the usual suspects.[2] At high temperatures, we give evidence that loss also arises and may be dominated by localized hopping transport. We will describe the physical principles that can be used to prepare material with minimal loss, while still attaining temperature compensation.

1. Shaojun Liu, Richard Taylor, N.S. Petrovic, Louisa Budd, Mark Van Schilfgaarde, and Nathan Newman, *J. of Appl. Phys.* **97**, 014105 (2005).
2. Lingtao Liu, Marco Flores and Nathan Newman, *Phys. Rev. Letters* **109**, 257601 (2012); Shengke Zhang, Alex Devonport and N. Newman, , J. Am. Ceram. Soc. **98**, 1188-1194 (2015).

C32: Field-effect surface chemistry: Gate-controlled photo-oxidation of grapheme

Ryo Nouchi

Nanoscience and Nanotechnology Research Center, Osaka Prefecture University, Sakai 599-8570, Japan
Email:r-nouchi@21c.osakafu-u.ac.jp, web site: http://www.nanosq.21c.osakafu-u.ac.jp/ttsl_lab/r_nouchi/e/

Atomic sheets obtained by exfoliation from layered materials have an ultrathin body which

is down to mono- to several atomic layers. Due to the ultimate thinness, electronic properties of atomic sheets are largely affected by various surface phenomena. In addition, an external electric field can penetrate into the sheets because the ultrathin body is insufficient to completely screen the field. Therefore, in the configuration of a field-effect transistor (FET; Fig. 1a), an electric field from the bottom gate electrode can penetrate to the top surface of the atomic sheet (Fig. 1b). In this talk, we will discuss the field-effect control of surface chemical reactions using the FET configuration with an atomic sheet channel.

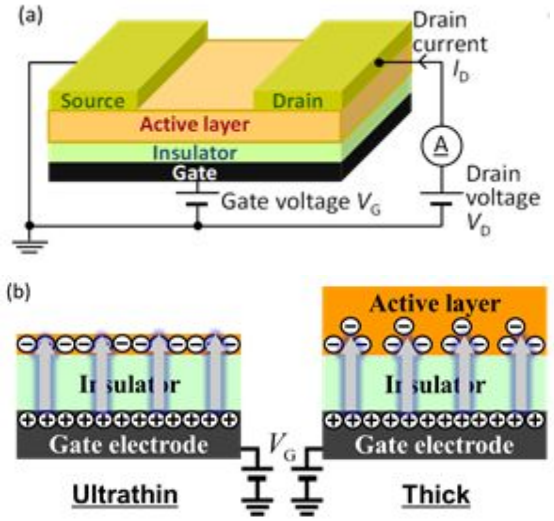

Fig. 1. (a) A schematic diagram of a FET with a universal back gate. (b) Penetration of the gate electric field to the top surface of the ultrathin material (left) and screening of the field near the bottom surface of the bulk counterpart (right).

As an example of the "field-effect surface chemistry" concept, gate-controlled photo-oxidation of graphene will be introduced (Fig. 2a) [1]. Graphene is single layer graphite, and all the constituent carbon atoms belong to its surface. Photo-oxidation of graphene can be easily achieved by exposure to ultraviolet (UV) light. Graphene oxide is known to have an insulating property, while pristine graphene is a semimetal with zero band overlap (often referred to as a zero-gap semiconductor). Thus, the oxidation can be detected by an increase in its electrical resistance. In addition, a structural change accompanied with the oxidation can also be identified by a change in Raman scattering spectra. Figure 2b shows the Raman scattering intensity mapping of a graphene FET before and after UV light irradiation to the FET in operation (thus, with application of finite drain and gate voltages) in air at room temperature. Edge-selective photo-oxidation is clearly seen. The oxidation was not observed under conditions with positive gate voltages and/or low drain voltages, indicating possible fine-tunability of the reaction by adjusting gate and drain voltages. The oxidation was found to proceed into the center region, which might enable us to fabricate graphene nanoribbons or nanoconstrictions.

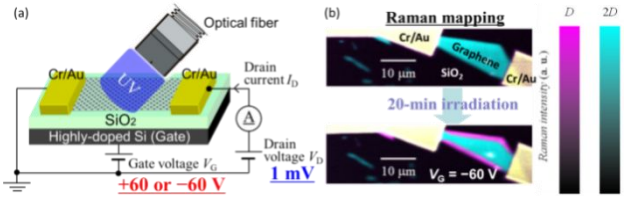

Fig. 2. (a) Experimental setup for gate-controlled graphene photo-oxidation by UV irradiation. (b) Intensity mapping of the Raman *D* and 2*D* bands of a graphene FET before and after 20-min irradiation of UV light with V_G of −60 V and V_D of 1 mV. The *D* band induction (oxidation) at graphene edges was not observed with V_G of +60 V.

The "field-effect surface chemistry" concept has been proven to work successfully in the case of photo-oxidation of graphene. The concept will offer a novel methodology to control various chemical reactions at a surface of ultrathin atomic sheets such as graphene, transition metal dichalcogenides, and transition metal oxides.

1. N. Mitoma and R. Nouchi, *Appl. Phys. Lett.* **103**, 201605 (2013).

C33: Bulk Photovoltaic Effects in $BiFeO_3$ Thin Films

Seiji Nakashima[1], Kouta Takayama[1], Hironori Fujsawa[1], and Masaru Shimizu[1]

[1]*Graduate School of Engineering, University of Hyogo, Himeji, Hyogo, Japan*
Email:nakashima@eng.u-hyogo.ac.jp

The bulk photovoltaic effect in ferroelectrics was extensively investigated for $LiNbO_3$, and

$BaTiO_3$ single crystals in 1970's. The mechanism is different from that of a conventional photovoltaic device using a *p*-(*i*)-*n* junction of semiconductors and can overcome the limitation by the band gap. Therefore, such photovoltaic effects which can generate photovoltage above band gap are called anomalous photovoltaic effects. Recently, an anomalous photovoltaic effect has been reported in striped-domain structured $BiFeO_3$ (BFO) thin film [1], and the report suggests novel mechanism of photovoltaic effects at domain walls. However, bulk photovoltaic effect has been also suggested in the striped–domain structured BFO [2]. In this research, Pt/BFO/Pt coplanar capacitors were prepared using single-domain structured BFO thin films without domain walls, and only the bulk photovoltaic effects in BFO thin films was investigated.

(111)- and (001)- oriented single-domain structured BFO thin films were grown on SrTiO3 (111) and 4° off-cut SrTiO3 (001) substrates by RF magnetron sputtering. Pt/BFO/Pt coplanar capacitors were fabricates by fabricating 100 x 100 um^2 Pt electrodes patterns with interelectrode distance of 260 um on BFO thin film. The photovoltaic property was characterized by using an electrometer (Keithley 6517A) to make current-voltage (*I-V*) measurements with/without illumination by a collimated violet laser (λ = 405 nm) with a power of 62 mW. The incident direction of the laser was fixed along the normal to the film's plane. The illuminated area was an ellipse with major and minor axis lengths of 800 and 580 μm, respectively.

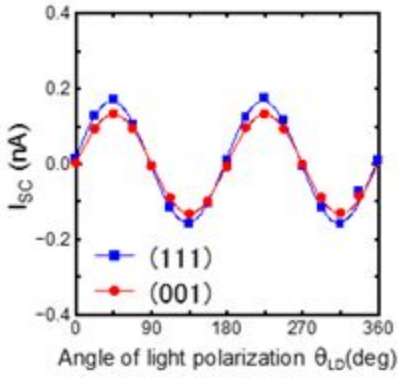

Fig. 1 Laser light polarization angle (LD) dependence of short circuit current (I_{SC}) of (111)- and (001)- oriented BFO thin films.

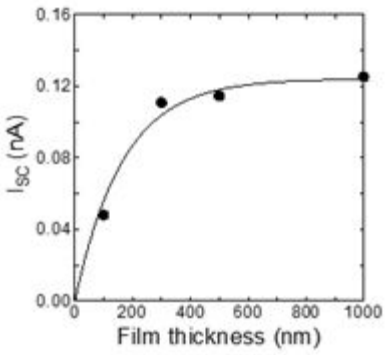

Fig. 2 Film thickness dependence of *I*sc in (111)-oriented BFO thin film.

Figure 1 shows laser light polarization angle (LD) dependence of short circuit current (I_{SC}) in (111)- and (001)- oriented BFO thin films. It can is found that the I_{SC} change as sin 2 LD, and these results are well explained by

$$\begin{pmatrix} I_x \\ I_y \\ I_z \end{pmatrix} = I \begin{pmatrix} 0 & 0 & 0 & 0 & \beta_{15} & -2\beta_{22} \\ -\beta_{22} & \beta_{22} & 0 & \beta_{15} & 0 & 0 \\ \beta_{31} & \beta_{31} & \beta_{33} & 0 & 0 & 0 \end{pmatrix} \begin{pmatrix} E_x^2 \\ E_y^2 \\ E_z^2 \\ E_y E_z \\ E_z E_x \\ E_x E_y \end{pmatrix} \quad \text{(eq. 1)}$$

, where ***I*** is short circuit current vector, is bulk photovoltaic tensor, and ***E*** is polarization vector of the incident light. Figure 2 shows BFO thickness dependence of Isc of (111)-oriented BFO thin film. It is found that the ISC increases with decreasing film thickness. This indicates photoconductivity of $SrTiO_3$ substrate is strongly affected in the thickness region of < 300 nm. These results are well explained by absorption coefficient of BFO ( ), and it is found that I_{SC} can be expressed by

$$I_{SC}(T) = \frac{G_{F0}(1-\exp(-\alpha T))}{G_{F0}(1-\exp(-\alpha T)) - \alpha G_{SO}\exp(-\alpha T)} I_F \quad \text{(eq. 2)}$$

, where G_{FO} and G_{SO} is photoconductance at BFO and $SrTiO_3$ surface, T is BFO thickness, and I_F is I_{SC} at T = ∞. Therefore, the abnormal photovoltaic effents in BFO thin films are due to socond-order electro-optical effects.

1. S. Y. Yang *et al*., *Nat. Nanotechnol.* **5**, 143 (2010).
2. A. Bhatnagar, A. R. Chaudhuri, Y. H. Kim, D. Hesse and M. Alexe, *Nat. Commun.* **4**, 2835 (2013).

Acknowledgments

This work was supported in part by the Japan Society for Promotion of Science, a Grant-in-Aid for Young Scientists (B) 26820115, a research grant from the University of Hyogo, Japan, JKA and its promotion funds from KEIRIN RACE, and a grant from the CASIO Science Promotion Foundation.

C34: Silicon Nanostructures for Nanoelectronics and Photovoltaics

Kunji Chen, Xinfan Huang, Linwei Yu, Yunqing Cao, Jun Xu, Zhongyuan Ma

State Key Laboratory of Solid State Microstructures, School of Electron Science and Engineering, Nanjing University, Nanjing 210093, P.R. China Email:kjchen@nju.edu.cn

Silicon based materials are the backbone materials for fabricating semiconductor devices and its process technologies are the basic of the modern VLSI technique. With the developments of nanoscale engineering, some silicon nanostructures now have been applied in the nanoelectronics and photovoltaics. In this talk we report recent progress in our group on silicon nano-crystalline dots (SiNC) and silicon nano-wire (SiNW) for application of nonvolatile memory, SiNWFET and solar cells etc.

1. Based on constrained crystallization principle in ultra-thin a-Si single layer or a-Si/a-SiN multilayers we obtained the size controlled uniform SiNC array, which has been employed to storage information for nonvolatile memory devices. This kind of discrete electron storage memories exhibit long retention and fast program speed characteristics. [1]

2. Based on band gap tunable Si Quantum dots (QDs) multilayers structure, we investigated the SiQD/SiC multilayers solar cells. The results shown that the range of light absorption spectrum was improved and both of EQE and IQE was also increased at the short wave edge.

3. A radial junction a-Si:H thin film solar cells, which built over a matrix of random SiNWs grown via a low temperature plasma-enhanced vapor-liquid-solid (VLS) process, have demonstrated that the carrier collection distance is greatly shortened, leading to a stronger built-in electric field and a largely improved stability against Staebler Wronski (SW) degradation.

4. The in-plane SiNWs on the silicon substrate have been investigated. A guided growth of SiNWs based on an in-plane solid-liquid-solid mechanism provides a general strategy to deploy SiNWs precisely into desired circuits. A simple bottom-gate SiNW FET structure was realized by connecting selected SiNW channels with Al electrode contacts and using the n^+ c-Si wafer as bottom-gate.[2]

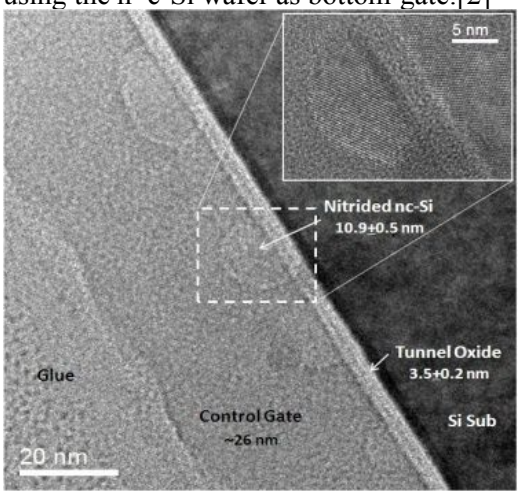

Fig.1. Cross-section TEM image of SiNC floating gate stacks.

1. X.Y.Qian, K.J.Chen, et. al., *J. Non-Cryst. Solids* **358**, 2344 (2012)

2. L.W.Yu, W.H.Chen, et. al., *Appl. Phys. Lett.* **99**, 203104 (2011)

C35: Engineered Soft Bionanocomposites

Vladimir V. Tsukruk

School of Materials Science and Engineering, Georgia Institute of Technology, Atlanta, USA

I discuss recent results from our research group on designing responsive biocompatible silk-based and cellulose nanocrystal nanomaterials for tunable LbL hollow microcapsules, conformal cell protection, and permeable biocomposites. [1, 2] Ultrathin silk fibroin shells are assembled in order to conduct surface modification and protection of microparticles, cells and cell assemblies. Microcapsules

designed in our study are formed at interfaces from various silk fibroins and their ionomer and pegylated derivatives and transferred to various yeast and bacterial cells. [3, 4,] pH-responsive behavior of silk ionomer, silk-graphene[5] , and cellulose nanocrystal nanoshells has been exploited for controlled loading and unloading model compounds such as labeled dextran macromolecules. Organized multiplexed arrays of ink-jet printed silk templates have been utilized for cell encapsulation with high viability and their long-term storage for biosensing arrays.[6]

1. I. Drachuk et al., Biomimetic coatings to control cellular function through cell surface engineering, *Adv. Funct. Mater.,* **2013,** *23,* 4437.
2. K. Hu, D. D. Kulkarni, I. Choi, V. V. Tsukruk, Graphene–Polymer Nanocomposites for Structural and Functional Applications, *Prog. Polym. Sci*., **2014,** *39,* 1934
3. C. Ye, I. Drachuk, R. Calabrese, H. Dai, D. L. Kaplan, V. V. Tsukruk, Permeability and Micromechanical Properties of Silk Ionomer Microcapsules, *Langmuir,* **2012,** *28*, 12235
4. Drachuk, R. Calabrese, S. Harbaugh, N. Kelley-Loughnane, D. L. Kaplan, M. Stone, V. V. Tsukruk, Silk Macromolecules With Amino Acid-Peg Grafts For Controlling LbL Encapsulation And Aggregation Of Recombinant Bacterial Cells, *ACS Nano,* **2015,** *9,* 1219
5. C. Ye, Z. A. Combs, R. Calabrese, H. Dai, D. L. Kaplan, V. V. Tsukruk, Robust Microcapsules with Controlled Permeability from Silk Fibroin Reinforced with Graphene oxide, *Small*, **2014**, *10*, 5087.
6. R. Suntivich, I. Drachuk, R. Calabrese, D. L. Kaplan, V. V. Tsukruk, Inkjet printing of silk nest arrays for cell hosting, *Biomacromolecules*, **2014,** *15,* 1428

C36: Understanding the formation of lipid-polymeric patchy particles

N. Rasheed[a-b], A. Abbas Khorasani[b-c], Juan Cebral[a-b], Fernando Mut[a], Rainald Löhner[d,], C. Salvador-Morales[a-b*]

[a]Bioengineering Department, George Mason University, 4400 University Drive MS 1G5, Fairfax, VA 22030, USA. [b]Krasnow Institute for Advanced Study, George Mason University, 4400 University Drive, MS 2A1, Fairfax, VA 22030, USA. [c]Department of Chemistry and Biochemistry. George Mason University, 4400 University Drive MS 3E2, Fairfax, VA 22030, USA, [d]Center for Computational Fluid Dynamics, College of Sciences, George Mason University.

Patchy polymeric particles have anisotropic surface domains that can be remarkably useful in diverse medical and industrial fields because of their ability to simultaneously present two different surface chemistries on the same construct. Such surface heterogeneity, for example, can be advantageous to achieve simultaneous interaction with both a substrate and a reporter biomolecule, thus decreasing the number of components in the system.

Using both experimental and computational approaches we investigated the role of the chemical and physical parameters in the formation of patchy particles. Experimentally, we found that the shear stress that the polymer blend undergoes during the particle's synthesis plays a pivotal role in the formation of these particles. Computational Fluid Dynamics (CFD) simulations corroborated this experimental finding. Furthermore, we found that the interplay of solvent-solvent, polymer-solvent and polymer-polymer-solvent interactions generates particles with different surface morphologies.

Understanding the mechanisms involved in the formation of patchy particles allow us to have a better control on the external physicochemical properties of patchy particles as well as on their internal structure. In addition, this fundamental study help us to address the scalability and batch control aspects of patchy particles which are essential for a successful clinical translation.

C37: Metal Nanoantimicrobials: a smart electrochemical solution to the quest for novel antibacterial agents, or just another toxic chemical?

R.A. Picca[1], M.C. Sportelli[1], C.D. Calvano[1], N. Ditaranto[1], N. Cioffi[1]

[1]*Chemistry Department, Università degli Studi Bari "Aldo Moro", 4 via Orabona, 70126 Bari, Italia*
Email:nicola.cioffi@uniba.it

Nanoantimicrobials based on metals (Ag, Cu, Zn, to cite a few) and their oxides are widely proposed as bioactive agents with low environmental and human toxicity for a number of applications, including food packaging, biomedicine, automotive and textile industries, and so on. [1-2]

The most desired nanoantimicrobials have the ability to release metal species in a controlled manner and eventually to slow down or inhibit at all the growth of bacteria or other pathogenic microorganisms. Direct nanophase release is absolutely unwanted and several approaches have been recently developed to quantitatively assess this point.[3] In our laboratories, we have been developing 1st and 2nd generation nanoantimicrobials for a number of industrial applications. Electrochemical methods, in particular, have been used for more than a decade to produce bioactive core-shell nanocolloids, which can be used as water-insoluble nano-reservoirs providing an excellent tuning of ionic release.[4-5] Laser Ablation synthesis in liquid media [6], and vacuum methods such as Ion Beam sputtering,[7] provide complementary materials with interesting antimicrobial properties.

In this talk, a survey of the pros & cons of each method will be provided, along with a detailed vision of the perspectives this field might encounter in the next future. Selected industrial applications will be also reported.

Moreover, we have recently moved a step into the assessment of bioactivity mechanisms, studied via a multi-technique approach combining materials science data, mass spectrometry (proteomics and lipidomics) studies of whole cell biological samples, along with analytical spectroscopies.

Several studies have already pointed out specific nanomaterial/microorganism mechanisms of interaction. However, to date, a systematic correlation between the nanomaterial's properties (bulk and surface chemical composition, structure and morphology) and the degree of antimicrobial efficacy (carried out at the molecular level), is infrequent.[8] Selected multidisciplinary examples in this field will be finally reported

1."Nano-antimicrobials, Progress and Prospects", N. Cioffi, M. Rai, Eds., Springer-Verlag Publisher, 1st Edition, ISBN 978-3-642-24427-8 (2012).
2. M.C. Sportelli, R.A. Picca, N. Cioffi, "Nano-antimicrobials based on metals", in "Novel antimicrobial agents and strategies", chapter 8, Phoenix, Harris, Dennison, Eds., Wiley-VCH Verlag Publisher ISBN: 978-3-527-33638-8. 352 (2014).
3. Y. Echegoyen, C. Nerìn, *Food and Chemical Toxicology*, **62**, 16 (2013).
4. N. Cioffi, L. Torsi, N. Ditaranto, G. Tantillo, L. Ghibelli, L. Sabbatini, T. Bleve-Zacheo, M. D'Alessio, P.G. Zambonin, E. Traversa, *Chemistry of Materials*, **17**, 5255 (2005)
5. N. Cioffi, N. Ditaranto, L. Sabbatini, G. Tantillo, L. Torsi, P.G. Zambonin, EP2157211-A1 (2008)
6. A. Ancona, M.C. Sportelli, A. Trapani, R.A. Picca, C. Palazzo, E. Bonerba, F. Mezzapesa, G. Tantillo, G. Trapani, N. Cioffi, *Materials Letters* **136**, 397 (2014)
7. M.C. Sportelli, M.A. Nitti, M. Valentini, R.A. Picca, E. Bonerba, L. Sabbatini, G. Tantillo, N. Cioffi, A. Valentini, *Science of Advanced Materials*, **6**, 1019 (2014).
8. J.A. Lemire, J..J. Harrison, R.J. Turner, *Nature Reviews Microbiology*, **11**, 371 (2013)

C38: High Speed and Low Temperature Deposition of SiC Film by Laser CVD

Takashi Goto

Institute for Materials Research, Tohoku University, Sendai, Miyagi, Japan
Email:goto@imr.tohoku.ac.jp, web site: http://www.goto.imr.tohoku.ac.jp/index.html

Silicon carbide (SiC) has commonly been used as a structural material due to its high hardness, thermal shock/oxidation resistance and mechanical strength. SiC body is generally fabricated by solid-state sintering with various sintering additives and impurities. However, these additives often degrade high temperature performance and would cause an impurity source. Therefore, highly pure and dense SiC body should be prepared. While chemical vapor deposition (CVD) has been employed to prepare thin films for semiconductor devices and protective coatings for cutting tools, thick films and bulky materials can also be synthesized by CVD. CVD SiC thick films have been prepared by thermal CVD using halide precursors, and thick CVD SiC plates and parts are used for industrial components such as susceptors for semiconductor fabrication. CVD and CVI (chemical vapor impregnation) are essential technique to prepare SiC fiber-reinforce SiC matrix (SiC/SiC) composite (CMC) for fabricating a channel box of nuclear power plant and a turbine blade of jet engines. On the other hand, SiC is a high power semi-conductor due to wide energy gap and high breakdown voltage. SiC single crystal has mainly been synthesized by sublimation, whereas it needs high temperature and a long time. CVD is also a versatile technique to prepare single crystal films by epitaxial growth on a single crystal substrate. However, the epitaxial growth rate of single crystal is generally too small.

We have prepared 3C-SiC thick film in a bulk form using halide precursors by thermal CVD. The deposition rates were about 1.0 and 2.0 mm/h by using $SiCl_4$+CH_4+H_2 and $SiCl_4$+C_3H_8+H_2 gases, respectively. The microstructure of SiC films changed depending on deposition conditions, in general a facetted surface texture with (111) orientation at lower deposition temperature around 1700 K and a cone-like surface texture with (110) orientation at more than 1800 K. In order to prepare high quality SiC film or bulky form at high deposition rate and/or low deposition temperature, a new technology is needed. We have developed laser CVD using continuous mode high power laser (~250W), and prepared oxide and non-oxide films at significantly high deposition rates more than several 100 times higher than that of conventional CVD. By using CO_2 laser and $Si_2(CH_3)_6$ as precursor, 3C-SiC film was prepared at 2.2 mm/h at 1500 K. The morphology changed from cone-like to cauliflower-like to granular to facetted with increasing deposition temperature from 1400 to 1800 K (Fig.1). By using diode laser, 3C-SiC film was prepared at 3.0 mm/h on Si single crystalline substrate at 1500 K, and epitaxial 3C-SiC single crystal film was prepared on Si substrate at 40 μm/h. By using $SiH(NCH_3)_2)_3$ as a precursor, a low temperature form of 2H-SiC film was prepared at 920 to 1050 K at 70 to 195 μm/h.

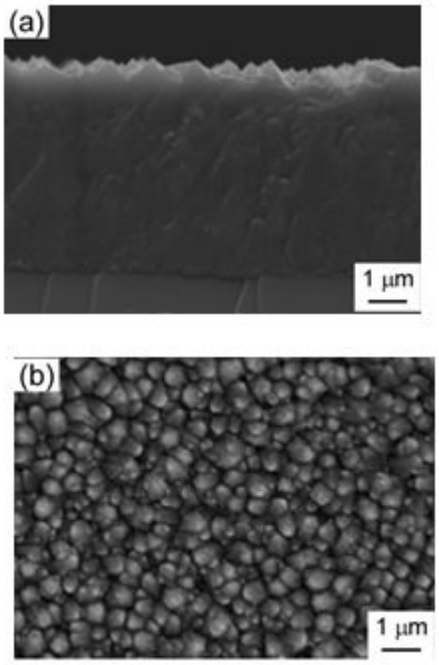

Fig.1 The surface morphology of SiC prepared by laser CVD: (a) cross-section, (b) surface.

1. S. Zhang, Q. Xu, R. Tu, T. Goto, L. Zhang, J. Amer. Ceram. Soc., **98**, 236 (2015).
2. S. Zhang, Q. Xu, R. Tu, T. Goto, L. Zhang, J. Amer. Ceram. Soc., **97**, 952 (2014).
3. S. Zhang, R. Tu, T. Goto, J. Amer. Ceram. Soc., **95**, 2782 (2012).
4. K. Fujie, A. Ito, R. Tu, T. Goto, J. Alloys Compounds, **502**, 238 (2010).

C39: In-situ TEM observation of Li battery reactions at electrolyte/electrode interface using liquid cell

Akihiro Kushima[1], Ju. Li[1]

[1]*Dept. of Nucl. Sci. and Eng., MIT, Cambridge, MA, USA*
Email:kushima@mit.edu, web site: http://web.mit.edu/kushima/www/AK

Understanding the reaction at the interface between electrolyte and the electrode is a key for improving the energy storage technology. For examples, electrolyte decomposed at the electrode surface can form solid electrolyte interface[1] (SEI) that affects the battery performance, and formation of lithium dendrites[2] can be an issue for next generation energy storages such as Li-metal, Li-sulfur, and Li-air(oxygen) batteries. These reactions, especially at the initial stages, are in the nano-scale. Here, in-situ transmission electron microscopy (TEM) enables direct observation of the phenomena in real time at unprecedented resolutions.[3,4]

We developed a liquid cell to confine the high-vapor pressure electrolyte for in-situ TEM observation of the electrochemical reaction at the electrolyte/electrode interface. While the cell is sealed to prevent the liquid from evaporating inside the TEM, it has electron beam transparent window for viewing the electrochemical reactions. The device can be used for various applications where solid-liquid interaction is important. In this talk some of our recent studies using the liquid cell are presented; 1) nucleation/growth of Lithium dendrites, 2) formation of SEI in Li-ion battery, and 3) lithium oxide formation/dissolution in Li-oxygen battery. (Fig.1) The information obtained from these in-situ TEM observations provides insights to understand the reaction mechanisms and the underlining science, and contributes to develop high performance energy storage devices.

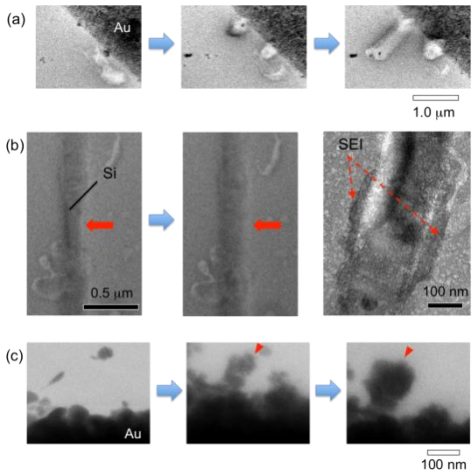

Fig. 1. In situ TEM observation of (a) Li dendrite nucleation/growth, (b) SEI formation on Si nanowire, and (c) Li_2O_2 growth during Li-oxygen battery discharge.

1. P. Verma, P. Maire, and P. Novák, Electrochimica Acta **55**, 6332–6341 (2010).
2. Z. Li, J. Huang, B. Yann Liaw, V. Metzler, and J. Zhang, J. Power Sources **254**, 168–182 (2014).
3. J.Y. Huang, L. Zhong, C.M. Wang, J.P. Sullivan, W. Xu, L.Q. Zhang, S.X. Mao, N.S. Hudak, X.H. Liu, A. Subramanian, H. Fan, L. Qi, A. Kushima, and J. Li, Science **330**, 1515 –1520 (2010).
4. X.H. Liu, Y. Liu, A. Kushima, S. Zhang, T. Zhu, J. Li, and J.Y. Huang, Adv. Energy Mater. (n.d.).

C40: Planar chiral nanostructures for biosensing

Lingling Huang[1]

[1] *School of Optoelectronics, Beijing Institute of Technology, Beijing 100081, China*
Email:huanglingling@bit.edu.cn

Planar chiral nanostructures (PCSs) are artificial two-dimensional or quasi three-dimensional nanostructures composed of achiral media and patterned with chiral features lacking any spatial inversion or mirror symmetry [1]. PCSs are extensively studied in recent years because they exhibit large chiroptical effects such as optical activity and circular dichroism (CD) much stronger than those in natural chiral media[2].

Based on these effects, PCSs may be developed as, e.g., compact polarization rotators, broadband circular polarizers, circularly polarized light emitting devices, light-driven chiral nanomotors, and negative refractive index metamaterials. In addition, it was reported that PCSs can be developed as novel biosensors[3] for the ultrasensitive detection and characterization of chiral biomolecules.

Here, we perform a thorough theoretical investigation on the sensibilities of the PCSs, by comparatively studying two complementary types of PCSs: a hole-type one and a particle-type one. In the chiral sensing operation, a pair of enantiomeric PCSs, i.e., two PCSs with the same geometry but opposite senses of chirality such as right-handed (RH) and left-handed (LH) chiral patterns, are covered with chiral analyte. Their CD spectra, which should be mirror symmetric to each other in an achiral environment, would be blue- or red-shifted depending on the light-matter interactions in the LH- and RH-PCSs. By inspecting the shift (both the direction and magnitude) of the two CD spectra, the conformational and constitutional chirality information of the chiral analyte can be achieved. We further evaluate from the near-field to get the insight physics. We find that the hole-type PCS can exhibit one order of magnitude larger chiral sensitivity than the particle-type counterpart, due to the excitation and coupling of surface plasmon polaritons and localized surface plasmons. The influence of the near-field excitation on the generated superchiral fields in the PCSs is studied, revealing the mechanism of the sensibility improvement.

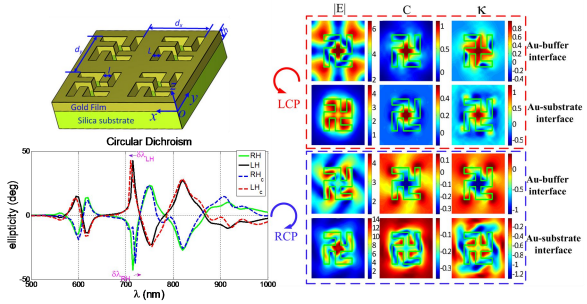

Fig1. Schematic geometries of the investigated hole-type PCSs, calculated CD spectrum shifts in both right-hand and left-hand patterns with chiral solution, and near-field excitation of superchiral fields.

1. A. V. Rogacheva, V. A. Fedotov, A. S. Schwanecke, and N. I. Zheludev, "Giant gyrotropy due to electromagnetic-field coupling in a bilayered chiral structure," Phys. Rev. Lett. **97**, 177401 (2006).
2. M. Decker, M. W. Klein, M. Wegener, and S. Linden, "Circular dichroism of planar chiral magnetic metamaterials," Opt. Lett. **32**, 856 (2007).
3. E. Hendry, T. Carpy, J. Johnston, M. Popland, R. V. Mikhaylovskiy, A. J. Lapthorn, S. M. Kelly, L.D. Barron, N. Gadegaard and M. Kadodwala, "Ultrasensitive detection and characterization of biomolecules using superchiral fields,"Nature Nanotechnology **5**, 783 (2010).

C41: Jahn-Teller Cu(II) ion induced mm wave energy levels in ferroelectric crystals of Cu(II):$Cd_2(NH_4)_2(SO_4)_3$

Dilip De; Yerima Benson
(*Department of Physics, Covenant University, Ota, Ogun State, Nigeria)*
(Department of Physics, Modibo Adamawa University of Technology, Yola, Nigeria)

The EPR studies of Cu(II) doped single crystal of ferroelectric cadmium ammonium sulphate: Cu(II):$Cd_2(NH_4)_2(SO_4)_3$. revealed for the first time orthorhombic Jahn-Teller effect of the ^{2}D Cu(II) with ^{2}E orbital ground state giving rise to the energy splitting of the three Jahn-Teller potential wells minima in the range of 25 -300 cm^{-1}. Detailed theoretical studies is presented along with experimental results to extract the energy parameters and other spin-hamiltonian parameters related to the Jahn-Teller Cu(II) ion. It may be possible to excite sub millimeter wave radiation by exploiting the Jahn-Teller effect due to Cu(II) ion in the ferroelectric crystal.

D26: Electromagnetic Coupling in Regular Arrays of Plasmonic Nanostructures

Anatoliy O. Pinchuk[1,2]

[1]*Department of Physics, University of Colorado Colorado Springs, Colorado, USA*

Email:apinchuk@uccs.edu, web site: http://www.uccs.edu/~apinchuk.html

[2]*Biofrontiers Institute, University of Colorado Colorado Springs, Colorado, USA*

Arrays of noble metal nanoparticles are of interest for multiple applications in subwavelength optics, optical waveguides, and biochemical sensors, to name just a few. When illuminated by an external light, such plasmonic systems exhibit collective surface plasmon resonance (SPR) excitations. The wavelength and width of the collective SPR depends on the size of the particles, distance between the neighbor nanoparticles, and polarization of the incoming light.[1,2] Depending on the distance between the particles, the coupling between them may be dominated by the near-field or far-field components of the induced dipole electromagnetic fields.[2]

Figure 1 shows schematics of the internal electric field induced by external and neighbor-particle fields. The magnitude of the internal field defines the frequency of the collective SPR resonance.[2] When the frequency of the external field is less than the SPR frequency of a single nanoparticle, as shown in Fig.1 (b), the internal field decreases, as a result of destructive interference, and no additional features are observed in the extinction spectra of the system. However, if the frequency of the external field is larger than the frequency of the SPR in a single nanoparticle, as shown in Fig.1 (a), the internal field is amplified, which leads to the appearance of an extra peak in the extinction spectra of the system. The extra peak shifts linearly as a function of the distance between the particles in the array.

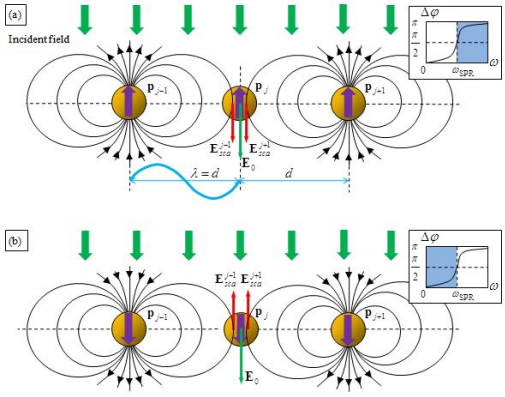

Fig1. Schematics of the induced dipoles and external electromagnetic fields creating internal electric fields which dives the collective SPR excitations in arrays of meatal nanoparticles.

1. VV Kravets, LE Ocola, Y Khalavka, AO Pinchuk, *Applied Physics Journal* **106**, 053104 (2015).
2. D.A. Smith, AO Pinchuk, *SPIE NanoScience+ Engineering*, 8457 (2012).

D27: Organic polariton condensates in all-dielectric microcavities: Polariton interactions and coherence properties

Ray Murray
Experimental Solid State Group
The Blackett Laboratory
Imperial College London, London, SW7 2AZ
United Kingdom
k.daskalakis11@imperial.ac.uk

Over the last two decades, polariton devices have attracted significant interest from researchers owing to the many fascinating phenomena observed such as stimulated scattering, parametric amplification, condensation and superfluidity. Cavity polaritons are bosonic half-light half-matter quasi-particles that, under the right conditions [1], form a macroscopic condensate in the ground state. This condensate decays through the cavity mirrors, thus providing coherent light-emission: a phenomenon termed polariton lasing. The threshold for polariton lasing can be significantly lower than that required for conventional photon lasing [2]. In inorganic semiconductors, the condensate's nonlinear character results principally from the Coulomb interaction between Wannier-Mott excitons. In contrast, interactions between the tightly bound Frenkel excitons — characteristic of organic semiconductors — are considerably weaker and were notably absent in the only reported demonstration of an organic polariton condensate [3].

In this work we demonstrate a room temperature organic polariton condensate that exhibits a

power-dependent blueshift due to nonlinear interaction between Frenkel excitons [4]. The studied samples consist of a thermally evaporated 2,7-bis[9,9-di(4-methylphenyl)-fluoren-2-yl]-9,9-di(4-methylphenyl)fluorene (TDAF) thin film enclosed in an all-dielectric (SiO_2/Ta_2O_5) microcavity (Fig. 1). On increasing the pump fluence, a threshold of 39 μJ/cm^2 is found that is followed by a superlinear increase of the photoluminescence (PL). This increase is accompanied by a simultaneous blueshift of the emission energy and a collapse, in momentum space, of the emission to the bottom of the lower polariton (LP) branch marking the onset of polariton lasing. In addition, by using a Michelson interferometer in a retroreflector configuration, we study the emergence of spatial coherence and demonstrate a number of unique features stemming from the peculiarities of this material set [5]. Despite its disordered nature, we find that correlations extend over the entire spot size and we measure $g^{(1)}(r, r')$ values of nearly unity at short distances and of 50% for points separated by nearly 10 μm. We show that for large spots, strong shot to shot fluctuations emerge as varying phase gradients and defects. These are attributed to modulation instabilities. Furthermore, we find that measurements with flat-top spots are significantly influenced by disorder and can, in some cases, lead to the formation of mutually incoherent localized condensates.

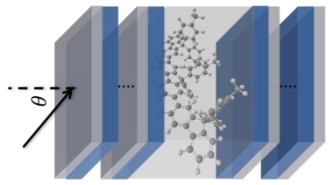

Figure 1. Schematic showing the fabricated structure which consists of two dielectric mirrors of alternating tantalum pentoxide (Ta_2O_5) and silicon dioxide (SiO_2) pairs enclosing a single layer of TDAF. The molecular structure of TDAF is shown between the mirrors.

[1] Dang et al., "Stimulation of Polariton Photoluminescence in Semiconductor Microcavity" Phys Rev Lett **81**(18), 3920-3923 (1998).

[2] Deng et al., "Polariton lasing vs. photon lasing in a semiconductor microcavity" Proceedings of the National Academy of Sciences **100**(26), 15318-15323 (2003).

[3] Kena-Cohen S, Forrest SR, "Room-temperature polariton lasing in an organic single-crystal microcavity" Nat Phot **4**(6)**,** 371-375 (2010).

[4] Daskalakis et al., "Nonlinear interactions in an organic polariton condensate" Nature Mater **13**, 271-278 (2014).

[5] Daskalakis et al., "Spatial coherence in a disordered organic polariton condensate" arXiv:1503.01373v1 (2015).

D28: Thermoelectronic Solar Power Conversion with Parabolic Concentrator

Dilip Kumar De and Olawole C. Olukunle

Department of Physics, Covenant University, Ota, Ogun State, Nigeria

Abstract

Solar energy can be focused by a parabolic concentrator mirror of diameter 2 m on to a small emitter surface (equal to the focused area) made of tungsten (coated with rare earth oxide or cesium to lower the work function) to raise the temperature to above 1000 C with solar insolation 600 to 1000 W/m^2. The temperature of the emitter depends on its height h from the center at the base, the diameter and focal length of the parabolic concentrator. Using modified Richardson Dushman constant we study the energy dynamics of the thermos electronic emission and the available power output from the thermos-electronic converter for different solar insolation, height h of emitter, reflectivity of parabolic mirror, assuming no space charge effect initially. We also investigate the advantage/disadvantage of cesiation of the tungsten surface and the cooling of the collector(anode) on the total power output in the solar thermos-electronic power conversion. The investigation discusses many novel ways the space-charge problem can be tackled and shows method of calculation of efficiencies which is also found to be dependent on solar insolation and the effect of space charge is modeled through introduction of a factor f($0<f\leq1$) and

consideration of energy dynamics of the thermos electronic power conversion. Part II of the paper considers in details the effect of space charge on above calculations and the extent of space charge reduction following the novel ways such as gate, magnetic field etc..

D29: Innovative therapeutic and diagnostic tools based on delivery and imaging of miRNAs by multifunctional carbon nanotubes

Stefano Bellucci, [1] Silvia Bistarelli, [1] Antonella Celluzzi,[2] Andrea Masotti,[2] Andrea Caporali,[3]

[1] INFN-Laboratori Nazionali di Frascati, Via Enrico Fermi 40, 00044 Frascati, Rome, Italy
[2] Gene Expression – Microarrays Laboratory, Bambino Gesù Children's Hospital, P.za S.Onofrio 4, 00165 Rome, ITALY.
[3] University of Edinburgh, University/BHF Centre for Cardiovascular Science, Queen's Medical Research Institute, 47 Little France Crescent, Edinburgh, EH16 4TJ

We used pristine and carboxy (COOH) functionalized carbon nanotubes (CNTs), obtained following well-established methodologies [1], for preparing functional nanomaterials coated with polyethylenimine (PEI) and polyamidoamine (PAMAM) polymers. The latter have been employed to obtain drug delivery vectors for *in vitro* and *in vivo* biomedical applications [2,3]. Simple physicochemical adsorption allowed us to coat CNTs, whereas polymer-conjugated CNTs have been obtained by amide bonds formation by taking advantage of COOH functionalities. Different functionalized CNTs display different solubility and toxicity properties, as a function of the polymer molecular weight. We evaluated the properties of these functional nanomaterials (i.e. DNA binding ability, toxicity, transfection efficiency) by specific *in vitro* assays (i.e., gel electrophoresis, cell cultures and fluorescence microscopy) on human primary endothelial cells. Our results illustrate the versatility of such innovative devices as multifunctional vectors for *in vitro* delivery of DNA/RNA-based oligonucleotides.

This work is supported in part by the Italian Ministry of Health research project "Delivery and imaging of miRNAs by multifunctional carbon nanotubes and circulating miRNAs as innovative therapeutic and diagnostic tools for paediatric pulmonary hypertension" (PE-2011-02347026 – Years: 2014-2017).

References

[1] Bellucci, S. 2005, Carbon nanotubes: physics and applications. *Phys. Stat. Sol. (c)*. 2: 34–47.
[2] Masotti, A. et al. 2007. Physicochemical and biological study of selected hydrophobic polyethylenimine-based polycationic liposomes and their complexes with DNA. *Bioorg Med Chem.* 15(3): 1504-15.
[3] Masotti, A. et al. 2008. A novel near-infrared indocyanine dye-polyethylenimine conjugate allows DNA delivery imaging in vivo. *Bioconjug Chem*. 19(5): 983-7.

D30: An efficient rule-based screening approach for discovering fast ion conductors using density functional theory and informatics

Randy Jalem,[1] Masanobu Nakayama[2,3]

[1]Global Research Center for Environment and Energy Based on Nanomaterials Science (GREEN) – National Institute for Materials Science (NIMS), Japan
[2]Nagoya Institute Technology, Japan
[3]JST-PRESTO, Japan

Battery technology has now hardly been able to keep up with the increasing demand in the electronics and electric vehicle market. This is especially true for lithium ion batteries, in which even higher energy densities, higher safety, and longer cycle life are much sought. With the ultimate goal which is to realize a major breakthrough, new material discovery and materials optimization are now being aided with state of the art material simulation techniques such as first-principles calculation within density functional theory (DFT) framework. One focus has been to build massive materials property datasets to provide insight and guidelines for

materials scientists. However, evaluation of properties by DFT is oftentimes involved with very time-costly calculation schemes, making data acquisition for large-scale materials screening for a broad range of materials very dependent on the level of available computational resources. Recently, augmenting DFT calculations with informatics-based techniques has become increasingly attractive for the exploration of vast computational search spaces. This presentation will highlight this approach, with the aim of efficiently screening a large number of compositions with respect to a target property that is critical to battery working operation – the lithium ion migration energy barrier. Structure-property relationships will also be explored using the statistical learning platform provided by the employed informatics techniques.

D31: Ultrafast Spectroscopic Study of Acoustic Transport and Phonon Interactions in Nanoscale Materials

Masashi Yamaguchi[1]

[1] Department of Physics, Applied Physics, and Astronomy, Rensselaer Polytechnic Institute, Troy, NY, USA
Email:yamagm@rpi.edu

Thermal transport properties of nanoscale materials are critical issues in many aspects of technology. For example, today's high performance microprocessors and electronic devices perform at a very high temperature. As such, one of the serious problems is that overheating of processors can cause the performance to deteriorate and result in a shorter working lifetime. Thermal transport, or device cooling, remains one of the challenges in microelectronics. Although pioneering work in this field was made a decade ago and considerable continuing efforts exist[1, 2], their foundation has not yet been well established as much as that of electronic and optical properties for nanometer scale materials[3, 4]. The problem is rooted in the fundamental phonon interactions rather than engineering issues. Length scale dependent phonon interaction is a key concept for the fundamental understanding of thermal transport in nanoscale materials. Thermally distributed phonons with various wavelengths belong to various transport regimes in nanoscale materials depending on the relative size of wavelength, mean-free-path vs. characteristic sizes of nanoscale materials.

Nanoscale confinement effects on acoustic transport and electron-phonon coupling in nanoscale arrays and nanoscale layers were studied by using GHz-sub THz acoustic spectroscopy and ultrafast transient reflectivity spectroscopy in nanoscale copper films. The tunable acoustic source in GHz-sub-THz frequency range was developed using ultrafast pulse shaping technique[5, 6]. Frequency dependent mean-free-path and group velocity directly was experimentally measured. We used two kinds of model structures for the phonon transport through nanolayers or nanorods to use with the acoustic spectroscopy. The structure consists of substrate, metal transducer and nanorod layers. Acoustic phonons are excited by photothermal process using femtosecond laser pulses in metal transducer layer deposited on sapphire substrate. Generated acoustic pulses propagate through the metal transducer layer, then they are partially reflected at the interface, and the rest continues to propagate into the nanorod arrays. Acoustic phonons can be detected as an echo signal at the transducer when the pulse returns, or at the other side of the sample. Frequency dependent phonon mean-free-path (MFP) was experimentally and directly measured for SiO_2 and ITO glasses. Furthermore, acoustic pulse transport and coupling to the eigen modes of vertically grown nanorod array will be reported. For electron-phonon coupling in spatially confined materials, we have used transient reflectivity measurement with tunable probe wavelength and measured around the d-band to Fermi surface. There are two competing relaxation processes of electrons in metallic materials. We demonstrate that electron-electron processes and electron-phonon scattering processes can be selectively measured within a framework of phenomenological model by changing the probe wavelength[7]. Also, we have observed the increase of electron-phonon coupling in epitaxially grown copper nanofilms

around 100 nm when the systems size becomes smaller[8].

[1]D. G. Cahill, W. K. Ford, K. E. Goodson, G. D. Mahan, A. Majumdar, H. J. Maris, R. Merlin, and S. R. Phillpot, J. Appl. Phys., **93**, 793-818 (2003).
[2]D. G. Cahill, et al., Applied Physics Reviews, **1**, 011305-011301-011345 (2014).
[3]H. Haug and A. P. Jauho, *Quantum Kinnetics in Transport and Optics of Semiconductors* (Springer-Verlag, Berlin, 1996).
[4]J. Bylander, T. Duty, and P. Delsing, Nature, **434**, 361 (2005).
[5]J. D. Choi, T. Feurer, M. Yamaguchi, B. Paxton, and K. A. Nelson, Appl. Phys. Lett., **87**, 819071-819073 (2005).
[6]C. Klieber, E. Peronne, K. Katayama, J. Choi, M. Yamaguchi, T. Pezeril, and K. A. Nelson, Appl. Phys. Lett., **98**, 211908 (2011).
[7]X. Shen, Y. P. Timalsina, T.-M. Lu, and M. Yamaguchi, Phys. Rev. B, **91**, 045129 (2015).
[8]Y. P. Timalsina, X. H. Shen, G. Boruchowitz, Z. P. Fu, G. G. Qian, M. Yamaguchi, G. C. Wang, K. M. Lewis, and T. M. Lu, Appl. Phys. Lett., **103** (2013).

D32: Mehcanical Manipulation of Skyrmion Crystal

Yoichi Nii[1*], T. Nakajima[1], A. Kikkawa[1], Y. Taguchi[1], T. Arima[1,2], Y. Tokura[1,3], and Y. Iwasa[1,3]

[1]*RIKEN Center for Emergent Matter Science (CEMS), Wako 351-0198, Japan*
**Email:yoichi.nii@riken.jp*
[2]*Department of Advanced Materials Science, University of Tokyo, Kashiwa 277-8561, Japan*
[3]*Department of Applied Physics and Quantum-Phase Electronics Center (QPEC), University of Tokyo, Tokyo 113-8658, Japan*

Nanometric spin swirling objects, Skyrmions, and its crystalline form called Skyrmion crystal (SkX) have been attracting growing attention owing to their potential applications for next generation memory as well as their emergent electromagnetic responses [1,2]. In spite of recent variety of theoretical proposals toward Skyrmion-based electronics (i. e., Skyrmionics) [3], few experiments have succeeded in creating, deleting and transferring Skyrmions, and the manipulation methodology has been so far limited. Here, we demonstrate a new approach for Skyrmion manipulation in terms of mechanical stress. By continuously scanning uniaxial stress at low temperatures, we created and annihilated Skyrmion crystal in a prototypical chiral magnet of MnSi. We also found that the SkX has a soft elastic stiffness [4], being consistent with the mechanical sensitivity of the SkX. All these results offer a new guideline for single Skyrmion control *via* scanning probe technique, which requires neither electric nor magnetic biases and consumes extremely low energy [5].

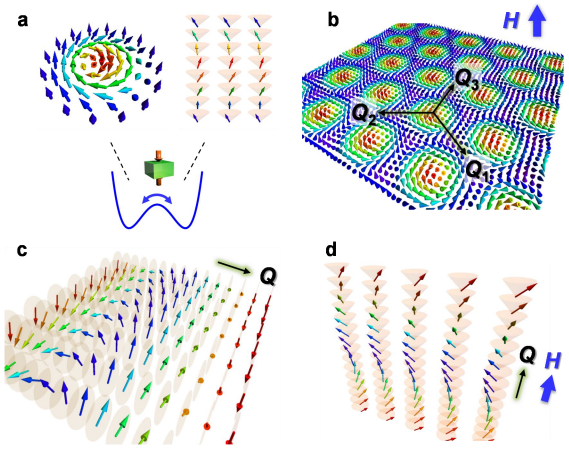

Fig. 1. (a) Mechanically controlled topological switching between Skyrmion and conical states. Spin textures in a chiral magnet of MnSi: (b) Skyrmion crystal, (c) Helical, and (d) conical phases.

1. S. Mühlbauer *et al*. *Science* **323**, 915-919 (2009)
2. N. Nagaosa and Y. Tokura, *Nat. Nanotechnol*. **8**, 899-911 (2013)
3. A. Fert, V. Cros and J. Sampaio, *Nat. Nanotechnol*. **8**, 152-156 (2013)
4. Y. Nii, A. Kikkawa, Y. Taguchi, Y. Tokura, and Y. Iwasa, *Phys. Rev. Lett.* **113**, 267203 (2014)
5. Y. Nii *et al., to be submitted*.

D33: Control of mesoscale phenomena in strongly correlated oxides

Zac Ward

Staff Scientist, Thin films and Nanostructures Group
Oak Ridge National Laboratory, USA

The strong electronic correlations arising from overlapping spin-charge-orbital-lattice order parameters in complex oxides are of fundamental importance to many desirable characteristics such as metal-insulator transitions, ferroicity, colossal magnetoresistance, and high T_C superconductivity. We will discuss our research progression on manganites which has taken us from creating a means of isolating and observing previously hidden mesoscopic phenomena to designing approaches that allow tuning of each of the individual order parameters. These methods will be put into the contexts of allowing us to explore the fundamental mechanisms at play in complex materials and providing a bridge toward next generation device functionality.

Supported by the US DOE Office of Basic Energy Sciences, Materials Sciences and Engineering Division.

D34: Huge spin-driven polarizations and optical-diode effect at room temperature in $BiFeO_3$

Jun Hee Lee

Oak Ridge National Laboratory

Although $BiFeO_3$ is one of the most investigated multiferroics, its magnetoelectric (ME) couplings and spin-driven polarizations are barely understood on an atomistic level. By combining a first-principles approach with a spin-cycloid model, we report hidden but huge spin-driven polarizations at room temperature in bulk $BiFeO_3$. One of the polarizations reaches ~0.03 C/m^2, which is larger than any other spin-driven polarization in a bulk material by one order of magnitude. By comparing our results with intrinsic measurements such as neutron scattering, Raman spectroscopy and IR directional dichroism, we quantitatively disentangle all the hidden spin-driven polarizations due to exchange-striction, spin-current, and single-ion-anisotropy. Interestingly, these polarizations contribute to a large uni-directional optical transmission which can be used as an optical diode at room temperature.

D35: Immunotoxicity of Nanomaterials

Andrij Holian

Center for Environmental Health Sciences, Department of Biomedical and Pharmaceutical Sciences, University of Montana, Missoula, Montana, USA
Email:andrij.holian@umontana.edu, web site: https://cehsweb.health.umt.edu/

The expanding use of engineered nanomaterials (ENM) has increased the need to describe the mechanisms responsible for initiating immunotoxic responses; develop reliable assessments to determine which ENM are most likely to cause harm; and determine the characteristics of ENM responsible for activation of the immune system. The majority of studies have focused on responses of the respiratory system to inhaled ENM. Most current evidence support the notion that ENM have to cause phagolysosomal membrane permeability (LMP) in innate immune cells to initiate "sterile" inflammatory responses that can progress to various adverse immune outcomes such as airway hyper-reactivity, fibrosis and autoimmune responses. LMP results in the release of a broad spectrum of proteases of which cathepsin B has been implicated in initiating NLRP3 inflammasome assembly, while other proteases initiate apoptosis and mitochondrial damage accompanied by ROS production. The apoptotic events result in the release of alarmins (e.g., HMGB1, IL-1 , etc) providing a "sterile" mechanism of activating the NF- B pathway necessary for the inflammatory response to accompany NLRP3 inflammasome activation and release of IL-1 . Therefore, the critical step in determining the bioactivity of ENM is LMP. Important factors in modulating LMP appear to be surface charge or wettability (more negative may be protective), stiffness (more rigid more LMP) and solubility under the slightly acidic environment of the phagolysosome. The mechanism responsible for

LMP has not been determined, but evidence suggests that perturbation of phospholipid metabolism and phospholipid/cholesterol content of the phagolysosome are important. Although ROS has been proposed as a mechanism ENM bioactivity, our studies demonstrate that it would not universally explain LMP. Alternatively, ENM effects on lysosomal lipid metabolism maybe critical. This work was supported in part by R01ES023209 from the NIH.

D36: Multifunctional rare-earth based nanoparticles for reactive oxygen species sensing and magnetic resonance imaging

Mouna Abdesselem,[1] Isabelle Maurin,[2] Olivier Clément,[3] Pierre-Louis Tharaux,[3] Thierry Gacoin,[2] Cédric Bouzigues,[1] Antigoni Alexandrou[1]

[1]Laboratoire d'Optique et Biosciences, Ecole polytechnique, CNRS, INSERM, 91128 Palaiseau Cedex
E-mail : antigoni.alexandrou@polytechnique.edu, web site: http://www.lob.polytechnique.fr/home/research/nanoimaging-and-cell-dynamics/
[2]Laboratoire de Physique de la Matière Condensée, Ecole polytechnique, CNRS, 91128 Palaiseau Cedex
[3]Paris Centre de Recherche Cardiovasculaire (PARCC), INSERM U970, 56 rue Leblanc, 75015 Paris, France

A deregulation of the reactive oxygen species (ROS) production is involved in numerous pathophysiological processes and in a variety of diseases like inflammation, neurodegenerative diseases and cancer. Understanding pathologies in their full complexity, enabling accurate diagnosis and design of novel therapeutic approaches requires collecting information on multiple pathophysiological parameters.

However, current ROS sensors are limited either in terms of quantitativity or in terms of time resolution. We have demonstrated that oxydoreduction processes of Eu^{3+} ions in $Y_{1-x}Eu_xVO_4$ nanoparticles result in luminescence modulation that can be used to detect intracellular H_2O_2 in cell signaling processes involving contraction and migration responses in a quantitative, time- and space-resolved manner [1]. In particular, we have shown that different stimuli elicit different dynamics of H_2O_2 concentration changes and that an asymmetric cell stimulation with the growth factor PDGF gives rise to an asymmetric intracellular H_2O_2 concentration profile (see figure 1) [2].

Replacing Y^{3+} ions with Gd^{3+} ions in the nanoparticle matrix, renders these particles multifunctional. Indeed, they conserve their luminescent and ROS detection properties, while they acquire the additional capability of providing contrast in magnetic resonance imaging (MRI). Injection of these nanoparticles in the mouse blood circulation results in MRI contrast enhancement in the bladder and the liver after 30 min (see figure 1) [3].

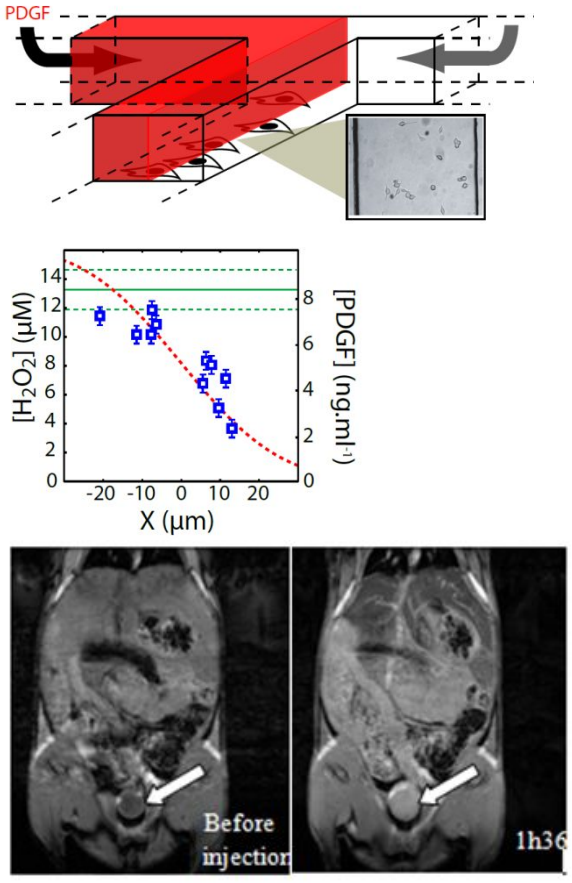

Fig1. Left: Asymmetric PDGF stimulation of HeLa cells grown in microfluidic channels (top). The measured intracellular H_2O_2 concentration (blue data points) follows the external PDGF gradient (dashed red line). In contrast, the detected H_2O_2 concentration is constant in the case of homogeneous stimulation

(green lines) (bottom). Right: Injection of $Gd_{0.6}Eu_{0.4}VO_4$ nanoparticles in the mouse blood circulation leads to nanoparticle accumulation in the bladder as is seen by the signal increase in T_1-weighted MRI images.

These multifunctional rare-earth vanadate nanoparticles pave the way for simultaneous optical and magnetic resonance detection, in particular for *in vivo* localization evolution and ROS detection in a broad range of physiological and pathophysiological conditions.

1. D. Casanova et al., *Nat. Nanotech.* **4**, 581-585 (2009)
2. C. Bouzigues et al., *Chem. Biol.* **21**, 647-656 (2014)
3. M. Abdesselem et al, *ACS Nano* 8, 11126–11137 (2014)

D37: Tumor penetrating pH-sensitive polymersomes for intraperitoneal tumor theranostics

Lorena Simón Gracia[1], Hedi Hunt[1], Pablo Scodeller[1,2], Gary B. Braun[2], Anne-Mari A. Willmore[1], Jens Gaitzsch[3],Venkata Ramana Kotamraju[2], Erkki Ruoslahti[2], Giuseppe Battaglia[3], Tambet Teesalu[1*].

[1]*Intitute of Biomedicine and Translational Medicine, University of Tartu, Tartu, Estonia Email:Lorena.Simon.Gracia@ut.ee, web site: www.cancerbiology.ee*
[2]*Cancer Research Center, Sanford-Burnham Medical Research Institute, La Jolla, California, USA.*
[3]*Department of Chemistry, University College London ,London, UK.*

Peritoneal carcinomatosis (PC) is the second cause of mortality in cancer patients, with a median survival estimate of 1–3 months [1]. Cytoreductive surgery combined with hyperthermic intraperitoneal chemotherapy (HIPEC) is the current clinical treatment. However, even with HIPEC, achieving curative drug accumulation and penetration in PC lesions remains an unresolved challenge [2].

Polymersomes (PS) are nano-sized polymeric vesicles that can be loaded with hydrophilic and hydrophobic drugs, biomolecules, and imaging agents. PDPA-based PS are stable at physiological pH and disintegrate rapidly at mildly acidic conditions in endosomes to release the contents intracellularly [3] (Fig.1A).

Here, we show that i.p. administrated POEGMA-PDPA (poly(oligoethylene glycol methacrylate)- poly(2-(diisopropylamino)ethyl methacrylate)) PS accumulate and penetrate in PC models of gastric and colon cancer (Fig.1B). Furthermore, i.p. treatment of MKN-45 gastric tumor-bearing mice with paclitaxel-loaded PS shows significantly reduced tumor growth and tumor nodules compared to free drug and Abraxane. Recently discovered tumor penetrating peptides (TPP) not only home to tumor vessels, but also spread through tumor parenchyma and internalize into malignant cells [4]. We found that in vitro cellular uptake and cytotoxicity of drug-loaded TPP-targeted PS are significantly higher compared to non-targeted PS in cell lines positive for TPP receptors. Moreover, after i.p. administration in mice bearing PC tumors, TPP-PS showed improved tumor accumulation and penetration compared to untargeted PS. Our studies indicate that i.p. administered TPP-functionalized pH-sensitive PS are suitable for selective cytoplasmic delivery of drugs and imaging agents deep into tumor tissue.

A

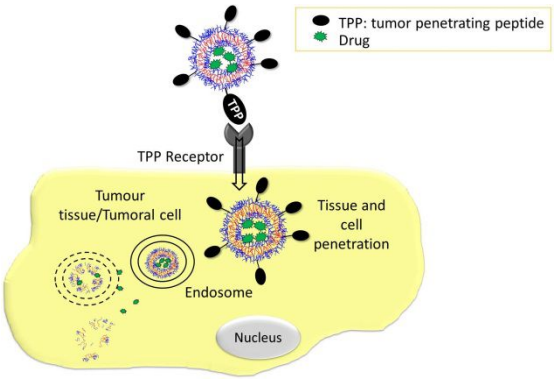

B

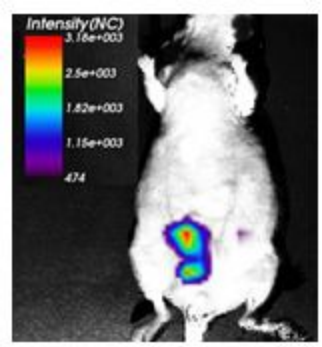

Fig1. A) Tumor penetration scheme of pH-sensitive TPP-PS and intracellular release of the loaded drug by disassembly of the vesicles inside the endosomes. B) In vivo imaging by ART OPTIX MX3 of fluorescent PS homing to gastric tumor MKN-45 after 24 hours of i.p. injection.

1. G. Montori, F. Coccolini, M Ceresoli, F. Catena, N. Colaianni, E. Poletti, L. Ansaloni. *International Journal of Surgical Oncology*, **2014**, 1 (2014).
2. M.J. Koppe, O.C. Boerman, W.J. Oyen, R.P. Bleichrodt. *Annals of Surgery*, **243**, 212 (2006).
3. C. Pegoraro, D. Cecchin, L. Simon Gracia, N. Warren, J. Madsen, S. P. Armes, A.Lewis, S. MacNeil, G. Battaglia. *Cancer Letters*, **334**, 328 (2013).
4. K. N. Sugahara, T. Teesalu, P. P. Karmali, V. R. Kotamraju, L. Agemy, O. M. Girard, D. Hanahan, R. F. Mattrey, E. Ruoslahti. *Cancer Cell*, **16**, 510 (2009).

D38: Molecular imaging nanosystems for cancer biology and therapy

Jamal Zweit, PhD, DSc
Virginia Commonwealth University, Richmond, VA
Email:jzweitr@vcu.edu

Molecular Imaging is concerned with the study of underlying biological pathways associated with disease processes and the working of therapies within the intact *in vivo* environment. Molecular nanotechnology deals with the applications of nano-materials in cell biology, drug delivery, targeted therapy and diagnostics. Combining molecular imaging with nanotechnology offers a powerful platform to specifically image and study multifunctional pathways associated with cancer biology and therapeutics. The Center for Molecular Imaging (CMI) at VCU, is a state-of-the-art multi-modality research facility, with expertise in molecular imaging Science (PET/SPECT/CT; MRI/MRS, Optical and Photoaccoustic imaging). The imaging technologies are underpinned by developments of targeted agents, including multi-modal hybrid nano-probes. Within the context of cancer biology and therapy, the combination of molecular imaging and nanotechnology offers real time investigations of tumor progression, the role of tumor micro-environment, and the interrogation of therapeutic interventions, all within the intact tumor and normal tissue environments. This presentation will highlight CMI research in these areas; which include i) image-guided chemotherapy, ii) radio-nanoparticle imaging and therapy; iii) dual-modal PET/MR imaging; iv) tumor associated microenvironment and v) image-guided normal tissue radioprotection. These research platforms highlight the use of combined technologies to enhance research in cancer biology and therapy within intact live subjects.

D39: Cerium Oxide Nanoparticles for Normal Tissue Protection During Radiation Therapy: Combining Molecular Imaging and Nanotechnology Approaches

Philip Reed McDonagh, Likun Yang, Minhao Sun, Purnima Jose, Gobalakrishnan Sundaresan, Ross Mikkelsen, Jamal Zweit

Virginia Commonwealth University, Richmond, VA
Email:mcdonaghpr@vcu.edu

Along with chemotherapy and surgery, radiation therapy (RT) is a leading treatment option for cancer as an element in the treatment plan of over 50 million cancer survivors worldwide. Even with advances in image guided therapies, RT is limited by damage to normal tissues. Both short and long term side effects have been associated with RT, including anemia, gastrointestinal distress, skin irritation, tissue fibrosis, and even secondary cancer, compromising the quality of life for many

patients. Our work investigates cerium oxide nanoparticles (CONPs) for their application as radio-protective agents administered during RT to prevent normal tissue toxicities. These nanoparticles have demonstrated an ability to reduce radiation side effects by reducing radicals and preventing radiation induced DNA damage, and doing so preferentially in normal tissue over tumor tissue.

Most research involving CONPs have been nanoparticles without a coating, without which the nanoparticles aggregate in solution, reducing the available surface area for radical scavenging. Previously, our lab has developed a synthesis method for polymer coated CONPs with a radionuclide incorporated into the core, allowing for PET or SPECT imaging and detailed biodistribution studies.[1] Synthesizing CONPs with a polymer coating allows the nanoparticles to dissolve in solution and significantly decreases the size, allowing more surface area for scavenging activity. Our current research focuses on incorporating zirconium-89, a clinically relevant PET isotope, into polymer-coated and uncoated CONPs, allowing for a comparison of pharmacokinetics and biologically activity. CONPs with the polymer coatings showed vastly improved biodistribution and clearance compared to uncoated CONPs, shown in images from dynamic PET scans in **Figure 1**. Uncoated CONPs showed immediate trapping in the lungs minutes after injection and further uptake by the liver and spleen over the first hour, with the nanoparticles persisting in these organs over twenty-four hours. PAA coated CONPs, by comparison, showed persistent signal from the blood over the first half hour, after which the nanoparticles began excretion through the kidneys and out through the urine. The uptake in relevant tissues was significantly higher in the polymer coated CONPs. These results demonstrate that polymer coated CONPs have much better pharmacokinetics and can get into tissues at the same concentration as uncoated CONPs at much lower doses.

We have also been able to determine the efficacy of the polymer coated CONPs, demonstrating that they are still able to both protect normal tissue and not protect tumors from radiation therapy. Experiments focused on the colon, a very radiosensitive organ, and a colon tumor mouse model. Normal tissue protection was demonstrated by examining the apoptosis in the colon after irradiation with and without polymer-CONP pre-treatment. Tumor protection was measured by comparing 18F-FDG PET images in the mouse colon tumor model before and two weeks after radiation treatment with and without polymer-CONP pre-treatment. The PET images showed a significant decrease in 18F-FDG uptake for irradiated mice with and without polymer-CONP pre-treatment, indicating that radiation caused the tumors to shrink. There was no significant difference in the amount that the radiation decreased tumor size between the groups, showing that polymer-CONPs were not protecting the tumor and had no effect on the efficacy of radiation treatment to the tumor.

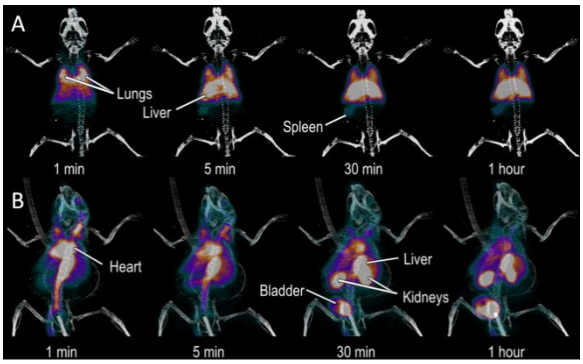

Figure 1: Dynamic PET scan of mice IV tail vein injected with ^{89}Zr labeled uncoated CONPs (**A**) and Poly(acrylic acid) coated CONPs(**B**). Uncoated CONPs show immediate accumulation in the lungs and liver, with an increased uptake in the spleen by 30 minutes.Poly(acrylic acid) CONPs show distribution in the blood with eventual uptake by the liver and kidneys and excretion in the urine by 30 minutes, demonstrating wide biodistribution of PAA-CONPs by the blood with fairly quick clearance.

1. Likun Yang, Gobalakrishnan Sundaresan, Minghao Sun, Purnima Jose, David Hoffman, Philip Reed McDonagh, Narottam Lamichhane, Cathy S. Cutler, J. Manuel Perez, Jamal Zweit. Intrinsically radiolabeled multifunctional cerium oxide nanoparticles for in vivo studies. J. Mater. Chem. B, 2013,1, 1421-1431.

D40: Nanotherapeutic approaches for the management of arthritis

Christine Pham

Washington University School of Medicine, USA
Email: cpham@dom.wustl.edu

Rheumatoid arthritis (RA) is a chronic and debilitating inflammatory arthropathy. Recent understanding of inflammatory responses in RA has led to the development of several effective treatment modalities. These include a number of "biologics" aimed at inhibiting the action of several inflammatory cytokines, including IL-1 , IL-6 and TNF- . Yet despite these advances, many patients with RA fail to respond to these new biologic agents. Moreover, studies have shown that around half of the initial responders eventually stop responding in the first year due to inefficacy or have to stop therapy altogether due to side effects. Thus there is a continued need for the development of new therapeutic agents. We have used a contact facilitated drug delivery (CFDD) system for the *in vivo*, $\alpha_v\beta_3$-integrin targeted administration of the anti-antiogenic drug fumagillin and the lipase-labile fumagillin prodrug to suppress clinical arthritis in a passive transfer model of RA at total drug doses far less than that required with the water-soluble fumagillin derivatives (50-300-fold reduction), especially when combined with the traditional anti-rheumatic disease-modifying drug methotrexate. In addition to suppression of clinical indices, injections of $\alpha_v\beta_3$-targeted fumagillin prodrug nanoparticles decreased the expression of local inflammatory markers, including IL-1 , IL-6, MCP-1, and TNF- . Combined with a favorable toxicity profile, these lipase-labile prodrugs used with lipid-based nanoparticles, offer a scalable and clinically translatable approach to improve the efficacy and safety of fumagillin and many additional targeted nanomedicines. Another approach was to use a self-assembling, peptide-siRNA nanocomplex to specifically silence the expression of NF- B and a broad array of downstream cytokine effectors for the effective suppression of inflammatory arthritis. We have demonstrated that a melittin-derived cationic amphipathic peptide, p5RHH, combined with anti-NF- B p65 siRNA homed to the inflamed joints and strongly suppressed inflammatory arthritis without affecting p65 expression in off-target organs or eliciting an adaptive immune response, even after serial injections. The results suggest that the peptide-siRNA platform may have real translational potential for the treatment of inflammatory arthritis and other disease processes amenable to siRNA silencing.

D41: Probing cell structure by atomic force microscopy

Luis F. Jiménez-García[1], A. Zamora-Cura[1], Y. Lozada-Villegas[1], R. Chávez-Rosales[1], G. Álvarez-Fernández[2], A.G. Almeida-Juárez[1], L.T. Agredano-Moreno[1], M.L. Segura-Valdez[1]

[1]*Department of Cell Biology, Faculty of Sciences, National Autonomous University of Mexico, Mexico City, D.F., Mexico. Email:luisfelipe_jimenez@ciencias.unam.mx*

[2]*Department of Biochemistry, Faculty of Medicine, National Autonomous University of Mexico, Mexico City, D.F., Mexico.*

Cell structure by light and electron microscopy has been well studied. However, much less studies deal with this topic by atomic force microscopy. Using an approach including processing of samples for transmission electron microscopy, sectioning with an ultramicrotome and mounting semithin sections on glass slides, we have been working treating every section as a surface. Several types of samples have been probed as plant material from *Allium cepa*, *Ginkgo biloba*, *Lacandonia schismatica, Araucaria heterophylla,* as well as animal cells as HeLa, Hep2, rat hepatocytes and thymocytes. Internal cell structure with high vertical resolution may be achieved in this way. It is the possible to recognize organelles as nuclei, nucleoli, mitochondria. Within the cell nucleus, nuclear pores, compact chromatin and nucleoplasm are visualized. In addition, the generation of profiles offers an opportunity for the characterization of such material. [1-5]

Figure 1 shows an atomic force micrograph of a cell from the ovary of the plant *Alloe vera.* Within the cell nucleus, the compact chromatin defines the reticulated type of nucleus, characteristic of many species. The nucleolus is compact. The cytoplasm is distributed as thin layers around the cell nucleus. Several cell types and different organelles are also observed, fitting well with images taken with light and electron microscopes.

Experiments monitoring variations in structures under different conditions will be performed.

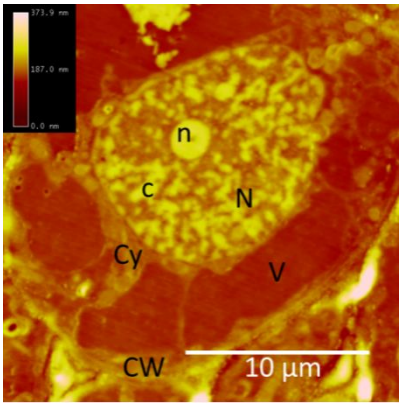

Fig1. Atomic force micrograph of an ovary cell of the plant *Aloe vera*. N, nucleus; n, nucleolus; c, compact chromatin; Cy, cytoplasm; V, vacuole; CW, cell wall.

1. L.F. Jiménez-García, M.L. Segura-Valdez, *Atomic force microscopy*. *Biomedical Methods and Applications* (Humana Press), 191 (2004).
2. A. Zamora-Cura and L.F. Jiménez-García, *J. Adv. Microsc. Res*. **9**, 296 (2014).

D42: How functional genomics informs nano-drug design for precision cancer medicine

Alexander H. Stegh

Ken and Ruth Davee Department of Neurology, The Northwestern Brain Tumor Institute, The Robert H. Lurie Comprehensive Cancer Center, International Institute for Nanotechnology, Northwestern University, Chicago, IL 60611, USA

High-throughput characterization and functional interrogation of cancer genomes has unraveled a complex landscape of genetic and epigenetic modifications, and has initiated the implementation of precision cancer medicine into clinical practice. The sheer complexity of genomic information, and the difficulty to concomitantly modulate the action of multiple 'undruggable' targets, however, pose significant challenges to drug development. Here, I will provide an overview of target gene identification in my laboratory, which has to led to the identification of critical cancer genes, in particular those implicated in the genesis and progression of malignant glioma. I will discuss how these findings can inform the design of RNA interference (RNAi)-based nanotechnological platforms, in particular siRNA *(1)* and microRNA-based spherical nucleic acids *(2)*, to overcome some of the most critical barriers to clinical progress, foremost the targeting of the undruggable oncogenome, and to enable precision (nano)drug design.

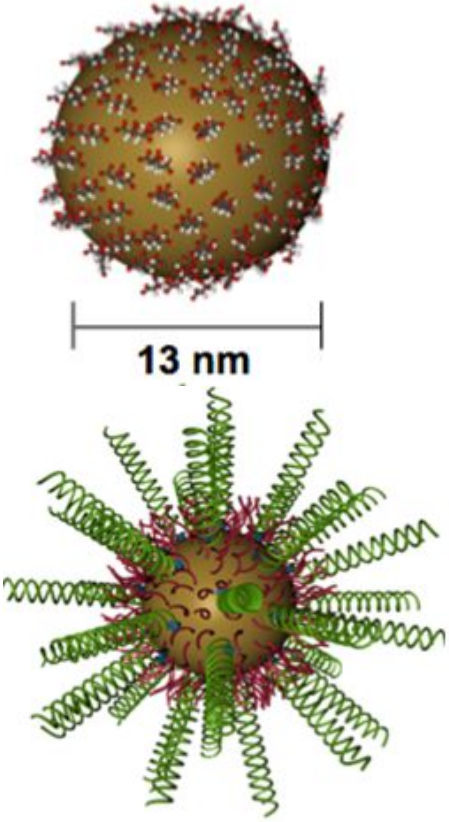

Fig. 1. Spherical Nucleic Acids (SNAs), i.e., PEGylated gold nanoparticles covalently conjugated with a corona of small interfering (si) or micro (mi)RNAs.

1. F. M. Kouri *et al.*, miR-182 integrates apoptosis, growth, and differentiation programs in glioblastoma. *Genes & development* **29**, 732 (Apr 1, 2015).
2. S. A. Jensen *et al.*, Spherical Nucleic Acid Nanoparticle Conjugates as an RNAi-Based Therapy for Glioblastoma. *Science translational medicine* **5**, 209ra152 (Oct 30, 2013).

Poster Session

P1: Solvent-Free Functionalization of Multiwalled Carbon Nanotube-Based Buckypaper with Amines

I. J. Ramírez-Calera[1], V. Meza-Laguna[2], E. Abarca-Morales[1], V. A. Basiuk[2] and E. V. Basiuk[1]

[1] *Centro de Ciencias Aplicadas y Desarrollo Tecnológico, Universidad Nacional Autónoma de México (UNAM), 04510 México D.F., Mexico; Email: elbg1111@gmail.com*

[2] *Instituto de Ciencias Nucleares, UNAM, 04510 México D.F., Mexico*

Buckypaper (BP), which is a thin film of carbon nanotube (CNT) network strongly aggregated through van der Waals forces, is of special interest for material science due to its high porosity, specific surface area, mechanical strength and flexibility. BP has a number of potential applications, for example, as thermally conductive and field emission materials, filter membranes, supports for growing biological tissues, as well as in the development of efficient sensors based on functionalized BP.

We developed a novel efficient approach for the covalent functionalization of BP based on oxidized multiwalled carbon nanotubes (MWNTs) with amine molecules of variable structure, which allows to avoid contamination with detergents and solvents. The functionalization protocol proposed consists in a solvent-free one-step treatment of BP with volatile amines under reduced pressure at a temperature of 160-180 °C. After the functionalization reaction, the excess amine is removed from the sample by simultaneous heating and pumping out. The functionalized BP samples were characterized by a number of experimental techniques including Fourier-transform infrared, Raman and X-ray photoelectron spectroscopy, thermogravimetric analysis, scanning and transmission electron microscopy, and atomic force microscopy (AFM). AFM imaging found important morphological differences between pristine and functionalized BP samples attributed to the presence of functionalizing organic moieties in the amine-treated materials. The suggested mechanism of covalent attachment of amines to BP is through the amidation of COOH groups of oxidized MWNTs. In addition to its simplicity, our approach allows for obtaining amide-derivatized BP materials without contamination with other chemical substances (solvents, condensing reagents, etc.), which is of crucial importance for a variety of applications, from nanoelectronics to nanomedicine.

Acknowledgements: We appreciate financial support from the grants UNAM-DGAPA-IN100815 and CONACyT-127299. I. J. R.-C. also thanks CONACyT and Posgrado en Ciencia e Ingeniería de Materiales UNAM for a doctoral fellowship.

P2: Interaction of a Ni(II) Tetraazaannulene Complex with Spherical Fullerenes and Short Carbon Nanotube Models: A DFT Study

V. A. Basiuk and L. V. Henao-Holguín

Instituto de Ciencias Nucleares, Universidad Nacional Autónoma de México, Circuito Exterior, Ciudad Universitaria, 04510, México, D.F., México Email: basiuk@nucleares.unam.mx

Noncovalently-bound nanohybrids of nickel(II) complex of 5,14-dihydro-6,8,15,17-tetramethyldibenzo[*b*,*i*][1,4,8,11]tetraazacyclotetradecine (or NiTMTAA for simplicity) with carbon nanotubes (CNTs) is a more complex and interesting case in structural terms as compared

to the related materials functionalized with porphyrins and phthalocyanines. Since NiTMTAA molecule has the shape of horse saddle, it can adopt several energetically non-equivalent orientations with respect to nanotube, depending on whether CH_3 or C_6H_4 substituents contact the latter.

The main goal of the present study was to provide information on the interactions of NiTMTAA with simple single-walled CNT (SWNT) models. To better account for noncovalent nature of these interactions, we employed three dispersion-corrected DFT functionals: M06-2X and LC-BLYP as implemented in Gaussian 09 package, and PBE GGA functional with Grimme empirical correction as implemented in the DMol^3 DFT module of Materials Studio 6.0 package from Accelrys, Inc. We considered one armchair (A) and one zigzag (Z) short closed-end SWNT models (which are often referred to as 'elongated fullerenes'), derived from hemispheres of C_{60} and C_{80} spherical fullerenes. The geometries obtained with M06-2X and LC-BLYP functional turned to be very similar. In most complexes, the interaction between NiTMTAA and SWNT was noncovalent. The exception was the geometry of one complex with Z, in which a new C-C covalent bond formed spontaneously: one C atom forming this bond belongs to the pentagon of the nanotube closed end, and another one is the γ-carbon atom of NiTMTAA. To explain this phenomenon, we performed an additional series of calculations with fullerene C_{60}, as well as with I_h and D_{5h} isomers of C_{80}. In the case of I_h C_{80}, from which (10,0) Z model is derived, we found again the covalent bonding with NiTMTAA in M06-2X calculations. The possibility of addition has likely to do, on one hand, with the reactivity of pentagonal defects responsible for spherical curvature and kinks of pristine nanotubes, and, on the other hand, with the known reactivity of the γ-C atom of transition metal complexes of TMTAA. In the case of PBE-Grimme calculations, all the complexes were found to be noncovalent. The general trend was that the 'embracing' contact of *o*-phenylene rings of NiTMTAA with SWNT surface allows for a stronger complexation due to π-π interactions.

Acknowledgements: We appreciate financial support from UNAM (grant DGAPA-IN101313) and CONACyT (grant 127299). L. V. H.-H. is indebted to the Doctorate Program in Chemical Sciences of UNAM and CONACyT for a Ph. D. fellowship.

P3: In Situ Functionalization of Multiwalled Carbon Nanotube Buckypaper with a Long-Chain Aliphatic Amine Polyethyleneimine

V. Meza-Laguna[1], M. Pérez-Ruiz[1], E. V. Basiuk[2] and V. A. Basiuk[1]

[1] Instituto de Ciencias Nucleares, Universidad Nacional Autónoma de México (UNAM), 04510 México D.F., México; Email: victor.meza@nucleares.unam.mx
[2] Centro de Ciencias Aplicadas y Desarrollo Tecnológico, UNAM, 04510 México D.F., México

Carbon nanotubes (CNTs) can be chemically fuctionalized, in either non-covalent or covalent way. In the functionalization, introduction of different chemical and biochemical functional groups/molecules into the nanotube structure is performed. The functionalities change physicochemical properties of CNTs. For biomedical applications, amine-functionalized carbon nanotubes seem to be the most promising because of strong electrostatic interactions between amine group and biological components, which can provide stable immobilization of biological compounds onto the nanotube surface. Polymeric aliphatic amines polyethylene glycol diamine (PEGDA) and polyethylenimine (PEI) have been used for the covalent functionalization of multiwalled CNTs (MWNTs) by direct heating in the melt. PEGDA and PEI functionalized MWNTs were found to be soluble in propanol [1]. Also, the dispersion of MWNTs in PEI has been used to prepare electrochemical sensors toward bioanalytes like ascorbic acid, dopamine, etc [2]. PEI functionalized single-walled CNTs graft polymer was also studied as a substrate for neural tissue cultures, and was found to promote neurite outgrowth and branching [3].

In this work we present the synthesis of MWNT buckypaper (BP)-PEI nanohybrid by *in situ* functionalization and its characterization. In a typical synthetic procedure, 20 mg of MWCNT and 20 mg PEI (1:1 w/w) were dispersed in ultrasonic bath with 100 ml of *n*-propanol for 15 min. The dispersion was cooled to -21°C, and ultrasonic probe agitation was applied for 10 min. The cooling and agitation cycles were repeated for two more times. After the last agitation step, the solution was filtered by means of glass vacuum filtration system, using 0.45 m pore size nylon filter membrane. PEI excess was removed by washing with additional 100 ml of *n*-propanol, and the sample was dried at room temperature. Finally, BP-PEI material obtained was peeled off from the filter.

The changes in morphology as compared to non-functionalized BP were observed by scanning electron microscopy. Characteristic absorption bands due to PEI were observed in ATR-FTIR spectra on both faces of the functionalized samples. The *I* vs. *V* curves measured showed that the presence of PEI in BP produces an increase in the electrical resistance as compared with non-functionalized BP. Additionally, the sample analysis by Raman spectroscopy was performed.

Acknowledgements: We appreciate financial support from the grants UNAM-DGAPA-IN100815 and CONACyT-127299.

1. Elena V. Basiuk (Golovataya-Dzhymbeeva), Omar Ochoa-Olmos, Flavio F. Contreras-Torres, Víctor Meza-Laguna, Edgar Alvarez-Zauco, Iván Puente-Lee, and Vladimir A. Basiuk. J. Nanosci. Nanotechnol. Vol. 11, No. 6 (2011).
2. M. D. Rubianes and G. A. Rivas, *Electrochem. Commun.* 9, 480 (2007).
3. H. Hu, Y. Ni, S. K. Mandal, V. Montana, B. Zhao, R. C. Haddon, and V. Parpura, *J. Phys. Chem. B* 109, 4285 (2005).

P4: Advances in Pd/Pt Nanoparticle Size decoration of mesoporous carbon spheres for energy application

Ryszard J Kaleńczuk, B. Zielińska, I. Turow, E. M. Mijowska

Institute of Chemical and Environment Engineering, West Pomeranian University of Technology, Szczecin, Poland
Email:rk@zut.edu.pl

In the past few decades, a variety of energy storage and conversion materials have been applied to high powered energy devices such as lithium batteries, supercapacitors, fuel cell and solar energy cells. [1] In comparison to the conventional energy materials, carbon nanomaterials have attracted extensive attention because of their unusual size and surface dependent properties useful in enhancing energy conversion and storage performance. [2] In particular, mesoporous carbons and mesoporous carbon materials modified by metals and metal oxides have been extensively studied due to their potential application in energy system.

Here, the palladium and palladium/platinum decorated mesoporous carbon spheres with different Pd and Pd/Pt nanoparticles size distribution have been prepared and analyzed in great details. The influence of palladium source (palladium acetyloacetonate, palladium acetate and palladium nitrate) and synthesis procedure on the Pd and Pd/Pt nanoparticles size distribution have been investigated (Figure 1). The obtained samples have been characterized by X-ray diffraction (XRD), transmission electron microscopy (TEM) together with Energy Dispersive X-Ray (EDX) as its mode, Brunauer-Emmett-Teller (BET) method, thermogravimetric analysis (TGA) and Raman spectroscopy.

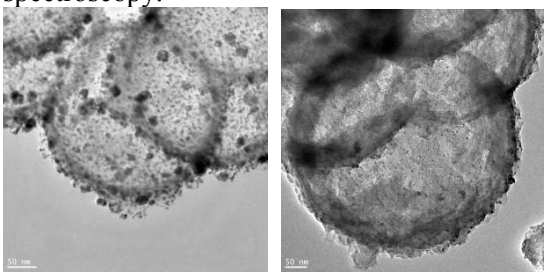

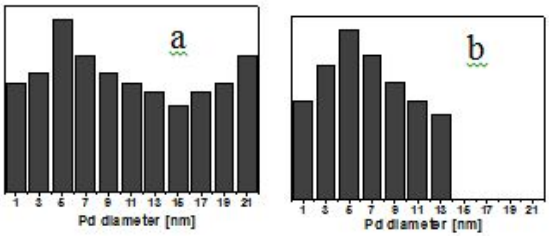

Fig1. TEM images and diameter distribution of Pd nanoparticles for palladium decorated mesoporous carbon spheres produced via reflux (a) and impregnation (b) methods.

1. J. Wang, H. L. Xin, D Wang, *Particle&Particle Systems Characterization* **31**, 515 (2013).
2. L. Dai, D. W. Chang, J. B. Baek, W. Lu, *Carbon Nanomaterials* **8**, 1130 (2012).

Acknowledgements: the research was funded by National Science Centre (DEC-2012/07/B/ST5/01925).

P5: Hig Brightness diode-pumped organic solid-state laser

Sébastien Forget[1,2], Zhuang Zhao[1,2], Oussama Mhibik[1,2], Malik Nafa[1,2], and Sébastien Chénais[1,2]

[1]Université Paris 13, Sorbonne Paris Cité, Laboratoire de Physique des Lasers, F-93430, Villetaneuse, France
[2]CNRS, UMR 7538, LPL, F-93430, Villetaneuse, France

Thin film organic solid-state lasers (OSSLs) have emerged as an important category of coherent sources, offering wavelength tunability over the whole visible spectrum[1,2].One of the main advantages of organic materials as gain media for lasers is their ability to be easily processed and their intrinsic low cost. OSSLs are generally optically pumped by frequency-doubled or tripled solid-state lasers, which are bulky and much more expensive than the organic laser structure itself, jeopardizing the promises of a truly low-cost system. Within the last decade, the spectacular progress in the field of high power inorganic blue laser diodes (LD) and light-emitting diodes (LED) enabled several teams to report on diode-pumped and LED-pumped OSSLs, thus demonstrating true low-cost systems. Nevertheless, as the peak power of such pumping sources is weak compared to the values achieved with pulsed solid-state lasers, very low threshold laser resonators such as DFB or microcavities are needed. As low threshold operation involves a low output coupling, minimizing threshold and maximizing output power are generally incompatible in a single laser device. As a consequence, the reported output powers of such diode-pumped lasers are very low and inefficient. Furthermore, DFB low loss compact resonators do not generally provide diffraction-limited beams, which combined with low output powers leads to a weak brightness.

In this paper we demonstrate high-power, diffraction-limited organic solid-state laser operation in a vertical external cavity surface-emitting organic laser (VECSOL)[3], pumped by a low-cost compact blue laser diode. The diode-pumped VECSOLs were demonstrated with various dyes in a polymer matrix, leading to laser emissions from 540 nm to 660 nm. Optimization of both the pump pulse duration and output coupling leads to a pump slope efficiency of 11% for a DCM based VECSOLs. We report output pulse energy up to 280 nJ with 100 ns long pump pulses, leading to a peak power of 3.5 W in a circularly symmetric, diffraction-limited beam and a two order of magnitude improvement in brightness when compared with previously published systems.

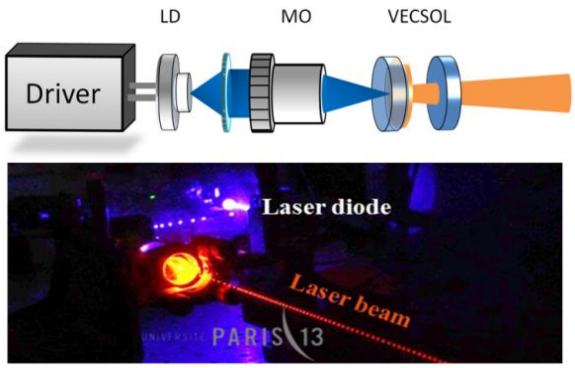

Fig.1: Schematic diagram of the diode-pumped plano-concave VECSOL resonator (MO : microscope objective, LD : Laser Diode). Inset: Long-exposure time photo of the working diode-pumped VECSOL.

[1] S. Forget and S. Chénais, *Organic Solid-State Lasers | Springer*, springer s (Springer-Verlag, 2013).
[2] S. Chénais and S. Forget, Polym. Int. **61**, 390 (2012).
[3] H. Rabbani-Haghighi, S. Forget, S. Chénais, and A. Siove, Opt. Lett. **35**, 1968 (2010).

P6: Simulations of Polyelectrolytes

Filip Uhlik

Department of Physical and Macromolecular Chemistry
Faculty of Science, Charles University in Prague, Czech Republic

Polyelectrolytes are polymers with ionizable groups. Under suitable conditions, polyelectrolytes are soluble in aqueous media. This property makes them attractive to biological, medicinal and environment-friendly applications that require organization of matter at nanoscale and can range from drug carriers, water pollutants removal, sea water desalination, coatings, oil recovery to nafion membranes in fuel cells. In some of them, e.g. as thickening agents, super-absorbents in diapers or flocculants, they have already reached mass production. Many of natural macromolecules (e.g. nucleic acids, proteins, pectins, heparins) are polyelectrolytes too.

Polyelectrolytes are conveniently divided into strong (also called quenched, e.g polystyrene sulfonic acid) and weak (also called annealed, e.g. polyacrylic acid). While strong polyelectrolytes remain fully ionized, the degree of ionization of weak polyelectrolytes can be influenced by both pH and ionic strength and is coupled to polymer conformations. This responsiveness to external stimuli makes weak polyelectrolytes particularly attractive to applications. However, their behavior is quite complex especially if we consider different conditions given by Bjerrum and Debye lengths, solvent quality, polymer concentration, branching and topology.

In this contribution we describe a general and efficient simulation technique based on hybrid Monte Carlo method in reaction ensemble suitable for studying polyelectrolytes under various conditions together with results for selected types of branching (e.g. polymer stars, combs and brushes), addition of salt with different valency, phenomena in polyelectrolyte gels and behavior of frustrated polyelectrolytes in poor solvents in order to illustrate both the capability of the method and the interesting phenomena in polyelectrolytes.

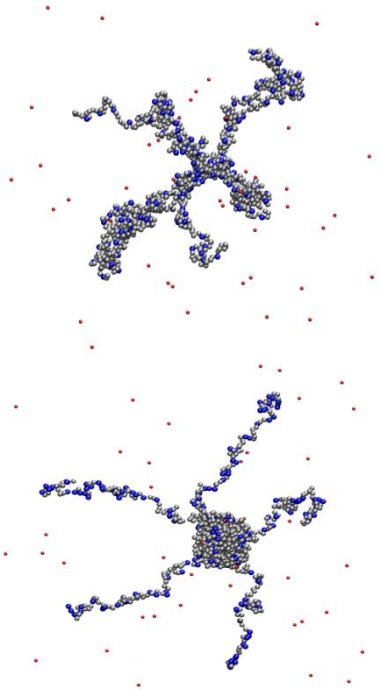

Qualitatively different behavior of otherwise same polyelectrolyte stars in poor solvent
(left: strong, right: weak; ionized monomer units: blue, neutral: gray, counter-ions: red).

P7: Coordination Functionalization of Graphene Oxide and Nanodiamond with Tetraazamacrocyclic Complexes of Nickel(II)

N. Alzate-Carvajal[1], L. V. Henao-Holguín[2], V. Meza-Laguna[2], A. Moreno-Bárcenas[3], J. F. Pérez-Robles[3], Elena V. Rybak-Akimova[4], V. A. Basiuk[2] and E. V. Basiuk[1]

[1] Centro de Ciencias Aplicadas y Desarrollo Tecnológico, Universidad Nacional Autónoma de México (UNAM), 04510 México D.F., Mexico; Email: elbg1111@gmail.com

[2] *Instituto de Ciencias Nucleares, UNAM, 04510 México D.F., Mexico; Email: basiuk@nucleares.unam.mx*
[3] *Centro de Investigación y de Estudios Avanzados, Instituto Politécnico Nacional, 76230 Querétaro, México*
[4] *Department of Chemistry, Pearson Chemistry Laboratory, 62 Talbot Avenue, Tufts University, Medford, MA 02155, USA*

The existence of COOH groups on the surface of graphene oxide (GO) and nanodiamond (ND) offers rich possibilities for the covalent, ionic and coordination functionalization of these important classes of carbon nanomaterials, and thus for broadening the spectrum of their useful properties and potential applications. For example, the attachment of tetraazamacrocyclic complexes to GO is extensively studied with an emphasis on hybrid nanomaterials for such application areas as organic photovoltaics, spin electronics and electrocatalysis.

The main goal of the present work was to explore the possibility of coordination functionalization of GO and ND with Ni(II) complexes of 1,4,8,11-tetraazacyclotetradecane (cyclam) and rac-5,7,7,12,14,14-hexamethyl-1,4,8,11-tetraazacyclotetradecane (tet *b*). Both $[Ni(cyclam)]^{2+}$ and $[Ni(tet\ b)]^{2+}$ are known to exist in diamagnetic square-planar tetracoordinated state in neutral and acidic media; on the other hand, these complexes can adopt a folded hexacoordinated conformation upon coordination with carboxylate ions in basic media (thus becoming paramagnetic complexes). It is the latter property which was employed by us for the attachment of $[Ni(cyclam)]^{2+}$ and $[Ni(tet\ b)]^{2+}$ to COOH functionalities existing in GO and ND. The functionalized samples obtained in this way were characterized by using Fourier-transform infrared, Raman, X-ray photoelectron and electron paramagnetic resonance spectroscopy, thermogravimetric analysis, scanning and transmission electron microscopy, as well as atomic force and scanning tunneling microscopy. An additional insight into structure and properties of the macrocycle–GO nanohybrids was afforded from density functional theory (DFT) calculations by using PBE GGA functional with Grimme dispersion correction in conjunction with the double numerical basis set DNP (as implemented in the DMol^3 numerical-based DFT module of Materials Studio 6.0 package from Accelrys Inc.).

Acknowledgements: Financial support from UNAM (grants DGAPA-IN100815 and IN101313) and CONACyT (grant 127299) is greatly appreciated. N. A.-C. and L. V. H.-H. are indebted to the Doctorate Program in Chemical Sciences of UNAM and CONACyT for a Ph. D. fellowship.

P8: Noncovalent Complexes of Phthalocyanines with Spherical Fullerenes and Short Nanotube Models: A DFT Study

Vladimir A. Basiuk

Instituto de Ciencias Nucleares, Universidad Nacional Autónoma de México, Circuito Exterior, Ciudad Universitaria, 04510, México, D.F., México Email: basiuk@nucleares.unam.mx

Noncovalent hybrids of phthalocyanines (Pcs) with fullerenes and carbon nanotubes (CNTs) is a subject of considerable research effort aimed to the development of efficient organic photovoltaic cells, heterogeneous catalysts, gas sensors, field effect transistors, lithium batteries, among other applications. Theoretical studies play an important role in the elucidation of structure and properties of the nanohybrids, however the number of relevant research reports is limited due to a large molecular size of both Pcs and carbon nanostructures.

The main goal of the present report was to provide information on the noncovalent interactions of free Pc ligand (H_2Pc) and its copper(II) (CuPc) and zinc(II) (ZnPc) complexes with spherical fullerenes C_{60} and C_{80}, as well as with short closed-end models of single-walled CNTs (SWNTs) by using DFT calculations. The armchair and zigzag SWNT models ANT and ZNT were derived from C_{60} and spherical C_{80} to form armchair (5,5) and zigzag (10,0) nanotubes, composed of 120 and 140 carbon atoms, respectively. The data were obtained by using the DMol^3 numerical-based DFT module of the Materials Studio 6.0 package (Accelrys Inc.).

We employed PBE GGA functional with Grimme empirical dispersion correction, in conjunction with the DNP double numerical basis set. Full geometry optimization and calculation of electronic parameters was performed by setting the quality and convergence criteria to 'fine', along with all-electron core treatment, Fermi orbital occupancy, and the global orbital cutoff of 4.4 Å (defined by the presence of Cu and Zn atoms). The calculated energies of complex formation ranged from -17.90 (for H_2Pc+C_{60}) to -37.12 kcal/mol (for ZnPc+ZNT). The interaction strength increased with increasing the size of carbon nanocluster, and, generally, with increasing atomic mass of the central atom. In all the complexes studied, Pc molecule lost its planarity to embrace carbon nanocluster and thus to augment the contact area. The optimized geometries were analyzed in terms of close contacts between the interacting components and N-M-N angles within the Pc coordination sphere. The HOMO-LUMO gap energies calculated were mainly defined by the magnitude of HOMO-LUMO gap for isolated carbon nanocluster rather than by the nature of central atom (H, Cu or Zn).

Acknowledgements: Financial support from UNAM (grant DGAPA-IN101313) and CONACyT (grant 127299) is greatly appreciated.

P9: Non-Covalent Functionalization of Multiwalled Carbon Nanotube Buckypaper with a Ni(II) Tetraazaannulene Complex

V. Meza-Laguna[1], M. Pérez-Ruiz[1], E. V. Basiuk[2] and V. A. Basiuk[1]

[1] Instituto de Ciencias Nucleares, Universidad Nacional Autónoma de México (UNAM), 04510 México D.F., México; Email: victor.meza@nucleares.unam.mx
[2] Centro de Ciencias Aplicadas y Desarrollo Tecnológico, UNAM, 04510 México D.F., México

The non-covalent functionalization of carbon nanotubes (CNTs) with aromatic compounds is a widely employed technique based on – - interaction that keeps the intrinsic electronic structure of CNTs totally intact and allows for combining unique properties of the two interacting components. Non-covalent functionalization of CNTs with aromatic polyazamacrocyclic ligands, usually porphyrins and phthalocyanines, and their transition metal complexes [1], have potential photovoltaic applications. Tetraaza[14]annulenes and related macrocyclic systems [2] are simpler compounds that exhibiting similar properties with potential use for photovoltaic, catalytic, electrochemical and other applications. Preparation of macrocycle–CNT hybrids by physical vapor deposition has been proposed due to high thermal stability of tetraazaannulenes. The synthesis of nanohybrids of single-walled and multiwalled CNTs (MWNTs) with Ni(II)-tetramethyldibenzotetraaza[14]annulene (NiTMTAA) has been successfully performed by vacuum sublimation method previously [3].

We have obtained non-covalent hybrids of MWNT buckypaper (BP) and NiTMTAA by ultrasonic agitation and vacuum filtration. Typically, 20 mg MWNTs and 2 mg were dispersed in 100 ml of *n*-propanol under ultrasonication for 15 min. After the solution was cooled to -21°C, ultrasonic probe agitation was applied for additional 10 min. The cooling and agitation cycles were repeated for two more times. After the last agitation, the solution was filtered by using a glass vacuum filtration system through a 0.45 m pore size nylon filter membrane. During drying step, the sample was peeled off by itself. In the filtration process, large particles are the first to precipitate, so it was expected that the faces of BP-NiTMTAA hybrid are different in morphology and properties. The both faces of pristine BP and BP-NiTMTAA were comparatively characterized by Raman and ATR-FTIR spectroscopy. SEM imaging showed that larges agglomerates of MWNTs with flat appearances are present in pristine BP samples, while the nanotubes in the functionalized samples were more dispersed. The electrical resistance measurements showed a decrease when the hybrid samples was exposed to ambient light; at the same time, this effect was observed only for one side of BP-NiTMTAA.

Acknowledgements: We appreciate financial support from the grants UNAM-DGAPA-IN100815 and CONACyT-127299.

1. R. Chitta, A.S.D. Sandanayaka, A.L. Schumacher, L. D'Souza, Y. Araki, F. D'Souza, O. Ito. Journal of Physical Chemistry C **111,** 6947–6955 (2007).
2. E.V. Basiuk (Golovataya-Dzhymbeeva), E.V. Rybak-Akimova, V.A. Basiuk, D. Acosta-Najarro, J.M. Saniger. Nano Letters **2**, 1249–1252. (2002)
3. Vladimir A. Basiuk, Laura Veronica Henao-Holguin, Edgar Alvarez-Zauco, Maria Bassiouk, Elena V. Basiuk. Applied Surface Science **270**, 634– 647 (2013).

Author Index

P** -page in **program** **A** -page in **abstract